JANUARY, 1952
IN TWO SECTIONS — SECTION I

Journal of METALS

January JOURNAL OF METALS Highlights:

"Melting Low Carbon Stainless Steel," - p. 20
"Removable Bulkhead Doors Speed Slag Removal," - p. 26
"Vacuum Impregnation of Castings," - p. 30

Basic values behind the trade mark

BASIC FURNACE REFRACTORIES

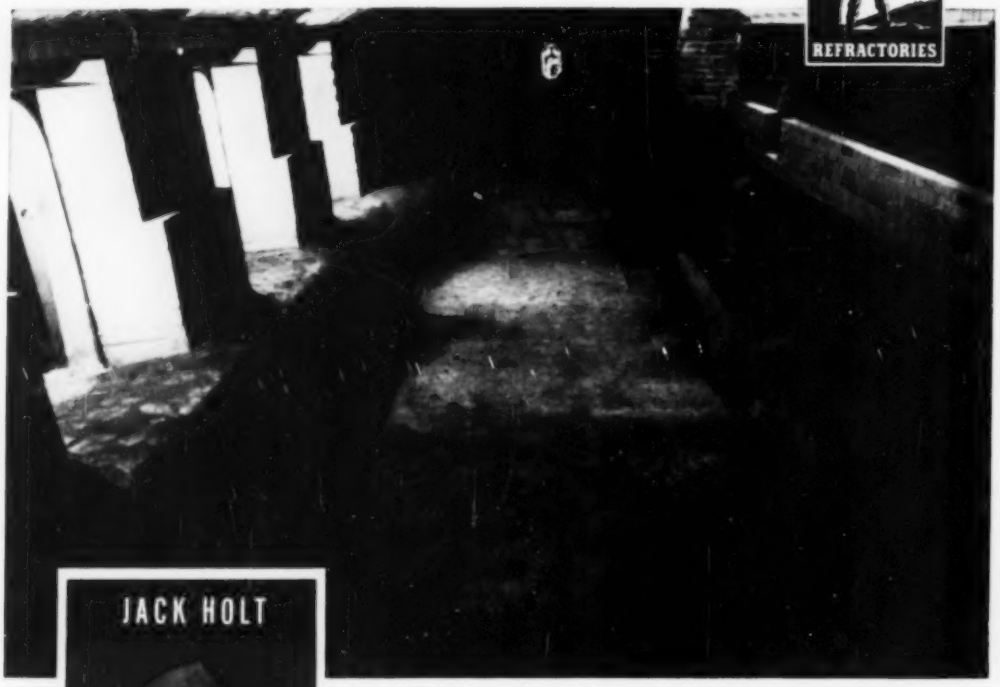

Jack Holt, member of the Basic Service Division, was open hearth superintendent in an Eastern shop before he joined our staff in 1950.

After this Ramset hearth — another Basic Service Division job — is brought up to temperature, and slagged, it will be ready for charging.

SERVICE WITH A SALE

A FAMILIAR trade mark identifies a dependable product. But quality of product is only one of the values that stand back of the "man with the shovel."

No product is completely sold unless it is properly serviced . . . We have always believed this. This belief led years ago to our product research program and to the development of installation techniques and tools. More recently it led to the establishment of a Service Division, manned by experienced ex-steelmakers. Incidentally, our Service crew has been booked solidly ever since we announced the new division.

These extra values add nothing to the price of Basic products. They are our contribution, intended to help reduce refractory costs per ton of steel—part of our effort to earn more of your granular basic refractory business.

Basic Refractories Incorporated 843 HANNA BUILDING, CLEVELAND 15, OHIO

Exclusive Agents in Canada: REFRACTORIES ENGINEERING AND SUPPLIES, LTD., Hamilton and Montreal

Journal of **METALS**

Published to provide a continuing, authoritative, and up-to-date record of technological, engineering, and economic progress in all branches of the metals industry by the
Metals Branch
American Institute of Mining and Metallurgical Engineers, Inc.
29 West 39th Street, New York 18

• • •

THOMAS E. LLOYD
Manager of Publications
Editor, Journal of Metals

• • •

A. S. COHAN — Associate Editor
D. G. GARRETT — MARGARET BAGG
Assistant Editors
GRACE PUGSLEY — Production Manager
W. J. SEWING — Asst. Prod. Mgr.

• • •

METALS BRANCH COUNCIL
C. C. Long — Chairman
E. O. Kirkendall — Secretary
R. M. Brick — IMD Chairman
T. L. Joseph — ISD Chairman
O. C. Ralston — EMD Chairman
M. Gensamer — D. S. Eppelsheimer
H. K. Work — Evan Just

TECHNICAL PUBLICATIONS COMMITTEE
J. T. Laudermilk — Chairman
E. J. Kennedy, Jr. — Secretary

AUXILIARY PUBLICATIONS COMMITTEE CHAIRMEN
M. Gensamer — Institute of Metals Div.
A. G. Forrest — Iron & Steel Div.
J. Glosser — Extract. Metal Div.

• • •

JAMES A. STANGARONE
Advertising Manager
B. C. SNELL
Regional Manager, Pittsburgh
1110 McDonald Place, Sewickley, Pa.

• • •

The AIME Publishes:
Journal of Metals
Mining Engineering
Journal of Petroleum Technology

Series 600 chromium carbide is now in the engineering appraisal stage at Carboloy Dept., General Electric Co., Detroit. The new carbide, produced from powdered metals, is expected to open new fields of application for metallic carbides. The photograph shows chromium carbide blanks about to be presintered.

Journal of Metals Reporter	19	New Products	12
Annual Meeting Program	97	AIME News	97
Employment Service	6	Coming Events	5
Meet the Authors	3	Personals	107
"Drift of Things"	17	New Books for Engineers	10

Melting Low Carbon Stainless Steel — Walter Crafts, H. P. Rowdabush — 20
Slag Pocket Cleanouts Speeded by Removable Open Hearth Bulkhead Doors — Roy E. Oven — 26
Hot Pressing Silver Powder — K. Ogawa, G. Matsumura — 28
Vacuum Impregnation of Castings — L. W. Hull — 30

Heats of Formation of Sodium-Tin Alloys Determined With a New High Temperature Colorimeter — F. L. McKisson, L. A. Bromley — 33
Constitution of the System Gallium-Indium — J. P. Denny, J. H. Hamilton, J. R. Lewis — 39
Solidification Mechanism of Steel Ingots — H. F. Bishop, F. A. Brandt, W. S. Pellini — 44
Constitution and Properties of Some Iron-Bearing Cupro-Nickels — E. W. Palmer, F. H. Wilson — 55
Volatility and Stability of Metallic Sulphides — C. M. Hsiao, A. W. Schlechten — 65
Crystal Structure of TiAl — Pol Duwez, J. L. Taylor — 70
Crystal Structure of TaCr$_2$ and CbCr$_2$ — Pol Duwez, H. Mathers — 72
Rolling Textures in Face-Centered Cubic Metals — Hsun Hu, P. R. Sperry, P. A. Beck — 76
Annealing Textures in Rolled Face-Centered Cubic Metals — P. A. Beck, Hsun Hu — 83
On the Solution of Diffusion Problems Involving Concentration-Dependent Diffusion Coefficients — Carl Wagner — 91

Secondary Recrystallization Texture in Copper — M. Shiraj, C. G. Dunn — 42
A Sensitive Method for Thermal Analysis of Very Low Melting Alloys — R. M. Evans, E. O. Fromm, R. T. Jaffee — 74
Method for Locating Two-Liquid Immiscibility Limits — R. F. Bunn — 81

Published the first day of each month by the American Institute of Mining and Metallurgical Engineers, Inc., 29 West 39th Street, New York 18, N. Y. Telephone: PEnnsylvania 6-9220. Subscription $8 per year for non-AIME members in United States and North, South and Central America; $9 foreign; $6 for AIME members, or $4 additional in combination with a subscription to "Mining Engineering" or "Journal of Petroleum Technology". Single copies, 75 cents; special issues, $1.50. The AIME is not responsible for any statement made or opinion expressed in its publications.
Copyright 1951 by the American Institute of Mining and Metallurgical Engineers, Inc. Registered cable address, AIME New York. Indexed in Engineering Index, Industrial Arts Index and Chemical Abstracts. Reentered as second-class matter Sept. 21, 1949, at the post office at New York, N. Y., under the Act of March 3, 1879. Additional entry established at Manchester, N. H.

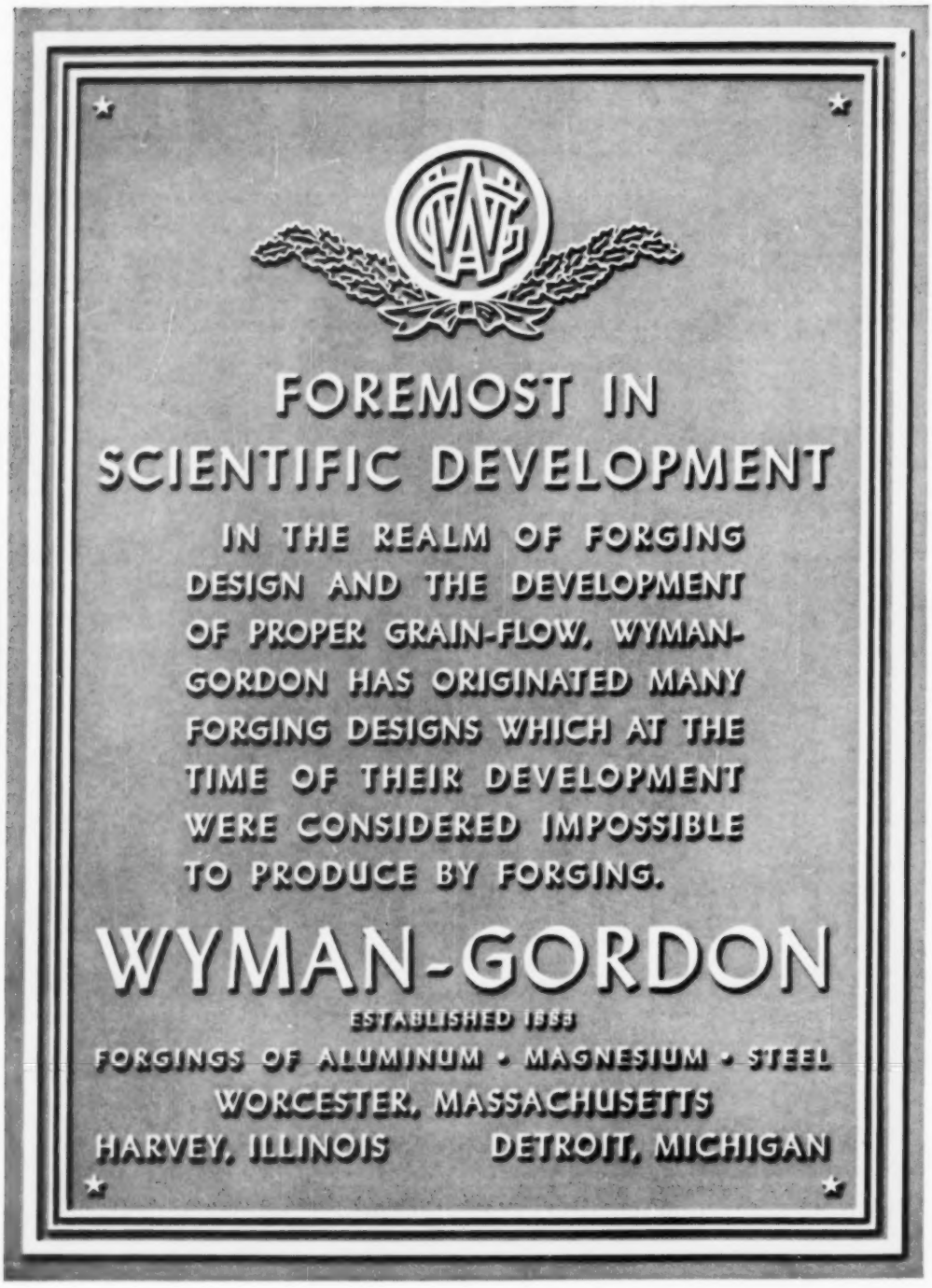
FOREMOST IN
SCIENTIFIC DEVELOPMENT
IN THE REALM OF FORGING DESIGN AND THE DEVELOPMENT OF PROPER GRAIN-FLOW, WYMAN-GORDON HAS ORIGINATED MANY FORGING DESIGNS WHICH AT THE TIME OF THEIR DEVELOPMENT WERE CONSIDERED IMPOSSIBLE TO PRODUCE BY FORGING.
WYMAN-GORDON
ESTABLISHED 1883
FORGINGS OF ALUMINUM • MAGNESIUM • STEEL
WORCESTER, MASSACHUSETTS
HARVEY, ILLINOIS
DETROIT, MICHIGAN

MEET THE AUTHORS

M. SHARP

C. G. DUNN

H. F. BISHOP

W. S. PELLINI

L. A. Bromley (p. 33) is an alumnus of Illinois Institute of Technology (M.S.) and University of California (B.S., Ph.D.), Berkeley, Calif. At the latter school he was research assistant and instructor, and is now assistant professor of chemical engineering. A member of AIChE and ACS, his hobbies are sailing and fishing.

J. P. Denny (p. 39), research metallurgist, General Electric Co., Lynn, Mass., was formerly associated with University of Utah, Battelle Memorial Institute, and served as Captain, USAF. He is a graduate of Colorado School of Mines and University of Utah (M.S., Ph.D.) and belongs to AIME, ASM, and Sigma Xi. Bowling, golf, chess, and skiing occupy his leisure time.

M. Sharp (p. 42) graduated from University of Michigan with chemical and metallurgical engineering degrees. Now engineer in the quality control dept. of Ryan Industries of Detroit, he was formerly with General Electric Co. This member of AIME and ASM enjoys chess and hiking.

C. G. Dunn (p. 42), a graduate of Montana State University (B.A.) and University of Illinois (Ph.D.), is research physicist for General Electric Co., Pittsfield, Mass. A previous contributor of papers to the Institute, he holds membership in AIME and APS. Bowling and photography are his hobbies.

H. F. Bishop (p. 44) is an alumnus of Michigan State College. A metallurgist in the metal processing branch, Naval Research Laboratory, Washington, D. C., his hobbies are bowling, tennis, and swimming.

F. A. Brandt (p. 44), metallurgist in the metal processing branch, Naval Research Laboratory, Washington, D. C., is a graduate of Columbia University (B.S.). His spare time is spent on maintenance of his house, listening to classical music, and photography.

W. S. Pellini (p. 44) is in charge of foundry and welding research at Naval Research Laboratory, Washington, D. C., and a graduate of Carnegie Institute of Technology. He served as Lieut. Cmdr., USN, and was associated with American Brake Shoe Co. and Atomic Energy Commission. Author of some 25 technical papers, and a member of AIME, AFS, AWS, and ASTM, he occupies his leisure hours with crafts and photography.

E. W. Palmer (p. 55), a graduate of Rensselaer Polytechnic Institute, is research metallurgist of American Brass Co., Waterbury, Conn., where he has been associated since 1930. A member of AIME, ASM, Institute of Metals, and Optical Society of America, he has authored several papers, and is an amateur photographer.

F. H. Wilson (p. 55) was born in Kuling, Kiangsi, China. He graduated from Princeton University, Wesleyan, and Yale University (B.S., M.A., M.S., and Ph.D.). He taught secondary school, then joined American Brass Co. in 1937, where he is now assistant research metallurgist. When not writing technical papers, this member of AIME and American Crystallographic Assn. enjoys music and gardening.

Chi-mei Hsiao (p. 65) was born in Hunan, China, and graduated from Tangshan Engineering College (B.S.) and Missouri School of Mines (M.S., Ph.D.). Now associated with Lindberg Steel Treating Co., Chicago, he has done research and development work on ferroalloys and tungsten steels in China, and spent one year with the National Bureau of Standards in China. A student associate of AIME, his hobbies are photography and stamp collecting.

R. M. Evans (p. 74), a graduate of Ohio State University, is associated with Battelle Memorial Institute, Columbus, Ohio. He has previously been connected with Buckeye Steel Castings Co., Bureau Agricultural Engineering, Civilian Conservation Corp., and Superior Molding Sand Co. A member of AIME, ASM, ASLE, he enjoys golf, camping, and model railroading.

Hsun Hu (p. 76) was born in China and studied at National Chiao-Tung University (B.S.), Lehigh University (M.S.), and University of Notre Dame (Ph.D.). A metallurgist at Institute for the Study of Metals, University of Chicago, he belongs to AIME, ASM, Sigma Xi, and British Institute of Metals. Ping pong, swimming, and music are his hobbies.

P. A. Beck (p. 76), research professor of physical metallurgy at University of Illinois, was formerly associated with University of Notre Dame, Cleveland Graphite Bronze Co., Beryllium Corp., and American Smelting & Refining Co. He was born in Budapest, Hungary, and graduated from Royal Hungarian University of Technical Sciences and Michigan College of Mining & Technology (M.S.), and has written numerous technical papers. Music, swimming, hiking, and golf are the recreations of this member of AIME, APS, American Crystallographic Assn., ASM, and ASTM.

P. R. Sperry (p. 76), a graduate of University of Notre Dame, is metallographer in the metallurgy dept. He has previously been associated with Glenn L. Martin Co. His hobbies are gardening and woodworking.

Carl Wagner (p. 91) was born in Leipzig, Germany, and received his doctorate at University of Leipzig. He was associated with several universities in Germany, and then became scientific advisor to Ordnance Research and Development Div. Suboffice (Rocket), Fort Bliss, Texas. He is now visiting professor at Massachusetts Institute of Technology, and is a member of AIME and numerous professional societies here and abroad.

CHI MEI HSIAO

R. M. EVANS

HSUN HU

CARL WAGNER

Advertisement

ELECTROMET *Data Sheet*

A Digest of the Production, Properties, and Uses of Steels and Other Metals

Published by Electro Metallurgical Company, a Division of Union Carbide and Carbon Corporation, 30 East 42nd Street, New York 17, N. Y. • In Canada: Electro Metallurgical Company of Canada, Limited, Welland, Ontario

MANGANESE . . .
Deoxidizer and Toughener for Steel

Manganese is one of the most important alloys used in making steel. It is practically indispensable as a deoxidizer and cleanser for improving the hot working properties of steels. When used as an alloying element, it makes steel stronger and tougher and it is therefore an important constituent of many structural and engineering steels.

Deoxidizes and Cleans Steel

The effectiveness of manganese in deoxidizing steel was first recognized in 1856, when it was used in the Bessemer process of steelmaking to counteract the bad effects of sulphur. In fact, manganese made this process a commercial success. Today manganese is used as a deoxidizer and cleanser in the production of nearly all grades of open-hearth and electric-furnace steel, as well as high-grade cast iron.

Research work carried out recently in ELECTROMET'S laboratories at Niagara Falls, New York, has provided new and important information on the value of manganese as a deoxidizer. This work shows that manganese is a more effective deoxidizer than has been previously realized, and that a combination alloy of silicon and manganese is a much stronger deoxidizer than either silicon or manganese by itself. Complete information is given in a report entitled "Solubility of Oxygen in Liquid Iron Containing Silicon and Manganese." If you would like a copy of this report, free of charge, write to the address above.

Improves Hot-Working Properties

By combining readily with sulphur, manganese performs another valuable job: it removes the principal cause of hot-shortness or brittleness, thereby giving steel better rolling and forging properties. In this reaction, the manganese combines with the sulphur to form manganese sulphide, as follows:

$$Mn + FeS = MnS + Fe$$

The manganese sulphide remaining in the steel is a less harmful type of inclusion than the iron sulphide would be, the hot-working properties of the steel are improved.

The weakening and embrittling tendencies of sulphur in cast iron can also be counteracted by the addition of manganese to the cupola charge.

Increases Strength, Toughness, and Wear-Resistance

When used as an alloying element in steel, manganese produces a steel with greater strength and toughness, and there is no serious loss of ductility. Additions of about 13 per cent manganese produce the well-known Hadfield manganese steel. High-manganese steels have exceptional resistance to wear, and consequently they have many applications in engineering jobs. Instead of wearing away quickly under conditions combining severe pressure, shock, and abrasion, these steels actually become harder through use. Thus, they last longer.

Because of the tendency of high-manganese steels to work harden, they serve industry in important and varied applications. Manganese steel castings, for example, are used for railroad frogs and crossings, rock-crusher parts, steam-shovel dipper teeth, and dredge-bucket lips. The chief applications of manganese steel are in rails used for special service, and light forgings subjected to heavy wear.

Dipper bucket teeth, cast of Hadfield manganese steel, actually increase in hardness under abrasive wear from gravel and rock in construction work — thus last many times longer than those of ordinary steel.

ELECTROMET Alloys

Manganese is produced by ELECTROMET in forms suitable for practically every use of the iron, steel, and non-ferrous metal industry. Some of the ELECTROMET products are listed below. For a complete description of these alloys, write for a copy of the booklet, "ELECTROMET Products and Service."

The terms "EM" and "Electromet" are registered trade-marks of Union Carbide and Carbon Corporation.

Alloys of Manganese and Their Uses

Standard Ferromanganese	The product most commonly used for adding manganese to steel for the purpose of alloying or deoxidizing and cleansing.
Low Carbon Ferromanganese	For adding manganese to steels having a low carbon content, such as stainless steels of the 18 per cent chromium, 8 per cent nickel type.
Medium Carbon Ferromanganese	Commonly used for making manganese steel containing 1.50 to 2.00 per cent manganese, and in the production of Hadfield manganese steel.
Low-Iron Ferromanganese	For applications in the nickel, aluminum, and copper industries where a low-iron alloy is required.
Silicomanganese	Used by the steel industry as a furnace block, as a deoxidizer, and also for manganese additions, particularly in the production of engineering steels containing 0.10 to 0.50 per cent carbon.
"EM" Silicomanganese Briquets	For adding manganese (with silicon) to cast iron in the cupola.
"EM" Ferromanganese Briquets	For adding manganese (without silicon) to cast iron in the cupola.

— Coming Events —

Jan. 8, 1952, Society for Applied Spectroscopy, Socony-Vacuum Training Center, 63 Park Ave., New York.

Jan. 9, AIME, Chicago Section, Chicago Bar Assn., Chicago.

Jan. 9, AIME, Connecticut Section, Hammond Metallurgical Laboratory, Yale University, New Haven, Conn.

Jan. 16, AIME, Bessemer Steel Committee, off-the-record meeting, Duquesne Club, Pittsburgh.

Jan. 16, AIME, Western Section, National Open Hearth Steel Committee, Rodger Young Auditorium, Los Angeles.

Jan. 16-18, Society of Plastic Engineers, Inc., annual national technical conference, Edgewater Beach Hotel, Chicago.

Jan. 17, AIME, New York Section, Mining Club, 33 Broadway, New York.

Jan. 23, AIME, New York Section, 29 W. 39th St., New York.

Jan. 31-Feb. 1, ASM, midwinter technical meeting, William Penn Hotel, Pittsburgh.

Feb. 8, AIME, Southwestern Section, National Open Hearth Steel Committee, Park Plaza Hotel, St. Louis.

Feb. 14, AIME, Philadelphia, Engineering Bldg., University of Pennsylvania, Philadelphia.

Feb. 18-21, AIME, annual meeting, Hotel Statler, New York.

Feb. 28, AIME, Cleveland Section, Lecture Room, Metallurgy Bldg., Case Institute of Technology, Cleveland.

Mar. 3-7, ASTM, spring meeting and committee week, Hotel Statler, Cleveland.

Mar. 12, AIME, Chicago Section, National Open Hearth Steel Committee, Del Prado Hotel, Chicago.

Mar. 16-19, American Institute of Chemical Engineers, Atlanta Biltmore Hotel, Atlanta.

Mar. 19, AIME, Western Section, National Open Hearth Steel Committee, Rodger Young Auditorium, Los Angeles.

Mar. 20, AIME, Philadelphia, Engineering Bldg., University of Pennsylvania, Philadelphia.

Mar. 22-Apr. 6, Chicago International Trade Fair, Navy Pier, Chicago.

Mar. 31-Apr. 2, AIME, annual conference, Blast Furnace, Coke Oven, Raw Materials Committee and Open Hearth Steel Committee, William Penn Hotel, Pittsburgh.

Apr. 17, AIME, Philadelphia, Engineering Bldg., University of Pennsylvania, Philadelphia.

Apr. 21, AIME, Chicago Section, National Open Hearth Steel Committee, Phil Smidt & Sons, Whiting, Ind.

Apr. 25-26, AIME, New England Regional Conference, Kenmore Hotel, Boston.

Apr. 26-May 11, Liege International Fair, Liege, Belgium.

May 1-7, American Foundrymen's Society, International Foundry Congress and Show, Convention Hall, Atlantic City, N. J.

May 6-9, Scientific Apparatus Makers' Assn., annual meeting, Edgewater Beach Hotel, Chicago.

May 22-24, American Society for Quality Control, annual convention, Onondaga County War Memorial, Syracuse, N. Y.

June 16-20, Industrial Finishing Exposition, International Amphitheatre, Chicago.

June 23-27, ASTM, 50th anniversary meeting, Hotel Statler, New York.

July 1-Sept. 30, Centennial of Engineering, Chicago.

Sept. 11-13, American Institute of Chemical Engineers, Palmer House, Chicago.

Sept. 22-25, American Mining Congress, Metal and Nonmetallic Mining Convention and Exposition, public auditorium, Denver.

Electro

ADAPTABILITY Could Be What You Need!!

As your requirements become more exacting and your practices more individual, your need for grinding wheels *engineered to your requirements,* becomes imperative.

For that reason, we operate with an unusual adaptability in resources and resourcefulness.

We are equipped both mentally and physically to depart from "standard practices" with grits, bondings and wheel forms, to produce wheels with a take-off efficiency that will pay off for you.

Gains of 45% from applying Electro adaptability are not unusual. Without obligation, may we demonstrate?

ELECTRO REFRACTORIES & ABRASIVES CORP.
344 Delaware Avenue, Buffalo 2, N. Y.
Regional Warehouse: Los Angeles 58, California
Canadian Plant: Cap-de-la-Madeleine, P.Q.

Electro SINCE 1910

Resin Bonded
ABRASIVE WHEELS FOR
CUTTING OFF
PRECISION GRINDING
SNAGGING
GRINDING WHEEL MANUAL 645 AND SPEED CALCULATOR
Free on Request
Write for Them *NOW!*

Electro
RESIN BONDED
GRINDING WHEELS

— Personnel Service —

New York 18 Detroit
San Francisco
Chicago 1

POSITIONS OPEN

Assistant to Sales Manager, mechanical or metallurgical engineering graduate, with at least 10 years' sales, sales promotion and product development experience in metal products fields, to perform staff duties in office and field covering new products and promotion of general business. Salary open. Location, New York. Y6361.

Chief Inspector to take charge of inspection covering stampings, welding and sheet metal products for jet engine accessories. Salary, $6000 a year. Location, New York. Y6357.

Physical Metallurgist, with three or four years' experience handling heat treatment of steels, hardening, etc. Salary open. Location, Brooklyn, N. Y. Y6347.

Metallurgist, 35 to 45, with degree, and with considerable experience in plant metallurgy on iron, steel and nonferrous materials. Salary, $6000 to $7200 a year. Location, New Jersey. Y6342.

Sales Engineer for agency specializing in domestic and foreign machine tools, i.e., metal working machine tools, automatic screw machines, engine lathes, light lathe, milling, hydraulic surface grinding machine tools. Salary, $3900 drawing against commission. Territory, New York. Y6333.

Research Fellowship in metallurgy at Eastern university. Post graduate work for Ph.D. degree. Selection of research problem in variety of fields, including welding, induction heating, powder metallurgy, electro-metallurgy and magnetic materials. Location, Pennsylvania. Y6330.

Junior Engineer, 26 to 30, B.S. degree in mechanical, metallurgical or mining engineering, with mining and milling equipment experience, or junior executive background with business school education, to assist in office engineering covering correspondence, purchasing, specifications, expediting, etc. Occasional trips. Salary, $4200 to $4500 a year. Location, New York. Y6325.

Metallurgist with degree in metallurgy or chemistry, and two years' or more ferrous products experience, to do physical or chemical testing, check heat treatment, and analyze production difficulties in steel products manufacturing plant. Salary, $4200 to $4800 a year. Y6323(a).

Chemist, graduate, with three or four years' industrial experience, including some metallurgy for laboratory of heavy equipment manufacturer. Salary, $4800 a year. Location, Pennsylvania. Y6307.

Metallurgical Engineers (2) with two to five years' experience in powder metallurgy, precision casting, finishing, etc., and/or general metal working industries, with some mechanical aptitude. Salary, to $6600 a year. Location, New York. Y6301(a).

Metallurgists, Project Leader, with M.S. degree and several assistants, graduates, for fatigue studies. Work will involve studies of grain size effect on high temperature fatigue, notch effects, fatigue gage for metals and related work. Salary, $4650 to $6240 a year. Location, New York State. Y6297.

DETERMINE CARBON IN MOLTEN STEEL IN 40 Seconds . . . AT THE FURNACE

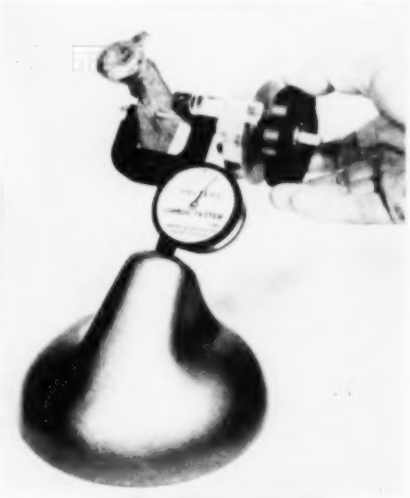

THE Dietert-Detroit Melters Carbon Test gives the carbon content of molten steel (range—.04 to .60% carbon) in 40 seconds. Only one man's attention is required. The test is carried out at the furnace. No time is lost in transporting the sample. Briefly, a test spoon of metal is poured into a mold, the test piece removed fifteen seconds later, quenched, ground and tested in a diamond cone hardness tester. The carbon per cent is read directly from the hardness tester scale.

Every minute of furnace time lost in waiting for preliminary analysis costs dollars. The Dietert-Detroit Melters Carbon Test will save these dollars for you and at the same time reduce the chances of an "off heat."

CONTROL EQUIPMENT
SAND · MOLD · MOISTURE
CARBON · SULFUR

HARRY W. Dietert COMPANY
9330 ROSELAWN AVE. · DETROIT 4, MICHIGAN

Assistant Professor, recent graduate, with Ph.D. degree, capable of working out courses in advanced physical metallurgy or metallurgical thermodynamics. For first two years will not be expected to teach more than one course a term. The rest of time will be devoted to helping carry out and supervise some of the research work. Excellent opportunity. Salary, $5400 a year depending on experience. Location, New Jersey. Y6295.

Metallographer with good understanding of the principles of physical metallurgy, to investigate and work on a new family of alloys; technically interesting work in a growing industry. Salary open. Location, Pennsylvania. Y6291.

Instructor in basic welding and heat treating laboratories, graduate metallurgical or mechanical engineer, possibly with some related industrial experience. Salary, $3000 for eight and a half months with opportunity for graduate work toward advanced degree, free of tuition. Location, Indiana. Y6289.

WANTED—MELTING DEPARTMENT SUPERINTENDENT

Immediate opening for person having experience in electric arc furnace melting of tool, high speed, stainless, and specialty steels in long-established mill in Pittsburgh district. Should have considerable practical experience, technical background, and ability for handling men. Reply giving complete record of experience, qualifications, age, and references.

Box K-17
JOURNAL OF METALS

FOR SALE Bausch & Lomb Research Metallograph. This equipment has been used, but is in good condition and is complete with objective lenses, eyepieces, etc. This equipment can be obtained at a substantial saving. Detailed information will be furnished upon request.
Box L-18 JOURNAL OF METALS

METALLURGIST—Position available to graduate metallurgist with 2 to 3 years' practical experience. 25 to 35 year age bracket preferred; however, will train recent college graduate. Great Lakes area. Please respond with statement of experience and background.
Box A-1 JOURNAL OF METALS

FOR SALE Revi-Duty electric furnace, Type HD-153012 muffle size 15" wide x 30" long x 12" high, 18KW at 220 volts single phase 2000°F max. built in 1942. Available immediately and can be seen by appointment in Philadelphia area.

Box A-2 JOURNAL OF METALS

Instructor or Assistant Professor, physical and/or process metallurgist, with Master's or preferably Doctor's degree, to teach elements of metallurgy, electro-metallurgy, ferrous metallurgy, metallurgical calculations, principles of physical metallurgy, metallography and the direction of advanced students in individual projects and research. Must be U. S. citizen. Location, West. Y6270.

Recent Graduate with some knowledge of metallurgy, particularly with reference to machinability, heat treatment and structure, both ferrous and nonferrous. Some experience in metallography with ability to polish and understand the structure of the more common steel and nonferrous alloys. Also qualified to conduct basic design studies and to operate physical testing machines normally found in a laboratory. Location, New York. Y6259.

Materials and Process Engineer for work involving the selection and testing of materials for precision engineered products. Five years' experience in work involving the evaluation of the application of a wide range of ferrous and nonferrous metals for precision equipment manufacture required. Mechanical, metallurgical or chemical degree. Salary, $6000 to $9000 a year. Location, Brooklyn, N. Y. Y6258(a).

Chief Engineer, 35 to 45, with five years' experience, preferably in ferrous foundry operations. Salary, $7200 to $8400 a year. Location, New York. Y6256.

Chief Metallurgist for an aluminum foundry. Must have had at least 4 years' experience in aircraft aluminum metallurgical work, and have knowledge of aircraft aluminum products. Will supervise aluminum metallurgical laboratory; test alloys; working to Navy specifications. Company will negotiate on fee. Location, Chicago. R8302(a).

Metallurgist to establish small control laboratory and be well grounded in heat treating and chromium plating. Salary open. Location, Alabama. T8379(a).

Metallographer, experienced in industrial radiography of light metals. Must have knowledge of magnetic particle inspection. Will take charge of metallurgical and heat treating laboratories. Salary open. Location, Indiana. T8389(b).

Production Metallurgist with at least three years' experience. Will assume technical control of production heat treating, magnetic particle inspection and fluorescent penetrant inspection. Salary open. Location, Indiana. T8389(c).

Mill Superintendent with mining, crushing and flotation experience, to take charge of equipment operation at kyanite project covering mining, concentration by flotation, drying, grinding, calcining, magnetic separation, etc. Salary, $4800 a year. Location, Southeast. Y6348.

MEN AVAILABLE

Foremanship, supervision; also desire opportunity learn purchasing, brokerage, ores and metals, or foundry work. Six years' process control and improvement, metallurgical accounting, production planning, supervise actual process and technical personnel in smelting and ore dressing. Age 40, B.S. in Chemical Engineering. M-658.

metallurgists

Key Positions
In An Important
NEW FIELD
with
SYLVANIA

A new and expanding division of Sylvania, recognized industrial leader for over 50 years with 30 plants throughout the U.S.A., has a few preferred positions for metallurgists.

Must have B.S. or Advanced Degree in Metallurgical Engineering, with experience in Powder Metal Metallurgy and Powder Metal Metallurgy Dies.

Please forward complete resume, including details of education and experience to:

SYLVANIA ELECTRIC

Manager of Personnel
Dept. 90B
40-22 Lawrence St.
Flushing, N.Y.C.

Ready to Roll!

● Ingot of invincibility! From the hot mass of this semi-molten metal will be rolled the weapons for our national defense . . . weapons to protect the way of life we cherish. And, we hope, that the future will find the output of this soaking pit going into refrigerators, bathtubs, and structural steel for the expansion of industry and added comfort to our daily lives.

The refractories industry has kept step with the steel industry in the amazing advance of production. General Refractories has constantly increased its capacity to meet the new demands. Today it offers industry the facilities of 43 mines, 29 plants, 18 sales offices and 200 distributing agencies.

Here, in this soaking pit, you'll find

GENERAL REFRACTORIES

GENERAL REFRACTORIES COMPANY
PHILADELPHIA

specially designed silica brick, fireclay brick, basic brick, high alumina brick, and Grefco plastic chrome ore, castables and mortars. But wherever else you look in the steel mill . . . blast furnace, open hearth, cupola . . . you'll find many another application for Grefco products.

And . . . beyond producing more and more of today's refractories products . . . General is engaged in an exhaustive research compaign to make possible even better refractories. In the world's most modern research laboratories, constant experimentation is carried on. All to the end that industry—steel, chemical, paper, glass—may count on General for a complete refractories service!

A Complete Refractories Service

Books for Engineers

Making, Shaping and Treating of Steel, based on original text by J. M. Camp and C. B. Francis. *U. S. Steel Co.* $7.50, 1584 pp.—Thoroughly revised, the content is a compilation of past and present practices in the iron and steel industry as summarized by specialists of the U. S. Steel Co., and based on their practical experience. In addition to extensive coverage of the processes named in the title, the work covers fundamental chemical and physical principles, refractories and fuels, fluxes and slags, cast iron, sponge and wrought iron, special steels, and mechanical testing methods. A detailed index is included.

Materials Handbook, by G. S. Brady. *McGraw-Hill Book Co.* $8.50, 913 pp.—This reference work gives practical data on approximately 9000 materials arranged under several hundred major headings. There are a detailed index and a section giving information on weights, measurements, physical property ranges, definitions, and various tables.

Machinability and Machining of Metals, by N. E. Woldman, R. C. Gibbons. *McGraw-Hill Book Co.* $7.50, 518 pp.—This book gives general principles of metal machining, metallurgical characteristics of the materials as they relate to various mechanical and thermal treatments, and the types and compositions of cutting tools. The approach is both theoretical and practical. One chapter is devoted to nonmetallic materials and another to cutting fluids.

Quality Control Handbook, edited by J. M. Juran. *McGraw-Hill Book Co.* $10.00, 300 pp.—This comprehensive volume covers the economics and specification of quality, how to organize for quality, the acceptance, control, and assurance of quality, statistical methods in the quality function, and forms and records for quality control procedures. Applications to specific processes and products are described by specialists in various fields.

Structure and Mechanical Properties of Metals (Monographs on Metallic Materials of the Royal Aeronautical Society, Vol. 2) by B. Chalmers. *John Wiley & Sons.* $3.50, 132 pp.—This book provides the simplest possible picture of the structure of metals and alloys and its relation to mechanical properties. The more important mechanical properties and their dependence on structure are considered.

Magnetic Materials, by F. Brailsford. *John Wiley & Sons.* $1.50, 156 pp.—This book is intended to give a comprehensive outline of the present state of knowledge of the subject. Chapters deal with ferromagnetism, properties and theory of single crystals, factors affecting magnetic properties, iron and silicon-iron alloys, nickel-iron and other alloys, and permanent magnet materials.

Phase Transformations in Solids (Symposium held at Cornell University, August 1948), edited by R. Smoluchowski and associates. *John Wiley & Sons.* $9.50, 650 pp.—This book contains theoretical discussions of crystallization, diffusion in solids, etc., transformations in nonmetals, and transformations in pure metals and alloys, by leading scientists in various fields.

Principles of Industrial Management, by L. P. Alford, revised and rewritten by H. R. Beatty. *Ronald Press Co.* $6.00, 779 pp.—This book presents basic principles and methods used in the management of an industrial enterprise. Questions for review, problems, and a bibliography follow each chapter.

Metallurgical Thermochemistry, by O. Kubaschewski, E. L. Evans. *Academic Press.* $6.00, 368 pp.—This monograph for research and process metallurgists serves both as an introduction to the subject and a work of reference.

Thermodynamics of Irreversible Process, by S. R. de Groot. *Interscience Publishers.* $4.00, 242 pp.—A review of the thermodynamic aspects of a recently developed macroscopic theory of irreversible processes based substantially on nonequilibrium thermodynamical functions.

Hot Working of Nonferrous Metals and Alloys (Institute of Metals Monograph and Report Series, No. 9). *Institute of Metals.* $2.50, 208 pp.—The monograph consists of papers with discussion reprinted from *Journal of the Institute of Metals*, which formed a symposium on the subject. Metals dealt with are aluminum, magnesium, copper, tin, lead, zinc.

U. S. Steel Co., 525 William Penn Place, Pittsburgh.
McGraw-Hill Book Co., 330 W. 42nd St., New York 18.
John Wiley & Sons, 440 Fourth Ave., New York 16.
Ronald Press Co., 15 E. 26th St., New York 10.
Academic Press, 125 E. 23rd St., New York.
Interscience Publishers, 250 Fifth Ave., New York.
Institute of Metals, 4 Grosvenor Gardens, London, S.W. 1, England.

Industrial Notes . . . . .

• *Defense Materials Procurement Agency has signed an agreement with Anaconda which may increase domestic copper output by more than 30,000 tons a year. This production will come from the company's Yerington mine in Nevada, which is now nonoperative.*

• Indications are that 1952 magnesium production including primary and secondary, will total 110,000 tons as compared with 43,000 tons in 1951.

• Ford Motor Co. of Canada will build an automobile and truck assembly near Oakville, Ont. It will take two years to build and eventually it will employ 500,000 workers. When the Oakville plant is in full operation, assembly of cars and trucks will be completely removed from Windsor.

• Orinoco Mining Co., subsidiary of U. S. Steel, has awarded a contract for the dredging and maintenance of a ship channel from the Gulf of Paria to Puerto Ordaz, for a railroad terminal to be built on the Orinoco River. This will provide a 170-mile channel that will permit ocean-going carriers with drafts up to 24 ft to proceed up the river to Puerto Ordaz where they will be loaded with iron ore from Cerro Bolivar. The channel will be completed in two years.

• **Anticipation of the development in the Trenton-Morrisville-Bristol area as a result of the completion of the new U. S. Steel Fairless Works, Pennsylvania Railroad will spend $9 million in expanding and modernizing their Morrisville freight yard near Trenton. The Morrisville yard, inactive for the past 5 years, will become one of the most important classification yards in the East. The rebuilt yard should be in operation by the end of 1953.**

• Sheffield Steel Corp., Houston, has awarded the Engineering & Construction Div., Koppers Co., Inc., a contract to design and construct a battery of 15 new chemical recovery coke ovens. The battery will be of the latest Koppers-Becker underjet design. Also, auxiliary equipment will be constructed for the present 47 oven battery.

• Cia Fundidora de Monterrey, S. A., Mexico City, D.F., increased its capital by $5,800,000 to install a new steel mill at a cost of about $5,220,000. The new mill will manufacture steel for the domestic market.

ASSURED SUPPLY FOR

321 STAINLESS Alloys of Titanium used in making Type 321 Stainless Steel are produced by TAM from North American Ores assuring continuous supply. Economic advantages spotlight increasing attention to excellent high temperature properties and other outstanding features. Complete technical data on request. Write our New York Office.

*TAM is a registered trademark.

TAM PRODUCTS

TITANIUM ALLOY MFG. DIVISION
NATIONAL LEAD COMPANY

Executive and Sales Offices: 111 BROADWAY, NEW YORK CITY
General Offices, Works and Research Laboratories: NIAGARA FALLS, N. Y.

New Products

New Products | New Literature | New Services

For Further Information on Literature or any Product, Fill in the Coupon and Send to JOURNAL OF METALS.
Students are Requested to Apply Directly to Manufacturers for Bulletins and Information.

1—OPTICAL DIVIDING HEAD: This dividing head with a fixed base was developed by the *F. T. Griswold Mfg. Co.* It can be used for checking angular dimensions such as spacing

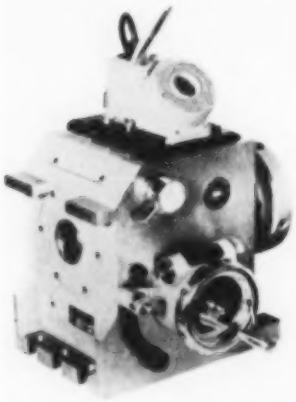

of spur gear and ratchet teeth, measuring accuracy of milling cutters, broaches, and for use on machine tools where precise positioning is required in either a horizontal or vertical plane.

2—PORTABLE CUTTING TOOL: A high-speed portable cutting tool that eliminates time consuming transportation of work to stationary machines has been introduced by *Composite Die Supply Co.* Among

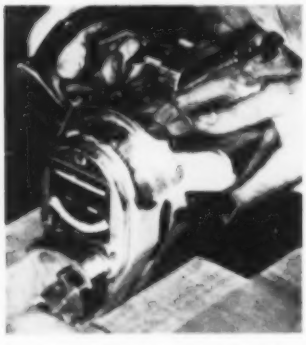

the uses of the machine are the cutting and shaping of wood, plywood, plastic, masonite, nonferrous metals and alloys. It has a 60 cycle 115 v and dc 18,000 rpm motor with a 12-ft extension cord; screwdriver blade, and head wrenches.

3—TANG BREAK-OFF TOOLS: A new line of automatic tang break-off tools for the removal of insetting tangs on helical-wire thread inserts is now available from the *Heli-Coil Corp.* Tang-removal operations at production rates on the following sizes and lengths of stainless-steel Heli-Coil thread inserts are possible: 6-32 to $\frac{1}{2}$-13 sizes in the National Coarse thread series to lengths of 1, $1\frac{1}{2}$, and 2 diam; and 10-32 to $\frac{1}{2}$-20 sizes in the National Fine thread series to the same lengths.

4—SHELL MOLD PERMEABILITY: Permeability of the shell can vary over a wide range with different sands, resin contests and flow characteristics. The No. 360 shell mold permeability accessory, offered by the *Harry W. Dietert Co.* is used in

conjunction with a permeability meter or permmeter. It is designed to read AFS permeability on a $\frac{1}{4}$ thick disc. Comparative permeability measurements may also be made on the mold itself.

5—CUTTING TOOL: A new special carbide tipped Thinsaw for extreme precision slitting has been developed by *Gay-Lee Co.* It is available in thicknesses down to 0.030 in. with tolerances held to 0.0002 in. and in diameters up to 5 in. These saws produce deep cuts without run-out and can be built flat with no protruding hub so they can be lined up side by side for close multiple cutting.

6—LIGHTWEIGHT ACETATE: Metallized acetates are now available in lighter weights as a result of the development of a 100 gage metallized material (0.001 thick) announced by *Coating Products.*

7—TREATED GLASS CLOTH: Silicone rubber treated glass cloth for motor and cable insulation is now in production at *General Electric Co.* Having high heat resistance and excellent flexibility and electrical properties, the material is ideal for motor and cable insulation.

8—REGUTRON MAGNETIC AMPLIFIER CONTROL: The new controller offered by *Electric Machinery Mfg. Co.* is used with the adjustable speed magnetic drive, an electromagnetic torque transmitting device which gives variable speed output when used in combination with a constant speed motor. This simplified magnetic amplifier control eliminates all the complicated electronic circuits of the previous electronic type amplifiers.

Free Literature

20—LEAD: The principal properties of lead and related data are contained in new booklet issued by *St. Joseph Lead Co.* The 47-page booklet describes the major uses of lead, its alloys and compounds and is divided into two parts.

21—JET-PIERCING: Detailed information on the fundamentals and practice of the Jet-Piercing process has now been made available in a pamphlet available from *Linde Air Products Co.* Actual piercing results are given, and new developments toward increasing overall process efficiency, are presented and discussed.

22—MACHINING STAINLESS STEELS: A revised edition of the fabricating manual *Machining of Armco Stainless Steels* has been published by *Armco Steel Corp.* A complete listing of grades with analyses and individual descriptions of grade characteristics are included.

23—HEAT TREATING SLIDE CHART: Chart contains data on type analyses of die steels, forging heat, annealing treatment and hardening treatment. Prepared by *Carpenter Steel Co.* it also includes facts on quenching, effect of drawing temperature on hardness, and others.

24—DECIMAL EQUIVALENT TABLE: Decimal equivalent decal transfer designed for application to slide rules, T-squares, drawing boards and other mechanical drawing equipment is offered by the *Meyercord Co.* The decal measures 6x1¼ in. and can be applied on any smooth surface.

25—METAL COATING: Anchorite 100, a paint anchoring corrosion resistant phosphate treatment for metals, is discussed in booklet published by *Octagon Process, Inc.* Common causes of paint failure are described and methods of application—immersion and spraying —of Anchorite are discussed. It meets specifications for Class C, Type II finish in U. S. Army specification No. 57-02C, as well as JAN-C-490, Grade I.

26—HEAT TREATMENT: Technical bulletin available from *E. F. Houghton & Co.* explains how maximum hardness and strength of aircraft and other steels can be developed to meet U. S. Government specifications MIL-H-6875. Charts show recommended temperatures for normalizing, annealing, and hardening certain types of steel and the quenching medium to be used.

27—TANTALUM EQUIPMENT: Useful information on the chemical and physical properties of tantalum, is contained in booklet offered by *Fansteel Metallurgical Corp.* Detailed engineering descriptions of single and multiple tube bayonet heaters, heat exchangers, and instrument protection are included.

28—CUTTING FLUIDS: To aid in selection of proper straight cutting oil or base for specific operations, *E. F. Houghton & Co.* has issued a 4-page bulletin giving general recommendations for the Cut-Max series of fortified and concentrated cutting fluids.

29—LOW-TEMPERATURE METAL TREATMENT: Advantages of low-temperature metal treatment are described in 8-page folder obtainable from Sub-Zero Mfg. Products Div., *Deepfreeze Distributing Corp.* Technical data on methods and results of sub-zero chilling of various metals and alloys are given.

30—SERVICE FACILITIES: Improved facilities for more quickly supplying steel from stock, are illustrated in brochure available from *Joseph T. Ryerson & Son, Inc.*

31—ANTI-RUST PAINT: New application bulletin, descriptive of Rust-Cure, anti-rust paint, has been issued by the *Monroe Co., Inc.* According to the manufacturer, the paint can be applied on rusted surfaces without wire-brushing, scraping or sandblasting. It also seals rusted surfaces and retards further rusting action.

32—BRAZE-CLAD METALS: Clad metal combinations of various base metals, ferrous and nonferrous, clad with a wide range of silver brazing alloys, are described in pamphlet issued by the *American Silver Co., Inc.* Technical information and useful applications are included.

33—CARBON AND GRAPHITE PRODUCTS: A new catalog section describing and illustrating *National Carbon Co.* carbon and graphite products is now available. Products in grades from porous to impervious for applications in the chemical and process, metallurgical, mechanical and electrical fields are fully described.

34—INDUCTION HEATING: Booklet obtainable from *Westinghouse Electric Corp.* presents case histories of how induction heating has increased production 50 to 2000 pct, reduced space up to 90 pct, and cut production costs. Modern induction heating apparatus are described as machine tools for hardening, heating, annealing, or joining metals in mass or batch quantities.

35—MACHINING NICKEL ALLOY STEELS: Detailed drawings and tables that will assist the user of nickel alloy steels in determining the most economical and satisfactory combination of microstructure, tool form, etc. are given in bulletin available from *International Nickel Co., Inc.*

36—SPECIMEN POLISHING: A 4-page folder describes the advantages of diamond abrasives for polishing metallurgical specimens. Diamet-Hyprez is offered in three different particle sizes, all in 5 g and 18 g gun applicators. *Buehler Ltd.*

37—MICROSCOPE THEORY: A non-mathematical exposition of how a microscope works with some notes on conditions which influence optical performance is available in limited quantities from *Bausch & Lomb Optical Co.* Objectives, eyepieces, condensers, filters, and types of illumination are treated in a nontechnical manner.

38—CAUSTIC SODA: Bulletin issued by *Pennsylvania Salt Mfg. Co.* provides references for particular problems on purchasing, handling and storage, equipment design and technical data. Detailed instructions for steaming and unloading 50 and 72 pct caustic soda as well as general information are included.

39—HEAT PROCESSING: Pamphlet now available from *Selas Corp. of America* emphasizes the increasing need for precision in heat processing. Principles of heat application to a wide variety of solid and fluid products are illustrated and described.

40—MAINTENANCE GUIDE: A new manual for electric heat treating furnaces is now obtained from *Hevi Duty Electric Co.* A check sheet is included to simplify maintenance schedules, reduce breakdowns and prolong furnace life.

41—RADIOACTIVITY CATALOG: Catalog containing sections on scalers and accessories, amplifiers, Geiger-Mueller tubes and accessories, may be had from *Tracerlab.* Illustrations and specifications of all instruments are given.

Journal of Metals
29 West 39th St.
New York 18, N. Y.

January

Please send me: More Information ☐ Free Literature ☐ Price Data ☐ on items indicated

1	2	3	4	5	6	7	8	9	10
11	12	13	14	15	16	17	18	19	20
21	22	23	24	25	26	27	28	29	30
31	32	33	34	35	36	37	38	39	40
41									

Name _____ Title _____

Company _____

Street _____

City and Zone _____ State _____

National Research

ONE

(A) 8-4 Booster Pump. Takes over at forepressures as high as 1 mm., handling large amounts of gas in range of 1 — 80 microns. Suitable for evaporators, furnaces, and other vacuum systems requiring high capacity in this range.

(B) H-2-P Purifying Diffusion Pump. Over 50 liters per second from 10^{-3} to 10^{-6} mm. range. Operates against forepressures as high as 0.800 mm. Blank-off 2×10^{-10} mm.

(C) Gas Free High Purity Metals. Copper, nickel, cobalt and iron. Special melts on request. Ingot weights up to 600 pounds.

(D) Alphatron® Vacuum Gauge. Accurate gauging from 10 mm. to 1 micron. A rugged metal ionization type instrument which can be adapted for recording, controlling, gas filling, and leak detection.

(E) 8-1 Booster Pump. A small pump designed for rotary exhaust equipment used in miniature and subminiature tube production. Useful where a small pump is required to quickly obtain pressures in the region of one micron.

(F) Type 710 Thermocouple-Ionization Gauge Control. One instrument for scientific and industrial vacuum gauging. Incorporates two thermocouple gauges (1 — 1000 microns) and one ionization gauge (10^{-3} mm. to 10^{-5} mm. Hg. range) in one control. Automatic input regulation and protective circuit.

(G) Standard Vacuum Furnace. A versatile packaged unit to melt, pour, heat treat, degas, sinter, and anneal under high vacuum or controlled atmospheres. Temperatures up to 2000° C.

(H) Vacuum Seals. For introducing motion, power, or connecting gauges.

(I) High Vacuum Valves. Available in sizes ⅛" to 16". Low rate of leak.

(J) Vacuum Fusion Gas Analyzer. Analyzes metals and alloys, including titanium, for combined or dissolved oxygen, nitrogen, and hydrogen.

(K) Type 701 Thermocouple Gauge Control. A light, portable instrument for vacuum testing in range 1 — 1000 microns. Compact and rugged.

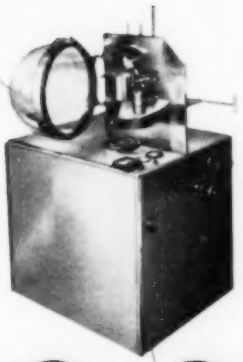

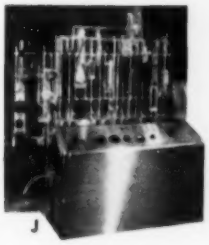

SOURCE!

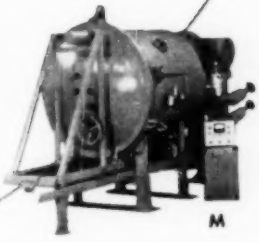

with a COMPLETE LINE *of* HIGH VACUUM EQUIPMENT

You may be using one or two of our products without realizing that at this one source you have available such a full line of high vacuum equipment.

You will find a unique quality in most of these products. They were created to "ideal" specifications drawn up by *manufacturers* who, in many cases, never dreamed we could fulfill their exacting requirements. The products are meeting these requirements day after day on production lines.

Let us supply all your high vacuum equipment needs. You will gain the benefits of a single source of supply plus the high standards of performance designed into National Research products. Write us for further details. National Research Corporation, Memorial Drive, Cambridge, Mass.

(L) H-16-P Purifying Diffusion Pump. Over 10,000 CFM in 10^{-5} range. Suitable for cyclotrons, commercial coating units, and other equipment demanding high pumping speed.

(M) Evaporators. Standard models from laboratory unit to high capacity tank type units.

INDUSTRIAL RESEARCH
PROCESS DEVELOPMENT
HIGH VACUUM ENGINEERING
AND EQUIPMENT

METALLURGY
DEHYDRATION
DISTILLATION COATING
APPLIED PHYSICS

National Research Corporation

Seventy Memorial Drive, Cambridge, Massachusetts

*Reg. U. S. Pat. Off.

FOUR TASIL LINED TREADWELL LADLES

Set NEW TONNAGE RECORD in Pittsburgh District!

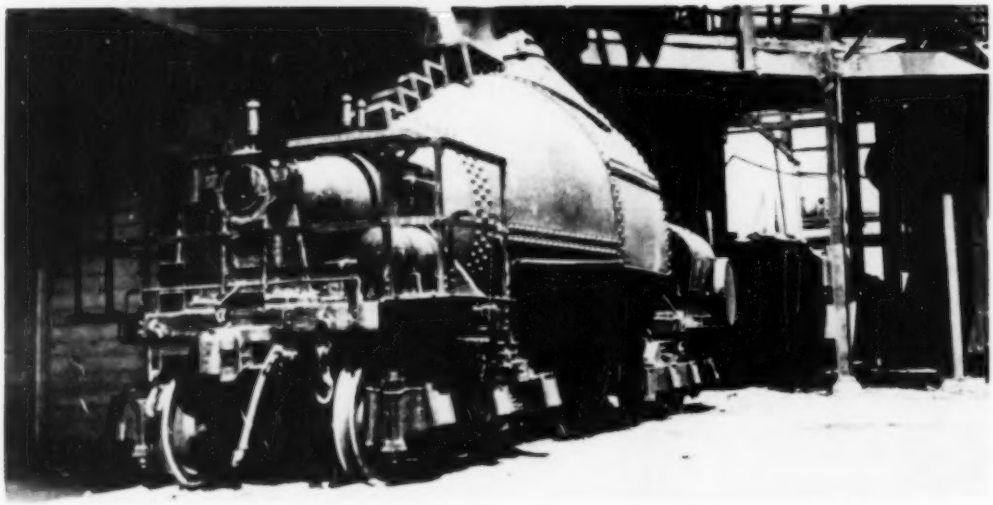

To keep a ready supply of hot metal available

"BALANCE" your linings with TASIL!

RESULTS OF RECENT TEST — Pittsburgh District	
LINING	AVERAGE TONNAGE BEFORE RELINED
Blast Furnace Quality Fire Brick	35,000 to 60,000 Tons
Super Duty Fire Brick	138,166 Tons
TASIL Balanced Super Duty Brick	168,305 Tons *

* Average of 4 linings

TASIL "BALANCED" TREADWELL LADLE LINING

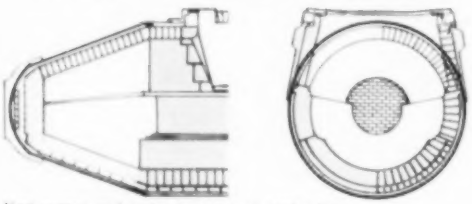

Half section and vertical section on center line

▭ - TASIL Brick and Cement

TAYLOR SILLIMANITE (TASIL) Brick and Cement extend the service life of Treadwell, Cling, and similar types of hot metal cars or ladles when used to reinforce or "balance" critical areas (see sketch). TASIL brick will not shrink or vitrify at service temperatures. Tough—they withstand the washing action of molten iron during charging, transportation and pouring.

TASIL No. 301 Air-Setting or No. 302 Heat-Setting Cement makes permanent weld-like joints and retards joint erosion. Used successfully with TASIL bonded mullite or super-duty brick linings.

In the above test, four TASIL "balanced" ladles carried 158,017 tons, 170,156 tons, 179,609 tons and 165,432 tons respectively. The average tonnage was 21-4 5% greater than that of all super-duty brick linings. TASIL brick projected 1½" beyond adjoining super-duty fire brick when cars were taken out for re-lining.

Keep your ladles and hot metal mixers working, reduce masonry and refractory costs, keep hot metal available at the Open-Hearth—use TASIL Brick and Cement to "balance" your linings. Bulletins 314 and 315 give complete data. Write for your copies.

Exclusive Agents in Canada:
REFRACTORIES ENGINEERING AND SUPPLIES, LTD.
Hamilton and Montreal

The CHAS. TAYLOR SONS Co.
A SUBSIDIARY OF NATIONAL LEAD COMPANY
REFRACTORIES SINCE 1864 • CINCINNATI • OHIO • U. S. A.

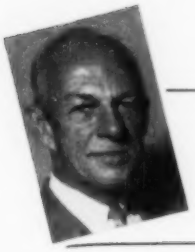

THE DRIFT OF THINGS

by Edward H. Robie

In late November and early December a considerable portion of our time was devoted to obtaining a business manager for Institute headquarters. The advisability of creating such a position was suggested in 1949 in the report of the Johnson committee. In that year, however, the Institute had a deficit of $72,000 so every effort was made to minimize expense. At that time most of the duties that normally would be assumed by a business manager were given to Newell Appleton who became office manager, convention manager, purchasing agent, and assistant to the secretary. So many responsibilities were his that he could not devote the necessary time to all of the many things that needed attention. H. H. Vasoll, representing a firm that made a study of Institute head office procedures early last fall, made a recommendation that "a business manager and controller from outside the present organization" be obtained, who would supervise the work of accounting, addressograph, purchasing, book and journal orders, filing, and mailing depts. He further recommended that Mr. Appleton be made administrative secretary, in which position he would act as head of an "Institute Activities Dept." He would devote his time to convention planning, meeting arrangements, travel accommodations, membership control and promotion, and public relations, and would assist the Secretary on special problems. Thus, Mr. Appleton retains some of his former responsibilities and will take more of the load off our shoulders in the conduct of affairs at Institute headquarters. The rest of his former work will be in the province of the newly created "Business Office Dept."

Peter J. Apol is the man finally selected for the post of business manager. He is a young man of 32, a native Michigander and a graduate of the University of Michigan where he received a B.S. degree in business administration in 1940. He then spent three years in the Navy and has the rank of Lieutenant in the U. S. Naval Reserve. Three more years were spent in the U. S. Maritime Service as chief purser, and another year as chief paymaster for the Pope & Talbot Steamship Co. The past four years have been spent as head of the Greenland Construction Co., Greenland, N. H., chiefly engaged in building construction.

Mr. Apol will endeavor to increase the efficiency of Institute headquarters operations and remove all possible causes for complaints of individual members. He will coordinate as seems advisable the work of various departments and install such modern business office machinery as seems applicable to our needs.

Irritating Our Best Friends

Though relations between the USA and Canada are entirely friendly, and armed conflict between the two countries is unthinkable, one of the editors of Canada's *Maclean's Magazine* recently told a New York Rotary Club audience that we irritate each other. For instance, he said that many on this side feel that Canada isn't pulling its weight in the military effort generally and in the Korean war in particular. The real reason, he said, is that there is a limit to the force that you can raise without conscription, and Canada does not have conscription. If Canada were in danger he indicated that conscription would probably be instituted. This strikes *us* as being a sane policy.

On the other hand, Canada is impatient with the mistrust that has developed in the United States over American foreign policy. They are afraid that we are going to drag them into a war. A second reason for Canadian anti-Americanism is that our differences at home undermine foreign confidence in American leadership. "In Canada we tend to get a picture of American policy as a catalog of calamity and ineptitude, conceived by men of no imagination and executed by men of no competence. We get the impression that that's what Americans think of their own government, and it is hardly surprising that some of use conclude that Americans ought to know."

Professionally, however, among mining men certainly, mutual respect and confidence are complete and the international boundary is unnoticed. Americans who go to the annual meeting of the Canadian Institute in Ottawa January 21 to 23 will be just as hospitably received as at their own meetings, and we hope to welcome equally as graciously the Canadian contingent who will be with us in New York February 18 to 21.

Famous Small Towns

The Census Bureau recently released the names of what it said were the three smallest towns in the country—Douglas, Ark., Ophir, Colo., and Mercur, Utah—with a population, respectively, of one, two, and three inhabitants. In Mercur, however, the poll taker is said to have become confused among the deserted shacks and counted three when there are actually only two people there. Two of these small towns are well known names to the mining man. Fifty years ago the Silver Bell, the New Dominion, the Suffolk, and the Caribeau mines made Mercur an important little mining town. Ophir was equally well known for its mine production. Its only inhabitant now is Mrs. Nellie Tatum, who came there in 1898. We understand that it is to have a new lease on life as its houses have been purchased by the Silver Bells Mining Co.

The names of many small places are thus familiar to mining men, but in traveling about the country often we run on to comparatively large cities whose names are unknown to us. We wonder how many of our readers can tell us just where Lakewood and South Gate are for instance. They are both big cities—over 50,000 population—and yet until we looked them up we could not have told in what state they were situated. If there are any AIME members in either of those cities they will no doubt wonder how ignorant can an engineering society secretary get.

The Difference

Speaking of Russia, we like the story related by a recent applicant for AIME membership now doing a fine job in this country following some unpleasant years in eastern Europe. An international group was investigating industrial conditions in various countries. In the USSR they visited a factory which they were assured was owned entirely by the workers. Seeing a couple of automobiles out front, they asked who owned those. "Oh, those belong to the directors," they were told. Later, visiting a factory in this country, they inquired as to its ownership, and were informed it was owned by capitalists. "And what about those hundreds of cars parked outside?" "Those are all owned by the workers."

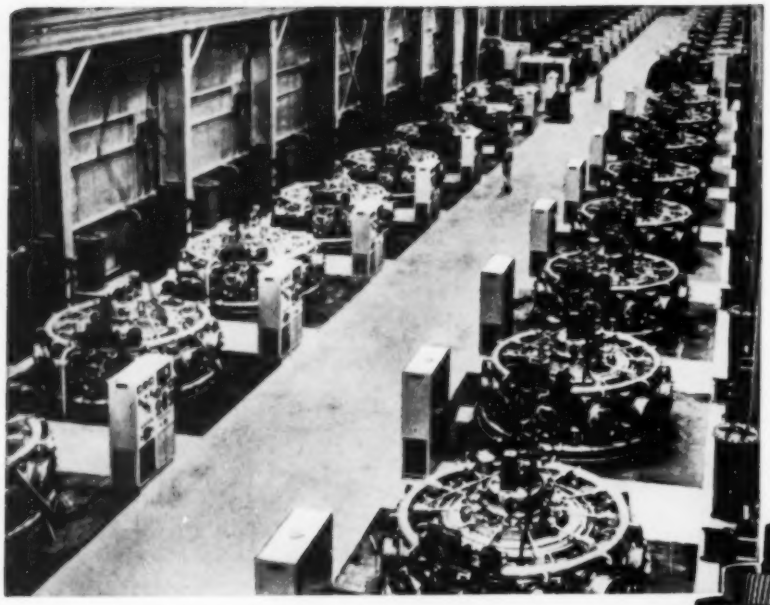

In world's largest internal combustion engine plant, operated by ALCOA, low cost power is essential for producing aluminum since every pound produced requires about 10 kilowatt hours of electrical power. *Right*: Nickel alloy cast iron crankshaft, weighing over 5,000 lbs., with gear train assembly, used in gas burning radial engine manufactured by Nordberg Mfg. Co., Milwaukee, Wisc.

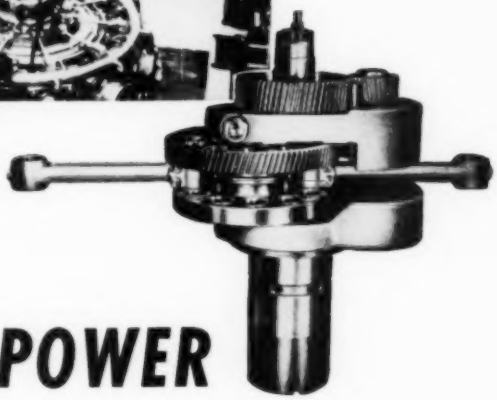

200,000 HORSEPOWER

24 hours per day on NICKEL CAST IRON CRANKSHAFTS

Here are some of the 120 Nordberg radial engines with vertical crankshafts of nickel cast iron which provide low cost power at the Point Comfort Reduction Works of the Aluminum Company of America, Port Lavaca, Texas.

High strength nickel alloy iron is used not only for these crankshafts, but also for the cylinder blocks. In addition, many highly stressed parts of these 11-cylinder engines are made from heat treated nickel alloy steels.

Powered by natural gas from nearby fields, these Nordberg units demonstrate how nickel alloyed irons and steels help to cut bulk and deadweight, and to render further economies by minimizing wear and corrosion.

At the present time the National Production Authority limits the applications for which nickel and its alloys may be used. However, we shall continue to issue information on user experience with nickel-containing materials as we believe that dissemination of technical data and service experience can help to promote the intelligent utilization of critical materials, so essential in these times.

INCO

THE INTERNATIONAL NICKEL COMPANY, INC. 67 WALL STREET NEW YORK 5, N. Y.

Sponge iron methods are again coming up for their perennial discussion among Government and industry officials. The shortage of scrap has sent steel producers scampering for new sources of metallics and as in the past, sponge iron is the No. 1 choice. West coast industrialists are intrigued by the possibilities. As far as known, none of the steel companies is yet contemplating producing sponge iron. At least one fabricator is considering direct reduction and continuous casting as a means of circumventing steel shortages.

Some months ago Cerro de Pasco announced it would build at its Peru smelter the first commercial Sterling electric arc furnace for smelting zinc concentrates. New Jersey Zinc Co., who developed the process, for several months has had in operation at its Palmerton plant a full scale furnace for development work. Also, New Jersey Zinc Co. has in an advanced stage of development a fluid bed roasting process for treating zinc concentrates.

One of the largest continuous annealing and pickling plants in the brass industry was placed in operation recently by Chase Brass & Copper Co. at Waterbury, Conn. The unit will process 140,000 lb of brass per day. It will accommodate material 25 in. wide and thicknesses up to 0.040 in. It will operate on a 24-hr day basis.

Sao Paulo, Brazil will have a steel plant "equal to that of Volta Redonda" according to the Governor of that Brazilian state. The works will probably be built outside the port of Santos and will be financed by private enterprise and the state.

Companhia Brasileira de Alumino will build a second aluminum reduction plant at Sao Paulo to produce an initial 7000 tons of metal a year. The bulk of the machinery will be bought in western Germany and Italy.

Mullins Mfg. Corp. will spend more than $1 million in enlarging and equipping its Liberty plant near Warren, Ohio, for cold extrusion of military shells. Heinz Mfg. Co. in Philadelphia has completed a new extrusion plant and is in production on a series of military shell contracts.

Nichols Iron & Cable Co., Davenport, Iowa is installing a new Properzi continuous casting machine for casting aluminum rod. The machine will have a capacity of 1 ton of rod an hr and the complete unit including a standard heating furnace, the casting machine, and a rolling mill with all control equipment will cost about $150,000.

Standerdization of engines and parts is paying off for Army Ordnance. In contrast to World War II practice of using six to ten different engines for the same tank, present design permits four engines to be used in 11 different vehicles. Sixty percent of the 2000 parts in these four engines are interchangeable. In the Walker Bulldog family, 11 vehicles, more than 60 machine components including engines, generators, ignition, and suspension systems are interchangeable.

A new million dollar plant for producing ferromanganese, ferrosilicon, and ferroalloys will be built by H. K. Ferguson Co. for the newly formed Tenn-Tex Alloy & Chemical Corp. on the Houston Ship Channel. The plant will have three electric furnaces and will produce about 2000 tons of ferroalloys a month.

Melting Low Carbon Stainless Steel

by Walter Crafts and H. P. Rassbach

THE major problems in melting 0.03 pct max carbon stainless steel are the attainment of a very low carbon level in the preliminary oxidation stage and prevention of carbon pickup in the refining period. It has been difficult to achieve these aims consistently and economically, because of fundamental problems in oxidation, reduction, and refining periods of basic electric furnace melting procedures used in producing low-carbon steels.

This paper reviews present-day trends in melting very low carbon stainless steel. While a detailed discussion of corrosion resistance is not warranted, Fig. 1 illustrates the influence of carbon content on the nitric acid corrosion resistance of 18-8 steel sensitized for 2 hr at 1200 F. These data demonstrate that minute changes in carbon content may affect resistance to sensitization, and that accurate carbon control is critical in melting this steel.

In the early 1930's, the production of Type 304 stainless with carbon contents under 0.08 pct was attended by many difficulties. This composition later became one of the major tonnage items of stainless steel production. Only a few years ago, melting stainless steels to a specification of 0.03 pct max carbon would have appeared impractical. With improvements in melting techniques, better process control and availability of purer raw materials, the 0.03 pct max carbon stainless has become a commercial product. Now that a wide area of application for these steels has been established, ways and means to produce them on a commercial basis have been worked out, and the manufacture of these steels in the future probably will be about as routine as is presently the case for such a grade as Type 304. Outstanding factors in the development of commercially practicable melting practices for such steels are the use of gaseous oxygen and exceedingly low-carbon content ferrochromium.

Fundamental problems involved in melting very low carbon stainless steels are much the same as in melting grades of normal carbon contents. Before

WALTER CRAFTS is Chief Metallurgist, Union Carbide & Carbon Research Laboratories, Inc., Niagara Falls, N. Y., and H. P. RASSBACH is Metallurgical Engineer, Development Dept., Electro Metallurgical Co., a division of Union Carbide & Carbon Corp., Chicago.
This paper was presented at the Electric Furnace Steel Conference, Pittsburgh, Dec. 6 to 8, 1951.

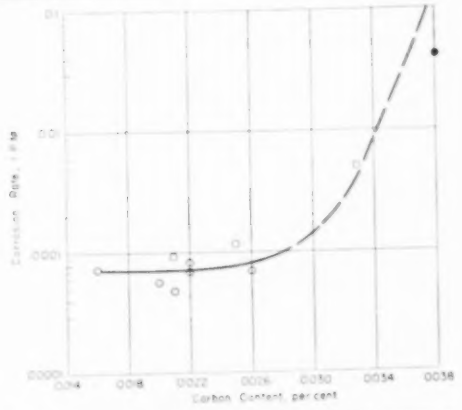

Fig. 1—Influence of carbon content on the nitric acid corrosion resistance of 18-8 sensitized 2 hr at 1200 F. Solid points denote averages of less than 48 hr boils.

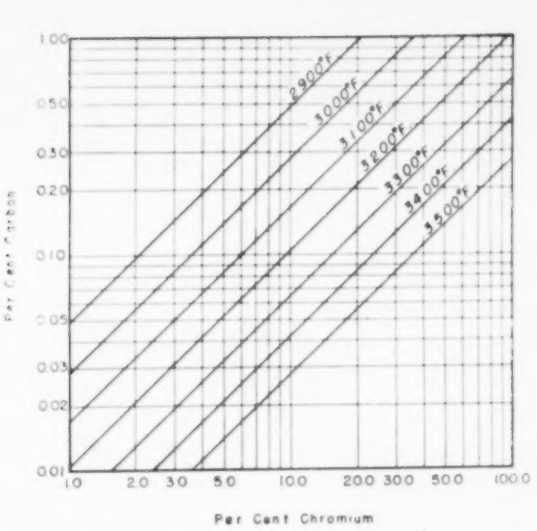

Fig. 2—Essential relations among carbon, chromium, and temperature under oxidizing conditions.[2]

1930, remelting of revert stainless scrap increased the carbon content above the specification so that most stainless steel was made with virgin charges by the addition of low carbon ferrochromium. Later, scrap was utilized by the time consuming process of oxidizing a chromium-free bath to low carbon and then adding stainless scrap to the bath.

The demand for larger tonnages of stainless steels increased sharply between 1930 and 1940, and producers accumulated sizable stocks of stainless scrap. During this period, a fair degree of success was attained with a practice using 40 pct or more of stainless steel scrap in the charge for the production of the 0.12 pct max carbon stainless steels. It was not, however, generally practical to use much revert scrap in the production of the 0.08 pct max carbon stainless steels.

The difficulties encountered in using substantial quantities of scrap in the era prior to the use of oxygen have been described adequately in the *Electric Furnace Steel Proceedings*. Some objectionable features of this practice, in which large quantities of iron ore or scale were added in the charge, were that carbon elimination was difficult, heavy losses of chromium occurred, removal of large volumes of heavy slag was laborious, recovery of chromium from scrap was low, and long heat times adversely affected refractories.

The advent of oxygen injection for decarburizing a chromium steel bath was a milestone in the progress of the stainless steel industry. The use of oxygen for carbon elimination in stainless melting subsequently has been adopted by most stainless producers. Proper utilization of oxygen has resulted in increased production, permitted larger stainless scrap charges, and contributed to increased chromium recovery from scrap.

After the carbon elimination period, the oxidized slags were treated with various reducing agents, generally silicon-bearing alloys, which resulted in recovering some chromium, iron, and manganese. In the two slag process, the first slag was removed and a new slag made. Sometimes the original slag was reduced to the desired degree and allowed to remain, in which case the practice was described as the single slag process. Necessary reducing and alloying additions were made when oxidation was completed.

Although suitable oxidation practices and low carbon ferrochromium have been available for a long time for producing low carbon stainless steel from virgin charges, utilizing stainless steel scrap has depended upon the economical lowering of the carbon content in a charge containing a substantial amount of chromium. The introduction of oxygen as the primary oxidizing agent has made it practical and economical to make grades such as Type 304 with high proportions of stainless steel scrap in the charge. However, under current operating conditions, lowering the carbon content of a chromium steel bath to the level necessary to make 0.03 pct max carbon stainless presents problems that require further study and evaluation.

Removal of carbon is a primary objective in the oxidizing period of a stainless steel heat; and the attendant loss of chromium and its corresponding effect on the slag are the main factors controlling the selection of the charge. The effects of temperature are equally important, and it has been recognized that the best temperature is the maximum compatible with economic maintenance of refractories. The reactions with oxygen are strongly exothermic. Consequently, high temperature is attained easily and must be maintained for a shorter time, so that the maximum temperature for safe furnace operation has been raised appreciably by oxidation with gaseous oxygen instead of ore. Thus, a higher chromium content may be retained at a low carbon level. In addition, the volume of slag is significantly less at higher temperatures. Since these factors are important in attaining low carbon content and in the economic utilization of stainless steel scrap, they have been given a great deal of study.

The essential relations among carbon, chromium, and temperature under oxidizing conditions were developed by Hilty in 1948,[2] and illustrated in Fig. 2.

While it must be realized that oxygen input, metal composition, and initial bath temperature can influence the results obtained, these relations may be used as a guide in establishing economically sound melting procedures for low carbon stainless steel.

At a constant temperature there is a definite relationship between carbon content and chromium content. Assuming carbon content to be a constant, the amount of chromium retained in the bath is a function of temperature. As there is a maximum temperature at which any melter may safely operate his furnace, the chromium content of the bath at the end of the oxidation period will be largely a function of the carbon content.

For example, if the chromium content of a furnace charge is 12 pct and the heat is decarburized to 0.05 pct carbon at 3300 F, the bath then will contain approximately 8 pct chromium and the balance of the chromium (4 pct) formerly in the bath will be in the slag in the form of chromium oxide. A similar charge containing 12 pct chromium, melted down and oxidized to 0.02 pct carbon maintaining the same temperature, 3300 F, will contain only 3 pct chromium in the bath and 9 pct of the initial charge will be in the slag as oxidized chromium. This relation is emphasized to show that it is possible to estimate the chromium content of the bath and the amount of chromium that may be oxidized.

The amount of iron and manganese oxidized simultaneously with carbon and chromium also is significant with respect to subsequent reduction, and affects the composition and fluidity of the oxidizing slag. In very low carbon heats, the addition of nonmetallic fluxes usually is undesirable because they further increase an already excessive slag volume. As a result, metallic oxides generally will comprise from half to two thirds of the slag. Increasing amounts of chromium oxide tend to stiffen the slags to such a degree that they may become solid, increasing the difficulty and cost of making a heat. Such slags may be so voluminous and heavy that they may limit the amount of chromium that can be included economically in the melt-down charge.

The total amount of metallics (chromium, iron, and manganese) oxidized must be known to estimate slag composition and character. A number of heats were melted in a 1-ton basic arc furnace and a survey was made to determine the amount of iron and manganese oxidized in relation to carbon, chromium, and temperature. Some heats were made with no stainless scrap in the charge and others were made with stainless scrap up to 11.5 pct chromium in the initial charge. The same amounts of lime (40 lb) and silica (20 lb) were added to each heat. After melting, the bath was blown with oxygen until the carbon reached the desired level in a range of 0.01 to 0.10 pct. At the temperatures reached in making these heats all of the slags were fluid, so that the analytical samples are believed relatively free from gross segregation. Slag weights at the end of the oxygen blow were calculated from a balance of final slag and metal weights with the charge and additions. The data shown in Figs. 3 and 4 represent the sum of the metal in the metallic oxides in the slag at the end of the oxygen blow in relation to the final carbon content and temperature.

The survey indicated that the total amounts of chromium, iron, and manganese oxide in the slag are determined by the attained carbon content and temperature of the bath, regardless of the chromium concentration in the initial charge. These indications must be considered conservatively and with certain reservations. The chemistry of the process is not well established and variable furnace conditions may affect the results. For example, a vigorous agitation might lower carbon with less oxidation of the metal. In addition, the slags in this investigation were fluid, and the relation with respect to the highly viscous slags ordinarily resulting from high chromium charges has not been determined. However, observations indicate that frequently it is more difficult to lower carbon below 0.03 pct in chromium bearing charges than in plain carbon steel charges. The main difference observed in the oxidation of high chromium charges at temperatures generally encountered in large furnaces is that the slags usually are

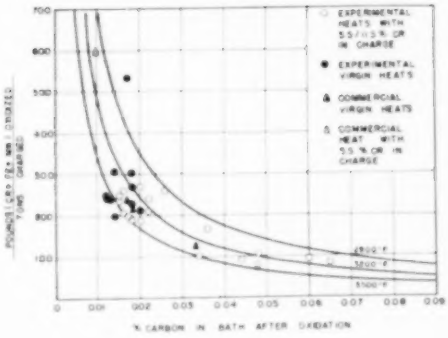
EXPERIMENTAL HEATS WITH 5.5 TO 5.9 % CR IN CHARGE
EXPERIMENTAL VIRGIN HEATS
COMMERCIAL VIRGIN HEATS
COMMERCIAL HEAT WITH 5.5 % CR IN CHARGE
3100 F
3200 F
3300 F
% CARBON IN BATH AFTER OXIDATION

UCC Develops New Low

The appreciation of the problems involved in the manufacture of very low carbon stainless steels led to research for improved alloying materials. A new ferrochromium alloy was developed having an extremely low carbon content and approximately 5 pct each of silicon and silica. This new material to a large extent has solved some of the major problems in the production of very low carbon steels. The carbon content of the alloy is so low that under most operating conditions its addition will tend to dilute the carbon content of the bath rather than to increase it, and because of its silicon and silica content, specific gravity, and its method of manufacture, it has excellent solubility.

When using regular ferrochromium, the alloy must be added gradually in several batches to prevent chilling onto the furnace bottom. In contrast, when using the new alloy on virgin heats of the 18 8 type where all of the chromium has come from ferrochromium, it has been possible to add all of the chromium to the bath in one batch. For example, in large heats complete solution of the alloy was accomplished in about 1 hr, whereas a similar addition of regular ferrochromium required 2 to 3 hr or longer.

The alloy is prone to pick up nitrogen when exposed to air at high temperature, so that it is subject to nitriding by the furnace atmosphere before it is dissolved in the steel. For this reason additions should be made so that they are rapidly submerged in the slag, and larger additions should be protected from the atmosphere by a fusible slag blanket to avoid a high nitrogen content in the steel. Additions of the alloy in several batches generally will limit the opportunity for high temperature exposure. In most instances this procedure will require relatively little more time than when all of the alloy is added in a single dose.

Time savings as great as 25 pct have been realized through

viscous to the degree that they are practically solid. The major criterion of the amount of stainless scrap that can be used effectively in making 0.03 pct max carbon stainless steel would, therefore, appear to be the maximum amount that can be introduced without producing a viscous slag.

At carbon levels above 0.05 pct, the amount of metal oxidized is relatively low and with gaseous oxygen does not present an impractical operating

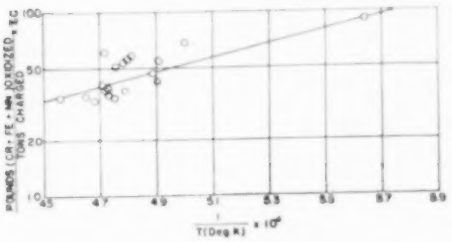

Fig. 3 (left)—Sum of the metal in the metallic oxides in the slag at the end of the oxygen blow in relation to the final carbon content.

Fig. 4 (above)—Sum of the metal in the metallic oxides in the slag in relation to temperature.

Carbon Ferrochromium

the use of this alloy with a single slag practice. While the saving of heat time is an important cost factor, in melting the very low-carbon steels this factor is secondary to the control of carbon content. While proper control of basicity aids in preventing carbon pickup, it is reasonable to assume that the shorter heat time during alloying will be equally beneficial in avoiding increase of carbon. Rapid solution of the ferrochromium addition also shortens the period during which the furnace is exposed to the corrosive action of a low basicity slag. Several other desirable characteristics of this material have been realized in tonnage commercial production. It has been noted that the susceptibility of carbon pickup from direct contact with the arc appears less for this alloy than when using normal ferrochromium. Also the alloy aids smooth operation in that it does not fuse or weld together in the melting process.

The normal analysis of this alloy, which is produced as walnut-sized pellets, is 62 to 66 pct chromium and 4 to 6 pct silicon, with extremely low carbon. The silicon: chromium ratio in this alloy is well adapted to use in single slag practice for control of slag reduction and silicon content of the bath. For example, in large heats of extra low carbon 18-8, made with a chromium free scrap charge, the silicon combined in an addition of all of the chromium in the form of the new alloy resulted in adequate reduction of the slag formed during oxidation. The residual silicon in the bath after complete solution of the low carbon chrome pellets was generally about 0.40 to 0.60 pct and the recovery of chromium above 90 pct. Where chromium scrap was used in the charge, it was found that supplementary silicon may be required and can be added in the form of ferrosilicon or other silicon-bearing alloys to reach the desired degree of reduction. This alloy has been used effectively in basic, chromite, and acid lined furnaces.

problem. Even with high chromium charges that result in relatively viscous slags, such slags do not interfere unduly with decarburization. For the 0.03 pct max carbon grades, if a viscous slag is to be avoided at 3250 F, the maximum chromium content of the initial charge should be in the neighborhood of 6 pct chromium. That is, about 25 pct of the final ingot weight may come from stainless steel scrap.

Arc furnace stainless steel melting practices may be separated roughly into two categories, two slag and single slag practices. In the two slag practice, the slag formed during oxidizing is removed and a new slag is made. The slag formed during oxidizing may or may not be treated with reducing agents to recover chromium, iron, etc. In the single slag practice, the oxidizing slag is treated with reducing agents to obtain a fairly high recovery of oxidizable elements and is not removed from the bath. When excessive volume becomes a factor, part of the slag is removed. In the single slag practice, phosphorus will not be eliminated to any large extent, and raw materials employed should have a phosphorus content within the required specification. Sulphur can be controlled within the standard AISI specifications.

In manufacturing low carbon stainless steels either of these practices may be used. In the two slag practice, substantial metallic losses may be experienced when there is partial reduction of metallic oxides from the slag prior to slag removal. Uncertainty as to the weight of metal in the bath has led some to the practice of tapping the furnace and weighing the metal. A further advantage of this practice is that with the good mixing action, metal samples will represent accurately the bath. Many shops do not have suitable mechanical equipment to permit weighing and returning metal to the furnace, and in such cases heat weight variation may be a problem.

In the two slag practice, after the original slag is removed and while the new slag is being made, it is possible for high lime slags to exist temporarily under the arcs while the new slag is being melted. These conditions can affect carbon control.

In the single slag practice, good metallic recovery is practical when reduction procedures are adequate. As there is no slag removal period, heat time may be saved, and because the metal always is covered by a slag there is less opportunity for accidental exposure to carbon.

Oxides of chromium, iron, and manganese from the highly oxidized slags, formed as a result of oxygen decarburization of a stainless steel bath, normally are reduced by 1—silicon in the form of ferrosilicon, ferrochromium-silicon, or other silicon-bearing alloys; 2—with aluminum; or 3—a combination of both. The extent to which such practices may be employed is limited largely by economic and physical factors.

Reduction of the metallic oxides with silicon is a reversible reaction that becomes more complete at lower temperatures. The intermediate product of the reaction, SiO_2, is stabilized by lime, so that chromium and iron are reduced more completely from a lime rich slag. Thus, as shown by Taylor,[3] reduction of oxides in the slag is more effective in slags of relatively high basicity. For example, if a low basicity slag containing a large amount of chromium oxide is treated with silicon, there will be a partial reduction of chromium oxide and the silicon content of the metal will be relatively high. However, if lime is added to the partially reduced slag, the chromium

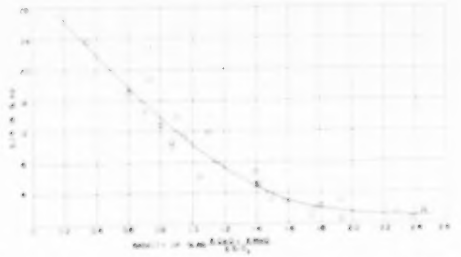

Fig. 5—Relation between chromium in the slag and basicity at the end of the slag reduction stages in a number of experimental and commercial heats of 18 pct Cr steel containing 0.30 to 1.00 pct Si.

oxide will be reduced further and the silicon content of the metal will become lower.

The relation found between chromium in the slag and basicity at the end of the slag reduction stage in a number of experimental and commercial heats of 18 pct chromium steel containing from 0.30 to 1.00 pct silicon is shown in Fig. 5. Basicity is expressed as the ratio of the sum of the CaO and MgO to the SiO_2 present. Compositions with less and more silicon tend to fall above and below the line in Fig. 5, but the correlation of silicon content with chromium in the slag for a given basicity is poor. Much is unknown about the chemistry of the reduction, and the difficulties entailed in obtaining samples representative of equilibrium conditions are formidable. Thus, although Fig. 5 is considered a good illustration of the effect of basicity, it should be considered a guide rather than accurate relation.

The sum of the unreduced metal oxides shows a similar relation with basicity, as shown in Fig. 6. The same reservations may be made for this chart as for Fig. 5, and the relation is useful for calculations aimed at evaluating different practices.

The amount of metallic oxide reduced from the slag per pound of silicon added is variable. In the available data on 0.03 pct max carbon stainless steels, in which several different types of silicon bearing alloys were used, it was found that 1 lb of silicon reduced an average of 3 lb of metal (chromium + iron + manganese). Variation in individual heats between 2.5 and 3.5 lb of metal reduced per pound of silicon was observed commonly.

It is thus evident that basicity is a primary factor

Fig. 6—Relation of the sum of the unreduced metal oxides with basicity.

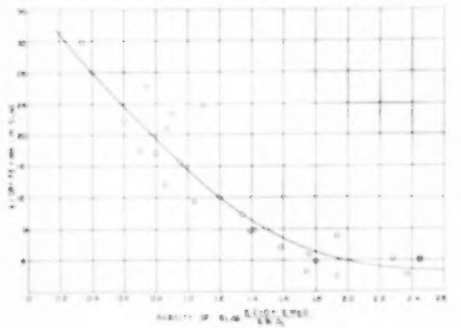

Table I. Calculated Heat Conditions After Reduction

Basicity Ratio	Lb Slag per Ton of Bath	Slag Volume, Pct	Si Required, Lb per Ton of Bath	Cr Recovery, Pct
1:1	315	20	68	88
2:1	700	39	91	97

in controlling the reduction of oxidized slags. Basicity especially is critical in the manufacture of 0.03 pct max carbon stainless steel in which the volume of oxidized slag is very large and the ratio of iron oxide to chromium oxide in the slag is relatively high. To illustrate the influence of basicity, a calculation was made using the relations described for the estimation of slag and metal weights that might result from reduction of low and high basicity slags. The hypothetical heats were assumed to contain 6 pct chromium in the initial charge, to be blown with oxygen to 0.015 pct carbon at a temperature of 3250°F, and to contain 0.50 pct silicon and 18.5 pct chromium at tap. With assumed basicity ratios of either 1:1 or 2:1, Table I shows conditions after reduction with silicon found by the calculation. These calculations show that while increasing the basicity from 1:1 to 2:1 improves the recovery of chromium, slag volume is increased 50 pct. These figures explain to a large extent the problems encountered in the shop in attempting to recover chromium from slags formed while oxidizing chromium steel baths to very low carbon levels.

Carbon pickup or creep may come directly or indirectly from the electrodes and arc and from accidental introduction in the materials used. All phases of the problem of carbon pickup have engaged the attention and interest of melters. Although the chromite hearth has been used, many operators retain basic linings in their melting furnaces and work has been initiated in investigating the transfer of carbon in basic slags.

Spoon test samples of a bath soon after a ferrochromium addition have shown not only higher chromium than the average of the bath, because of incomplete diffusion, but also higher than average carbon. For example, in one heat the carbon content after the oxygen blow was 0.020 pct and the spoon sample taken soon after the ferrochromium addition contained 0.030 pct carbon and 22.01 pct chromium. The carbon content of the ferrochromium was only 0.012 pct. Consequently, if dilution of the bath was the only factor involved, a decrease in the carbon content of the heat should have occurred. That there was actually a local and temporary enrichment of carbon is indicated by the fact that the final composition was 0.020 pct carbon and 18.90 pct chromium. This same phenomenon has been observed on a number of heats.

These samples of stratified metal, taken before chromium was diffused uniformly throughout the bath, suggested an accelerated transfer of carbon contained in the slag during the addition of the ferroalloy rather than from a direct introduction of car-

Table II. Carbon Content of Lime-Silica Slags vs. Basicity

	Lime-Silica Ratio		
	1:2	1:1	2:1
Carbon-Slag, Pct	0.012	0.014	0.039

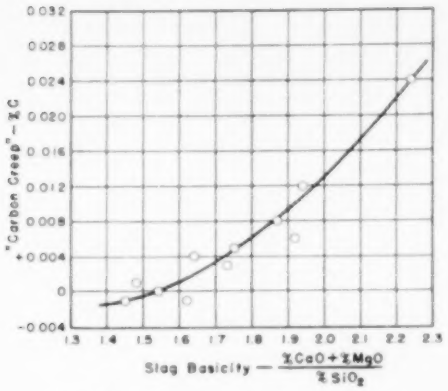

Fig. 7.—Relation between carbon pickup and basicity

bon from the electrodes. A preliminary study then was made on the effect of slag composition on the solubility of carbon in slags of various compositions. In this experimental work, synthetic lime-silica slags, with 5 pct alumina to give fluidity, were melted in a graphite induction furnace crucible and held at 1600 C for 30 min. As shown in Table II, the carbon content of lime-silica slags increases with basicity. Although the carbon contents found in these synthetic slags probably are not the same as might be found in furnace slags, the relative increase of carbon content of the slag with the basicity of the slag is considered very significant. At high temperatures, such as may be reached locally under the arc, basic slags have been observed to contain several percent of carbon.

Review of the metal and slag anaylses of a number of heats of 0.03 pct max carbon stainless steel made in a 1-ton basic arc furnace demonstrated the effects of basicity. These heats were made using either single or double slag practices with additions of standard 0.03 pct max carbon ferrochromium or 5 pct silicon-ferrochromium pellets. Carbon analyses after the oxygen blow and in the final metal were compared to find the amount of carbon picked up during the reducing and finishing periods. As shown in Fig. 7, the pickup of carbon was negligible when the basicity: $\frac{\text{CaO Pct} + \text{MgO Pct}}{\text{SiO}_2 \text{ Pct}}$ was below 1.5 and increased in an ascending curve with higher basicity.

This principle has been applied to large basic furnace operation with good effect in that carbon pickup may be controlled closely. It has been demonstrated also in these heats that the silicon content need not be limited to avoid carbon creep.

Summary

The slag and metal relationships outlined for oxidation, reduction, and addition steps in melting low carbon stainless steel have been determined with sufficient accuracy to indicate the major trends. Although data and understanding are limited, the following conclusions have been drawn to summarize this complex subject.

Decarburization with oxygen will oxidize the metal to a greater degree as the carbon is lowered and to a lesser degree as the temperature is raised. Under conditions resulting in a fluid slag, the total amount of iron, chromium, and manganese oxidized is not dependent on the chromium content of the charge, but that the ratio of iron oxide to chromium oxide changes. Except at relatively high temperatures, high concentrations of chromium in the charge result in viscous slags that greatly increase the difficulty of decarburizing to very low levels. To avoid large slag volumes and excessive metal losses, it appears desirable in making 0.03 pct max carbon stainless steel to oxidize at a high temperature and adjust the chromium content of the charge so that the oxidizing slag is relatively small in volume and is fluid at very low carbon contents.

After decarburization to a very low carbon level, carbon pickup during subsequent working of the heat is a serious problem, especially in basic lined furnaces. Carbon from the electrodes tends to dissolve in basic slag and transfers indirectly to the metal. The less basic slags dissolve less carbon and experimental steels made under low basicity slags have shown little carbon creep. Under commercial conditions, the use of low basicity slags facilitates the control of carbon in making 0.03 pct max carbon stainless steel in basic lined furnaces.

Basicity is a primary factor in the reduction of the oxidizing slag, a high degree of basicity being essential to high-chromium recovery. Further, in addition to carbon pickup in very low carbon heats, the slag volume is so large as to constitute a serious operating problem that is materially aggravated by the lime additions required to attain a high basicity. In higher carbon stainless steels, decarburization to a level of 0.05 pct carbon or higher results in the formation of a relatively smaller slag volume, presenting no abnormal reduction problems. If the reduction slag is highly basic, a high recovery of chromium is realized and a high chromium charge may be used more effectively. Thus, the overall utilization of revert stainless steel scrap appears to be facilitated by the use of a higher proportion in the higher carbon grades.

The new ferrochromium alloy possesses two characteristics particularly useful in making very low carbon stainless steels. The carbon content of the alloy is so low that in most instances an addition will lower rather than increase the carbon content of the steel bath. The high solubility of the material decreases the danger of carbon pickup by shortening the alloying period and it offers opportunity for substantial savings in heat time.

Acknowledgments

The authors wish to express grateful appreciation of the generous and valuable cooperation of D. C. Hilty, research metallurgist, Union Carbide & Carbon Research Laboratories, Inc., as well as the helpful assistance of R. K. Kulp, assistant manager, development dept., Electro Metallurgical Co.

References

D. C. Buck, J. J. Heger, F. J. Phillips, and B. R. Queneau: Corrosion Resistance and Mechanical Properties of Low-Carbon Austenitic Stainless Steels. *Special Technical Publication #93*, ASTM (1950), pp. 30-54.

[2] D. C. Hilty: Relation Between Chromium and Carbon in the Refining of Chromium Steel. *Electric Furnace Steel Proceedings*, AIME (1948), pp. 140-148.

[3] C. R. Taylor: Some Observations on the Metallurgy of Electric Furnace Melting. *Electric Furnace Steel Proceedings*, AIME (1950), pp. 91-97.

Slag Pocket Cleanouts Speeded By Removable Open Hearth Bulkhead Doors

by Ray E. Over

REMOVING the slag from open hearth slag pockets at the end of a campaign can be costly and time consuming. The usual deposit in conventional silica furnaces is highly silaceous and forms a monolith that requires explosives and air hammers to break it into pieces convenient to handle. The operation will take from one to seven days, depending upon the plant and the methods employed.

Open hearth units utilizing suspended basic end construction usually have slag deposits of an entirely different nature, by virtue of keeping silica contamination to a minimum. On some of these units the granular slag has been removed completely from one end in 30 min by mechanical equipment.

While the slag removal problem was simplified by the use of suspended basic ends, removing the bulkhead brickwork and later replacing it required considerable time and effort. In one plant it involved the complete removal and subsequent replacement of 8000—9x4½x3 in. clay brick. While some of the original brick was salvaged, the additional handling was costly.

At the Houston, Texas, plant of the Sheffield Steel Co., F. Ray McFarland, division manager, suggested that this operation could be made more efficient by using a removable bulkhead mounted on the furnace structure. Based on this suggestion, a top-hinged door was designed. This door could be opened for slag removal and then closed and sealed when the furnace was ready to operate with little loss of time or material.

The door designed for this purpose consists of a rigid structural steel frame hinged from the top and lined with fully suspended 9 in. thick basic brick. Basic brick was used to keep slag adhesion to a minimum and because of the wear-resistant qualities. This door is 9 ft, 7 in. wide and 15¼ ft high and has a total weight of approximately 18 tons. Of this 18 tons, the framework comprises six tons with the lining at 12 tons. A beam running across the lower portion of the door acts as a stop and is bolted to the furnace columns to keep the door closed. With the top outside hinges, the door remains open for about 18 in. at the bottom until forced shut. A loose course of brick installed around the outside insures an air tight seal.

Fig. 1 shows the door under construction from inside of the slag pocket. The complete installation of brick and hangers, including the seal course around the outside, takes two masons 9 hr each.

Fig. 1—Door under construction from inside of the slag pocket.

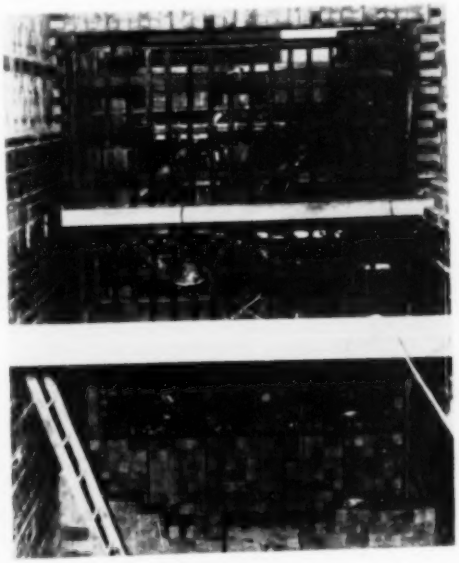

RAY E. OVER is Manager of the Open Hearth Dept., M. H. Detrick Co., Chicago.

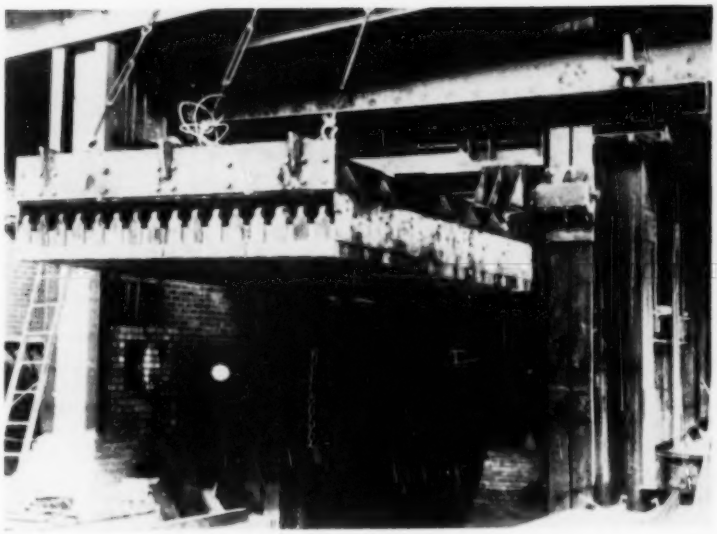

Fig. 2—The door is shown here in its raised position.

Fig. 2 shows the door in its raised position. The three supporting cables clear the back stand and tie into the upper furnace structure. Turnbuckles make certain that each cable carries a proportionate part of the weight.

In this particular plant, the slag pocket level is about 5 ft below the pit level, necessitating a sloping ramp for cleanout. Rather than dig a new ramp each time, concrete sides were installed and then capped off with an old bottom pour casting at pit level. This covers most of the ramp and cuts down the amount of fill.

At the end of a campaign the doors are kept closed for about 12 hr. Opening for cleanout is done in the following manner: (1) Bottom pour slabs are removed and ramp is cleared of all debris by Traxcavator. (2) Bolts holding bottom of door in position are burned off, which allows door to swing open approximately 18 in. at the bottom. In the event that the door does not swing out by itself, a tug by the Traxcavator frees it quickly. (3) A cable is fastened to the lifting lug in the center of the door and tied to the pit crane. (4) The pit crane raises the door to a position slightly above horizontal. The two outside supporting cables are fastened and the crane transfers the load to them. The center cable is then secured and adjusted to carry its share of the weight.

The actual lifting and securing of the door usually takes three men about 5 min. The Traxcavator then cleans out the pocket in about 30 min.

The closing operation is simply the reverse. A false wall of old checker brick is built inside, lapping the bottom of the door by about 4 in. The Traxcavator is used to push the door into the closed position, and bolts holding it shut are installed. The door is then sealed from the outside using chrome brick and chrome ore at the sides and top, capped off with about 1 in. of Plastic Insulation.

Fig. 3 shows the same door shown in Figs. 1 and 2 at the end of the sixth campaign or 862 heats without repair. The bottom edge of the supporting casting is 5 in. from the outer face of the door. This door and its mate have been in continuous service since February 1950, without repair and have about 1200 heats. Where space permits, doors of this type could be side hinged or, if desired, removed completely and stored until required.

Fig. 3—The same door is shown at the end of the sixth campaign (862 heats) without repair.

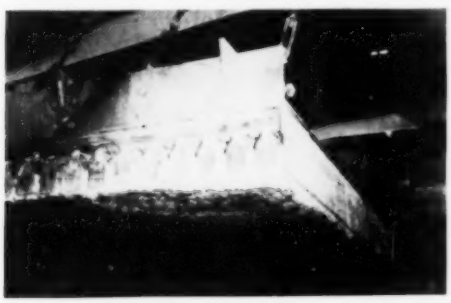

With top hinged doors, positive supports hinged to the furnace buckstays and shaped like the triangular fold-away legs used under kitchen tables in small apartments could be employed. On wide slag pockets, a door just wide enough to permit the easy passage of a Traxcavator could be used. Another variation would be the top-hinged or side-hinged door starting about 6 ft above the slag pocket paving. A sliding overhead trolley similar to that used on garage doors might be applicable in some cases.

Removable slag pocket doors were developed primarily to cut costs in an area where skilled and unskilled labor are at a premium. While the initial cost is high, the overall cost is favorable. This is borne out by the fact that the initial installation has been followed by installations on six additional furnaces.

The swing-out or removable section could be applied to other portions of the open hearth furnace.

HOT SILVER

by K. Ogawa

THIS project was instituted to study the change of the aggregated state of silver powders at various temperatures, and to find the temperature range in which the effect of hot pressing is most marked. Accordingly, an experimental method was adopted whereby the compressibility of powder under low pressures at different temperatures was measured, and from these experiments, three degrees of change of the aggregated state at each temperature could be observed. The initial temperature of the first range (about 200° to 550° C) corresponds to the temperature of stopping of the stirring wire in G. Tammann's experiment.[1] In the second range (about 550° to 800° C), an interlocking of powder particles takes place because of the softening of particle edges which collapse and fill up the bridge space. The third range (about 800° C to melting point) corresponds to the softening temperature of the particle itself. In spherical powders where mechanical interlocking cannot occur, the second range could not be found. From these results, it became apparent that in the second range, the effect of compacting pressure is mainly to fill up the bridge space, whereas in the third range, it is to improve the conditions of contact between particles. Moreover, in the third range, the effect of compacting time is also important.

Lastly, it was found that, in compacting at low pressures (not exceeding 85 psi) and for long times in the third temperature range, the mechanical properties of the specimen thus obtained were far better than those of the usually cold pressed and subsequently sintered specimen.

Several reports of hot pressing methods for metal powders have been made since 1926 by F. Sauerwald,[2] copper and iron; W. Trzebiatowski,[3] gold and copper; C. G. Goetzel,[4] copper, brass and bronze; and W. D. Jones,[5] cast iron and copper alloys. In these researches, the main object was to produce ductile and highly dense materials, in comparison with those that are normally compacted and sintered. The compacting pressures applied in these experiments were relatively high (7100 psi) and the compacting temperatures, 500° to 600° C, were in most instances below the melting point of the metals.

The specimen was molded in a graphite die at room temperature, and after coming to the desired temperature, pressure was applied. As raw materials, electrolytic acicular silver powder, heat decomposed granular silver powder, and molten spherical silver powder,[6] were used. Each powder was −250 mesh.

In Fig. 1, the density of hot pressed granular silver powder compacts is plotted against temperature for compacting pressures varying from 0 to 85 psi for loading times of 30 min. At about 200° C, which corresponds to the initial temperature of the first range of sintering, the specimens became compact. At 500° or 600° C, which corresponds to the initial temperature of the second range, the density began to increase to a marked extent.

A plot of density against time for the same powder hot pressed at 28 psi and various temperatures showed that up to 800° C, the density increased much more rapidly than at higher temperatures. This phenomenon was distinct when using granular powder.

The same powder was hot pressed with a tubular punch at 71 psi for 30 min. Below 800° C the powder mass was not strongly compacted so that by external force it could be crumbled readily, but above 850° C,

KAZUMIKO OGAWA and GENTARO MATSUMURA are members of the Faculty of Science, Metallurgical Laboratory, Kyoto University, Kyoto, Japan.

Fig. 2—Results of bend test on silver powder

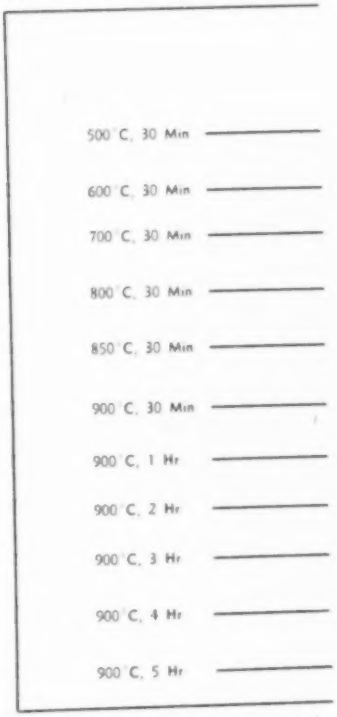

Fig. 1—Plot of density vs. sintering temperature for hot pressed granular silver powder compacts

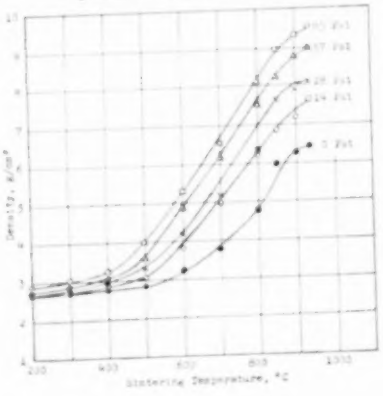

PRESSING POWDER

and G. Matsumura

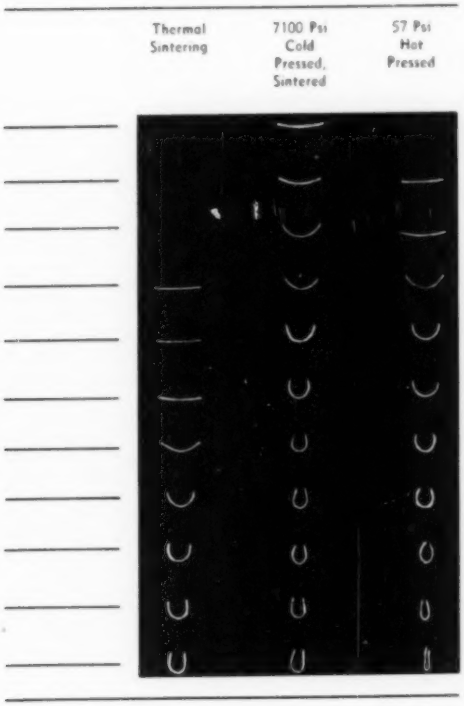

Fig. 3—Properties of silver compacts at optimum cold and hot pressing pressures.

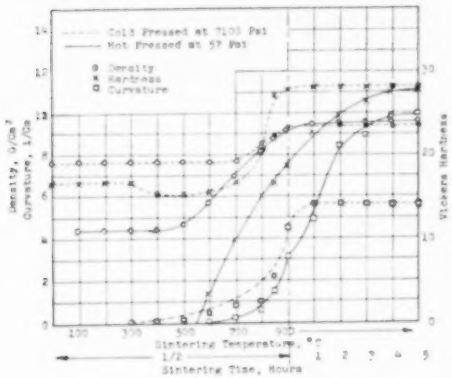

the particles adhered to each other to form one massive body. This latter point corresponds to the initial temperature of the third range of sintering.

The tap density of the spherical powder is greater than that of the granular, which means that in the granular powder, there are many more bridge formations present. There is no unusual increase corresponding to the second range in the curve for the spherical powder as compared to that for the granular powder; rather, the increase is continuous. This indicates that for the granular powder in the second temperature range, the bridges begin to break down and the pores begin to be filled with other powder, without the occurrence of appreciable deformation. In the case of the spherical powder where no mechanical interlocking takes place, no break down of the bridges, and thus no subsequent increase of density, occurs. In the case of the spherical powder, compaction begins only at fairly high temperatures, e.g. about 500° C, because of the lack of mechanical interlocking. Thus, the three ranges are not fixed, but vary with the particle shape and size, and are found to correspond to those obtained in wire pulling experiments."

To establish the mechanical properties of hot pressed specimens, Vickers hardness, density, and workability were measured. The workability was investigated by means of a bending test as follows: The specimen, 1 mm wide, was wound upon cylinders whose diameters varied successively from large to small, and when the first crack in the surface became visible to the naked eye, the curvature of the neutral fiber of the specimen was measured. Fig. 2 is a photograph of a group of silver powder compacts prepared by hot pressing, cold pressing and subsequent sintering, and thermal sintering under different conditions, and subjected to this test.

In the case of cold pressed and subsequently sintered specimens, a pressure of 7100 psi produces the best properties; 28,400 psi gives very inferior properties because of thermal expansion, but in each instance, saturation values were obtained after about 1 hr.

In the case of the hot pressed specimen, the properties take a fairly long time to be saturated, but the values are much higher than in the cold pressed and subsequently sintered specimen. A pressure of 57 psi gave better properties than a pressure of 28 psi with the properties taking a shorter time to be saturated. It appears worthwhile to investigate further the question why, after 2 hr, the density is saturated and the workability is not. Fig. 3 shows the properties at optimum cold and hot pressing pressures.

Acknowledgments

The authors wish to thank Professor Keizo Iwase for his continued advice, and Dr. C. G. Goetzel for his help in preparing this article for publication.

References

[1] G. Tammann and Q. A. Mansuri, *Z. anorg. allgem. Chem.*, **126**, 119 (1923).

[2] F. Sauerwald, *Z. Metallkunde*, **21**, 22 (1929).

[3] W. Trzebiatowski, *Z. physik. Chem.*, **A169**, 91 (1934).

[4] C. G. Goetzel, *Trans.* ASM, **28**, 909 (1940).

[5] C. G. Goetzel, *Trans.* AIME, **161**, 580 (1945).

[6] C. G. Goetzel, *Trans.* ASM, **30**, 86 (1942).

[7] W. D. Jones, *Met. Ind.* (London), **56**, 69 (1940).

[8] W. D. Jones, *Met. Ind.* (London), **56**, 225 (1940).

[9] F. Sauerwald and L. Holub, *Z. Elektrochem.*, **39**, 750 (1933).

[10] K. Iwase, K. Ogawa and A. Yasumori, *Science of Powder* (Japan), **2**, 24 (1948).

VACUUM IMPREGNATION OF CASTINGS

by L. W. Hull

CASTINGS are an important part of the nation's metal tonnage. Anything, therefore, that contributes to economies in metal and the labor of handling it is important. Vacuum impregnation of castings and of some weldments achieves this objective, chiefly in terms of labor, both wage labor and executive, and to some extent in terms of metal. For example, thinner structural walls in castings are sound practice if properly impregnated.

Casting, with notable exceptions such as Asarco continuous-cast shapes and Federated Metals' Castomatic solders, is not an exact science. Poor casting design, defects from physical or chemical causes, and improper foundry practice lead to porosity in castings. For many years the cost of poor castings was hidden beneath the casual theory that the rejects were returned for remelting and nothing was lost.

The cost of defective castings is cumulative and monumental. Foundry labor is the first and obvious loss, to which can be added the expedients for repair or otherwise making suspect castings fit for service. Worst of all perhaps is the waste in machining and finishing, because final inspection may first discern a defect which was born with the casting.

The greater part of such costs can be avoided by vacuum impregnation of castings. Proper impregnation eliminates rejects under buyers' tests and insures against failure in service. The cost is so low that it often is found cheaper to impregnate and be sure of sound castings than to test and ship castings that have passed foundry tests. Even the latter, as pointed out, may develop previously undetected flaws when machined. Impregnation, formerly used only for salvage and repair and once widely considered a dubious risk, is increasingly a part of standard operating procedure for treatment of all castings as delivered from the molds.

Standard techniques for impregnation of castings are now recognized and used by military and government departments. There are various bulletins available for the guidance of manufacturers. Such sources stipulate that impregnation is to be used for correction of seepage or fine porosity; not for major porosity, sponginess, blowholes, mechanical cracks and the like. This conforms with standard practices of the technique. Sand castings, permanent mold castings, and diecastings of ferrous and nonferrous metals are treated successfully by impregnation, though nonferrous castings predominate because of their greater liability to porosity.

Impregnation commonly is done after machining, although it does not affect machinability. It is al-

L. W. HULL is Manager of the Vacuum Equipment Div., F. J. Stokes Machine Co., Philadelphia.

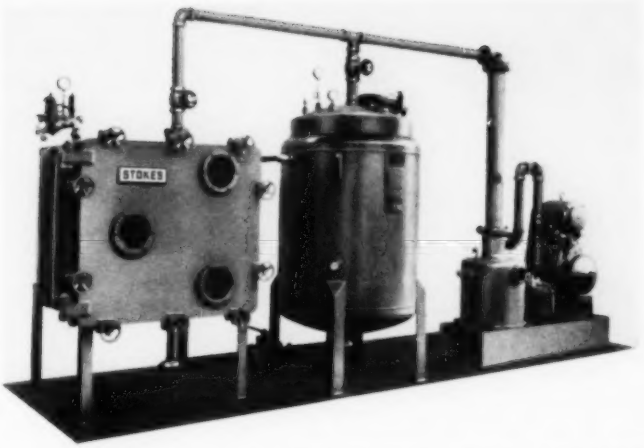

Typical vacuum impregnation unit, consisting of chamber at left with shelves or racks for small castings, impregnant storage tank, center, condenser and Microvac pump at right.

ways possible that machining may uncover subsurface or noncapillary defects, which would not be corrected by impregnation and would not be disclosed by normal wear. Still, one big Canadian company making jet engine components applies vacuum impregnation before machining on castings that are not to be machined on opposite faces of the same section. The latter castings are impregnated after machining, in conformity with the prevailing practice.

Impregnating Materials

Four groups of materials are used for impregnation. These are given in historical order; types (1) and (2) are little used since the more modern types have become available.

(1) Sodium silicate type, with or without metal flours. The latter are fillers and commonly referred to as colloidal. Semicolloidal probably is a more accurate description since they are usually 500-mesh iron and copper powders, usually require agitation in process, and do not exhibit the Brownian movement of true colloids. Metal powder fillers also offer the risk that particles will filter out of solution and bridge microscopic pores, later to be ruptured under wear and unseal a capillary duct. Sodium silicate itself shrinks on baking, is reactive with some metals, and somewhat abrasive, so that subsurface residue may injure bearing surfaces when finish polishing is done after machining. However, it has exceptional dielectric properties and tolerates unusually high temperatures and pressures. Yet there is a strong trend toward resin-styrene compounds as described as type 3.

(2) Linseed or tung oils. These, like sodium silicate and its compounds, are baked after impregnation is complete. They are subject to gradual oxidation that may run to complete deterioration in time.

(3) Resin and resin-oil combinations. Styrene with linseed oil or dehydrated castor oil, several General Electric *Permafils*, Dow's *Styrene DMI*, Western Sealant's *PE-1* (pure resin), and certain Bakelite resins are examples of these combinations. These are thermosetting compounds, varied in properties and in the incidence and type of volatile and

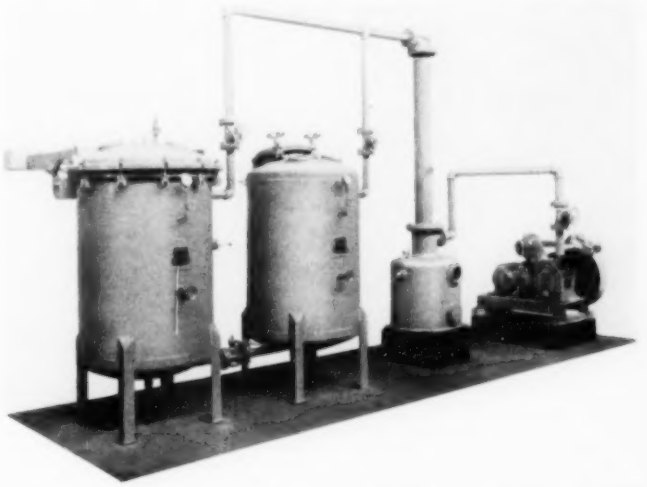

Large vacuum impregnation units are often set below floor level so work can be handled easily at top of tank. Large pieces are lowered into the vacuum chamber by chain hoist.

resin constituents, resistant to temperature changes, solvents and chemicals.

(4) New compounds. Typical of these are Kirk White Chemical Co.'s *Rawpak* and Metallizing Co. of America's *Mogul Cast Seal Type B.* These are air setting and require no baking. Many, but not all, of groups 3 and 4 are described as 100 pct solids in true solution, which suffer no shrinking during drying or curing.

In general, it may be said that the best impregnants are those of low viscosity, preferably of low volatility, which dry or cure to solid infusible materials with little or no loss of volume. They should tolerate temperatures of 300 F, and have no effect on machinability of the impregnated part.

There are five methods by which impregnation is or has been practiced.

(1) Immersion of the casting in the impregnant in a pressure-tight vessel to which pressure is applied. This is the oldest method. The obvious flaw is that the impregnant, under pressure, compresses air in macroscopic holes or capillary passages. After decompression the air will force the impregnant out of some of the pores and to that extent defeat the purpose of impregnation. Even though small bridges of solid impregnant cover other pores they are liable to rupture in service.

(2) Internal pressure method by which sizeable castings are sealed off except for a single port. Impregnant is introduced and pressure applied at the entrance port. The pores and capillaries are thus filled from the inside outward. This method is expensive because of the preliminary sealing involved and suffers the same post treatment hazards as the first method.

(3) External pressure by batch immersion. This suffers the same disadvantages as the first method, but treats more parts at less cost per unit.

(4) Vacuum impregnation by batch immersion, followed by pressure. This method is applicable equally to large pieces when equipment of practical size will permit only one at a time to be handled, or to batches of smaller parts that can be handled in trays or baskets.

(5) Vacuum alone is used in a process by which all ports are sealed with a vacuum connection at one port. The casting is submerged in the sealing compound and vacuum drawn to pull the sealant through the walls from outside to inside.

Government agencies do not recognize the first method, of the other three, methods 2 and 4 are preferred. It may be said that the first three methods merely seal off the openings, creating the risk that service wear, corrosion, or (with some impregnants) electrolysis, may expose new defects.

Vacuum impregnation followed by pressure is indisputably the most successful of all processes for assuring the soundness of castings. Its success leads to the thought that the expression "sealing of castings," common in literature on the subject, may be dropped as vacuum impregnation is more widely used and older methods progressively abandoned.

The first step in vacuum impregnation is thorough cleaning and degreasing. Scrubbing with various alkaline cleaners is customary. *Solvesso # 2, Ansco A,* and hydrogenated naptha are among the cleaners commonly used. It is recommended that unmachined magnesium castings be pickled in 3 to 10 pct H_2SO_4 long enough, usually 1 to 2 min, to remove 0.002 in. of metal; then rinsed in cold water followed by hot water to accelerate drying.

Castings then should be dried at mild heat, 250 F, to eliminate surface moisture, solvents, and gases that may be trapped in the pores. Magnesium, again, requires special attention. Recommendations run from heating at 225 F for 2 hr to 350 F for 1 hr. All castings should be cooled to room temperature. They are then loaded into the vacuum chamber of equipment such as that shown in the adjacent pictures. When small parts are treated in batches, it is desirable to arrange them to avoid cupping, for convenience in handling when they are removed. Vacuum is drawn to 29 in. or more, or until the gage is steady, and held for 20 min. By this time the casting should be completely free, in practical terms, of air and moisture. The capillary ducts, microscopic channels and pores, are void of air and offer no resistance to the entry of the impregnant.

To admit impregnant to the vacuum chamber, the interconnecting valve between the vacuum tank and the impregnant storage tank is opened. Air is admitted to the latter while the vacuum pump continues to draw on the vacuum tank. The impregnant then flows into the vacuum tank (some operators make a point of slow transfer) until the parts are covered as observed through the sight glasses.

Pressure is applied to the impregnant by introducing inert gas or air above it after closing the interconnecting valve and shutting off the vacuum line—60 to 100 psi is conventional, and 20 to 40 min is the usual time under pressure. One successful operator allows 15 min for each $\frac{1}{4}$ in. of depth to be penetrated, equal to $\frac{1}{2}$ hr for a maximum 1 in. section, considering that pressure applies equally from both sides.

After air pressure is relieved, the impregnant is drawn back to its tank by vacuum and reverse valving. The castings are removed, drained, and rinsed in acetone, butyl acetate, *Solvatone, Oakite* in water, or similar cleaners.

Baking follows except when air curing impregnants are used. Manufacturers of impregnants furnish complete instructions adapted to the curing of their products. Temperatures commonly run from 250 to 300 F, but time varies so widely, 10 min to 5 hr, that it would be unwise in this discussion to be specific. With the conclusion of the baking operation, castings are ready for cooling and testing, usually done at 50 pct above working pressure. Some impregnants should not be tested until after a lapse of 48 hr.

Magnesium castings are sometimes cured in an oil bath and require an extra washing and drying operation before cooling and test. A single impregnation usually is sufficient for castings which can be made leak proof, but occasionally second and third impregnations are desirable.

A process identical with that of vacuum impregnation is currently being used for the bonding of dissimilar materials where fairly broad faces are in contact. Plastics and steel, steel and aluminum, copper and neoprene, and numerous other materials, severally and mutually, are bonded in this way after preparation in fixtures to hold together the faces which are to adhere. It is reported that very high shear and tensile strengths are noted. Impregnants of high dielectric properties, used in this way, effectively prevent electrolysis between metals of different anodic characteristics.

Heats of Formation of Sodium-Tin Alloys Determined With A New High Temperature Calorimeter

by Raleigh L. McKisson and LeRoy A. Bromley

A high temperature calorimeter designed for use up to 1500°K is described and the theory of its operation presented. This calorimeter was used to measure the heats of formation of Na-Sn alloys ranging in composition from tin to $NaSn$. The values tend to support those reported by Kubaschewski and Seith.

ONE method of obtaining the heat of formation of an alloy is to measure the heat of mixing of the elements at high temperature. The principal advantage of this method is that the desired quantity is measured directly, while in conventional room temperature methods the differences of the heats of solution of the elements and the alloy in a suitable solvent are measured. A method of improving the accuracy of the high temperature measurements, when the precision of the measurement is lower than that of the heat capacity values for the elements, is to add one component at room temperature to the other at the high temperature, so that part of the heat of reaction is dissipated in heating the cold component to the high temperature. Thus, only a fraction of the heat of reaction is measured, and a result of higher precision is obtained. The limitations of the high temperature technique are that volatile systems cannot be studied, and that many alloys melt at temperatures higher than those at which the calorimetric apparatus operates readily. Nevertheless, a calorimeter operating at 1500°K would be useful in investigating many of the lower melting alloy systems and the low melting mixed oxide systems. A unit designed for these applications was built and is described here.

The Na-Sn system was chosen for investigation because the temperature involved, 880°K, would adequately test the operation of the calorimeter. Further, the data reported in the literature for the various alloys of sodium and tin differ markedly, and it was hoped that this investigation would help to fix the values of the heats of formation in this system.

R. L. McKISSON, formerly with the University of California, is now with California Research and Development Co., Livermore, Calif., and L. A. BROMLEY is Assistant Professor of Chemical Engineering, Radiation Laboratory, University of California, Berkeley, Calif.

Discussion on this paper, TP 3182DE, may be sent, 2 copies, to AIME by March 1, 1952. Manuscript, Oct. 2, 1950, revision, June 25, 1951. St. Louis Meeting, February 1951.

Design of Apparatus

A detailed discussion of the considerations involved in the calorimeter design is given by McKisson and Bromley,[1] and a brief summary follows. Fig. 1 shows a sectional view of the calorimeter.

The inner graphite chamber is maintained at constant temperature by means of the circulating molten tin bath in which it is submerged. The tin is contained in a graphite vat. This unit comprises a thermostat whose heat capacity is about 7000 cal per °C. The main heating element consists of a machined graphite spiral with a room temperature resistance of about ½ ohm. These parts are separated from the powdered carbon external insulation by the cage, a cylindrical graphite chamber. The electrical insulators and separators, the auxiliary heater spool, and the loading tube liner are made of sintered alumina. The tin vat stirrers, the sample stirrer, the melt thermocouple well, and the power leads are made of molybdenum. The auxiliary heater is wound with molybdenum wire and serves to compensate for the heat loss up the loading tube. All of the individual components in the high temperature region of the calorimeter will withstand at least 2000°K, and the various contacting materials should easily withstand 1500°K. The external container for the insulating carbon powder is a copper shell upon which copper tubes are soldered to serve as cooling coils.

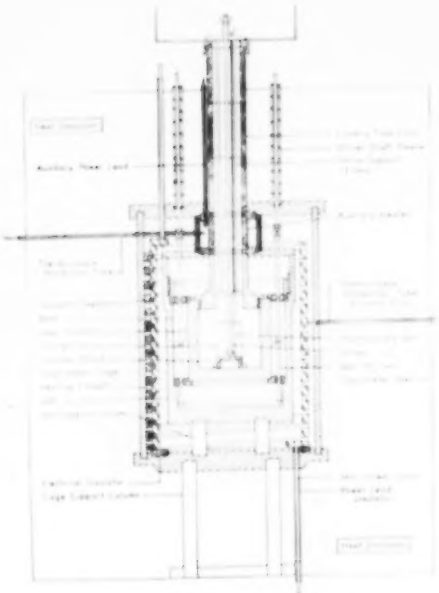

Fig. 1—High temperature calorimeter

The sample dispenser unit, Fig. 2, rests on the top of the loading tube and carries the samples from the sample chamber to the melt. The lower end is a cell, closed by a trap door, into which the samples are placed. When the sample tube has been cranked down through the loading tube to its lowest position, the ejector mechanism forces the sample out into the melt.

The calorimeter power supply consists of a 220 v 7.5 kva Variac, whose secondary feeds a 4:1 step-down transformer. The output from the step-down transformer is fed into the main heating coil of the calorimeter. The control of the main power supply is obtained by varying the Variac setting to correct the temperature of the heating element. This temperature is continuously read by a Wheelco Potentiotrol unit which operates from a thermocouple in contact with the main heating element. The Potentiotrol unit is wired to control a reversible motor which is geared to the Variac shaft. When the temperature of the heating element is low, the motor increases the emf delivered by the Variac; when the temperature is high, the emf is decreased. In addition to this control, movable limiting switches are mounted so that the maximum variation in the Variac emf can be set to give the best degree of constancy in the temperature cycle of the tin bath.

The recording instruments are a controller-recorder, a precision potentiometer, and a timer. In normal operation, the controller-recorder unit is used to record the temperature-time trace of the sample, another unit controls the tin-bath temperature as previously described, and the potentiometer in conjunction with the timer is used to read the temperatures of the sample, at known times. The controller-recorder trace and the potentiometer-timer reading constitute the data obtained from the calorimeter.

The gas system used consists of a tank of argon and a tank of helium, each piped through manometers and drying tubes to the calorimeter. The drying tube on the argon line consists of a bubbler unit in which the gas bubbles through the liquid alloy of sodium and potassium to remove water and oxygen. The dry argon then flows into the heating element region, and also into the inner graphite chamber, providing an inert atmosphere around the heating element and around the sample. The drying tube on the helium line consists of a column of phosphorus pentoxide. The dry helium then flows to the top of the sample dispenser unit. Thus the argon fills the inner graphite container displacing any lighter gas and overflows into the sample chamber where it meets the helium which displaces heavier gas in the upper part of the dispenser unit. The sample chamber does not have a gas-tight seal with the loading tube, and the two gases escape through this joint and thus provide the calorimeter with an inert atmosphere.

Derivation and Application of Equations

The data obtained from the apparatus consist of a temperature-time trace of the crucible and its charge, together with a number of checks of temperatures on this curve from readings taken on the potentiometer. The problem is, then, to devise a method of calculating the heat liberated in a reaction using these data. McKisson[1] previously analyzed a system similar to the one concerned here, and this derivation will follow a similar approach.

The rate of heat transfer from the crucible at temperature, T, when the surroundings are at temperature, t, is:

$$q = \sigma A \epsilon (T^4 - t^4) + hA(T - t) \qquad [1]$$

where: q is the rate of heat transfer, cal per min; σ,

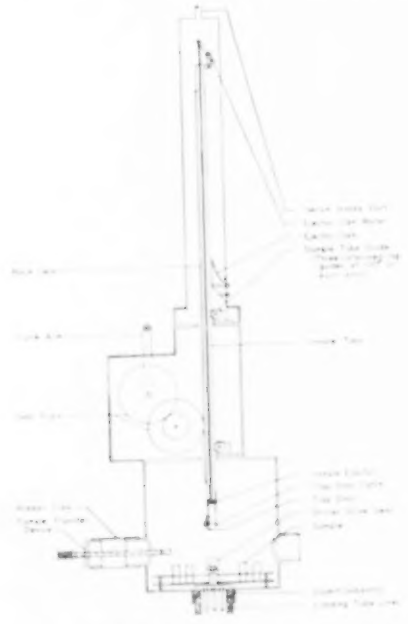

Fig. 2—Sample dispenser unit

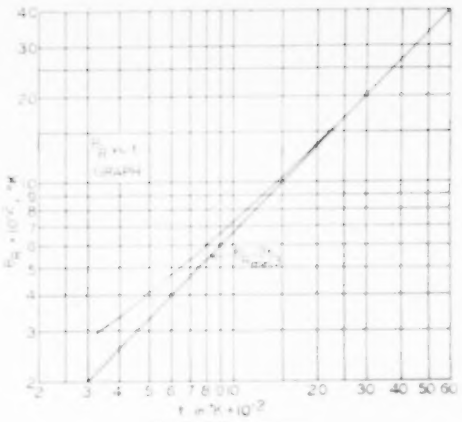

Fig. 3—T'/t vs. t curve.

the Stefan-Boltzmann constant, cal per min sq cm °K⁴; A_r, the area of crucible system for radiative heat transfer, sq cm; A_c, the area of crucible system for convective heat transfer, sq cm; ϵ, the effective emissivity of the crucible; T, the temperature of crucible, °K; t, the temperature of cavity, °K; and h, the heat transfer coefficient for convection, cal per min sq cm °C.

$(T' - t')$ can be expanded in terms of $(T - t) = \Delta T$, thus:

$$(T' - t') = 4t^3\Delta T + 6t^2\Delta T^2 + 4t\Delta T^3 + \Delta T^4 \quad [2]$$

If ΔT is less than $0.1t$, neglecting the last two terms of the expansion will give an error of less than 1 pct. Then, substituting the first two terms of eq 2 into eq 1 and rearranging:

$$-q = (4\sigma A_r t^3 + hA_c)\,\Delta T + (6\sigma A_r t^2)\,\Delta T^2 \quad [3]$$

In eq 3, the Stefan-Boltzmann constant, σ, is a constant for all conditions. The emissivity, ϵ, is a function of T, but can be considered constant during a run. The effective area for radiative heat transfer, A_r, and the effective area for convective heat transfer, A_c, are functions of melt-height. The convection heat-transfer coefficient, h, is a function of melt-height, melt temperature, T, and ΔT, but the dependence on ΔT is small. Because of the small variability of these quantities, they can be considered to be constant during an individual addition.

Now let:

$$(4\sigma A_r t^3 + hA_c) = P \quad [4]$$

and:

$$(6\sigma A_r t^2) = R \quad [5]$$

Substituting eq 4 and eq 5 in eq 3:

$$-q = P\Delta T + R\Delta T^2 \quad [6]$$

Eq 6 gives an expression which relates the rate of heat transfer from the crucible to the temperature difference between the crucible and the cavity through the quantities P and R. Since $q = dQ/d\theta$, plotting q against time, θ, will give an area which is proportional to the heat liberated in the reaction. Such a plot may be constructed if P and R are known. The ratio of P to R can be written, using eq 4 and eq 5:

$$\frac{P}{R} = \frac{4\sigma A_r t^3 + hA_c}{6\sigma A_r t^2} \quad [7]$$

In eq 7 if $hA_c = 0$, the minimum value of the ratio (P/R) can be calculated as:

$$(P/R)_{hA_c=0} = \frac{2t}{3} \quad [8]$$

The system can be analyzed by means of heat transfer correlations given by McAdams[7] and the ratio P/R calculated within 5 pct. The results of such an analysis are shown in Fig. 3. Details of this calculation are given by McKisson.[8] These values are used only in estimating R once P is known, since $R\Delta T^2$ represents only a correction term in eq 6. The problem, then, is to obtain the best value for P.

When no heat is being liberated in the system, the expression relating the heat, Q, to the heat capacity of the system is $dQ = C_v\,dt$, and when this is combined with the expression for Q in terms of time, θ:

$$-q = -C_v\frac{dT}{d\theta} = P\Delta T + R\Delta T^2 \quad [9]$$

Now, since $\Delta T = (T - t)$, then $d\Delta t = dT$. Using this equality in eq 9 and rearranging:

$$\frac{d\Delta T}{P\Delta T + R\Delta T^2} = -\frac{1}{C_v}\,d\theta \quad [10]$$

Eq 10 is integrable, yielding:

$$\frac{\theta}{C_v} = \frac{1}{P}\ln\frac{P + R\Delta T}{\Delta T} + C \quad [11]$$

or, rearranging in more useful form:

$$\theta = -\frac{C_v}{P}\ln\frac{\Delta T}{1 + (R/P)\Delta T} + C_1 \quad [12]$$

Eq 12 indicates the relation between θ and ΔT for the system when no reaction is occurring. By plotting $\ln(\Delta T/[1 + (R/P)\Delta T])$ vs. θ for the addition of an inert material, a straight line is obtained whose

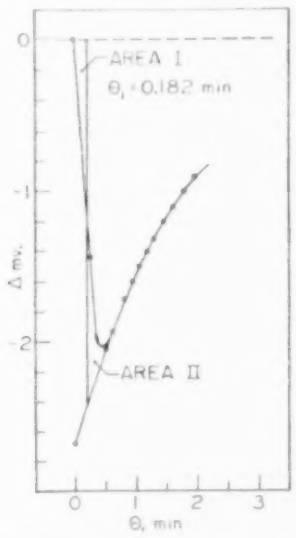

Fig. 4—Mv vs. θ curve.

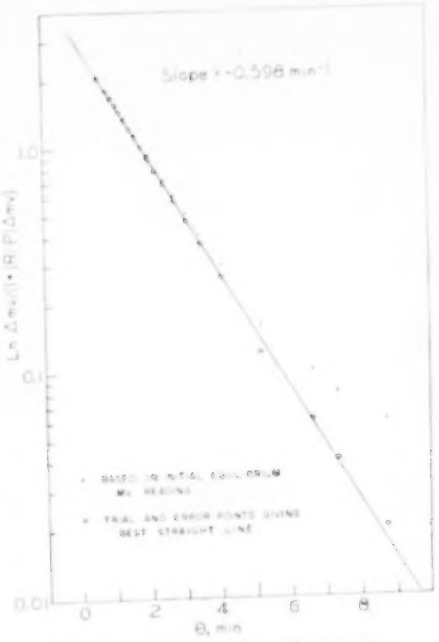

Fig. 5—Ln [Δmv/[1 + (R/P)Δmv]] vs. θ curve.

slope is $-(P/C_c)$. In eq 12 it is more convenient to use Δmv, the millivolt difference reading of the melt thermocouple from the equilibrium millivolt value, provided that a linear relation exists between mv and temperature. When C_c is known the slope yields P, and the q vs. θ plot can be made.

The C_c of the system can be determined from the addition of an inert material to the melt. The procedure is outlined as follows:

1—Plot the T vs. θ curve or the Δmv vs. θ curve using data from the addition of an inert material of known heat capacity (Fig. 4) and estimate the average temperature of the addition.

2—Refer to Fig. 3 and find the value of P/R corresponding to this average temperature.

3—Calculate values of $\Delta mv/[1 + (R/P)\Delta mv]$ and plot $\ln (\Delta mv/[1 + (R/P)\Delta mv])$ vs. θ (Fig. 5). The slope of the resulting line is $-(P/C_c)$. In the event that the final equilibrium temperature differs from the initial equilibrium temperature, the one that more accurately represents the true equilibrium temperature must be determined. This is most easily done by plotting the data corresponding to both temperatures on the $\ln (\Delta mv/[1 + (R/P)\Delta mv])$ vs. θ plot and determining which gives the best straight line. Such a case is shown in Fig. 5, where use of the final equilibrium temperature gives a straight line over the entire time range but the initial equilibrium temperature does not.

4—Extrapolate the $\ln (\Delta mv/[1 + (R/P)\Delta mv])$ vs. θ curve back to low values of θ and plot the corresponding extrapolated curve of Δmv vs. θ (Fig. 4).

5—Estimate Δmv_i (ΔT_i is the first approximation of temperature drop of mixing, when inert material is added) in the Δmv vs. θ curve (Fig. 4) by adjusting θ_i so that Area I equals Area II. The significance of this equalization is explained under item 9, below.

6—Calculate the value of C_{c_i} corresponding to ΔT_i from the known heat content of the inert material:

$$\Delta H_{inert} = (C_{c_i} - C_{c_{inert}})\ \Delta T_i \qquad [13]$$

In eq 13, $C_{c_{inert}}$ is calculated at the average temperature of the addition. The heat capacity, C_{c_i}, which is operative in the warming process, includes the heat capacity of the inert material added.

7—Evaluate the slope of the $\ln (\Delta mv/[1 + (R/P)\Delta mv])$ vs. θ curve, calculate P_i from this slope and the value of C_{c_i} from eq 13, and find the corresponding value of R, R_i, from the P/R ratio.

8—Calculate values of q_i:

$$q_i = P_i\Delta T + R_i\Delta T \qquad [14]$$

and plot q_i vs. θ (Fig. 6), including values corresponding to the extrapolated Δmv's from 4.

9—Now, since areas in the q vs. θ plot (Fig. 5) are equivalent to heat, a time, θ_{ii}, may be found for which the total area between the curve plotted from the measured data and the base line ($q = 0$) is equal to the total area between the extrapolated curve and the base line. This is equivalent to finding the time of a fictitious instantaneous temperature equilibration between the melt contents and the inert material. The time θ_{ii} corresponds to a Δmv_{ii} (ΔT_{ii}) on the Δmv vs. θ plot (Fig. 4). In general, θ_{ii} will be slightly less than θ_i and ΔT_{ii} will be slightly larger than ΔT_i. The procedure of item 5 is analogous to the one described in 9 except that in 5 it is assumed that (R/P) is negligible and q is directly proportional to Δmv.

10—Calculate the value of $C_{c_{ii}}$ using ΔT_{ii} in eq 13. Then calculate the corrected values P_{ii} and R_{ii}.

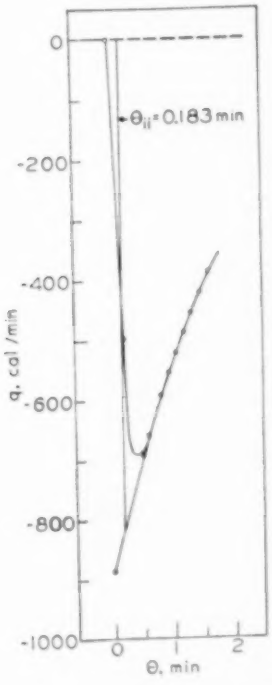

Fig. 6—q_i vs. θ curve.

11—Evaluate the values of q_{θ_n} using eq 14 and repeat steps 8 through 10 until successive calculations show P and C_x to be constant. In most cases, it is not necessary to calculate q_{θ_n} since θ_n and θ_{n-1} will differ only slightly, if at all.

The final values of P and C_x calculated as above apply only to the alloy melt to which the inert material was added. In order that an individual heat of reactive addition be calculable, a value of P for the particular addition is needed. The estimation of P for any particular addition can be effected by interpolation between quantities directly determined. These points must be taken from the addition of nonreacting material, since this is the only way to be certain that there are no rate of reaction effects to affect P. An initial point can be readily obtained by adding a piece of the melt metal to the crucible containing only this metal. Other points must be taken by the addition of an inert material.

When the values of P for each addition have been determined, the graphical solutions to the equation can be made:

$$Q = \int q \, d\theta \qquad [15]$$

for each addition. The quantity Q is the heat effect for the reaction:

(Cold Reactant) + (Hot Alloy$_1$) ⟶ (Hot Alloy$_2$)

Sample Measurement

The sodium samples were cast from Mallinkrodt analytical reagent sodium in a dry-box.[5] The tin stock was obtained from the American Smelting and Refining Co.; and from the Reynolds Metals Co.; and samples were prepared by casting. Spectrographic analysis of the prepared samples indicated a purity of 99.9+ pct for each component. The calibration samples were tin (added to pure tin only) and molybdenum (added to alloy melts).

About 18 hr before starting a measurement, the samples were placed in the sample chamber, the Variac was set to give the desired equilibrium temperature, and the inert gases were introduced. The measurement was started after the system had been at the desired equilibrium temperature for 30 min.

The measurement proper consisted of recording the temperatures of the reaction crucible melt, the two tin bath thermocouples, and the sample chamber. The sample was transferred to the dispenser tube (with the helium flow turned up to about 0.10 cu ft per min) and a final check on the reaction crucible temperature was made. The timer was started when the sample was ejected into the melt and temperatures (emf) were read on the precision potentiometer as rapidly as possible. The emf was recorded, together with the corresponding times. This record was then compared with the trace of the temperature vs. time from the controller-recorder and if there was a gap in the potentiometer data, the controller-recorder tracing was used to provide supplementary data.

The initial melt was tin, and the first addition was pure tin, to provide an initial determination of P and C_x. Subsequent additions were sodium plus a protective wrapping of tin foil. These were used until the melt had reached one of the check points, then several additions were made using samples whose Na-Sn ratio was identical with that of the melt. Then a molybdenum sample was added to provide a final determination of P and C_x. This

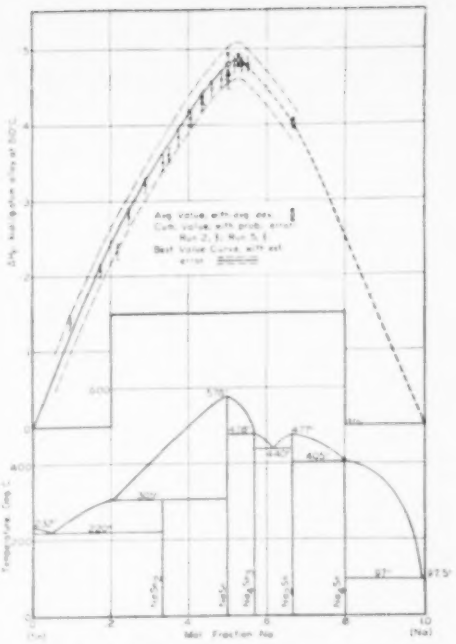

Fig. 7—Heat of formation and phase diagram for Na-Sn alloys.

sequence yields a number of heats of formation of tin-rich alloys plus several direct measurements for a single composition. In the determinations for the sodium-rich alloys, the step-wise measurements could not be made, and only the measurements for which the sample composition and the melt composition were identical were made. The calculations were made as outlined above using the data of Kelley[7] for the heat capacities of the elements.

Six runs were completed, yielding 58 individual measurements. One entire run, consisting of 11 additions, was discarded because the stirring was inadequate; and 7 other additions were discarded; 5 because of stirring rate, and 2 because of obvious experimental error. Thus 40 additions were usable, yielding 40 individual measurements. Of these, 12 were for the composition NaSn, 6 for the composition $Na_{1.1}Sn$, and 4 for the composition Na_4Sn. These three averages are plotted in Fig. 7 together with the other 18 results. The phase diagram shown below the curve of experimental results is taken from Hansen.[6]

Discussion

It was found that the heats found in the q vs. θ plots for the same reaction varied widely. For the 12 direct determinations of the composition NaSn, these values average +898 cal per mol with an average deviation of 267 cal per mol or 30 pct. This greatly exceeds the maximum probable error (±10 pct) estimated. However, for the four direct determinations of the composition Na_4Sn, the q vs. θ plot values average +3148 cal per mol with an average deviation of 230 cal per mol or 7.3 pct. This is of the order of the estimated probable error.

The cause of the very large average deviation above cannot be positively determined, but one

Table I. Heats of Formation of Na-Sn Alloys

Composition	$-\Delta H$, Kcal per g-atom	Temperature, °K	References
[illegible]	0	298	3
	0.2	298	10,11,12
	0.85 ± 0.25	880	This research
[illegible]	3.5	298	3
	0	298	10,11,12
	0	Room	13,14,15
	4.9 ± 0.2*	873	9
	4.80 ± 0.14	882	This research
$Na_{...}Sn_{...}$	4.66 ± 0.04	881	This research
$Na_{...}Sn_{...}$	5.1	298	3
	0	298	10,11,12
	4.83 ± 0.21	880	This research
Na_2Sn	4	298	3
	5	298	10,11,12
	4.0	Room	13,14,15
	4.03 ± 0.60	885	This research
Na_4Sn	4.2	298	3
	6.6	298	10,11,12
	2.9	298	13,14,15
	2.5 ± 0.5	880	This research

* Recalculated value.

factor which would have a marked effect on these quantities is the stirring rate, or more particularly, the extent to which uniformity of composition and temperature was attained. The development of the equations used is based on a uniform temperature in the reaction crucible, and the entire Run 1 was discarded because its results deviated markedly from those of the later runs. Since the stirring rate in Run 1 was about 250 rpm, and the rate was increased to ~400 rpm in the later runs (which gave better agreement), the slower stirring was assumed to be the cause of the poor results. It is possible that the stirring rate, although high, in the NaSn additions was not always effective in maintaining a uniform temperature and composition in the crucible. Although the 30 pct deviation is large, its effect on the ultimate result is minimized by the fact that the total heat effect is ~9590 cal, which means that the inaccurate measurement involves less than 10 pct of the total heat effect. This is because the q vs. θ plot measures the heat for the reaction: cold sodium plus cold tin to yield hot alloy; and more heat is required to heat the reactants up to the high temperature (10,490 cal), than is liberated in the reaction (9590 cal); therefore there is a net heat absorption by the crucible. The heat capacities of tin and sodium are known to within 1 pct so that the large error in the q-θ plot heat is absorbed in the final result.

The only data on the Na-Sn system taken at high temperature was that of Barber et al.[3] The other values by Biltz and Holverscheit,[4] Biltz and Meyer,[5] Biltz, Bichowsky and Rossini,[6] Kubaschewski and Seith,[7] Kubaschewski and Wittig,[8] and Kubaschewski,[9] are reported at 298°K. Table I lists all the available values for the heats of formation of Na-Sn alloys, together with the temperature of the measurement and the reference.

The results at high temperature check very well with those of Barber et al.[3] A quantitative comparison between the results of this research and the other values shown in Table I is possible only if the heats of fusion and heat capacities are known for all the alloys and the elements. Since these data are not available for the alloys, only a qualitative comparison is possible. Such a comparison can be made by solving for the various combinations of heat capacities and heats of fusion which are required to compute ΔH_{298}. Any result requiring absurd values of heat capacity and/or heat of fusion cannot be considered compatible with the results presented here. The limits considered acceptable for the liquid alloy heat capacity are from 7 to 10 cal per deg g-atom; for the entropy change in melting, 1.5 to 3.5 e.u. per g-atom; and for the solid alloy heat capacity, 6 to 9 cal per deg g-atom.

A comparison of the limits noted above with the data of Table I shows that all of the values of Biltz and Holverscheit,[4] are within the compatible range, that all the values of Kubaschewski[9] and Kubaschewski and co-workers[7,8] are near the center of the compatible range, but that the values reported by Bichowsky and Rossini,[6] who reviewed the work of Biltz,[5] and Biltz and Meyer,[5] are higher than the upper compatible limit.

Conclusion

A new high temperature calorimeter has been designed, constructed, and used for the determination of heats of formation of Na-Sn alloys at 880°K. The results tend to support the values originally reported by Kubaschewski and Seith. The results of the measurements are shown in Table I and Fig. 7.

Acknowledgment

Grateful acknowledgment is made to the Standard Oil Co. of California for financial aid in the form of a research fellowship to R. L. McKisson, and to Leo Brewer of the University of California for his helpful suggestions. This work was performed under the auspices of the U. S. Atomic Energy Commission.

References

[1] R. L. McKisson and L. A. Bromley: A New High Temperature Calorimeter. Atomic Energy Commission Unclassified Report UCRL-688. University of California Radiation Laboratory (1950).

[2] R. L. McKisson: Master's Thesis, University of California, Berkeley, Calif. (1948).

[3] W. Biltz and W. Holverscheit: *Ztsch. anorg. allgem. Chem.* (1924) **140**, p. 261.

[4] W. H. McAdams: *Heat Transmission*. (1942) New York. McGraw-Hill Book Co.

[5] R. L. McKisson: Ph.D. Thesis, University of California (1950).

[6] R. K. Edwards, R. L. McKisson, and L. A. Bromley: Liquid Sodium Pump for the Purification of Inert Atmospheres. Atomic Energy Commission Unclassified Report UCRL-687. University of California Radiation Laboratory (1950).

[7] K. K. Kelley: Contributions to the Data on Theoretical Metallurgy. U. S. Bur. Mines, *Bull.* 476 (1949).

[8] M. Hansen: *Der Aufbau der Zweistofflegierungen*. (1943) Ann Arbor, Mich. Edwards Bros. Inc.

[9] G. R. Barber, L. Brewer, L. A. Bromley, and R. L. McKisson: Application of the High Temperature Calorimeter to the Determination of the Heats of Formation of Na-Sn and Li-Sn Alloys. U. S. Atomic Energy Commission Document AECD-2294. (1949).

[10] W. Biltz and F. Meyer: *Ztsch. anorg. allgem. Chem.* (1926) **176**, p. 23.

[11] W. Biltz: *Ztsch. Metallkunde* (1937) **29**, p. 73.

[12] F. R. Bichowsky and F. D. Rossini: *The Thermochemistry of the Chemical Substances*. (1936) New York. Reinhold Pub. Corp.

[13] O. Kubaschewski and W. Seith: *Ztsch. Metallkunde* (1938) **30**, p. 7.

[14] O. Kubaschewski and F. E. Wittig: *Ztsch. Elektrochem.* (1941) **47**, p. 433.

[15] O. Kubaschewski: *Ztsch. Elektrochem.* (1942) **48**, p. 646.

Constitution of the System Gallium-Indium

by John P. Denny, J. Hugh Hamilton, and John R. Lewis

The constitution of the Ga-In system was determined by thermal methods. An experimentally determined metastable equilibrium line (an extension of the indium-rich liquidus) was obtained. The various alloys were studied metallographically using polished samples obtained by a casting method. These low melting alloys required a special dry-ice assembly to maintain a suitable temperature.

RECENT interest in alloys that are liquid at room temperature has led to rather extensive investigation of gallium-base alloys. Widely distributed over the earth, gallium could be produced in substantially larger quantities than at present, if a significant demand existed.[1] One study[2] has established its presence in 12 out of 14 zinc blends, in all of 15 aluminum ores, in 4 out of 12 manganese ores, in 35 out of 91 iron ores, and in all of 7 magnetite ores. It occurs as a rule in minute amounts, however, leading to high extraction costs. Recent quotations run from $2.50 to $7.50 per g.

During the course of the present investigation, portions of the system Ga-In have been redetermined, and the results of this study are presented herein. Thermal and metallographic methods have been employed.

Lecoq de Boisbaudran, the discoverer of gallium, conducted the first investigation[3] on Ga-In alloys in 1885. The temperatures of incipient melting, and of completion of melting, were determined at four alloy compositions. In 1936, Hansen[4] constructed a eutectic-type phase diagram for the system Ga-In, based on Boisbaudran's work. The existence of a Ga-In compound was regarded as improbable by Hansen, and subsequent investigations are in agreement.

French, Saunders, and Ingle[5] conducted a more complete study of the system in 1938, using thermal methods. Their phase diagram is a eutectic type, containing a unique concave-upward liquidus. The solid-solution range of gallium in indium was reported as 9.5 pct by weight, and that of indium as less than 1 pct, at the eutectic temperature. The eutectic composition, determined as being bracketed by the compositions showing a true horizontal at the eutectic temperature (16°C), was reported as 76 ± 0.5 pct Ga and 24 ± 0.5 pct In.

Experimental Procedure

The preparation of Ga-In alloys is simplified by the low melting points involved. Various compositions were prepared by melting in pyrex tubes, using a cover of distilled water or paraffin to prevent the alloys from wetting the glass wall. In all cases, the melts were homogenized by stirring.

Where possible, both cooling and melting curves were determined. The extensive undercooling of gallium was found to prohibit a satisfactory cooling-curve analysis of gallium-rich alloys, however, and transition points on the gallium side of the eutectic could be determined only by melting curves. The inverse rate method of thermal analysis proved to be most satisfactory and was used to a great extent. Various heating and cooling rates were used, ranging from 0.2° to 5.0°C per min.

Low temperature melting analyses were conducted within a constant temperature bath, maintained at about 70°C. The alloys were solidified (under water or paraffin) within a pyrex tube, using dry ice; the tube was then sealed within a cold Dewar flask, the unit transferred into the constant temperature bath, and periodic temperature readings taken.

The high temperature melting-curve determinations and all cooling-curve determinations were made in a vertical tube furnace. At near-eutectic compositions, the furnace was placed within a refrigerated room held at −20°C. Accordingly, the furnace on cooling approached −20°C asymptotically and permitted the determination of those phase transitions occurring below room temperatures.

Temperatures were measured with a 30-gage iron-constantan thermocouple, immersed directly in the alloy. To prevent contamination of the melt, the leads and junction were coated with Lucite, applied by painting with a solution of Lucite in ethylene dichloride. Electromotive force measurements were made with a Leeds and Northrup precision potentiometer, type 8662. The couples were calibrated against the boiling point of water and, at lower temperatures, against a calorimeter thermometer having a Bureau of Standards certificate.

The melting points of gallium and indium used in the present investigation were determined as 29.77° and 156.1°C, in good agreement with previously reported values of 29.78°C[6] and 156.4°C.[7] The spec-

J. P. DENNY, Member AIME, is now Research Metallurgist, General Electric Co., Lynn, Mass.; J. H. HAMILTON, Member AIME, is Director of Utah Engineering Experiment Station and Professor of Metallurgy, and J. R. LEWIS, Member AIME, is Professor and Head, Department of Metallurgical Engineering, University of Utah, Salt Lake City.

Discussion on this paper, TP 3204E, may be sent, 2 copies, to AIME by April 1, 1952. Manuscript, Oct. 16, 1950; revision, Oct. 1, 1951. New York Meeting, February 1952.

This paper represents part of a thesis by J. P. Denny submitted in partial fulfillment of requirements for the degree of Doctor of Philosophy to the University of Utah.

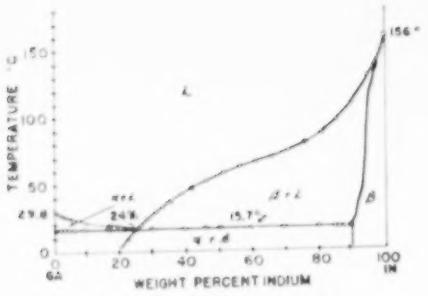

Fig. 1—Ga-In constitution diagram.

trumpic analyses were: gallium (Eagle Pitcher Co.) —0.01 pct Cu, 0.01 pct Si, 0.005 pct Pb, 0.0007 pct Ag, balance Ga; and indium (Indium Corp. of America)—0.0005 pct Mg, balance In.

Discussion of Results

The Ga-In phase diagram is presented in Fig. 1. The liquidus and eutectic horizontal are plotted from experimental points obtained in the present investigation, while the indium-rich solvus is taken from the work of French et al.[1] In contrast to previously reported diagrams, the indium-rich liquidus is found to be concave downward from the eutectic to approximately 70 pct In. The gallium-rich liquidus, eutectic temperature (15.7°C), and eutectic composition (24 pct In) are in reasonable agreement with the investigation of French and coworkers.

The liquidus inflection at about 70 pct In is suggestive of a third phase which undergoes peritectic decomposition. Careful thermal analyses have failed to indicate such decomposition, however, and the reported diagram is therefore similar to the system Cd-Pb.

Confirmation of the eutectic temperature was obtained when a slightly undercooled eutectic alloy was nucleated. The temperature subsequently rose to 15.7°C, where it remained until solidification was complete. Under certain conditions, it was found possible to quench the eutectic alloy to −25°C without complete solidification. Slight undercooling of the indium-rich alloys was also apparent. On cooling, a short, nearly horizontal arrest was found to accompany the initial crystallization of indium, and, in a few instances, a small temperature rise was observed. The supercooling of indium is not nearly so extensive as that of gallium, however, and good checks were obtained by melting and cooling the indium-rich alloys.

In general, cooling-curve transitions along the indium-rich liquidus were better defined than the melting curves. The melting transitions were particularly slight at compositions lying between 24 and 35 pct In, rendering their detection extremely difficult or impossible, and cooling-curve values have accordingly been plotted in this portion of the diagram. The better defined cooling-curve transitions may be attributed to the slight undercooling of the indium; after undercooling, the initial crystallization is accompanied by a relatively large thermal effect.

An interesting feature of the present diagram is an experimentally determined metastable equilibrium line, shown as an extension of the indium-rich liquidus in Fig. 1. If an alloy containing 80 pct Ga in 20 pct In is cooled slowly, it ordinarily will not undergo a phase transition at either the gallium-rich liquidus or the eutectic, due to the absence of proper nucleating agents. It will, however, crystallize out the indium-rich solid when the temperature has fallen to 5.2°C. After solidification and heating, a transition will be seen at the eutectic temperature.

Portions of the liquidus reported in the present investigation differ from the previously reported diagrams by as much as 25°C. Considering the low temperatures involved in this system, the difference is quite significant. A visual test at the composition 62 pct Ga-38 pct In was used to demonstrate the correctness of the diagram reported herein. This composition was found to be definitely semisolid at room temperatures, a fact that is in agreement with the diagram shown in Fig. 1, and not in agreement with the diagrams reported previously.

A series of experiments were conducted at high indium compositions, in which the constituents were melted, homogenized by stirring, slowly cooled to room temperature, held in a water bath for 30 min at the eutectic temperature, quenched in dry ice-acetone, and then subjected to inverse rate melting analysis. It is noteworthy that a distinct transition was observed at the eutectic temperature at all compositions up to 99 pct In. This result appears to be in contradiction to the French solvus line. It is felt, however, that the hold at the eutectic temperature during sample preparation was not of sufficient duration to insure equilibrium. X-ray diffraction studies are desirable.

Metallography

Both casting and microtome polishing techniques have been found to be satisfactory for Ga-In alloys. Casting has the advantage of more rapid surface preparation and has been used to a larger extent.

In the casting method, the liquid alloy was solidified between clean glass plates. Although liquid gallium wets glass, the solidified alloy may be detached readily from the plates, either on prying with a razor blade or on slight impact by a glass rod. The sides adjacent to the glass plates are found to be in a highly polished condition, and readily adapted to metallographic examination. It is possible that the cast surface is nonhomogeneous because of selective wetting of oxides and alloy, but this film is very thin and may be removed by a suitable etching reagent.

To prevent melting of the polished specimens, the etching solutions were kept in an ice bath. The following etchant, previously developed by Rhines,[2] was found to be quite satisfactory: 50 ml distilled water, 1.5 g potassium dichromate, 5 ml sulphuric acid, 3 ml saturated sodium chloride solution, 20 ml hydrofluoric acid, and 10 ml nitric acid. In order to control the rate of etching, one part of the etching solution was normally mixed with three parts of water. The solution etches glass, and is preferably kept in a wax container. Best results are obtained when it is freshly prepared.

In order to prevent melting during metallographic examination, a small assembly containing dry ice (or other coolant) was placed in direct contact with the specimen. The formation of frost on the polished surface was prevented by enclosing the entire objective assembly and specimen within a plastic cover containing a quantity of desiccant. An alternate and simpler method, applicable during periods of low humidity, was to play a stream of dried

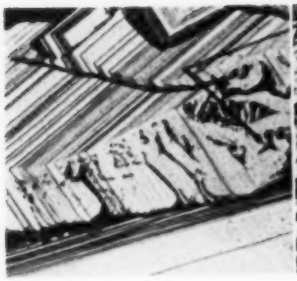

Fig. 2—Pure gallium, unetched. Quenched to —25° C. X110.

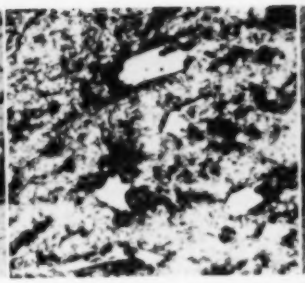

Fig. 3—90 pct Ga-10 pct In, etched. Quenched to —25° C. X200.

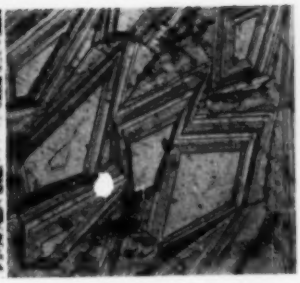

Fig. 4—76 pct Ga-24 pct In, unetched. Quenched to —35° C. X110.

nitrogen on the specimen throughout the entire period of examination.

By treating various Ga-In alloys with the above etching reagent, it was determined that the finely divided eutectic is fast etching, that the indium-rich phase is slow etching, and that the gallium-rich phase is very slow etching. The reported Ga-In eutectic composition (24 pct In) was subsequently confirmed as correct. A 24 pct In sample, homogenized and cooled to approximately 15.7° C and seeded with a small solid particle of the same composition, had only the finely divided eutectic structure.

A characteristic of the gallium-rich structures has been found to be their large grain size. Once seeded, gallium crystals grow at a fairly rapid rate, and the large grain size is therefore attributed to a slow rate of nucleation. Even after quenching in dry ice-acetone mixtures (—78° C), or in liquid nitrogen (—195.8° C), the grains were found to be visible to the naked eye after etching. The liquid nitrogen quench was found to produce the smallest grain size, 1/16 to $\frac{1}{8}$ in. in width and radiating from the edges of the sample inward to the center.

An unexpected result of the metallographic investigation was the observation of striking striations at the gallium-rich compositions. These are apparently associated with the gallium crystal growth process and result from the method of polishing (casting).

Typical micrographs are presented in Figs. 2 through 7. Striations are to be observed in Figs. 2, 4, and 6. Their spacing is apparently a function of the temperature to which the alloys were quenched; the lines were quite dense in specimens quenched to low temperatures, whereas at higher quenching temperatures, they were less numerous, with greater distances existing between adjacent lines.

A typical gallium-rich alloy is shown in Fig. 3, representing the composition 90 pct Ga-10 pct In. The light etching gallium-rich phase is surrounded by a finely divided eutectic mixture; under the microscope, the gallium-rich phase was found to be striated.

A typical indium-rich alloy, shown in Fig. 5, contains elongated indium-rich particles (light) intimately associated with the eutectic (dark). This microstructure contains what appears to be a smaller amount of eutectic than is dictated by the equilibrium diagram. During sample preparation, the indium-rich phase precipitates out continuously as the temperature is lowered below the indium-rich liquidus, whereas the composition of the liquid apparently tends to follow the metastable line shown in Fig. 1. When the supercooled liquid finally solidifies, it is much richer in gallium content than indicated by the stable portion of the diagram, leading to the anomalous structure.

Chemical Analysis Method

A rapid method for the chemical analysis of Ga-In alloys was evolved during the present investigation. As finally developed, the analyst was able to determine the compositions of unknowns within about 0.5 pct, and several determinations could be made in one afternoon. The method is thus preferable, in the case of simple Ga-In mixtures, to the more complex cupferron and tannin methods.

The weighed Ga-In sample is dissolved in nitric acid. To facilitate solution, small amounts of hydrochloric acid may be added, and the acids may be warmed slightly. After the alloy has dissolved, the liquid is boiled to remove any chlorides that may remain; these would otherwise cause subsequent volatization of the indium.

The solution is neutralized with 20 pct NaOH, and a few drops added in excess so as to dissolve the

Fig. 5—70 pct Ga-30 pct In, etched. Quenched to —25° C. X60.

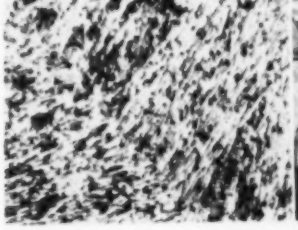

Fig. 6—76 pct Ga-24 pct In, unetched. Quenched to —35° C. X110.

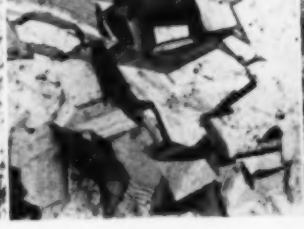

Fig. 7—76 pct Ga-24 pct In, etched. Same area as shown in Fig. 6. X110.

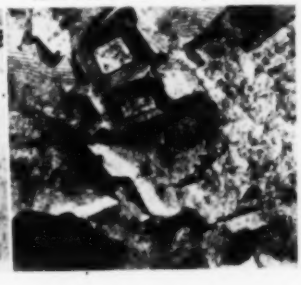

amphoteric gallium. The $In(OH)_3$ precipitate is allowed to settle, is filtered through a fairly coarse filter paper, and washed several times with water. The filtrate and washings may be discarded, or analyzed for gallium.

The precipitate is dissolved from the paper with dilute nitric acid, and the paper washed thoroughly with water. The solution is brought to a boil and reprecipitated with ammonia solution in slight excess. After settling, it is filtered through the same paper and washed thoroughly with water. The precipitate and paper are charred slowly in a tared porcelain crucible (not platinum), the temperature is gradually raised, and a final ignition is given over the full blast. The crucible is cooled in a desiccator and weighed, the difference in final and tare weights is the indium oxide, In_2O_3.

$$\text{Calculation: } \frac{\text{Wt } In_2O_3 \times 82.7}{\text{Wt Sample}} = \text{Pct In}$$

Summary

The constitution of the system Ga-In has been studied using thermal and metallographic methods. In contrast to the previously reported diagrams, the indium-rich liquidus is found to be concave downward from approximately 70 pct In to the eutectic. Metastable experimental points have been determined along the extension of the indium-rich liquidus. The gallium-rich liquidus, eutectic temperature, and eutectic composition are found to be in reasonable agreement with the investigation of French and coworkers. The eutectic point is located at 15.7 C and 24 pct In.

Metallographic techniques applicable to the study of those alloys which are liquid at room temperature have been developed and are described. A rapid method for the chemical determination of Ga-In alloys is presented.

Acknowledgments

The present investigation was sponsored by the Office of Naval Research as Project NR 052 109, Contract N7 onr 451, Task Order II. The authors gratefully acknowledge the contributions of George D. Barnes, who assisted in the metallographic and thermal analysis work, and W. J. Savournin, who is responsible for the chemical analyses. The spectroscopic analyses have been determined by Harold R. Bradford, of the University of Utah.

References

[1] Fred Schulman: Gallium Steps Out. Monthly Research Report of U. S. Office of Naval Research. (January 1948).

[2] W. N. Hartley and H. Ramage: The Wide Dissemination of the Rarer Elements and the Mode of Their Association in Common Ores and Minerals. *Journal* Chem. Soc. (1897) **71**, pp. 533-550.

[3] Lecoq de Boisbaudran: Alloys of Indium and Gallium. *Comptes Rendus* Acad. Sci. (1885) **100**, pp. 701-703.

[4] M. Hansen: *Aufbau der Zweistofflegierungen*. (1936).

[5] S. J. French, D. F. Saunders, and G. W. Ingle: The System Gallium-Indium. *Journal of Physical Chemistry* (1938) **42**, pp. 265-274.

[6] W. F. Roeser and J. I. Hoffman: Freezing Point of Gallium. Bur. Stds. *Journal of Research*, R. P. 735 (1934) **13**, pp. 673-676.

[7] W. Roth, I. Meyer, and H. Zeumer: Atomic Heats, Heats of Fusion and Heats of Transition for Gallium, Indium, and Thallium. *Ztsch. anorg. allgem. Chem.* (1933) **214**, p. 316.

[8] F. N. Rhines, W. M. Urquhart, and H. R. Hoge: Constitution of the System Indium-Tin. *Trans.* A.S.M. (1947) **39**, pp. 694-712.

Technical Note

Secondary Recrystallization Texture in Copper

by M. Sharp and C. G. Dunn

THE orientations of 137 crystals of copper produced by secondary recrystallization in a cube texture matrix have recently been obtained. Although the crystals were not prepared for the purpose of determining a secondary recrystallization texture, the orientations obtained proved to be rather interesting, as they confirmed, in part, published results and also disclosed additional preferred orientations in the texture.

The investigation of Dahl and Pawlek,[1] Bowles and Boas,[2] and Kronberg and Wilson[3] showed respectively that the orientations of secondary grains growing in a cube texture matrix were related to those of the primary grains by a rotation of approximately 30° about [001], the rolling direction, by 30° about a <111> direction, and by either 22° or 38° about a <111> direction. Kronberg and Wilson also obtained a component of the texture similar to that of Dahl and Pawlek except the angle of rotation about [001] was 19°. When the cube texture matrix was deformed a small amount, Kronberg and Wilson also obtained large grains on subsequent annealing corresponding to a rotation of 15° about the normal to the sheet, but these grains should not be classified as secondary recrystallization grains since they were produced subsequent to mechanical straining.

The particular texture obtained, of course, depends on the composition of the copper and the processing schedule employed, since these factors markedly affect the primary recrystallization texture and the sharpness of any cube texture produced. In the present investigation, pieces of OFHC copper in the form of ½ in. round bars were cold forged to a thickness of about 0.40 in., annealed 1 hr at 350°C in an atmosphere of hydrogen, and cold rolled crosswise to a thickness of 0.200 in. These pieces were given a penultimate anneal of 1 hr at 350°C in hydrogen and a 90 pct cold-rolling reduction lengthwise to a thickness of 0.020 in. Indentations generally were put in one end of the as-cold-rolled strips to promote earlier formation of secondary grains.

M. SHARP and C. G. DUNN are associated with General Electric Co., Pittsfield, Mass.

TN 99E. Manuscript, Sept. 24, 1951.

This work was supported by the U. S. Atomic Energy Commission under Contract No. W-31-109-Eng-52.

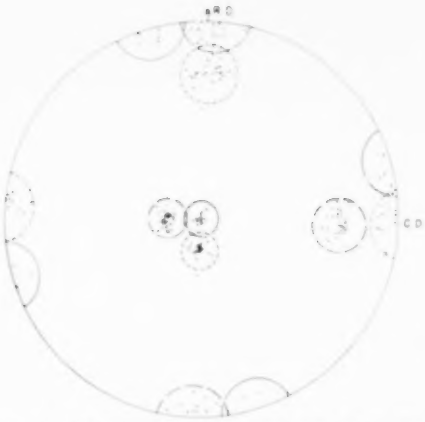

Fig. 1—{100} poles of 61 crystals related to the cube texture by rotations about <100> axes.
Circles with long dash lines — Component *A*
Circles with short dash lines — Component *B*
Circles with solid lines — Component *C*

Specimens were lowered at a speed of ½ cm per hr through a high temperature gradient into a furnace operating just below the melting point of copper. Under these conditions growth of secondary grains occurred at temperatures near 1050 C. The cold-rolled structure recrystallized at lower temperatures, of course, to a matrix of small grains of about 0.1 mm diam and, according to X-ray and micrographic data, had a strong cube texture plus a small amount of twinned structure.

During growth of the large grains, twinning and even repeated twinning occurred. Twins often formed as narrow lamellae; at other times they became large grains. X-ray data were taken only of the large crystals, i.e., those of 15 mm to several centimeters length.

Plots of the cube poles for each of the 137 crystals were made and the texture determined. Results showed that the texture consisted of a number of preferred crystal orientations, which could be simplified by combining those of the same kind.

Fig. 1 shows three kinds of preferred orientations designated in the legend by the letters *A*, *B*, and *C*. In this and in Fig. 2 circles of 10° radius are used to show the sharpness of each component of the texture. Component *A* consists of 30 crystals that are related to the cube texture by a rotation of 21° about R.D. or [001]. Component *B* contains 24 crystals that correspond to a rotation of 18° about C.D. or [010]. This is a new preferred orientation. Component *C* contains 7 crystals that correspond to a 19° rotation about the normal to the sheet or [100]. The three preferred orientations *A*, *B*, and *C*, therefore, correspond to rotations of approximately 19° about <100> axes of the cube texture and comprise a complete set of such possible orientations. In crystallographic terms *A*, *B*, and *C* have the orientations (130) [001], (130) [310], and (100) [013] respectively. The first of these agrees well with the data of Kronberg and Wilson.

Fig. 2 shows 59 crystals related to the cube texture by an average angle of rotation about a <111> axis of 28°. This result agrees with the 30° value reported by Bowles and Boas.

Within the accuracy employed so far, the orientations of the remaining 17 crystals may be described as twins of the above orientations. Seven crystals in orientations of the form (212) [547], are related to component *C* of Fig. 1. They may be derived from the cube texture by a rotation of 54° about the axis [375]. Others that were twin-related to components *A* and *B* of Fig. 1 had the orientations (815) [122] and (574) [221] or had these after a 90° rotation about the normal to the sheet. They could be derived from the cube texture by a rotation of 54° about an axis of the type <357>. Finally, there were a few crystals in twin orientation to the preferred orientation given in Fig. 2. These could be derived from the cube texture by a rotation of 47° about a <523> axis.

If the above texture had been determined by {200} and {111} pole figure plots, as is done for fine-grained materials, it might wrongly be concluded that there were some cube orientations present (contribution from the 61 crystals of Fig. 1 or the 59 crystals of Fig. 2 respectively).

Regarding orientations for good growth in a cube texture matrix, the present results show that there are several and that these require four different types of axes to relate them to the cube texture.

The orientations obtained represent a larger number than have been reported by other investigators. The reason for this is not clear, but the use of indentations in the present work may account for part of the differences. On the other hand, significant differences in texture, regardless of cause, in themselves indicate differences in the orientations of grains that grow (active nuclei) and, therefore, a lack of randomly oriented nuclei in the cube texture matrix that become restricted to a limited number of active ones by a selective growth process. This is not to say that selective growth plays no significant role. It means, however, that one begins to explain the results obtained in terms of a restricted number of available nuclei.

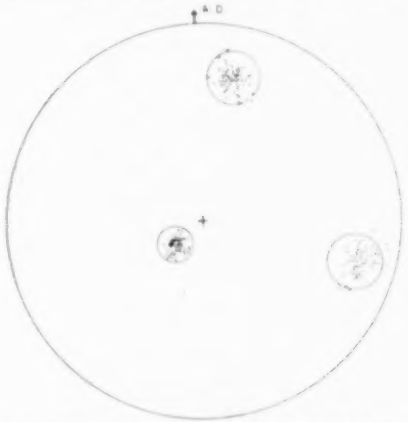

Fig. 2—{100} poles of 59 crystals related to the cube texture by rotation about a <111> axis.

References

[1] O. Dahl and F. Pawlek: *Ztsch. Metallkunde* (1936) **28**, p. 266.

[2] J. S. Bowles and W. Boas: *Journal* Inst. Metals (1948) **75**, p. 449.

[3] M. L. Kronberg and F. H. Wilson: *Trans.* AIME (1949) **185**, p. 501; JOURNAL OF METALS (August 1949).

Solidification Mechanism of Steel Ingots

by H. F. Bishop, F. A. Brandt, and W. S. Pellini

The solidification mechanism of experimental steel ingots (7x7x20 in.) was studied by thermal analysis. It was determined that solidification proceeds in wave-like fashion at rates which are determined by the carbon level, superheat, and mold thickness. The thermal cycles of the mold walls were related to the course of solidification.

DESPITE marked advances in the field of solid state transformation, metallurgical research has contributed comparatively little exact quantitative data on the mechanism of solidification of metals. There is, therefore, a great need for such data in the various metallurgical industries.

The mechanics of solidification of ingots have been investigated in the past primarily by studies of the rate of skin formation as indicated by bleeding or "pour out" tests. The "pour out" method, however, is a tool which gives only approximate information. In the case of alloys with wide solidification ranges, such as irons and certain nonferrous alloys, the method will not work at all; in the case of alloys of intermediate solidification ranges, such as commercial steels, the information may be misleading. Thus, the general adoption of this method has resulted in divergent conclusions regarding the solidification process.

Chipman and Fondersmith[1] by means of bleeding tests have shown that the linear growth of a solidifying ingot wall follows a parabola of the general form, $D = K\sqrt{t} - C$, with the start of solidification delayed until superheat is exhausted, as indicated by the constant C. These tests were carried only to a wall thickness of about 5 in. using an ingot of approximately 17x39 in. in cross-section; hence the latter stages of solidification were not studied. Matuschka[2] indicated that linear solidification of ingots is rapid at first, then slow, but toward the end of solidification the rate becomes extremely rapid again. Spretnak's[3] bleeding studies indicated that wall growth is expressed more rigorously by two parabolas, and that their point of intersection corresponds to a change of solidification mode from columnar to equiaxed. Spretnak also showed that the K values of the first parabola are always the same regardless of superheat. Nelson[4] bled ingots of square cross-section and found that linear wall growth is initially rapid but decreases continually until the end of solidification. He also concluded that rate of solidification in ingots of square cross-section increases 2.15 pct for every 10 pct increase in cross-sectional area of the mold. The mold ratios considered (ratio of cross-sectional area of the mold to cross-sectional area of the ingot) were all less than 2 to 1.

The subject of solidification has also been treated mathematically in many cases, but because of the lack of accurate thermal constants and the simplifying assumptions required, as their authors generally acknowledge, they represent only approaches to the actual conditions of ingot solidification.

A third method of studying solidification is the electrical analogue method promulgated by Paschkis[5] and by Jackson and coworkers.[6] This method treats solidification as a heat transfer problem with the solidification cycle synthesized on an electrical circuit. Paschkis in his treatment of solidification considered the fact, which was generally ignored, that solidification of steel is not simply the growth of a plane solid wall but a more complex process occurring over a temperature range as indicated by the constitution diagram. Undoubtedly, the anomalous results obtained by bleeding tests arise from the inability to measure quantitatively this mushy condition. The shape of Paschkis' solidification curves are more nearly in accord with those of Matuschka, in that they indicate rapid linear solidification at the beginning and end of solidification with intermediate solidification occurring at a slower rate. Paschkis indicates a definite lengthening of solidification time with increasing superheat.

Thermal analysis is a direct method providing exact information for all types of metals regardless of solidification range and was thus adopted in the present program to follow the entire course of solidification from the surface to the centerline of the ingots. The method has the added advantage of being adaptable to following the thermal cycle of the ingot mold during the course of solidification.

Fig. 1—Test assembly

Test Methods

The ingots studied were of square cross-section, 20 in. long, tapered from 7 1/4 in. at the top to 6 3/4 in. at the bottom, and fed with a hot top 7 in. in diam and 12 in. high. The molds were uniform in wall

H. F. BISHOP and F. A. BRANDT are Metallurgists and W. S. PELLINI, Associate Member AIME, is Head, Metal Processing Branch, Metallurgy Div., Naval Research Laboratory, Washington, D. C.

Discussion on this paper, TP 3208E, may be sent, 2 copies, to AIME by April 1, 1952. Manuscript, Aug. 13, 1951. New York Meeting, February 1952.

thickness from top to bottom and were made of gray iron containing approximately 3.50 pct C, 2.00 pct Si, and 0.80 pct Mn. To prevent damage to the thermocouples extending into the mold cavity it was necessary to gate the ingots into the bottom as shown in Fig. 1. The ingates were molded in sand and the bottoms of the ingots were also sand instead of the conventional chill.

Temperatures were measured across both the ingot and the mold in a plane at the midheight of the ingot. At this position bottom and riser gradients were essentially eliminated and solidification could be considered unidirectional; i.e. as growth of a solid skin in a direction perpendicular to the vertical mold surface. Steel temperatures were measured by means of Pt-Pt-Rh (13 pct) thermocouples enclosed in $\frac{1}{8}$ in. OD, 1/16 in. ID quartz tubes which extended completely through the ingot and mold (Fig. 2) parallel to and at varying distances from a reference mold wall. All hot junctions were immersed equally in $3\frac{1}{2}$ in. of steel and thus temperature inaccuracies due to conductivity losses along the thermocouple wires were minimized. The $\frac{1}{8}$ in. OD quartz tubes were the smallest which could protect the thermocouples from the erosive action of the metal, and even these softened to some extent and were bowed upward by the buoyant force of the liquid steel. X-ray examination of sections containing the tubes showed, however, that the deformation was never more than 1 in. and was entirely in the vertical plane, so that the beads maintained the correct alignment with respect to the interface.

The temperatures in the ingot molds were measured by means of chromel-alumel couples flash welded to the bottoms of 3/32 in. diam holes which were drilled in the mold wall to the desired distance from the interface. These couples were spaced $\frac{1}{2}$ in. apart along the vertical centerline of one of the mold surfaces near its midlength.

Interface temperatures were measured on both the mold and hot metal side of the interface. The metal interface temperatures were obtained by means of a couple enclosed in a quartz tube which lay against the inner mold surface and extended through the mold in the same manner as the other thermocouple tubes. In this case, however, a protection tube of only 1/16 in. OD was adequate since the metal solidified rapidly at this position. The interface temperature on the ingot mold side was obtained by first drilling a hole through the mold wall until the point of the drill pierced the inside surface. The bead of the chromel-alumel couple was flash welded into this opening so that it was flush with the inside mold surface. The partially exposed bead was then covered with a thin coating of silica wash. Except at this point no mold wash was used in any of the tests; the oxide coating which had formed on the molds when they were cast was not removed and served to prevent welding of the ingots to the mold walls.

The platinum and platinum-rhodium wires were 26 gage, the chromel and alumel wires 28 gage. The ingot temperatures were recorded on a 16 point automatic potentiometer recorder, 1500° to 3000°F scale, with an accuracy of 0.25 pct of full scale and a sensitivity of 0.1 pct. The mold temperatures were recorded on a similar instrument 0° to 2500°F scale. These instruments permitted sequential temperature readings from 16 thermocouple stations within 30 sec. Since in the majority of tests there were not over 8 couples attached to each instrument, readings

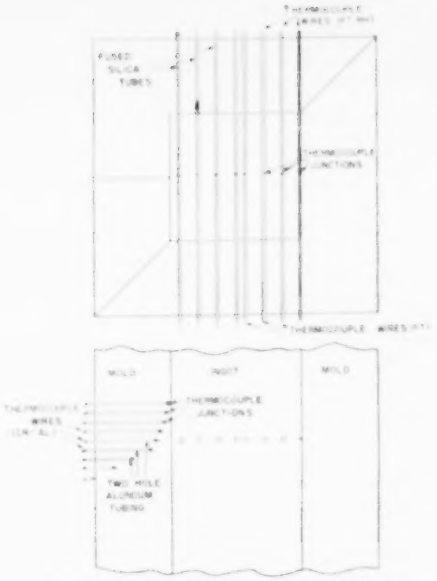

Fig. 2—Thermocouple locations in ingot and mold.

were obtained from each thermocouple on 15-sec cycles. The response characteristics of the thermocouple bead in the quartz tube were studied by sudden immersion into molten steel. Near metal temperatures were reached in approximately 5 sec, and full equalization was obtained in the ensuing 10 sec. It was concluded accordingly that the response to temperature changes which occurred during solidification was of the order of 10 sec.

The effect of the following three variables on solidification were studied: 1—mold ratio (ratio of the cross-sectional area of the mold to the cross-sectional area of the steel ingot); 2—pouring temperature, and 3—carbon content. Specifically, the ingot molds employed had wall thicknesses of $1\frac{1}{2}$, $2\frac{1}{2}$, and $4\frac{1}{8}$ in., thus making the mold ratios approximately 1 to 1, 1 to 2, and 1 to 4. The ingots were poured at three different temperatures (measured in the ladle with a Pt-Pt-Rh immersion couple) which were equivalent to superheats of between 25° and 200°F. The effects of these mold ratio and superheat variations were studied with steels of two nominal carbon contents: 0.08 and 0.60 pct C. The steels were melted in a 1000 lb induction furnace and 0.10 pct Al was added to the ladle as a final deoxidizer. Liquidus and solidus temperatures were determined from inverse rate cooling curves of the couple located at the center of the ingot. These curves were determined by plotting the time required for the temperature to drop consecutive steps of 5°F. It is estimated that the accuracy of the liquidus and solidus determinations was ±3°F. The solidus in these experiments represents a "technical solidus," indicating essential solidity except for possible thin films of interdendritic liquid metal, the solidification of which cannot be determined thermally.

Temperature Distribution in Ingot and Mold

Figs. 3a and 4a show the temperature cycles at various locations in the 0.60 pct C steel ingots and

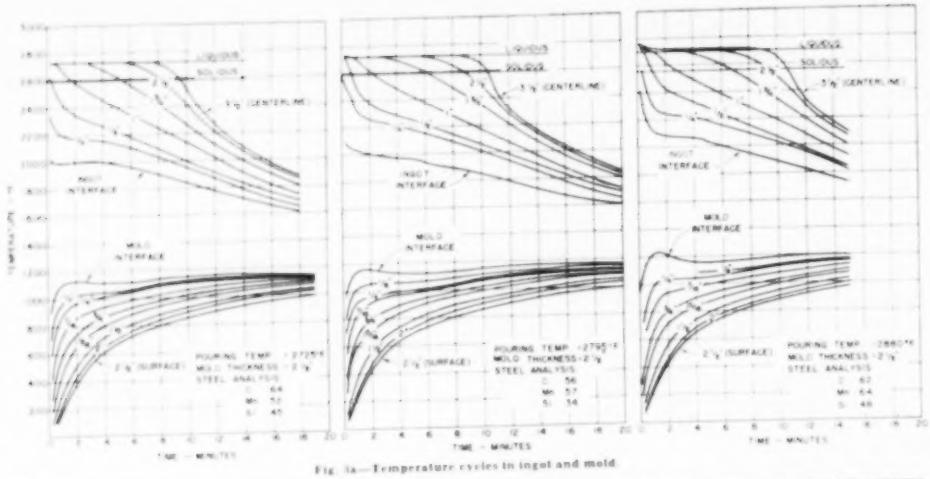

Fig. 3a—Temperature cycles in ingot and mold.

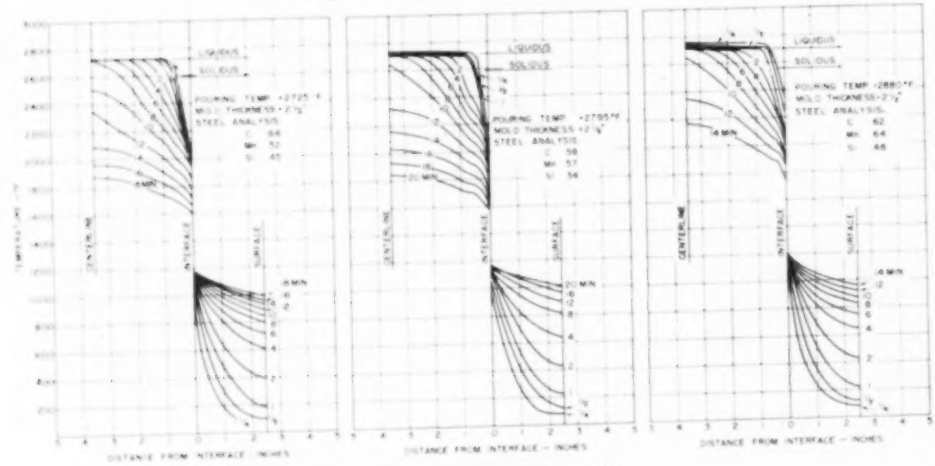

Fig. 3b—Thermal gradients in ingot and mold.

Fig. 3—Superheat series for high carbon steel.

mold walls during the solidification process. These data are replotted in Figs. 3b and 4b to show the thermal gradients from the casting centerline to the outer edge of the chill wall at various times after pouring. Fig. 3 illustrates the thermal effects resulting from increasing superheat and Fig. 4 of increasing mold wall thickness. Figs. 5 and 6 show similar data for 0.08 pct C steel ingots.

Thermal Course of Mold Walls. It is apparent from Figs. 3 and 5 that the superheat condition has relatively little effect on the thermal course of the mold walls. Temperature differences can be observed mainly at the mold interfaces for the first 2 min after pouring. This is due to the initial temperature differences in the metal in contact with the mold. The higher pouring temperature is reflected in a higher rate of heating and a higher maximum temperature at the interface. The differences are greatly reduced in the later stages of the solidification process.

Variations in the volumetric thermal capacities of the mold walls, however, develop pronounced effects on the entire thermal course of the walls. Figs. 4 and 6. The effects are not marked during the period of initial surface heating of the walls, for during this period the walls are heated appreciably only near the interface. At this stage all of the walls, $1\frac{1}{2}$ to $4\frac{1}{8}$ in. thick, behave essentially as if of the same thickness. However, as solidification proceeds and general heating occurs throughout the walls, the various volumetric heat capacities of the mold walls begin to be reflected markedly in the thermal course of the mold walls.

The first indication of the heat capacity effect is shown by the timing and nature of a thermal disturbance at the interface due to the formation of an air gap. In the systems with the thinnest walls this disturbance is developed at approximately 1 min after pouring, as indicated by inflections in the thermal course of the ingot and mold interfaces. The systems with the intermediate and large size molds undergo a gradual temperature reversal in the chill side at about $1\frac{1}{2}$ min. When the air gap forms in

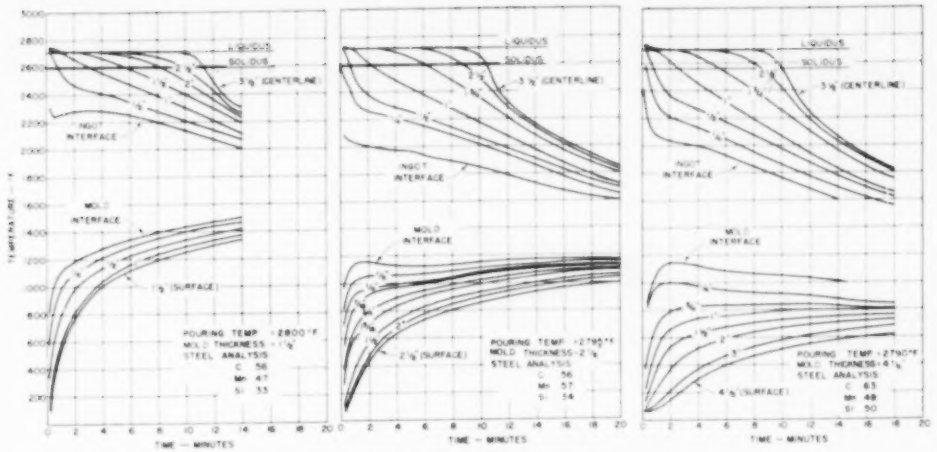

Fig. 4a—Temperature cycles in ingot and mold.

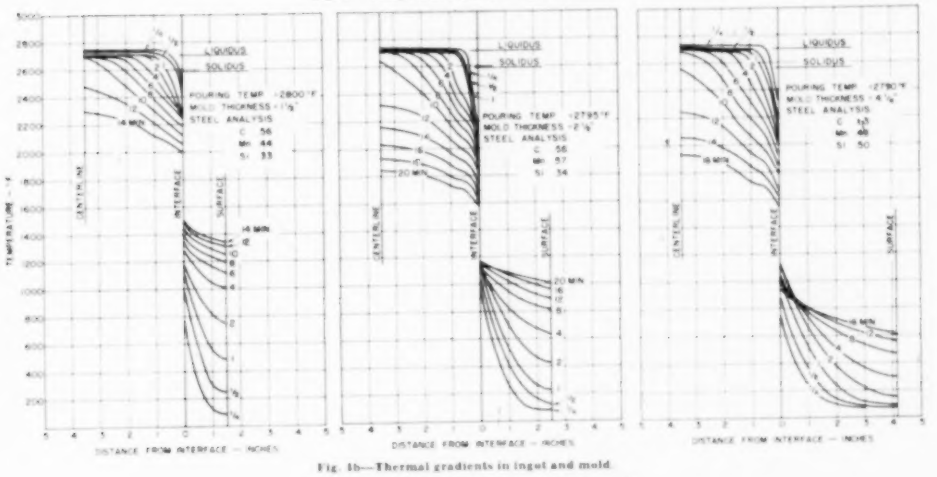

Fig. 4b—Thermal gradients in ingot and mold.

Fig. 4—Mold thickness series for high carbon steel.

these systems, the cooling rates of the ingot side of the interfaces are markedly reduced. That these temperature disturbances are the result of air gap formation was verified experimentally by pouring a similar ingot against a $2\frac{1}{2}$ in. thick mold with a 45° tilt such that the bottom face remained in continuous contact with the mold, while the opposite side could shrink away to form an air gap. The mold interface temperature on the top side fell when the air gap formed, but on the bottom side it climbed steadily throughout solidification.

The air gap times noted in these experiments are in close agreement with the air gap time found by Matuschka[7] in a 0.65 pct C, 10 in. diam ingot cast into a mold having walls $3\frac{3}{8}$ in. thick. Matuschka found that an electrical circuit through the mold and the ingot was broken by the air gap 1 min and 25 sec after pouring.

The fact that an air gap forms earlier with thin molds than with thick molds is ascribed to the more rapid heating of the thin mold, which then expands and pulls away from the ingot.

Following the stage of air gap formation with its consequent drop in rate of heat transfer across the interface, further indications of the relative heat capacities of the mold walls are provided by the temperature course of the various mold walls. The thinnest mold wall shows insufficient heat capacity to prevent continued rapid heating throughout the entire wall. The intermediate mold wall has sufficient heat capacity to maintain an approximately constant interface temperature, while the heaviest is over-sufficient in that the interface temperature falls.

An indication of the relative heat capacities of the three mold wall sizes can be made by comparing outer surface temperatures at a given time. For example 2 min after pouring, the surface temperature of the $1\frac{1}{2}$, $2\frac{1}{2}$ and $4\frac{1}{8}$ in. molds, Fig. 6, are 770°, 425°, and 140° F, respectively.

Solidification Course of Ingots

For a basic understanding of the process of solidification from mold walls, it is essential to consider the nature of heat transfer from the ingot to the

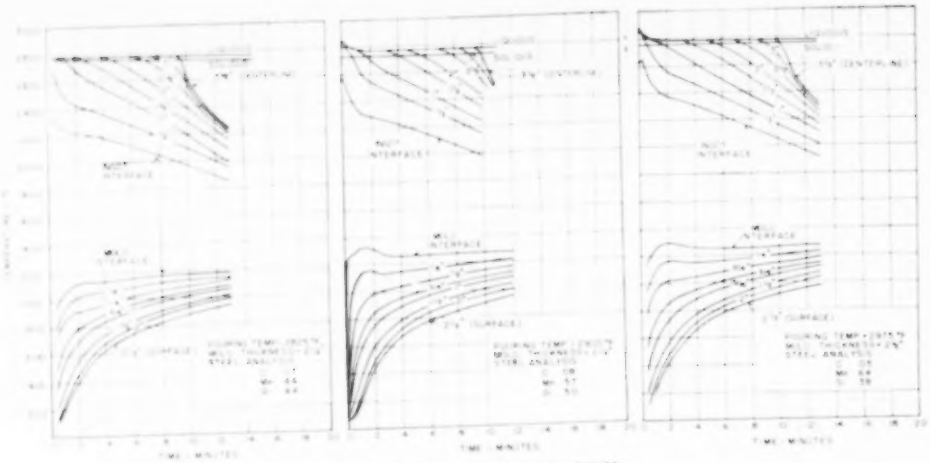

Fig. 5a—Temperature cycles in ingot and mold.

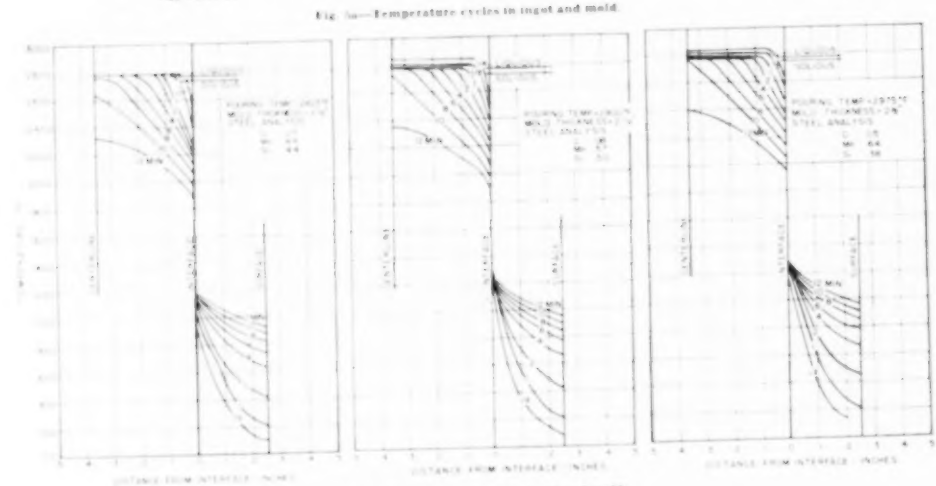

Fig. 5b—Thermal gradients in ingot and mold.

Fig. 5—Superheat series for low carbon steel.

mold. This may be deduced from the shape of the thermal gradient curves shown in Figs. 3 to 6. It is recognized that heat from three sources is metered from the ingot to the mold during solidification: 1—specific heat of liquid metal, 2—heat of solidification, and 3—specific heat of the solid metal which has already formed. The nature and progression of solidification at any given time is governed by the rates at which these various heat components are metered to the mold.

It will be noted from Figs. 3 to 6 that the usual continuous thermal gradients generally associated with heat flow are disturbed by the formation of a "knee" in the temperature range of transformation from liquid to solid. The abrupt change in gradients at the knee is due to the necessity of removing heat of solidification from this zone before the thermal gradients can move inward. The knee zone thus represents a band of active solidification which forms a "thermal block" to the central liquid portion of the ingot. The development of this thermal block occurs early in solidification during the formation of the initial skin on the mold wall. Since the solidification knee zone becomes established at and below the liquidus temperature, it will not act to block the specific heat of the metal above that temperature. Thus, during the formation of the initial skin at the wall surface, the superheat of the liquid metal is simultaneously metered out at a very rapid rate, as indicated by the short time required for the gradient curves in the central portion of the casting to reach the liquidus temperature. It will be noted for example that the 180°F superheat in the ingot of Fig. 3 poured at 2880°F is lost in little over a minute and in this time a completely solid skin $\frac{1}{2}$ in. in thickness has also been formed.

Since significant cooling of the central portion of the ingot below the liquidus temperature cannot occur because of the thermal block, the central portion of the ingot gravitates to an essentially isothermal condition at the liquidus temperature and remains as such until reached by the solidification

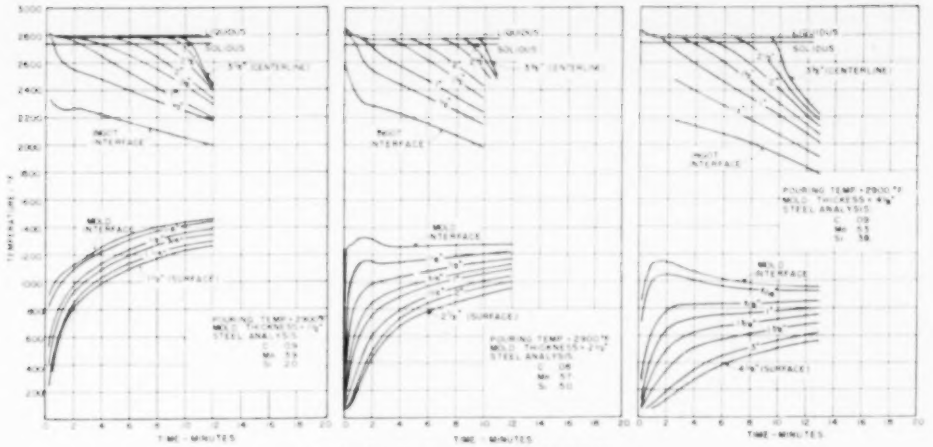

Fig. 6a—Temperature cycles in ingot and mold.

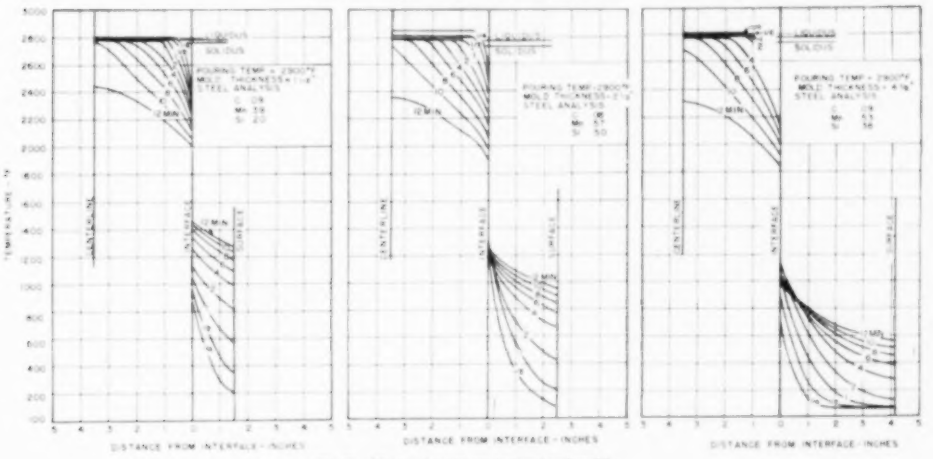

Fig. 6b—Thermal gradients in ingot and mold.

Fig. 6—Mold thickness series for low carbon steel.

knee. The passage of the solidification knee is denoted by a temperature drop which is consequent to the removal of heat of solidification; for example, the center of the ingot poured in the small size mold, Fig. 4, remains near the liquidus temperature until 10 min after pouring; however, in the interval between 10 and 11 min, during which time solidification is completed, a drop of approximately 125° occurs. With the passing of the transformation knee the remaining, now solid, metal on the mold wall side of the knee cools further, thus contributing specific heat of solid to the total flow of heat to the mold. These basic features of solidification are observed to hold for all the test ingots.

The specific contributions of superheat and mold wall thickness to solidification may be observed more readily by replotting the thermal data in terms of the progression of solidification waves or "fronts" through the ingot. Fig. 7 shows the course of solidification of the high and low carbon steel ingots thus summarized from the thermal data of Figs. 3 to 6. The progression of the forefronts and ends of the knee zones, which represent the position of the two freezing waves, are shown as "start of freeze" and "end of freeze" curves respectively. These data are also plotted on square root of time basis in Fig. 8.

The effects of superheat and mold thickness on the course of solidification are shown in both the "start" and "end" curves; the specific effects being similar for both curves but somewhat more pronounced for the "end" curves. Thus, in order to simplify discussion, and because of the greater practical significance of the "end of freeze" curves, further discussion will be restricted to the wave of complete solidification.

It was observed earlier from the gradient curves that superheat is lost rapidly during the stage of initial skin formation. Since the mold has a limited capacity for accepting heat, the presence of superheat necessitates a reduction in the flow of solidification heat. The bottom graphs of Fig. 7 show that this is reflected in decreased initial rates of solidification. Following the complete release of superheat the rates of solidification of all ingots of a given

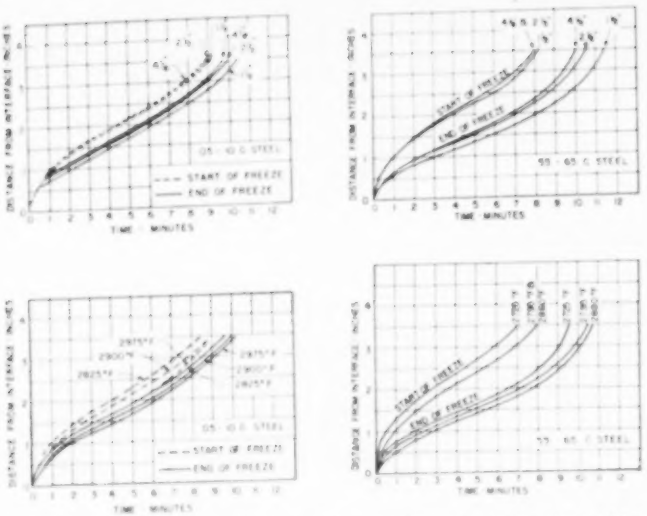

Fig. 7—Effect of mold ratio (upper graphs) and superheat (lower graphs) on linear progression of solidification.

carbon level become essentially equal regardless of initial superheat, i.e. the solidification curves are thereafter displaced by a time interval which is proportional to the amount of initial superheat. This time displacement is retained throughout the remainder of solidification. For the high carbon steel an increase in superheat from 25° to 180°F increases solidification time approximately 13 pct (9.5 to 10.7 min); for the low carbon steels an increase in superheat from 50° to 200°F increases solidification time approximately 6 pct (9.8 to 10.4 min).

The volumetric heat capacities of the mold walls also affect solidification as shown in top graphs of Fig. 7. During the first ½ min the solidification rates of the three ingots in each series are identical. This should be expected inasmuch as during this period only the mold wall surfaces are heated, hence all act as of infinite thickness. After the first ½ min the solidification of the ingots in the lowest heat capacity mold wall (1½ in.) becomes slower. The solidification rates of the high carbon steel ingots in the two larger molds (2½ and 4½ in. walls) are identical for the first 4 min after which the rate for the intermediate 2½ in. wall becomes somewhat slower. This divergence is not as pronounced in the low carbon ingots, the solidification rates in the two larger molds remaining essentially the same throughout the entire process. It is noted for the high carbon steels that the time of total solidification is decreased approximately 13 pct (11.5 to 10 min) by increasing the chill thickness from 1½ to 4½ in. Increasing the chill thickness from 1½ to

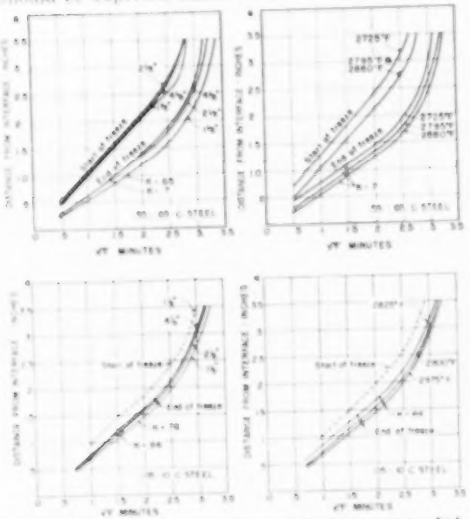

Fig. 8—Linear progression of solidification showing extent to which the parabolic relationship [illegible] is valid. Superheat, upper graphs, and mold ratio, lower graphs.

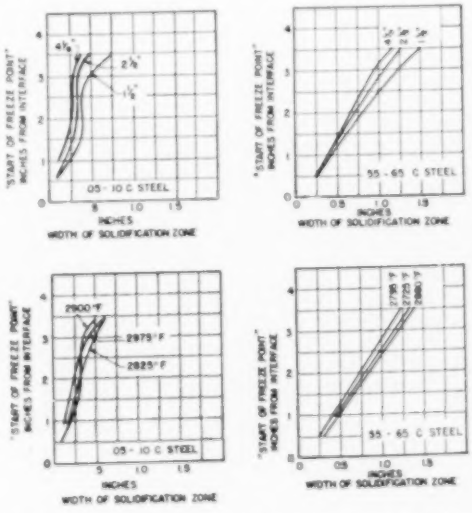

Fig. 9—Effect of mold ratio (upper graphs) and superheat (lower graphs) on width of solidification band.

$2\frac{1}{2}$ in. decreased the solidification time by approximately 9 pct (11.5 to 10.5 min) while an increase from $2\frac{1}{2}$ to $4\frac{1}{8}$ in. further decreased this time only 5 pct ($10\frac{1}{2}$ to 10 min), thus indicating rapidly diminishing returns in this mold ratio range. A similar trend is noted in the low carbon steels.

While variations of chill thickness or of superheat may have approximately the same effect on the time for final solidification, the mechanisms by which this time difference is developed are markedly different. The retarding effect of low heat capacity mold walls does not begin until after considerable solidification has occurred and then becomes increasingly greater as solidification progresses, while the superheat effect retards the solidification process only during the initial stage of solidification.

From Fig. 8 it can be seen that growth becomes approximately parabolic soon after pouring. However, when the wall has solidified for approximately half of its total thickness, growth rates deviate rapidly from the parabolic condition. These solidification curves have shapes very similar to those indicated by the work of Matuschka and Paschkis.* The constants for the period of parabolic relationship ($d = k\sqrt{t}$) are indicated on the curves of Fig. 8. If the straight line portions are extrapolated back (as a straight line) to zero thickness, the superheat delay factor C of the classic solidification formula $d = k\sqrt{t - C}$ may be deduced. The effect, however, is not a simple initial postponement in the start of freezing as predicted by this formula, but rather is one of decreasing solidification rates due to the presence of superheat as shown by the various curves of Fig. 7. Thus, the delay factor has physical significance only after superheat has been eliminated completely and a fixed lag in the progression of solidification has been established. The lag is retained essentially without change to the end of solidification.

It was observed that solidification of steel from metal, the term "wall thickness" or "skin thickness"

* Similar studies for sand mold walls (ref. 10) indicate a general rather than a "band" solidification mechanism for the solidification of the same steels and ingot sizes.

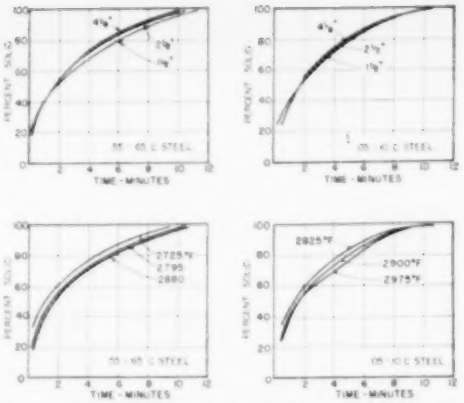

Fig. 10—Effect of mold ratio (upper graphs) and superheat (lower graphs) on volumetric progression of solidification.

ceeds as a band of solidification by the simultaneous travel of "start" and "end of freeze" waves. The space separation of these two waves is relatively narrow, hence the solidification process consists basically of the movement of the solidification band from the mold wall into the near-isothermal liquid which is retained essentially at the liquidus temperature. However as the solidification zone moves inward, the perimeter of the liquid center decreases and the width of the solidification zones increases as shown in Fig. 9. It can be noted for the high carbon steel that the solidification zone widths in the ingots of the pouring temperature series are approximately the same at comparable locations, the maximum difference being about $\frac{1}{8}$ in. However in the mold ratio series of both steels there is a difference of as much as $\frac{3}{8}$ in. in zone widths of the ingots cast in the smallest and largest molds.

Because of the presence of the solidification zone, which represents a mixture of liquid and solid metal, the term "wall thickness" or "skin thickness"

Pouring temperature 2880°F. Pouring temperature 2795°F.

Fig. 11—Effect of pouring temperature on macrostructure of 0.60 pct C steel ingots.

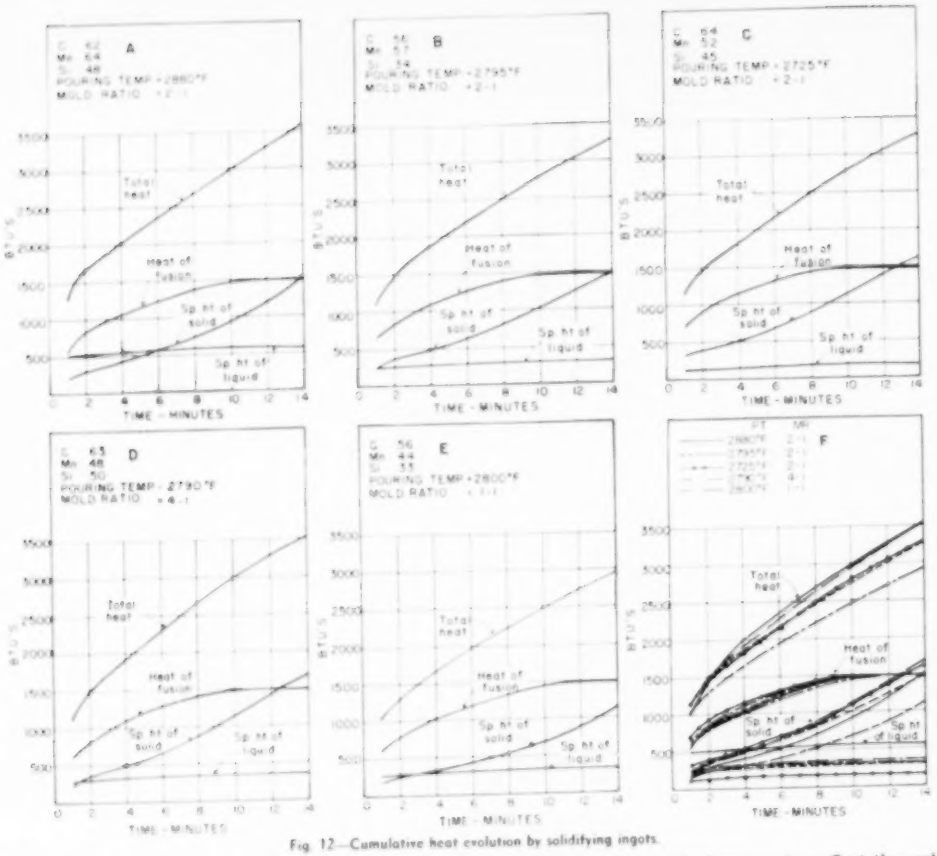

Fig. 12—Cumulative heat evolution by solidifying ingots.

in describing solidification phenomena of steel ingots is ambiguous. Furthermore, the constantly decreasing solidification perimeter as solidification progresses toward the center of the ingot results in possible misleading conceptions of solidification when linear rates alone are considered. Accordingly, the volume rate of solidification, including the solid which is present in the mushy region, was determined for the various ingots and plotted in Fig 10. It will be noted from these curves that the volume rates of solidification constantly diminish during the solidification cycle, whereas linear rates of solidification become very rapid at the end of freezing cycle. The increased rates of linear solidification result from the increased proportion of solid developed in the central regions (general solidification) as the "end of freeze" wave moves toward the center and also from the decreasing perimeter of the solidification front which gravitates to a point as the center is approached. The increase in linear rates is, however, insufficient to prevent a decrease in volume rates resulting from a decreasing perimeter. It is of interest to note that half of the liquid metal becomes solid in approximately 1½ min, while an additional 8 to 10 min is required for the last half of the liquid to solidify.

Variations in thickness of chill wall were found to have no significant effect on the macrostructural characteristics of the ingot. Increasing superheat, however, produced a marked coarsening effect throughout the ingot. Fig. 11 shows typical macrostructures of the high carbon ingots resulting from variations in superheat. It is hypothesized that the fine structures present when superheat is low result from the formation of many small crystallites during pouring which are uniformly distributed throughout the liquid and serve as nuclei or centers of growth as the "start of freeze" wave moves through the casting. With high superheat fewer nuclei are developed, hence the start of the freeze wave moves through comparatively nuclei-free liquid providing conditions for the growth of fewer but larger crystals.

Heat Transfer in Solidifying Ingots

Fig. 12 shows the cumulative amounts of the various heats (the determination of which is given in the appendix)—liquid and solid specific heats and heat of fusion—which are liberated from a 1 in. thick segment at the midheight of each of the high carbon steel ingots. The heat of fusion curves are, of course, the same as the volume solidification curves plotted as Btu's rather than percent. While the rate at which heat of fusion is liberated diminishes with time, the rate at which heat is liberated from the metal that has already solidified increases and nearly balances the diminishing rate of heat evolved by solidification. Thus the rate of total heat evolved from an ingot after the air gap is formed is nearly constant.

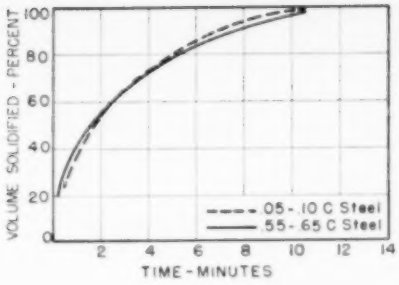

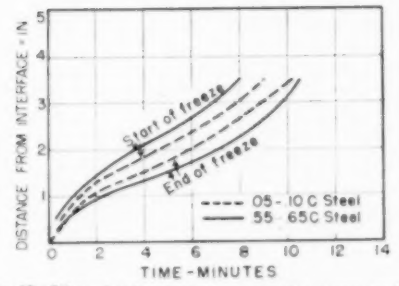

Fig. 13—Effect of carbon content on volumetric (upper graph) and linear (lower graph) progression of solidification.

Most of the liquid specific heat is lost very early as superheat and the small amount remaining is lost as the liquid cools into the mushy region.

The heat evolution curves of the various ingots are plotted in one group, Fig. 12F, in order to afford an easier quantitative comparison. It is noted that there is a marked spread between ingots only in the amounts of total heat and of specific heats of liquid and solid metal evolved. The spread between the heat of fusion curves is relatively nil. The heat components of ingots poured at the same temperature into molds of small and large mold ratios indicate interesting relationships. More total heat is absorbed by the heavy mold than by the thin mold at any given time, but this extra heat is specific heat from the solid metal which has already solidified. Similarly when the mold ratios are the same and superheat is varied, more total heat is absorbed by the mold when superheat is high. This extra heat is primarily specific heat of liquid. Thus while thin molds and high superheat prolong solidification times, these differences are not as great as would be expected from a consideration of only the heat capacities of the molds or the initial heat within the liquid metal.

Effect of Carbon Content on the Solidification

The wide range of carbon contents between the two steels studied permits evaluation of the combined effect of differences in phase transformation, temperature range of solidification, and temperature level of solidification on the solidification mechanism of steel ingots. The 0.08 pct C steel solidifies to δ iron over the temperature range of 2775° to 2740°F (35°F) while the 0.60 pct C steel solidifies to γ iron over the range of 2700° to 2570°F (130°F).

A complete evaluation of the carbon effect necessitates consideration of the entire course of solidification. As discussed in the foregoing sections solidification proceeds by the development and movement across the ingot of three distinct zones: 1—a completely solid zone adjacent to the mold wall, 2—a completely liquid zone at the center of the ingot, and 3—a solidification zone located between zones 1 and 3 which is a mixture of liquid and solid metal. It should be noted that variations in the temperature range of solidification arising from differences in carbon contents affect only the relative widths of the three zones leaving the basic mechanism of solidification essentially unchanged.

The major effects of variations in the temperature range of solidification are illustrated in the linear and volumetric solidification curves of the high and low carbon steel ingots poured at intermediate temperatures into molds of 2 to 1 mold ratio, Fig. 13. It may be noted from the linear curves that at comparable times in the solidification process the "start of freeze" front in the high carbon steel is more advanced and its "end of freeze" front is less advanced than the comparable fronts of the low carbon steel. While the "start of freeze" front of the high carbon steel is active, the rate of travel of the "end of freeze" front of the high carbon steel is slower than that of the low carbon steel. During this period, as can be seen at the bottom of Fig. 13, the separation of the "end of freeze" waves of the two steels is constantly increasing. However, with the completion of the "start of freeze" wave the central portion of the high carbon steel ingot is in a partially solid condition with the consequent result that the "end of freeze" wave thereafter moves forward at a more rapid linear rate than that of the low carbon steel. After completion of the "start" wave the relative rates of travel of the "end" waves for the two steels are reversed as should be expected.

Despite the differences in distribution of solid within the two ingots freezing over wide and narrow solidification ranges, Fig. 13 (lower graph), the volumetric solidification rates are very nearly alike as shown in the top graph of Fig. 13. The high carbon steel requires a slightly longer time (approximately 5 pct) to complete solidification than does the low carbon steel poured under comparable conditions of superheat and mold ratio, as shown in Fig. 14. This is ascribed in part to the lower temperature differential between the mold and metal for the high carbon steel which results in a lower rate of heat transfer, and also to the fact that the high carbon steel, in

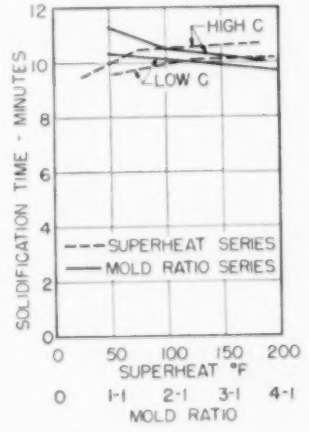

Fig. 14—Effect of carbon content, mold ratio, and superheat on solidification time.

solidifying over a temperature range of approximately 130 F must liberate concurrently with heat of fusion more specific heats of both the liquid and solid components of the metal within this temperature range than the low carbon steel which solidifies over a range of only 35 F.

Conclusions

1—The lateral solidification of steel in ingot molds is characterized by the simultaneous travel of "start" and "end of freeze" fronts by encroachment into liquid which remains essentially isothermal at the liquidus temperature. The space separation of these fronts, which indicates a zone of intermixed liquid and solid, is proportional to the width of the liquidus to solidus temperature range and, within limits, inversely proportional to mold ratio.

2—Linear solidification rates based on "end of freeze" are parabolic only during approximately the first half of the solidification cycle, after which there is a rapid deviation from the parabolic condition. The classic relationship thickness $= K\sqrt{\text{time}}$ applies only to this first stage. The K values of the parabolic relationship increase as the carbon content decreases.

3—Ingots of 7x7 in. cross-section solidified completely in 10 to 12 min within the limits of carbon content, superheat, and mold thickness investigated. These ingots developed an air gap at 1 to $1\frac{1}{2}$ min after pouring with consequent marked temperature fluctuations at the ingot-mold interface.

4—Volumetric solidification rates of 0.08 and 0.60 pct C steels poured under like conditions are closely similar. Linear solidification rates of the low carbon steels are greater during the early period of parabolic progression and slower in the later stages of solidification. This is the result of the difference in widths of the zones of intermixed liquid and solid in the two steels.

5—Superheat is completely liberated at early stages of solidification. During the period of superheat elimination the progression of solidification is retarded. Following this period linear solidification rates become essentially equal irrespective of initial superheat. Increasing superheat produces a general coarsening of the macrostructure.

6—Variations in mold thickness under like conditions of superheat and steel composition have no effect on solidification rates in the very early stages of solidification. At early stages molds of lower heat capacity show reduced rates of solidification. Mold ratio variations in the range of 1 to 1 to 4 to 1 do not affect macrostructure.

7—Heat balance determinations show that following the formation of the air gap the total heat transfer of any particular ingot in a given mold remains essentially constant. A constant rate of heat transfer is maintained by the simultaneous metering of the various heat components (specific heat of liquid, specific heat of solid, and heat of fusion) to the mold as solidification progresses.

Appendix

The various components of the total heat liberated after any time in the solidification process were calculated from the gradient curves shown in Figs. 3 to 6. The following thermal constants were employed:

Specific Heat Liquid Steel	0.2 Btu per lb, °F
Specific Heat Solid Steel	0.165 Btu per lb, °F
Heat of Fusion	117 Btu per lb
Density (Liquid and Solid Steel)	0.26 lb per cu in.

To determine heat of fusion which had been liberated up to any given time it was necessary to determine the amount of solid present not only in the completely solid region which had cooled below the solidus temperature, but also in the mushy region above the solidus temperature. The percentage of solid in the mushy zone of each ingot was determined by averaging the percentage of solid at three equispaced points within the mushy zone. The fractional part of the temperature range between the liquidus and solidus through which each point had cooled was determined from the gradient curves of the particular ingot under consideration. This point was transferred to the comparable location on the Fe-C equilibrium diagram and the percentage of solid was determined by the lever arm relationship.

In calculating specific heats of liquid and solid metal liberated between the liquidus and solidus temperature, where liquid and solid coexist, transformation from liquid to solid was considered as occurring isothermally at a temperature where, according to the equilibrium diagram, the metal was 50 pct liquid and 50 pct solid. This condition exists in 0.55 to 0.65 pct C steels when the metal has cooled to a point below the liquidus equal to one third of the temperature range of solidification.

The heat liberated by the liquid metal as specific heat up to any given time included: 1—superheat, 2—specific heat of the liquid within the mushy region, and 3—specific heat of the solid metal below the solidus temperature which necessarily had to give up specific heat as a liquid within the mushy zone before it solidified.

The cumulative amounts of specific heat liberated by the cooling of solid metal include the heat liberated by the solid at temperatures both within and below the mushy zone. All of the solid present in the ingot at any particular time is considered to have cooled from the 50 pct liquid-50 pct solid point. The heat evolved in cooling below the solidus was obtained by figuratively dividing the ingot element into $\frac{1}{2}$ in. wide concentric rings and from the gradient curves obtaining the mean number of degrees below the solidus that each ring had cooled. This figure for each ring when multiplied by the density and specific heat of the steel, and by the volume of the ring is the specific heat of solid evolved by the ring. The total of the heats evolved by the ingot is equal to the sum of the heats evolved by each ring in the ingot.

References

[1] J. Chipman and C. R. Fondersmith: Rate of Solidification of Rimming Ingots. *Trans.* AIME (1937) **125**, pp. 370-377.

[2] B. Matuschka: The Solidification and Crystallization of Steel Ingots. The Influence of Casting Temperature and Undercooling Capacity of the Steel. *Journal* Iron and Steel Inst. (1931) **124**, pp. 361-386.

[3] B. Matuschka: Solidification in Open Topped and Closed Topped Ingot Molds. *Journal* Iron and Steel Inst. (1938) **137**, No. 1, pp. 109-126.

[4] J. W. Spretnak: Kinetics of Solidification in Killed Steel Ingots. *Trans.* A.S.M. (1947) **38**, pp. 569-676.

[5] L. H. Nelson: Solidification of Steel in Ingot Molds. *Trans.* A.S.M. (1934) **22**, pp. 193-226.

[6] V. Paschkis: Studies on Solidification of Castings. *American Foundryman* (December 1945) **8**, pp. 26-37.

[7] V. Paschkis: Theoretical Thermal Studies of Steel Ingot Solidification. *Trans.* A.S.M. (1947) **38**, pp. 117-147.

[8] R. Jackson, R. Sarjant, J. Wagstaff, N. Eares, D. Hartree, and J. Ingham: Variable Heat Flow in Steel. *Journal* Iron and Steel Inst. (1944) **150**, No. 2, pp. 211-268.

[9] B. Matuschka: Heat Equilibrium Between Ingot and Ingot Mold Wall. *Archiv. f. Das Eisenhuttenwesen* (1929) **2**, pp. 405-411.

[10] H. F. Bishop, F. A. Brandt, and W. S. Pellini: Solidification of Steel from Sand and Chill Walls. *Trans.* Amer. Foundrymen Soc. AFS Preprint No. 51-21 (1951).

Constitution and Properties of Some Iron-Bearing Cupro-Nickels

by E. W. Palmer and F. H. Wilson

The solid solubility of iron in 2 to 10 pct cupro-nickels increases with temperature and nickel content. Property changes accompanying various heat treatments indicate typical precipitation hardening behavior. Iron content also affects softening temperature and subscale formation. These factors, as well as impingement corrosion resistance, influence the optimum iron content of commercial alloys.

FOR many years Cu-Ni alloys have been used extensively in the form of tubes, pipes, and plates for the construction of salt-water lines and surface condensers on shipboard and in tidewater power stations. The 30 pct Ni alloy has been considered more resistant to rapidly flowing sea water than alloys of lower nickel content, and has been standard on ships of the U. S. Navy. Some ten years ago, the still better corrosion resistance obtained by modifying the 30 pct Ni alloy with approximately 0.5 pct Fe was recognized, and the iron-bearing alloy rapidly superseded the plain alloy as the standard material for severe service. In 1945, Tracy and Hungerford[1] published a study of the effect of iron on the corrosion of various cupro-nickels in sea-salt solutions, and their data indicated that the 10 pct Ni alloy containing about 0.75 pct Fe was equivalent to the 30 pct Ni alloy containing 0.5 pct Fe. This was confirmed by LaQue in discussion of the above paper, and by results in an experimental condenser set up at the Kure Beach marine test station of The International Nickel Co., reported by Freeman and Tracy.[2]

The 10 pct Ni iron-bearing alloy is now being very widely used in applications where the 30 pct Ni iron-bearing alloy was formerly considered standard. While this "substitution" has undoubtedly been stimulated by the present extreme shortage of nickel, it must be emphasized that it involves no loss of service performance, and would have occurred anyway in the course of time, for economic reasons. In view of the increasing use of the 10 pct alloy, it seems desirable to make generally available the results of several investigations of Cu-Ni-Fe alloys carried out in the Metallurgical Research Laboratory of The American Brass Co. in recent years.

The present paper deals with the constitution of these alloys in the copper-rich corner of the system, and with the variations in hardness and tensile properties resulting from the heat treatment of alloys containing various amounts of iron. Most of this work is concerned with alloys containing 10 pct Ni. With over about 0.75 pct Fe, the 10 pct Ni alloy is susceptible to precipitation hardening, and the consequences of this in connection with commercial production are examined in some detail.

E. W. PALMER and F. H. WILSON, Members AIME, are Research Metallurgist and Assistant Research Metallurgist, respectively, American Brass Co., Waterbury, Conn.

Discussion on this paper, TP 3203E, may be sent, 2 copies, to AIME by April 1, 1952. Manuscript, Aug. 23, 1951. New York Meeting, February 1952.

Table I. Compositions of Alloys Studied

Series	Alloy No.	Cu, Pct	Ni, Pct	Fe, Pct	Mn, Pct	Total C, Pct
2 Pct Ni						
A	5148	97.93	1.98	0.005	0.08	
	5149	97.85	2.01	0.097	0.09	
	5150	97.72	2.00	0.25	0.09	
	5151	97.44	2.01	0.50	0.08	
	5152	97.22	1.99	0.75	0.09	
	5153	96.94	2.03	1.03	0.08	
	5154	96.45	2.01	1.52	0.09	
5 Pct Ni						
A	5155	95.17	4.78	0.005	0.077	
	5156	94.79	5.01	0.097	0.090	
	5157	94.80	4.92	0.26	0.090	
	5158	95.54	4.92	0.50	0.090	
	5159	94.14	4.99	0.76	0.094	
	5160	93.95	5.03	1.00	0.095	
	5161	93.43	5.04	1.50	0.075	
10 Pct Ni						
B	6788	89.63	9.94	0.11	0.32	0.004
	6789	89.48	9.98	0.21	0.33	0.002
	6790	89.42	9.94	0.30	0.34	0.001
	6791	89.29	9.97	0.41	0.33	0.001
C	6758	89.67	9.98	0.01	0.32	0.017
	6759	89.20	9.99	0.48	0.32	0.010
	6760	89.00	9.95	0.71	0.32	0.016
	6761	88.75	9.97	0.95	0.32	0.014
	6762	88.48	10.00	1.19	0.32	0.006
	6763	88.18	10.05	1.44	0.32	0.006
	6764	87.56	10.14	1.96	0.33	0.008
D	7288	86.56	10.02	3.08	0.34	0.021
	7289	85.69	9.95	4.00	0.34	0.024
	7290	84.78	9.98	4.88	0.32	0.025
E	7423	88.59	10.07	1.03	0.30	0.012
	7424	88.27	10.03	1.46	0.23	0.010

Alloys

Several series of cupro-nickel alloys containing iron were used in these investigations. Most of them were prepared in the laboratory, but two samples of commercially fabricated alloys were included.

Series A—Nominally 2 and 5 pct Ni, each with 0 to 1.5 pct Fe.
Series B—Nominally 10 pct Ni with 0.1 to 0.4 pct Fe.
Series C—Nominally 10 pct Ni with 0 to 2 pct Fe.
Series D—Nominally 10 pct Ni with 3 to 5 pct Fe.
Series E—Nominally 10 pct Ni with 1 and 1.5 pct Fe.

Fig. 1—Vertical section through the solvus surface of the Cu-Ni-Fe phase diagram at 5 pct Ni.

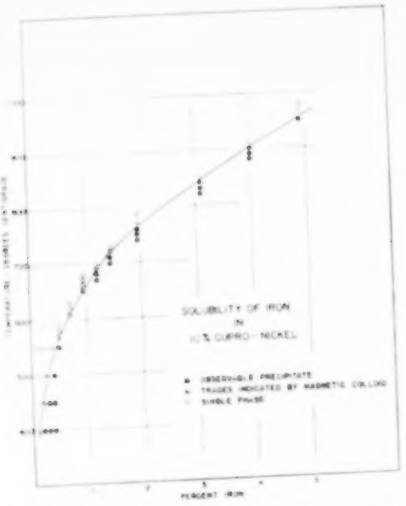

Fig. 2—Vertical section through the solvus surface of the Cu-Ni-Fe phase diagram at 10 pct Ni.

Series A contained about 0.1 pct Mn and the others about 0.3 pct Mn. Series A, B, and D were cast as $\frac{3}{4}$x1$\frac{1}{4}$x6 in. bars, while Series C consisted of 6 in. ingots 2$\frac{1}{2}$ in. square at the bottom and 3$\frac{1}{4}$ in. square at the top, hot forged to $\frac{3}{8}$x3x27 in. bars. Series E was two commercially cast heats, hot rolled to $\frac{3}{4}$ in. thick plate. The compositions as determined by analysis are given in Table I.

For both mechanical tests and for solubility limit studies, Series A bars were scalped, cold rolled to 0.16 in., annealed 1 hr at 800°C, quenched, cold rolled to 0.060 in., annealed 1 hr at 850°C, quenched, and cold rolled to 0.040 in. Series B bars, used only for the phase-diagram studies, were hot rolled at 900°C to 0.2 in., annealed 1 hr at 900°C, quenched, and cold rolled to 0.1 in. For mechanical tests, the forged Series C bars were annealed 2 hr at 900°C, quenched, and fabricated to 0.040 in. by the same schedule as Series A, except that the annealing temperatures were 900°C. Bars $\frac{3}{8}$ in. thick from Series C and D, used for the solubility limit studies, were heated 2 hr at 1085°C, quenched, and cold rolled to 0.1 in.

None of these procedures completely eliminated from alloys of 1 pct or more iron the nonhomogeneous distribution of iron concentration arising from dendritic solidification. It was found possible to make the 10 pct Ni alloys homogeneous by three cycles of alternate cold rolling and annealing for 2 hr at 1085°C, and further samples of alloys requiring this treatment were so processed for equilibrium studies.

Constitution

An understanding of the behavior of the iron-bearing cupro-nickels must necessarily be based on knowledge of the extent to which iron is soluble at various temperatures under equilibrium conditions. Using metallographic techniques, the solid solubility of iron in 5 and 10 pct cupro-nickels containing small amounts of manganese (less than 0.35 pct) has been determined. The results are shown in Figs. 1 and 2 as partial vertical sections of a ternary Cu-Ni-Fe phase diagram. (For the purpose of plotting, the presence of manganese in the alloys has been disregarded.) Isothermal points from these two solubility curves, and data on the solubility of iron in copper from Tammann and Oelsen,[5] provide three points on the ternary diagram defining the limit of iron solubility at a given temperature. The boundaries of the α solid solution at 500°, 600°, 700°, 800°, and 900°C as determined thereby are drawn in Fig. 3.

In their survey of the whole Cu-Ni-Fe diagram as determined by X-ray diffraction studies, Bradley, Cox, and Goldschmidt[7] show peculiar humps in the iron solubility lines in this portion of the diagram, which indicate very much higher solubilities of iron than were found in the present work. It appears that the X-ray diffraction technique must have missed some of the iron-rich phase, for there is considerable evidence, both metallographic and in the response of the alloys to heat treatment, that the solubilities they indicate cannot be correct. It is exceedingly doubtful that the presence of small amounts of manganese in the present alloys could have such a profound effect.

Complete homogenization of the high iron alloys used in this investigation required a very drastic treatment (three 2 hr anneals at 1085°C, alternated with 50 pct reductions by cold rolling), but results identical with those reported here were obtained on definitely nonhomogeneous samples fabricated according to commercially reasonable schedules. Ap-

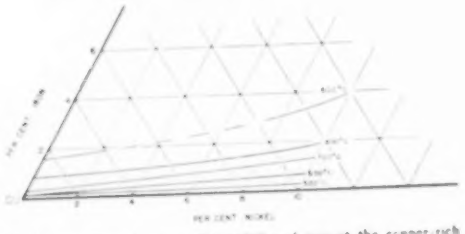

Fig. 3—Isotherms showing solid solubility of iron at the copper-rich corner of the Cu-Ni-Fe phase diagram.

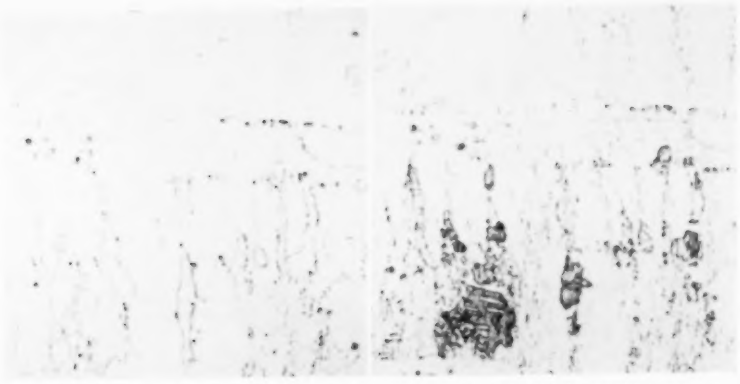

a—As revealed by electropolishing. b—As etched lightly with bichromate.

Fig. 4—Precipitation in 2 pct Fe-10 pct Ni alloy annealed 2 hr at 700° C. Sample previously cold rolled 50 pct after quenching from above solvus. X150

parently the local variations in iron concentration in the partially homogenized alloys, while causing heavier precipitation in some places than in others, were too small to affect conclusions drawn from successive anneals near the boundary differing by 10° C in temperature.

Establishment of the solvus surface depended upon positive recognition of the iron-rich phase, and it was found necessary to use special techniques for this purpose. Micrographic examinations were made after annealing and quenching, from a series of temperatures, both hard-worked samples and samples prequenched from a solution anneal. At 750° C and above, the annealing time was 1 hr; from 500° to 750° C, the time was 2 hr; and at lower temperatures a series of times up to 1 week were employed. The specimens were polished electrolytically in an electrolyte of 100 parts 85 pct orthophosphoric acid and 15 parts water. This technique revealed any optically resolvable particles of the iron-rich precipitate without the aid of etching; in fact, etching effects tended to mask clear evidence of precipitate on the polished surface.

Samples containing at least 1 pct Fe quenched from above the solvus developed a grain boundary pattern during the electrolytic polishing, the intensity of the effect increasing with iron content. It was established that the pattern resulted from a greater rate of solution at the boundaries. This is an interesting phenomenon not commonly found in the electrolytic polishing of single-phase alloys, but it seems to be the same as that described by Chaudron[7] for an Al-Zn alloy. The breadth of these boundary lines is greater than boundaries revealed by mechanical polishing and etching with bichromate.* Although not studied in detail, there appeared to be a tendency for these heavy boundaries to disappear when samples showing them were electrolytically polished after an anneal at temperatures causing precipitation.

In general, hard specimens recrystallized over an appreciable range of temperatures, the range increasing with iron content. Specimens annealed within this range showed precipitation accompanying recrystallization. Thus, for example, Fig. 4a shows a beaded grain boundary precipitate as electropolished, and Fig. 4b shows the same field following a very light bichromate etch. This occurrence of the precipitate at the boundaries of new grains in compositions which, if quenched from above the solvus, showed the grain boundary effect on electropolishing, made it difficult to identify the precipitate positively at temperatures near the solvus. Nor was it certain that the precipitate had formed in the grain boundaries of high iron specimens which were quenched from above the solvus and reheated. The best technique available for detecting small amounts of precipitate at the grain boundaries was the use of polarized light. The heavy grain boundaries appeared bright against a dark field, and small discontinuities in this bright line were assumed to be precipitate, since they were very rare (inclusions, etc.) in samples quenched from temperatures definitely above the solvus.

Detection of optically unresolvable precipitation was not difficult when it occurred locally in small areas associated with grain boundaries. Such areas of relatively dense precipitation were shown by Gordon and Cohen[6] for Cu-Fe and Cu-Co alloys. This "patch" type of precipitation was found only in alloys quenched from a solution anneal and re-

Fig. 5—Patch type precipitation in 1.5 pct Fe-10 pct Ni alloy annealed 1 hr at 500° C after quenching from 900° C. X150

* Etch No. 5 in *Metals Handbook*, p. 901 (1948 Ed.) A.S.M. Cleveland.

a—Magnetic colloid on mechanically polished surface. b—Same field as electropolished.

Fig. 6—Pattern of magnetic colloid compared with precipitation pattern shown by electropolishing in sample annealed below the recrystallization temperature. 5 pct Fe 10 pct Ni cold rolled 50 pct and annealed 1 hr at 850 C. X50

heated. For a given iron concentration it occurred only at and below a certain temperature, and this temperature was lower as the iron content increased. Samples of the 1.5 pct Fe–10 pct Ni alloy, quenched from a solution anneal and reannealed at 600 C, show this form, but at 700 C the precipitation is rather uniformly distributed. The alloy containing 3 pct Fe and 10 pct Ni precipitated mostly in patches at 500 C and mostly as generally distributed particles at 600 C, while the 5 pct Fe–10 pct Ni alloy did not precipitate in patches even when annealed at 300 C for 24 hr.

The general appearance of this patch form of precipitation is illustrated in Fig. 5 for a 1.5 pct Fe–10 pct Ni alloy which was annealed 1 hr at 500 C following a solution anneal. The patches, which are very dark after an ammonia-peroxide etch, are not contrasted in color from the rest of the structure when a bichromate etchant is used. The structure was usually observed directly after electropolishing and the patches had a splotchy brown appearance as if a deposit formed during polishing and was not entirely removed during rinsing.

Two observations concerning the patch-type precipitation, which were found to be quite generally true, are typified in Fig. 5. First: in direct correspondence to the observations of Forsyth, King, Metcalfe, and Chalmers on Be-Cu, it will be noted that the relative orientations of the grains at whose boundary a patch grows have an effect on the growth of the patch. Several examples of patches which are made discontinuous where a twin boundary meets a grain boundary can be seen. Second: no examples were observed in which a patch grew in both directions from the same part of a boundary, although this did not indicate preference for one orientation as against the other since growth into the other grain occurred at other places in the same boundary. Rather it would appear that whatever it may be in the boundary that nucleates precipitation in a patch is consumed by the nucleation. The arrow in Fig. 5 indicates a typical example of this second observation.

A method for detecting small amounts of optically unresolvable precipitate not occurring in patches involves the use of magnetic colloid. A magnetic field can be set up in a drop of a colloidal suspension of magnetic iron oxide on the polished surface of the sample by placing a permanent magnet close behind a thin specimen. Since the unresolvable precipitate

a—Magnetic colloid pattern. b—Same field immediately after removal of magnet.

Fig. 7—Optically unresolvable ferromagnetic precipitate revealed by magnetic colloid 2 pct Fe–10 pct Ni alloy quenched from 900 C and annealed 2 hr at 550 C. X500

Table II. Effect of Iron on Hardness of Quenched, Cold-Rolled and Reheated Cupro-Nickels (2 and 5 Pct Ni) Rockwell F Hardness

Alloy No.	Ni, Pct	Fe, Pct	As Quenched 850°C	Cold Rolled 6 B&S No. Hard	Reheated 1 Hr At				
					400°C	450°C	500°C	600°C	700°C
5148	1.98	0.005	24.5	90.6	89.5	50.6	40.1	35.0	27.3
5149	2.01	0.097	23.4	92.0	90.6	50.4	40.2	35.2	27.1
5150	2.00	0.25	26.2	93.4	90.8	63.6	45.2	38.2	33.0
5151	2.01	0.50	27.5	92.7	91.3	61.3	49.9	49.6	37.6
5152	1.99	0.73	26.2	94.0	92.0	84.2	56.0	56.1	56.0
5153	2.03	1.01	34.8	93.6	92.6	85.7	82.5	67.3	64.6
5154	2.01	1.52	30.9*	94.7	94.3	90.6	72.0	73.7	72.9
5155	4.78	0.005	26.6	90.6	91.7	79.9	45.5	41.2	37.3
5156	5.01	0.097	30.1	93.7	92.3	84.6	45.7	41.5	38.0
5157	4.92	0.25	33.5	94.2	92.7	89.0	47.4	43.1	37.9
5158	4.92	0.50	31.3	93.7	93.6	93.0	53.3	48.3	42.3
5159	4.99	0.76	40.6	95.1	94.9	92.6	68.0	59.2	48.2
5160	5.03	1.00	44.0	92.6	95.1	92.4	81.6	73.0	61.5
5161	5.04	1.50	46.9	95.5	95.6	93.0	89.9	87.7	85.2

* Quenched from 900°C.

is ferromagnetic, the colloid will tend to congregate in the areas of precipitation. A comparison can be made between this technique and that of electropolishing for a resolvable precipitate in the case of a 5 pct Fe-10 pct Ni alloy quenched from above the solvus, cold rolled, and then annealed for 1 hr at 850°C, a temperature below the recrystallization temperature for this alloy. By viewing the same field first with magnetic colloid on a mechanically polished surface (Fig. 6a) and then as electropolished (Fig. 6b), it can be seen that heavy precipitation is revealed by the colloid. Neither sample was etched. The use of magnetic colloid in a case where the precipitate is too fine to be resolved after electropolishing, is shown by micrographs, Figs. 7a and b, of the same field of a sample of the 2 pct Fe-10 pct Ni alloy quenched from 900°C and annealed 2 hr at 550°C. The local aggregation of the colloid shown in Fig. 7a disappears upon removal of the magnet as shown by b. There is no resolvable precipitation, nor can any be found in these areas at magnifications up to X2000, even when the specimen is etched.

The appropriateness of this technique for establishing the limits of solubility is indicated by the fact that for each alloy there is a temperature above which quenched samples show no pattern of the colloid in a magnetic field. In alloys with 0.5 pct Fe or less, the limit of solubility was determined by the presence or absence of very narrow patches in the electrolytically polished surface. However, for higher iron contents the criterion employed was detection of any magnetic colloid pattern. Simple magnetic tests, based on the pull exerted on the specimen by a strong permanent magnet, were also used, and indicated diminishing attraction with progressively higher annealing temperatures below the solvus. This paralleled weakening magnetic colloid patterns, but in general a colloid pattern could be detected in samples given an anneal at a temperature slightly higher than the highest one for which samples showed attraction to the permanent magnet.

The equilibrium phase diagram for Cu-Ni-Fe in the copper-rich region shows that the solubility of iron increases gradually as the nickel content increases and appreciably as the temperature increases. The room-temperature solubility in the 10 pct Ni alloy is less than 0.1 pct and increases to more than 5 pct at temperatures above 950°C. Compositional variations due to dendritic segregation in these alloys are not easily eliminated, but ordinary fabrication procedures reduce them sufficiently so that the equilibrium diagram may be usefully applied to commercially wrought materials.

Properties

The rather pronounced increase with temperature in the solubility of iron in these alloys indicates that above certain iron contents precipitation hardening effects may be expected during fabrication.

That such effects occur in 2 and 5 pct Ni alloys is indicated in Table II, which shows the Rockwell F hardness of specimens of Series A alloys (quenched from 850°C, rolled 6 B&S numbers) reheated 1 hr

Fig. 8—Effect of iron content on precipitation hardening of 10 pct cupro-nickels quenched from 800°C.

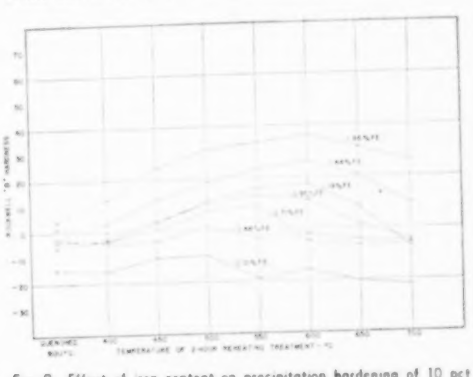

Fig. 9—Effect of iron content on precipitation hardening of 10 pct cupro-nickels quenched from 900°C.

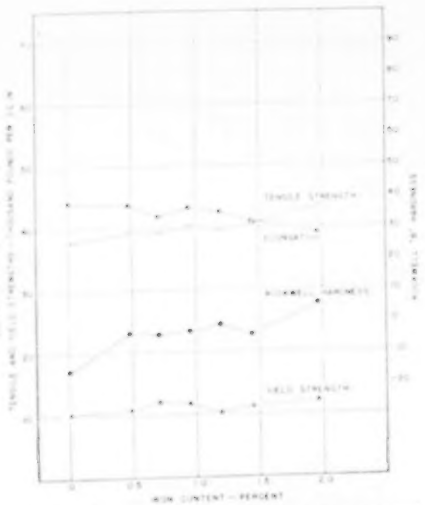

Fig. 10—Effect of iron content on the tensile properties and hardness of 10 pct cupro nickels quenched from 900° C.

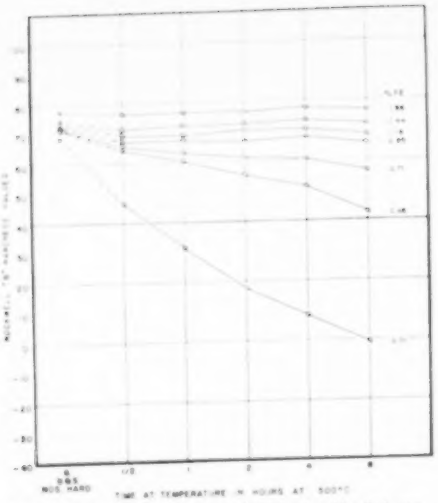

Fig. 12—Changes in hardness with time of cold rolled iron-bearing 10 pct cupro-nickels annealed at 500° C. Quenched from 900° C prior to rolling.

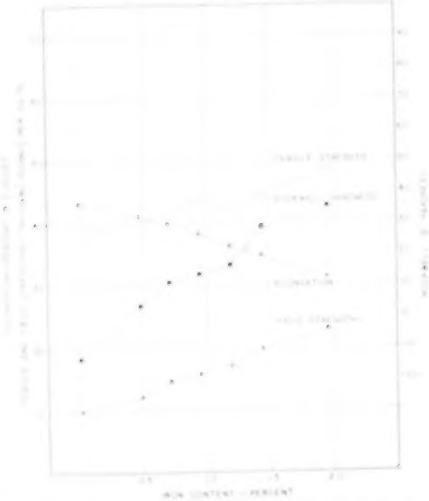

Fig. 11—Effect of iron content on the tensile properties and hardness of 10 pct cupro nickels quenched from 900° C and reheated 2 hr at temperatures giving maximum hardness (see Fig. 9).

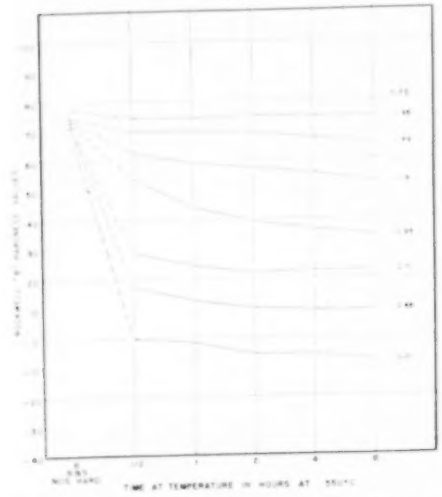

Fig. 13—Changes in hardness with time of cold rolled iron-bearing 10 pct cupro-nickels annealed at 550° C. Quenched from 900° C prior to rolling.

at temperatures from 300° to 700° C. The normal softening behavior of the low iron content alloys is in sharp contrast with the marked retention of hardness by the alloys containing 1.0 and 1.5 pct Fe. However, these low nickel content alloys were considered inferior to the 10 pct Ni alloy for commercial development, chiefly on the score of corrosion resistance, and hence the precipitation hardening characteristics of the lower nickel alloys have not been investigated in detail. Most of the work has dealt with the 10 pct Ni alloy group.

The effect of iron in producing precipitation hardening characteristics in 10 pct cupro-nickels is indicated in Figs. 8 and 9, which show Rockwell B hardness results on specimens of Series C alloys quenched from 800° and 900° C, respectively, and reheated 2 hr at temperatures from 400° to 700° C. It will be noted that little, if anything, is gained by quenching from 900° rather than 800° C. With both quenching temperatures, the alloy containing 0.48 pct Fe seems free from any precipitation hardening tendency, but slight hardening at about 550° C is noted on reheating the 0.71 pct Fe alloy. With higher iron contents, increasing amounts of precipitation hardening are found. A reheating temperature, for a 2 hr treatment, of 550° to 600° C seems to produce maximum hardness in these quenched alloys.

Tensile property changes associated with precipi-

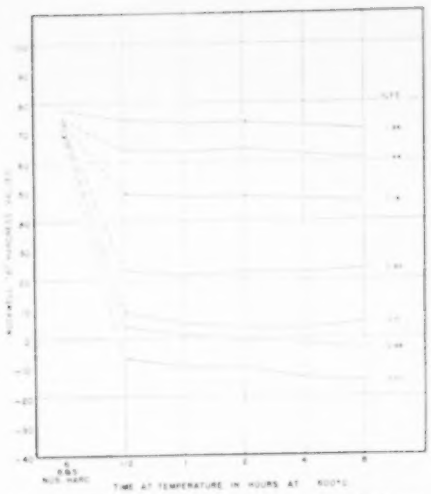

Fig. 14—Changes in hardness with time of cold rolled iron-bearing 10 pct cupro-nickels annealed at 600° C. Quenched from 900° C prior to rolling.

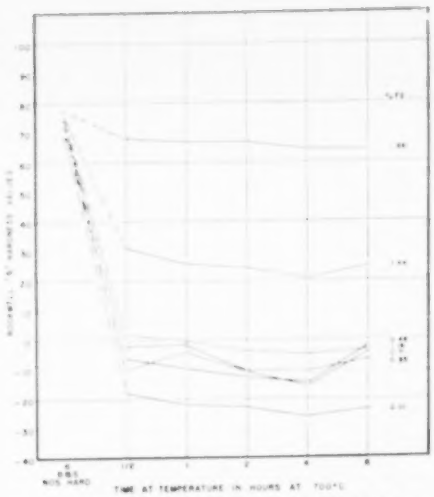

Fig. 16—Changes in hardness with time of cold rolled iron-bearing 10 pct cupro-nickels annealed at 700° C. Quenched from 900° C prior to rolling.

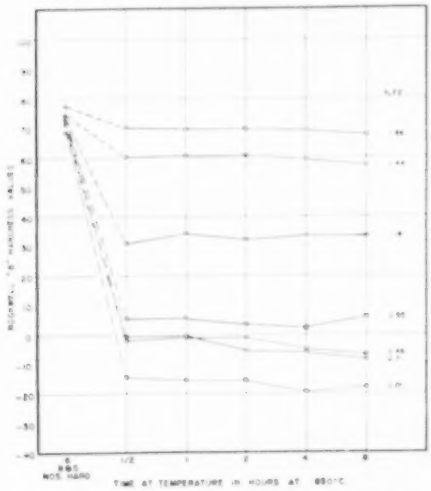

Fig. 15—Changes in hardness with time of cold rolled iron-bearing 10 pct cupro-nickels annealed at 650° C. Quenched from 900° C prior to rolling.

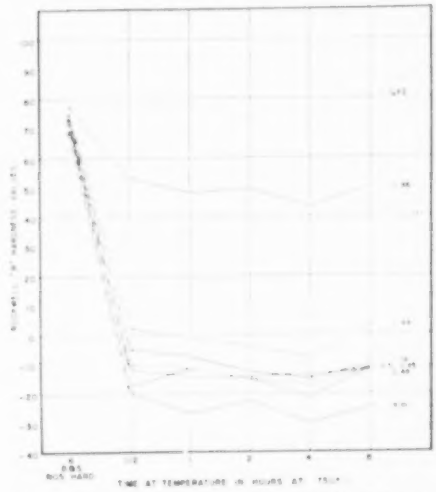

Fig. 17—Changes in hardness with time of cold rolled iron-bearing 10 pct cupro-nickels annealed at 750° C. Quenched from 900° C prior to rolling.

tation hardening are indicated in Figs. 10 and 11. Fig. 10 shows the effect of iron content on the tensile properties of 0.040 in. strip of 10 pct cupro-nickels (Series C) quenched from 900° C. There is a slight upward trend in tensile strength and Rockwell hardness with iron content, and a downward trend in elongation, but the yield strength remains essentially constant. Fig. 11 shows the same alloys reheated 2 hr at temperatures giving maximum hardness, as taken from Fig. 9. It is apparent that precipitation hardening of these iron-bearing cupro-nickels can reach substantial proportions. For example, the yield strength of a precipitation hardened alloy containing 2 pct Fe is more than twice that of the iron-free alloy given the same treatment.

The effect of iron on the softening behavior of the 10 pct cupro-nickels during anneal is of great interest to the fabricator. In studying this point, specimens of Series C alloys (quenched from 900° C and rolled 6 B&S numbers hard to 0.040 in. gage) were reheated for times of ½, 1, 2, 4, and 8 hr at temperatures from 500° to 800° C. The results of Rockwell hardness measurements on these specimens are given in Figs. 12 to 18. Fig. 19 shows softening curves for the same alloys for a 2 hr treatment at various reheating temperatures. It is apparent that, while in no case does the precipitation treatment result in a hardness above that of the cold-rolled stock, the precipitation of iron does have a profound effect on softening behavior. The iron-free alloy is completely

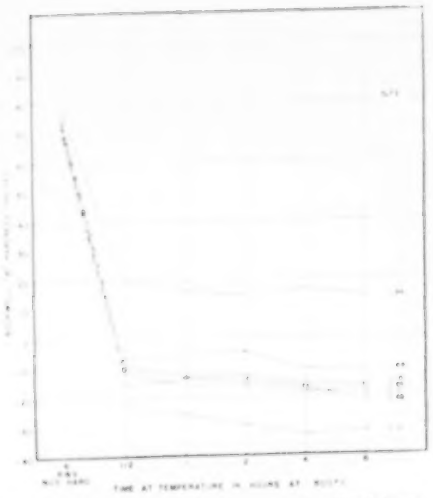

Fig. 18—Changes in hardness with time of cold rolled iron bearing 10 pct cupro nickels annealed at 800 C. Quenched from 900 C prior to rolling.

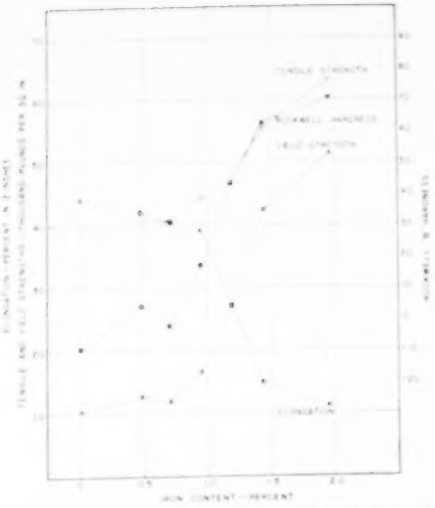

Fig. 20—Effect of iron content on the tensile properties and hardness of cold rolled 10 pct cupro nickels heat treated 8 hr at 650 C. Quenched from 900 C prior to rolling.

softened by a 30 min anneal at 500 C. With 1.96 pct Fe, the alloy does not fully soften even at 800 C. An interesting point brought out by Figs. 12 to 18 is the small effect of time of reheating on these cold-worked and reheated alloys.

In order to study the effect of rather full precipitation, tensile specimens of Series C alloys were reheated 8 hr at 650 C. Results of tensile tests and Rockwell hardness measurements are given in Fig. 20 and indicate once again the marked effects of iron content and heat treatment on the properties of this alloy.

Since this same 10 pct cupro-nickel is also used for tube sheets, the properties to be expected in commercially produced hot-rolled plate are of interest. Table III gives the results of a series of tensile tests made on two such plates, one containing approximately 1 pct and the other 1.5 pct Fe (Series E). The hot-rolled plates were $^{3}/_{4}$ in. thick, and threaded-end tensile specimens having 0.505 in. diam over a 2 in. gage length were machined from specimens cut longitudinally from the plate. These specimens were variously heat treated, as noted in the table, to explore the range of properties that might be obtained in alloys containing these two amounts of iron. It will be noted that while the two alloys have very similar properties after a solution anneal (800 C for 1 hr) and quench, the higher iron alloy shows a much greater response to a reheating treatment (600 C for 2 hr). Also, the 1.5 pct Fe alloy shows as much increase in tensile and yield strength when simply slowly cooled from a solution anneal as it does after a reheating treatment, while the 1 pct Fe alloy is relatively unaffected in either case. Of considerable interest is the fact that both alloys show excellent properties as-hot-rolled. It should also be noted that a reheating treatment applied directly to hot-rolled specimens causes a loss of strength in the 1 pct alloy, but a slight gain in the 1.5 pct alloy, indicating that the latter is supersaturated with respect to iron after hot rolling.

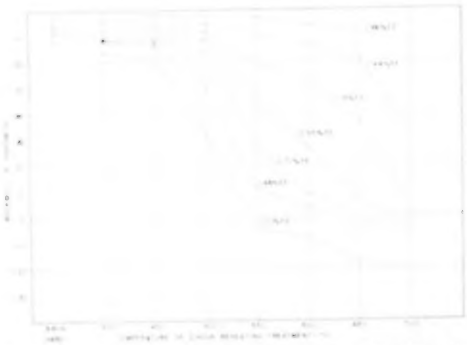

Fig. 19—Effect of iron content on softening behavior of cold rolled 10 pct cupro nickels. Strip cold rolled 50 pct after quenching from 900 C.

A further factor requiring consideration in the fabrication of these iron-bearing cupro-nickels is their susceptibility to subscale formation during annealing. As is shown in Figs. 12 to 19, the higher iron content alloys require progressively higher temperatures for full anneal. Unfortunately, the extent of subscale formation increases rapidly with annealing temperature. This is illustrated in Figs. 21a, b, and c, where alloys containing 0.71, 1.44, and 1.96 pct Fe, respectively, have been annealed in air for 2 hr at temperatures such as might be used in the commercial fabrication of these alloys. Only negligible subscale is formed on the 0.71 pct Fe alloy annealed at 650 C, but the 1.44 pct Fe alloy annealed at 750 C, and the 1.96 pct Fe alloy annealed at 850 C, have amounts of subscale sufficient to cause great difficulty in pickling operations. Pickling the interior of a condenser tube is difficult, at best, and there would seem to be a possibility, with the high iron alloys, that the removal of subscale might not be complete. Whether or not small areas of subscale might serve as foci for corrosion attack is not def-

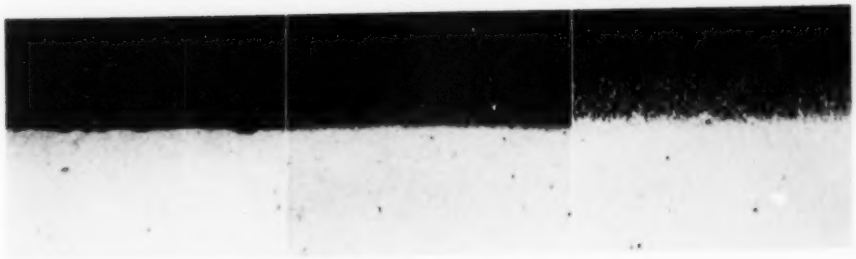

a b c

Fig. 21—Subscale formation on 10 pct cupro-nickels containing iron. X500.

	Depth, In.	
	Black Scale	Sub-scale
a—0.21 pct Fe annealed 2 hr at 650°C	0.001	0.0001
b—1.44 pct Fe annealed 2 hr at 750°C	0.002	0.0005
c—1.96 pct Fe annealed 2 hr at 850°C	0.007	0.0010

initely established, but some effect of this type would be anticipated.

Discussion

The iron-bearing 10 pct cupro-nickel has become an important industrial alloy primarily because of its exceptional resistance to sea-water corrosion. Since the amount of iron required for optimum corrosion resistance is in the range where precipitation hardening effects are encountered, the selection of an ideal iron content must take into consideration the effects of iron on fabrication as well as on corrosion resistance. The data reported above give information as to the equilibrium solubility of iron at various temperatures, and the nature and extent of physical property changes that may be expected from various fabrication procedures.

It must be recognized that precipitation hardenability is not a particularly desirable attribute of an alloy for condenser tubes or salt-water lines. While the hardening characteristics are of interest in several other uses of the iron-bearing 10 pct cupro-nickel, they are unimportant, as such, in these major applications, which depend almost entirely on the unique corrosion resistance of the alloy. Condenser tubes, at the ends, at least, must be soft enough to be rolled into tube sheets, and salt-water lines often require bending to shape in order to follow the contours of marine construction. The precise properties required are more readily obtained with a judicious amount of temper, rather than by utilizing precipitation hardening characteristics.

It appears, from unpublished work carried out by the Corrosion Research Laboratory of The American Brass Co. (some of it in collaboration with other laboratories), that the impingement corrosion resistance of the 10 pct cupro-nickel in sea water improves steadily with increasing iron contents up to about 2 pct, provided the iron is in solid solution. By far the greater part of the total improvement is obtained with the first 0.75 pct Fe; thereafter increased iron results in only slight, though definite, improvement. Alloys containing precipitated iron behave as though the precipitated iron were not there. Only the amount of iron in solid solution is effective. (Precipitated iron does affect the appearance of corroded specimens: with increasing amounts of free iron, the golden brown film characteristic of specimens in which the iron is completely in solution rapidly darkens, and finally becomes black.) While free iron does not appear to be a significant factor in impingement corrosion, which is unquestionably the chief determinant of the useful life of these materials in "pure" sea water, in polluted coastal waters, where oxygen concentration cells may form and cause local pitting, there is some evidence, not yet conclusive, that free iron is harmful. High iron content condenser tubes containing free iron have shown pitting in such waters, while comparison tubes

Table III. Tensile Properties of Hot-Rolled Plate

10 Pct Cupro-Nickel with 1 and 1.5 Pct Fe

Fe, Pct	As Hot-rolled	Hot-rolled and Reheated	Solution Annealed, Quenched	Solution Annealed, Quenched, Reheated	Solution Annealed, Air-cooled	Solution Annealed, Slowly Cooled
			Yield Strength (0.5 Pct Extension), psi			
1.03	26,025	29,850	15,060	17,975	14,230	15,350
1.46	35,675	36,200	15,100	22,625	16,605	23,000
			Tensile Strength, psi			
1.03	48,425	47,250	40,575	42,675	41,250	42,800
1.46	51,900	52,625	41,510	46,600	44,050	48,800
			Elongation in 2 In., Pct			
1.03	36.5	39.3	52.5	50.5	53.0	51.3
1.46	35.0	33.5	51.0	45.0	50.0	41.3
			Reduction of Area, Pct			
1.03	71	69	80.5	79.5	80	80
1.46	72	70	77	76	79	75.5

Solution Anneal: 800°C for 1 hr.
Reheating Treatment: 600°C for 2 hr.

containing 0.73 pct Fe, all of which was in solid solution, have been practically free from pitting.

The ideal iron content for a 10 pct cupro-nickel, then, would appear to be the maximum amount that can be retained in solid solution throughout the fabrication processes necessary to the production of the finished pipe or tube. While Fig. 2 indicates an equilibrium solubility of 2 pct Fe at about 770 C, Fig. 18 indicates that the 2 pct Fe alloy is not completely softened at 800 C, and an annealing temperature in excess of this would be required in commercial fabrication. Retention of the iron in solid solution would require a quench from this annealing temperature. While some products might be so treated, it is difficult to imagine such a quench being carried out on a typical condenser tube, say $\frac{7}{8}$ in. in diam and 20 ft long. And in present day tube mill furnaces, which do not have atmospheres that are nonoxidizing at such high temperatures, a substantial layer of subscale and serious pickling difficulties would be anticipated. Obviously the 2 pct alloy would be very difficult to fabricate.

On the other hand, an alloy containing only 0.75 pct Fe, an amount sufficient to give an impingement corrosion resistance comparable to the standard iron-bearing 30 pct cupro-nickel, is homogeneous above 815 C, is fully softened by annealing at 650 C, where negligible subscale is encountered, and, because of the low rates of diffusion at the required annealing temperature, will retain the iron in solid solution if simply air cooled in accordance with regular mill practice. It is because of this ease of fabrication that the 0.75 pct Fe alloy has undergone considerable commercial development.

Where impingement corrosion resistance greater than that possessed by the 0.75 pct Fe-10 pct cupro-nickel is required, it may be obtained, to a limited extent, by increasing the iron content and selecting fabrication procedures that will ensure that as much iron as possible is in solid solution in the finished product. Alloys with iron contents of perhaps 1.0 to 1.25 pct appear not too impractical from a fabrication viewpoint. At present there are few if any applications where the slight improvement in corrosion resistance produced by still higher iron contents justifies the much greater difficulty of fabrication involved.

An iron content above 0.75 pct may also serve a useful purpose in condenser tube sheets, which are usually heavy gage plates produced by hot rolling. Here the increased iron does not add to the already adequate corrosion resistance, since it is largely precipitated, but by raising the softening temperature it does permit the production of a hot-rolled plate having higher strength than would be obtained with the 0.75 pct Fe alloy. In certain other applications, such as heat exchanger tubes for high pressure-high temperature service, where high strength is a major consideration, it may also prove practical to raise the iron content to the point where useful improvement in strength is obtained through precipitation hardening effects.

Conclusions

1—The solid solubility of iron increases rapidly with increasing temperature in cupro-nickels of low nickel content. For the 5 pct Ni alloy, the solubility of iron increases from about 0.2 pct at 500 C to 0.85 pct at 750 C. For the 10 pct Ni alloy, the solubility of iron increases from less than 0.10 pct at 400 C to 4.8 pct at 950 C.

2—Alloys containing sufficient amounts of iron are susceptible to precipitation hardening by suitable heat treatment. In 10 pct cupro-nickels, an iron content in excess of about 0.7 pct is required to produce an appreciable amount of hardening.

3—With the higher amounts of iron, the softening temperature of a 10 pct cupro-nickel is raised to the point where commercial annealing becomes impractical because of subscale formation and consequent pickling difficulties. While a 0.75 pct Fe alloy can be completely softened at 650 C, about 850 C is required for an alloy containing 2.0 pct Fe.

4—Since the iron-bearing 10 pct cupro-nickel is useful primarily because of its excellent resistance to impingement corrosion in sea water, and improved physical properties are of little interest (except perhaps in tube sheets and tubes for high pressure-high temperature heat exchangers), the precipitation hardening characteristics of the alloy are important chiefly because they dictate fabrication procedures and allowable iron content.

5—While maximum impingement corrosion resistance of the 10 pct cupro-nickel appears to be obtained with maximum iron in solid solution, fabrication difficulties limit the iron content to perhaps 1.25 pct. An alloy containing about 0.75 pct Fe can be fabricated without changing the usual mill procedures for cupro-nickel, and fortunately is only very slightly inferior in impingement corrosion resistance to alloys of higher iron content.

Acknowledgment

The authors would like to thank The American Brass Co. for permission to publish this paper, and to record their indebtedness to John R. Freeman, Jr., Technical Manager, under whose general supervision this work was carried out. Very helpful discussions with A. W. Tracy, Assistant Metallurgist, are also gratefully acknowledged.

Addendum

Since this manuscript was prepared, the results of extensive researches on the iron-bearing cupro-nickels by the British Non-Ferrous Metals Research Association have been reported by G. L. Bailey.[9] Although these results are in general agreement with those reported by Freeman, Tracy, Hungerford and the present authors, they have led to a recommendation of somewhat higher iron contents. The basis for this discrepancy lies in the fact that, in British condenser tube practice, the tubes are finished hard. This permits the British manufacturers to retain iron in solution by quenching the tubes at a size which can be readily handled, after which they are not again heated. In the United States, condenser tubes must be soft enough to withstand rolling into the tube sheets and this requires an anneal at a stage where the tubes are too long for proper quenching and too small in diameter for proper cleaning after a high temperature solution-anneal.

References

[1] A. W. Tracy and R. L. Hungerford: *Proc.* A.S.T.M. (1945) **45**, p. 591.

[2] J. R. Freeman, Jr. and A. W. Tracy: *Corrosion* (1949) **5**, p. 245.

[3] G. Tammann and W. Oelsen: *Ztsch. anorg. allgem. Chem.* (1930) **186**, p. 257.

[4] A. J. Bradley, W. F. Cox, and H. J. Goldschmidt: *Journal* Inst. Metals (1941) **67**, p. 189.

[5] G. Chaudron: *Journal* Inst. Metals (1949) **76**, p. 1.

[6] R. B. Gordon and M. Cohen: Symposium on Precipitation Hardening, A.S.M., Chicago (October 1949).

[7] P. J. E. Forsyth, G. J. Metcalfe, R. King, and B. Chalmers: *Nature* (London) (1946) **158**, p. 875.

[8] G. L. Bailey: *Journal* Inst. Metals (1951) **79**, p. 243.

Volatility and Stability of Metallic Sulphides

By C. M. Hsiao and A. W. Schlechten

The apparent vapor pressures of a number of metal sulphides were determined by measuring their rate of weight loss when they were heated under vacuum. The calculated pressures are due in some instances to the volatility of the sulphide and in others to the decomposition pressure.

THE direct reduction of metallic sulphides, as in the precipitation method for lead or antimony, is not a widely used process today. However, it might be employed for the production of a number of metals if the operation were carried out under reduced pressures. Two general procedures are possible; the reducing agent could form a stable nonvolatile sulphide from which the valuable metal could be removed by volatilization or liquation. The other approach would be to choose a reducing agent which would form a sulphide that could be volatilized away from the valuable metal. A vacuum operation would serve to protect the sulphides and metals from oxidation and would increase the evaporation rates.

A related process is the separation of metallic sulphides by selective volatilization either at atmospheric pressure or under vacuum. This procedure is already used commercially for the elimination of lead and cadmium as PbS and CdS from zinc calcines; it might well have other applications.

To predict such processes it is necessary to know the relative volatilities of the metallic sulphides and to know whether they volatilize as sulphides or whether the predominant weight loss is due to decomposition. Such data would also be of value in studying problems such as the use of sulphides for refractories, as described by Brewer,[1] or in the evaluation of the theory of ore deposition from the vapor state, as proposed by Brown.[2]

Qualitative statements concerning the volatility of metallic sulphides can be found frequently in the literature and are well summarized by Mellor, but accurate determinations of rates of evaporation or vapor pressures are very scarce. Kelly[3] lists vapor pressure data only for PbS, his reference being to the work of Schenck and Albers,[4] who measured the vapor pressure of PbS by a dynamic method between 830° and 995° C. More recently Veselovskii has determined the vapor pressures of the sulphides of antimony, lead, cadmium, and zinc at temperatures ranging from 360° to 1000° C using Knudsen's method. A second Russian worker, Pogorelyi,[5] determined the vapor pressures of CdS and ZnS at temperatures from 900° to 1250° C. The results obtained by these workers are shown in subsequent graphs in comparison with the data of this paper. Brewer and coworkers[1] have studied some of the metallic sulphides to determine their suitability as refractories in vacuum.

Veselovskii's determinations on PbS checked well with those of Schenck and Albers, and his determinations of CdS check almost exactly with Pogorelyi. For the vapor pressure of ZnS the data of Veselovskii and that of Pogorelyi are in fair agreement, as shown in Fig. 1, but it should be pointed out that Lumsden[6] has discovered that the equation given by Veselovskii for the vapor pressure of ZnS:

$$\log P_{(mm)} = \frac{-14{,}200}{T} + 9.495$$

is in error by a factor of ten when compared to the experimental data.

In contrast with the scarcity of data on vapor pressures, the decomposition pressures of many metal sulphides have been determined and are summarized by Smithells.[7]

Theoretical Considerations

The experiments described in this paper consisted of determinations of the rate of weight loss of certain metallic sulphides under very low pressures at different temperatures. These data plus observation and analyses of the products reveal the mechanism of the weight loss and also provide a basis for the calculation of the vapor pressure or apparent vapor pressures of the sulphides.

C. M. HSIAO and A. W. SCHLECHTEN, Member AIME, are Graduate Student and Chairman, respectively, Dept. of Metallurgical Engineering, Missouri School of Mines and Metallurgy, Rolla, Mo.

Discussion on this paper, TP 3215D, may be sent, 2 copies, to AIME by April 1, 1952. Manuscript, July 30, 1951; revision, Oct. 31, 1951. New York Meeting, February 1952.

This paper represents part of a thesis by C. M. Hsiao submitted in partial fulfillment of requirements for the degree of Doctor of Philosophy to the University of Missouri.

Fig. 1—Apparent vapor pressure of ZnS as obtained from evaporation rates compared with results of other workers using different methods

Langmuir determined that the maximum rate of evaporation of substances of low volatility when heated in a vacuum is related to the vapor pressure as follows:

$$W = P\sqrt{\frac{M}{2RT}} \qquad [1]$$

or more simply

$$W = 5.833 \times 10^{-2} P\sqrt{\frac{M}{T}} \qquad [2]$$

where W is the maximum rate of evaporation in g per sq cm per sec; P, the vapor pressure in mm of mercury; M, the molecular weight in g; R, the gas constant; and T, the absolute temperature.

Langmuir's equation as shown above assumes that when an evaporating surface is in equilibrium with the vapor above it, every vapor atom or vapor molecule returning to the surface condenses and is not reflected. If this is not so, the term to the right must be modified by a "condensation coefficient" or "accommodation coefficient," otherwise the calculated vapor pressures are lower than their true value. Practically no data are available on such coefficients and most workers assume a value of unity, as has been done in this paper.

A question arises as to the composition of the vapor above the heated sulphide. The vapor above very stable sulphides may be composed almost entirely of metal sulphide molecules, while the vapor above easily decomposed sulphides would consist mainly of sulphur and possibly of the metal. Between these two extremes there can be examples of sulphides that partially evaporate as such and partially decompose.

Because of the uncertainty as to the extent of decomposition and the correct value of the accommodation coefficient, our results are labeled "Apparent Vapor Pressures." Subsequent discussion will bring out in each instance how close these may be to true vapor pressures. In any event, the apparent vapor pressure will give a true measure of the rate of weight loss of the metallic sulphide that will occur in a vacuum, no matter what the mechanism may be.

Experimental Apparatus and Procedure

The vacuum furnace used consisted of a 2¼ in. diam porcelain tube 40 in. long supported in a vertical position and with the upper closed end heated by a resistance coil. The details of the furnace, the controls, and the vacuum system have been described in a previous publication.[7] The sulphides used in the experiments were the highest purity obtainable from Fisher Scientific Co., and no attempt was made to refine them further.

The general procedure was to place a sample of the metal sulphide powder in an alundum crucible and carefully tamp it down to form a compact with a smooth and even surface of known area. The weighed crucible and charge was then placed in a graphite tube which was in turn inserted in the furnace tube so that the sample was in the heated zone. The furnace was evacuated to a few microns of residual gas pressure and the sample was heated at a given temperature for a determined time. After the furnace was cooled, the sample was removed and weighed to determine the weight loss.

To correct for the weight loss during the heating and cooling time, a second run was made with the same heating and cooling rate but a different holding time at the same temperature. The difference in weight loss between the two runs was then the result of volatilization at the holding temperature for the time equal to the difference between the two runs. Expressed in equation form:

$$G = (W_1 - W_2)/(t_1 - t_2)$$

where G is the rate of evaporation in g per sec; W_1 and W_2, the weight losses of runs 1 and 2; and t_1 and t_2, the total times of those runs. If G is divided by

Table I. Sublimation Data for ZnS

Run No.	Vacuum, Microns	Temperature, °C	Time, Sec	Area, Sq Cm	Loss, G
ZnS-23	12.0	704	12,900	5.52	0.0387
ZnS-20	12.5	704	5,900	5.52	0.0338
ZnS-22	12.5	804	1,560	5.52	0.0375
ZnS-19	12.5	804	5,320	5.52	0.1483
ZnS-18	12.0	804	17,340	5.52	0.2294
ZnS-16	12.5	904	1,560	5.52	0.4050
ZnS-15	12.5	904	5,580	5.52	1.0915
ZnS-14	12.0	904	14,400	5.52	2.8713
ZnS-21	12.5	904	20,760	5.52	1.2920
ZnS-24	12.5	1008	900	5.52	1.0290
ZnS-25	11.5	1008	2,520	5.52	1.8230

Table II. Volatility and Vapor Pressure of ZnS

Run No.	Temperature, °K	Volatility × 10⁶, G per Sq Cm-Sec	Log P_{mm}
ZnS-25-26	977	0.999	5.271
ZnS-15-19	1073	2.27	3.997
ZnS-19-20	1073	2.21	3.901
ZnS-15-19	1073	1.99	3.944
ZnS-18-22	1173	25.23	2.822
ZnS-18-21	1173	27.37	2.794
ZnS-14-21	1173	24.92	2.844
ZnS-14-16	1273	207.1	1.890
ZnS-23-24	1278		

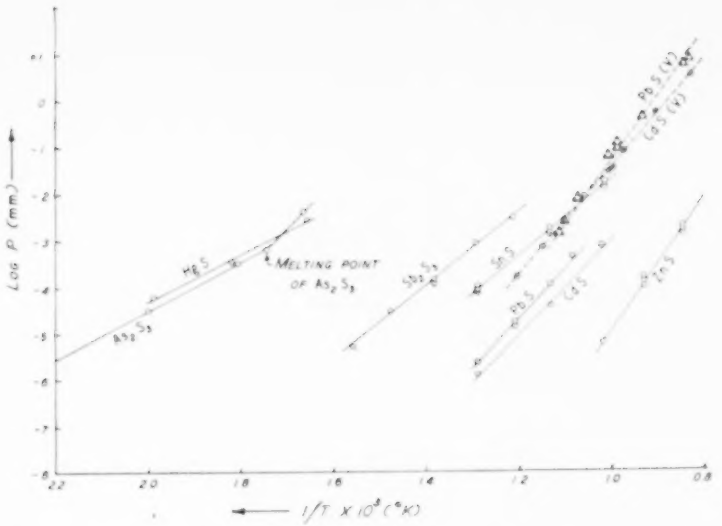

Fig. 2—Apparent vapor pressures of certain volatile sulphides.

The dotted lines refer to the determinations of Veselovskii.

the area of the sulphide surface the rate of evaporation in g per sq cm-sec is obtained.

Various possible sources of experimental error were investigated and evaluated. Blank runs using an empty alundum crucible showed that the weight loss of the crucible when heated in vacuum at 1100 C for 5½ hr was less than 0.3 mg and, therefore, could be ignored.

The temperature was measured outside of the porcelain tube, but preliminary experiments with a thermocouple in the sample position showed that there was no great lag between inside and outside temperatures. For example, the inside temperature reached 800 C less than 2 min after the outside temperature; at higher temperatures this lag was even less.

The pressure measured in the furnace, which would be that of the residual gases, was almost constant for any one run, but varied from 8 to 14 microns in the experiments reported here. This is sufficiently low to prevent oxidation, but there may be some question as to the effect of this residual gas pressure on the rate of evaporation. When volatile substances such as zinc or magnesium are evaporated in vacuum, experience has shown that there is no measurable change in the rate of evaporation at residual gas pressures below 100 microns. For substances with lower volatilities, such as the metallic sulphides, the effect of residual gas pressure is not known as well, but the work of Carman[7] indicated that if the furnace pressure is in the neighborhood of a few microns, the rate of evaporation is not sensitive to small variations of the pressure.

It might be supposed that the surface resulting from the compression of sulphide powders would be rough and therefore have more area than a truly flat surface. The presence of surface crevices has been shown mathematically by Melville[8] to have no influence on the effective surface if the accommodation coefficient is unity, and very little effect if the coefficient is less than one. To check this premise, experiments were run on the evaporation rate of copper powders using the same technique as used for the sulphides. At 1000 C rates were obtained of 0.334 to 0.40×10^{-3} g per sq cm-sec which compares very favorably with results of 0.35 to 0.54×10^{-3} g per sq cm-sec obtained by Marshall, Dornte, and Norton[9] who used solid pieces of copper.

As mentioned before, some doubt may exist as to how much of the apparent vapor pressure is the result of evaporation and how much the result of dissociation. Data are available for the dissociation pressures of many of the metal sulphides, in other instances the dissociation pressure can be calculated from the free energy of dissociation obtained by indirect means. Examination of the residue and distillate from the volatility experiments will also give indications of dissociation.

On the basis of such information, the sulphides have been divided into two groups, the volatile sulphides which lose weight mainly by the evaporation of metal sulphide molecules, and the nonvolatile sulphides which lose weight chiefly by dissociation and the subsequent evaporation of sulphur and of the metal individually.

Experimental Results

Volatile Sulphides: The data for ZnS are listed in detail and the methods of calculation are shown. Only the final data are shown for other volatile sulphides which are treated in the same manner as given for ZnS.

The weight losses for ZnS heated in a vacuum are

Table III. Apparent Vapor Pressures of Certain Volatile Metal Sulphides

$\text{Log } P_{\text{mm.}} = A \cdot T + B$

Sulphides	A	B	Temperature Range, °C	Pressure Range, Log $P_{\text{mm.}}$
ZnS	13.861	8.979	704-1008	−3.27 to −1.69
CdS	10.500	7.372	503-704	−5.96 to −3.16
HgS	5.586	6.669	230-330	−4.41 to −2.58
SnS	8.380	6.728	503-704	−4.09 to −1.91
PbS	11.160	9.358	503-654	−5.56 to −3.35
As_2S_3	5.098	4.672	180-330	−5.54 to −2.42
Sb_2S_3	7.674	6.764	352-553	−5.43 to −2.56

shown in Table I. The weight losses for two or more runs at the same temperature are combined to eliminate the error of heating and cooling and the rate of loss is calculated. This rate is then substituted in Langmuir's equation and the apparent vapor pressure is calculated. Table II shows the results calculated from the data in Table I, and the experimental points give a measure of the reproducibility of the results. The data for log P_{atm} plotted against 1/T gives a straight line. The equation of the line is

$$\log P_{atm} = -13,981/T + 8.979$$

Fig. 1 shows these results in comparison with the values obtained by other workers using different methods of determination.

In Table III are listed the data for a number of sulphides that were treated in a manner similar to that just described for ZnS. The data for ZnS are repeated for ease of comparison. These data are presented graphically in Fig. 2.

The calculated dissociation pressures of the above sulphides are much less than the calculated pressures listed in Table III, indicating that most of the weight loss was due to actual volatilization of the sulphide molecules and not to decomposition. This conclusion is supported by observations of the residue and condensate, which showed no change from the original composition. However, experiments on the sublimation of PbS at temperatures higher than those listed in Table III showed formation of metallic lead in the residue; data for these experiments were not used in the apparent vapor pressure determinations.

Some doubt exists as to the behavior of As_2S_3. There is a possibility that it decomposes to As_2S_2 and sulphur, both of which volatilize, although there was no free sulphur in the condenser to substantiate this theory.

The lack of agreement between our apparent vapor pressure determinations and the vapor pressure measurements of Veselovskii shows that the maximum rate of evaporation as predicted from Langmuir's equation is not achieved, if Veselovskii's results are correct.

Nonvolatile Sulphides: In contrast with the behavior of the volatile sulphides are the results obtained for MnS, FeS, CoS, NiS, Cu_2S, and MoS. For most of these the observed apparent vapor pressures are close to the dissociation pressures determined by other workers. Further evidence of dissociation was shown by the decrease of the percentage of sulphur in the residue and the appearance of free sulphur in the condensate.

The apparent vapor pressures of the nonvolatile sulphides referred to above are listed in Table IV. In making these calculations the molecular weight of the metal sulphide was used for the value of M in Langmuir's equation. The data of Table IV are presented in Fig. 3.

MnS: The results are very close to the P_{S_2} above MnS as determined by Cox and coworkers,[9] although considerably higher than the results reported in the older work of Jellinek and Zakowski[4] and that of Britzke, Kapustinsky, and Wesselowsky.[5]

FeS: The results intersect the P_{S_2} curve of Cox and are almost identical with the P_{S_2} curve of Sudo.[10] However, chemical analyses show a transfer of Fe to the condensate, if it can be assumed that this was the result of FeS evaporation, then about 20 pct of the total weight loss was due to FeS transfer in the range 900° to 1100°C.

CoS: The apparent vapor pressure is somewhat more than the decomposition pressure reported by Jellinek and Zakowski. Chemical analyses show a transfer of Co to the condensate, and, if this is entirely due to CoS volatility, then the weight loss is 54 pct, the result of dissociation at 804°C increasing to 75 pct at 1006°C.

NiS: The apparent vapor pressure is almost the same as the decomposition pressure reported by Jellinek and Zakowski. Chemical analyses indicate that the weight loss is at least 90 pct due to dissociation. Hayward[7] has reported that NiS readily loses sulphur upon heating until the residue attains the relatively stable composition of Ni_3S_2.

Cu_2S: The apparent vapor pressure of Cu_2S does not follow the pattern of the other sulphides. The weight loss, especially at lower temperatures, is much greater than that expected on the basis of dissociation pressures determined by other workers by a factor of 1000. However, the formation of fine metallic copper wool on the surface of the sample is evidence of dissociation. The wool was collected

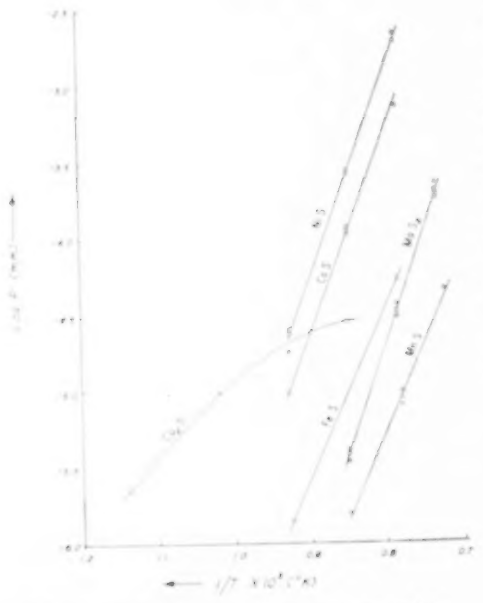

Fig. 3—Apparent vapor pressures of certain nonvolatile sulphides.

Table IV. Apparent Vapor Pressure-Temperature Relation for Certain Nonvolatile Metallic Sulphides

$$\text{Log } P_{atm} = -\frac{A}{T} + B$$

Sulphide	A	B	Temperature Range, °C	Pressure Range, Log P_{atm}
MnS	11,937	4.853	904–1106	−5.79 to −4.32
FeS	10,350	4.162	804–1006	−5.84 to −4.26
CoS	12,630	6.731	804–1006	−4.99 to −3.13
NiS	9,213	5.84	604–804	−4.65 to −2.70
Cu_2S			604–904	−5.64 to −4.54
MoS	13,639	6.678	904–1106	−5.40 to −3.69

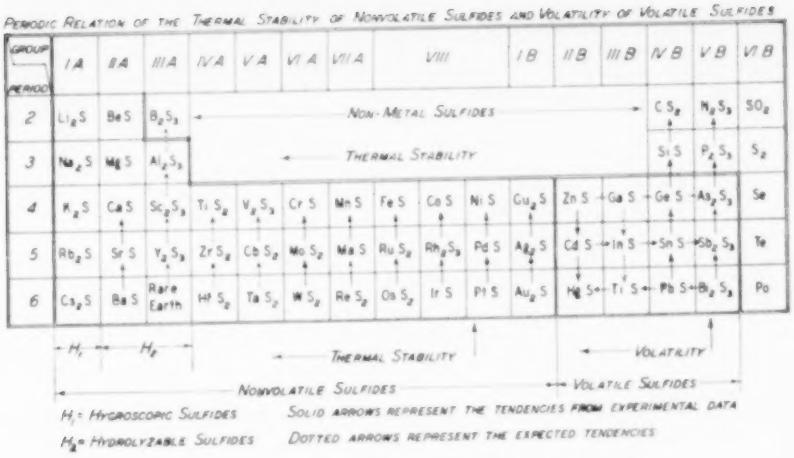

Fig. 4—Probable volatility and stability relationship of metallic sulphides.

carefully and weighed; the results show that the dissociation was roughly 38 pct at 704°C, increasing to 45 pct at 904°C.

The unusual shape of the Cu_2S curve may be the result of the formation of this fine metallic copper wool or moss copper on the surface of the sulphide sample which retards the escape of the vapor. Schuhmann and Moles[7] have shown how sensitive the sulphur pressure above Cu_2S is to a variation from the theoretical composition.

MoS$_2$: The apparent vapor pressure is even less than the dissociation pressure calculated from the free energy data of Kelley. It can be assumed that the weight loss is mainly due to dissociation.

Miscellaneous Experiments: An experiment with CaS showed so little loss of weight even at 1100°C for extended times that no figures could be obtained for the vapor pressure. It suffices to say that CaS has an extremely low vapor pressure and great stability. Experiments with Al_2S_3 and with Na_2S failed because the moisture picked up from the air gave erratic weight readings.

Relation of Sulphide Volatilities and Position of the Metal in the Periodic System: On the basis of the data presented and the semiquantitative values to be found in the literature, an attempt has been made to systematize the behavior of metallic sulphides as to volatility and stability.

For purposes of discussion the sulphides have been classified into two groups, volatile sulphides, those which lose weight chiefly by volatilizing as such, and nonvolatile sulphides, those which dissociate rather than evaporate. This classification superimposed on a periodic arangement of the elements is shown in Fig. 4.

The magnitude of the volatilities and the trend of sulphide stability are shown with arrows. Solid arrows are based on experimental data either from this paper or from other sources; dotted arrows represent expected tendencies.

Summary

The rate of weight loss vs. temperature has been determined for a number of metallic sulphides when heated under vacuum. These data are presented in the form of apparent vapor pressures. The sulphides are classified as volatile or nonvolatile sulphides on the basis of whether the weight loss is chiefly the result of evaporation of the sulphide molecule, or whether it results mainly from dissociation. A proposed classification has been made of a large number of sulphides.

It is felt that the information gathered is a basis for determining the practicality of the selective volatilization of the sulphides, as well as giving information necessary for planning direct reduction processes for metallic sulphides.

References

[1] L. Brewer et al.: *Chemistry and Metallurgy of Miscellaneous Materials*. Chap. 4 (1950) New York. McGraw-Hill Book Co.

[2] J. S. Brown: *Ore Genesis*. (1948) Hopewell Press.

[3] K. K. Kelley: U. S. Bur. Mines *Bull.* 383 (1935) p. 61.

[4] V. R. Schenck and A. Albers: *Ztsch. anorg. allgem. Chem.* (1919) **105**, pp. 145-146.

[5] B. K. Veselovskii: *Journal of Applied Chemistry* (Russian) (1942) **15**, pp. 422-435.

[6] A. D. Pogorelyi: *Journal of Physical Chemistry* (Russian) (1948) **22**, pp. 731-745.

[7] J. Lumsden: Memorandum dated January 1950.

[8] C. J. Smithells: *Metals Reference Book*. (1949) Interscience Pub. Co.

[9] W. J. Kroll and A. W. Schlechten: *Journal* Electrochem. Soc. (1948) **93**, p. 247.

[10] P. C. Carman: *Trans.* Faraday Soc. (1948) **44**, pp. 529-536.

[11] H. W. Melville: *Trans.* Faraday Soc. (1936) **32**, p. 1017.

[12] A. L. Marshal, R. W. Dornte, and F. J. Norton: *Journal* Amer. Chem. Soc. (1937) **59**, pp. 1161-1166.

[13] E. M. Cox et al.: *Trans.* AIME (1949) **185**, p. 27; JOURNAL OF METALS (January 1949).

[14] K. Jellinek and J. Zakowski: *Ztsch. anorg. allgem. Chem.* (1925) **142**, p. 1.

[15] E. V. Britzke, A. F. Kapustinsky, and B. Wesselowsky: *Ztsch. anorg. allgem. Chem.* (1933) **213**, p. 69.

[16] K. Sudo: *Sci. Rep.* Research Inst. Tohoku Univ. (1950) **A2**, No. 3.

[17] C. R. Hayward: *Trans.* AIME (1914) **48**, p. 141.

[18] R. Schuhmann, Jr. and O. W. Moles: *Trans.* AIME (1951) **191**, p. 235; JOURNAL OF METALS (March 1951).

Crystal Structure of TiAl

by Pol Duwez and Jack L. Taylor

THE present knowledge of the Ti-Al system is limited to the portion of the diagram extending from pure aluminum to the intermetallic compound $TiAl_3$. A preliminary investigation of the titanium-rich Ti-Al alloys revealed that the solubility of aluminum in α titanium is quite extensive and that the transformation temperature of titanium is raised by alloying with aluminum. From an X-ray diffraction study of alloys containing up to 75 atomic pct Al (TiAl$_3$), the phase boundaries at 750° C were located as follows: the α titanium solid solution extends from 0 to about 36 atomic pct Al, a two-phase region exists from 36 to 46 atomic pct Al, and an intermediate phase of varying concentration extends from 46 to 62 atomic pct Al. The purpose of the present paper is to describe the crystal structure of this new phase.

The alloys were prepared by melting in a helium arc furnace on a water-cooled copper plate, using a furnace essentially the same as that described in ref. 2. The titanium metal was of the iodide type furnished by the New Jersey Zinc Co., and a piece of pure aluminum (99.99 pct) was obtained through the courtesy of the Aluminum Co. of America. After melting, the samples, weighing approximately 5 g, were sealed in evacuated fused silica tubes and homogenized for 4 hr at 1000° C. The specimens were then held for 10 days at 750° C and rapidly cooled to room temperature. Filings were then taken from each sample, sealed in evacuated vials, annealed at 750° C for 4 hr, and rapidly cooled to room temperature by quenching the vials in water. Powder diffraction patterns were obtained with a 14.32 cm diam camera, using $K\alpha$ copper radiation filtered through a nickel foil.

Structure Determination

The X-ray diffraction patterns of the alloys containing 46, 50, 55, 60, and 62 atomic pct Al were identical, except for a slight shift in the positions of the reflections. The alloy containing 55 atomic pct Al was chosen for structure determination. The powder pattern contained 37 reflections and the α_1-α_2 doublets were well resolved in the back-reflection range. The relatively small number of reflections and the sharpness of the pattern were considered as an indication of a simple atomic arrangement in a relatively small unit cell of high symmetry, and an attempt was therefore made to solve the structure without single crystal work. A satisfactory fit was found on a large scale Hull-Davey tetragonal chart for an axial ratio of approximately 1.45. All the reflections were readily indexed and the tentative unit cell dimensions were computed to be $a = 2.81$ kX, $c = 4.07$ kX, and $c/a = 1.448$.

The indices (hkl) and the values of d and $\sin^2\theta$ are given in Table I. The agreement between observed and computed $\sin^2\theta$ is quite satisfactory. Once the unit cell was known, the details of the structure were readily found. First, it is obvious that the number of atoms per unit cell cannot exceed two, since more than two atoms would lead to a density greater than that of pure titanium. The next logical step is to assume that the two atoms occupy the corner and center of the cell. If this assumption is correct, the structure may be described as follows: space group $D^1_{4h} - P\,4/mmm$; one titanium atom in a: 000, one aluminum atom in d: $\frac{1}{2}\frac{1}{2}\frac{1}{2}$; and no extinctions.

Assuming this structure to be the correct one, intensities were computed by means of the usual equation:

$$I = p\,F^2 \frac{1 + \cos^2 2\theta}{\sin^2\theta\cos\theta}$$

where F is the structure factor; θ, the Bragg angle; and p, the multiplicity factor. The calculated values of intensities are compared in Table I with the visually estimated intensities. The agreement is quite satisfactory and the structure is therefore confirmed.

The crystal structure of TiAl just described is the same as that of AuCu ordered. The AuCu ordered

P. DUWEZ and J. L. TAYLOR, Members AIME, are Associate Professor of Mechanical Engineering and Chief of the Materials Section, and Research Engineer, respectively, Jet Propulsion Laboratory, California Institute of Technology, Pasadena, Calif.

Discussion on this paper, TP 3211E, may be sent, 2 copies, to AIME by April 1, 1952. Manuscript, Aug. 3, 1951. New York Meeting, February 1952.

structure, however, is not generally described on the basis of the smallest possible tetragonal unit cell (containing two atoms) used in the present study. The usually accepted representation of the AuCu ordered structure is by means of a slightly deformed cubic structure for which the a parameter is $\sqrt{2}$ times larger than the parameter of the small cell considered above, and the c parameter is the same. In order to conform to the accepted nomenclature, the structure of TiAl may then be described as type $L1_0$ (AuCu ordered), space group $D^1_{4h} - P\,4/mmm$, with one titanium atom in a: 000; one titanium atom in c: $\frac{1}{2}\frac{1}{2}0$; and two aluminum atoms in e: $0\frac{1}{2}\frac{1}{2}$ and $\frac{1}{2}0\frac{1}{2}$. If the AuCu type unit cell is used, new indices (hkl) have to be assigned to the reflections of the powder pattern. These (hkl) are listed in the seventh column of Table I. It may be noted that with the AuCu ordered type unit cell, only the (hkl) for which $h + k = 2n$ are observed, as a result of the special atomic positions e of the D^1_{4h} space group.

Lattice Parameter Variation with Composition

Because of the difference in the atomic diameters of titanium and aluminum, it may be anticipated that the size of the unit cell of TiAl will vary with composition. As stated above, the range of homogeneity of the TiAl phase extends from 46 to 62 atomic pct Al at 750°C. Within this range of concentration, the lattice parameters of various alloys were computed (on the basis of the primitive unit cell) by applying the least-squares method to the high angle reflections of the powder patterns. The results, presented in Fig. 1, show that the a parameter decreases regularly, whereas the c parameter increases steadily with increasing aluminum concentration. The change in the axial ratio c/a is shown in Fig. 1.

Table I. Diffraction Data for TiAl (55 atomic pct Al)

hkl Small Cell	d kX	Sin²θ		Relative Intensity		hkl Large Cell
		Observed	Calculated	Observed*	Calculated	
001	4.06	0.0358	0.0357	w	96	001
100	2.80	0.0734	0.0748	w	73	110
101	2.31	0.1107	0.1107	s	1000	111
002	2.04	0.1420	0.1433	w	169	002
110	1.99	0.1492	0.1492	m	305	200
111	1.78	0.1844	0.1844	vw	28	201
102	1.65	0.2170	0.2170	vw	20	112
112	1.421	0.2926	0.2921	m	200	202
200	1.404	0.2998	0.2984	w	96	220
003	1.350	0.3242	0.3218	vvw	1	003
201	1.328	0.3351	0.3340	vvw	9	221
210	1.260	0.3722	0.3733	vvw	7	130
103	1.222	0.3957	0.3963	w	118	113
121	1.201	0.4097	0.4089	m	224	131
202	1.157	0.4414	0.4413	w	100	222
113			0.4710		4	203
212	1.069	0.5171	0.5161	vvw	10	132
004	1.018	0.5702	0.5712	vw	19	004
220	0.9942	0.5978	0.5969	vw	36	400
203			0.6197		4	223
221			0.6328		4	401
104			0.6463		4	114
300			0.6716		3	330
213	0.9230	0.6936	0.6946	w	137	313
301	0.9133	0.7084	0.7074	vw	68	331
114	0.9056	0.7203	0.7208	vw	70	204
222	0.8924	0.7403	0.7399	vw	68	402
310	0.8894	0.7470	0.7462	vw	70	420
311	0.8791	0.7805	0.7818	vvw	12	421
302			0.8145		6	332
204	0.8243	0.8696	0.8696	w	90	224
312	0.8152	0.8892	0.8932	m	193	422
005			0.8991		1	005
223	0.8026	0.9173	0.9181	vvw	10	403
124	0.7914	0.9435	0.9446	vw	23	314
105	0.7820	0.9663	0.9677	m	183	115
320			0.9702		17	510
303	0.7716	0.9940	0.9932	m	197	333

*s, indicates strong; m, medium; w, weak; vw, very weak; and vvw, very very weak.

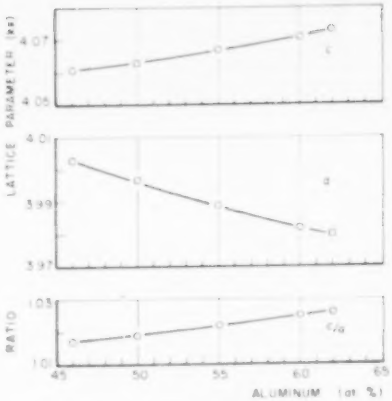

Fig. 1—Lattice parameters and axial ratio of TiAl phase vs. aluminum concentration.

It is therefore demonstrated that the substitution of aluminum for titanium into the TiAl phase results in an expansion of the unit cell in the c direction, and the contraction which would normally be expected on the basis of atomic size takes place only in the basal plane of the tetragonal cell.

A very similar change in the shape of the unit cell has been found for dilute solid solutions of various elements in hexagonal metals like magnesium (see for example ref. 3). In this case, theoretical considerations have shown that the lattice expansion in the direction of the c axis was related to the electron concentration of the solid solution.[4] It is very probable that the increase in electron concentration with aluminum addition is also responsible for the change in the c/a ratio of the TiAl phase.

Conclusions

The crystal structure of TiAl is tetragonal, type $L1_0$ (AuCu ordered). At 750°C, the TiAl phase extends from 46 to 62 atomic pct Al. Within this range, the a parameter decreases and the c parameter increases with increasing aluminum concentration. The axial ratio c/a increases regularly from 1.017 to 1.026.

Acknowledgment

This work was done at the Jet Propulsion Laboratory, California Institute of Technology, under contract number DA-04-495-ORD-18 with the Army Ordnance Department, Washington, D. C. The authors wish to thank this agency for the permission to publish the results of this investigation.

References

[1] W. L. Fink, K. R. Van Horn, and P. M. Budge: Constitution of High Purity Aluminum-Titanium Alloys. *Trans.* AIME, (1931) **98**, pp. 421-436.

[2] C. H. Schramm, P. Gordon, and A. R. Kaufmann: The Alloy Systems Uranium-Tungsten, Uranium-Tantalum and Tungsten-Tantalum. *Trans.* AIME (1950) **188**, pp. 195-204; JOURNAL OF METALS (January 1950).

[3] G. V. Raynor: The Lattice Spacings of the Primary Solid Solutions of Silver, Cadmium, and Indium in Magnesium. *Proc.* Royal Soc. (1940) **174A**, pp. 457-471.

[4] W. Hume-Rothery and G. V. Raynor: The Apparent Sizes of Atoms in Metallic Crystals with Special Reference to Aluminum and Indium and the Electronic State of Magnesium. *Proc.* Royal Soc. (1940) **177A**, pp. 27-37.

Crystal Structure of $TaCr_2$ and $CbCr_2$

by P. Duwez and Howard Martens

IN two papers published in 1949, [1,2] alloys of chromium with the refractory metals tungsten, molybdenum, tantalum, and columbium were investigated in view of their possible use as high temperature resisting materials. For the Cr-Ta system, a partial phase diagram was presented and the only intermediate phase was identified at $TaCr_2$. A phase of the same composition was also observed in the Cb-Cr system. The X-ray diffraction data presented in these papers, however, were insufficient for crystal structure determination.

It is shown in the present study that the only intermediate phase in both the Ta-Cr and the Cb-Cr systems corresponds to the ideal stoichiometric ratio $TaCr_2$ or $CbCr_2$. Both structures are cubic, MgCu$_2$ type. At high temperature, however, $TaCr_2$ has a hexagonal MgZn$_2$ type structure, which can be retained at room temperature by fast cooling.

The alloys were prepared by melting in a helium arc furnace on a water-cooled plate. The design of the furnace was essentially the same as that described in ref. 3. Some alloys were also obtained by sintering compacts made of the mixed powders pressed at 80,000 psi. The sintering was carried on for 4 hr at 1375° C.

The tantalum and columbium powders were supplied by Fansteel Metallurgical Corp., North Chicago, Ill. The tantalum powder was the reagent grade, with a particle size smaller than 400 mesh and a total impurity content less than 0.1 pct. The columbium powder was smaller than 325 mesh and contained approximately 0.1 pct C and traces of Fe, Ti, and Zr. The electrolytic chromium powder from Charles Hardy, Inc., New York, was smaller than 300 mesh and contained about 0.1 pct Na, 0.05 pct Ca, and traces of Cu, Al, Mg, Si, and Co.

Powder diffraction patterns were obtained with a 14.32 cm camera, using copper K_α radiation filtered through nickel foil. The powder pattern of the $TaCr_2$ alloy obtained by sintering at 1375° C was different from that obtained on the same alloy rapidly cooled from the melt. Contrary to this result, the powder pattern of $CbCr_2$ was the same, whether the alloy was made by sintering at 1375° C or by melting, and was similar to that of the $TaCr_2$ sintered. It was also found that the structure of the $TaCr_2$ specimen obtained by melting was retained after heating for 4 hr at 1590° C, but transformed into the structure found in the sintered specimen after heating for 4 hr at 1375° C. Hence, the structural change of $TaCr_2$ appears to be a reversible polymorphic transformation.

$CbCr_2$ and $TaCr_2$ Structure, Low Temperature Form

By using large scale Hull-Davey charts, the powder pattern of $CbCr_2$ and of the low temperature form of $TaCr_2$ were readily interpreted on the basis of a face-centered cubic lattice with a parameter of approximately 6.95 kX. The indices of the reflections together with the values of $\sin^2\theta$ are given in Tables I and II. From this list of observed reflections, it appears that the (200), (600), (024), (046), and (028) reflections are missing. The lack of $(h00)$ reflections for $h = 4n$ indicates a four-fold screw axis. The missing $(0kl)$ spectra for $k + l = 4n$ indicate the existence of a diamond glide d. The combination of these symmetry elements can be found in the $O_h^7 - Fd3m$ space group, which is therefore the most probable one.

After having determined the approximate density of $TaCr_2$ by the immersion method, the number of molecules per unit cell was calculated and found to be nearly eight. This information, added to the fact that the most probable space group is O_h^7, leads to the consideration of a structure of the MgCu$_2$ type, in which the atoms have the following positions: 8 magnesium in a and 16 copper in d. On the basis of this structure, intensities were computed by means of the usual formula:

$$I = pF^2 \frac{1 + \cos^2 2\theta}{\sin^2\theta \cos\theta} \qquad [1]$$

where F is the structure factor; θ, the Bragg angle; and p, the multiplicity factor. As shown in Tables I

P. DUWEZ, Member AIME, is Associate Professor of Mechanical Engineering and Chief of the Materials Section and H. MARTENS is Research Engineer, Jet Propulsion Laboratory, California Institute of Technology, Pasadena, Calif.

Discussion on this paper, TP 3210E, may be sent (2 copies) to AIME by April 1, 1952. Manuscript, Aug. 3, 1951. New York Meeting, February 1952.

Table I. Diffraction Data for $CbCr_2$

hkl	d kX	$\sin^2\theta$ Observed	$\sin^2\theta$ Calculated	Relative Intensity Observed	Relative Intensity Calculated
111			0.0364		37
220	2.46	0.0976	0.0971	ms	490
311	2.10	0.1340	0.1335	s	1000
222	2.01	0.1463	0.1457	m	210
400			0.1942		1
331			0.2307		8
422	1.424	0.2914	0.2914	m	170
511-333	1.335	0.3361	0.3278	ms	275
440	1.233	0.3887	0.3885	m	214
531	1.176	0.4273	0.4249	vw	8
620	1.102	0.4866	0.4856	w	73
533	1.065	0.5229	0.5220	w	110
622	1.030	0.5560	0.5542	w	73
444			0.5827		<1
711-551			0.6191		2
642	0.9025	0.6792	0.6798	w	135
553-731	0.8930	0.7167	0.7163	m	300
800	0.8719	0.7773	0.7770	w	75
733			0.8134		2
822-660	0.8223	0.8739	0.8741	m	150
555-751	0.8036	0.9165	0.9165	ms	410
662	0.8000	0.9253	0.9226	w	135

s indicates strong; ms, medium strong; m, medium; w, weak; vw, very weak; and vvw, very very weak.

and II, the observed and computed values of $\sin^2\theta$ agree well and there are no flagrant discrepancies between the computed intensities and those estimated visually. In the powder pattern of $CbCr_2$, the few reflections that were not observed have the weakest computed intensities.

The lattice parameters of the two compounds were computed by applying the least squares method to eight high-angle reflections. These parameters are: for $TaCr_2$, $a = 6.947$ kX; for $CbCr_2$, $a = 6.976$ kX. The interatomic distances are: in $TaCr_2$, Ta to Cr, 2.880 kX; Ta to Ta, 3.008 kX; Cr to Cr, 2.456 kX; and in $CbCr_2$, Cb to Cr, 2.892 kX; Cb to Cb, 3.021 kX; Cr to Cr, 2.466 kX.

In view of the fact that the atomic diameters of tantalum and columbium are almost identical, it is not surprising to find almost identical lattice parameters for the two compounds $TaCr_2$ and $CbCr_2$. In this connection, it is also interesting to note that the structure of $TiCr_2$ is also face-centered cubic with a parameter equal to 6.929 kX.[4] Since the three atoms titanium, columbium, and tantalum have almost the same size, it is most probable that an uninterrupted series of solid solutions would exist between the three isomorphous phases, $TaCr_2$, $CbCr_2$, and $TiCr_2$.

TaCr$_2$ Structure, High Temperature Form

The powder patterns obtained on $TaCr_2$ samples either after melting or after heating for 4 hr at 1590°C contained 34 reflections and the high angle reflections were not clearly resolved into doublets. Annealing the powder would probably have improved the sharpness of the pattern, but in order to retain the high temperature form, it would have been necessary to anneal above 1375°C, and at such a temperature it would have been difficult to prevent the powder from sintering and from absorbing residual oxygen or nitrogen of the helium atmosphere. In spite of the lack of sharpness of the high angle reflections, the indexing of the pattern was achieved after a satisfactory fit was found on a Hull-Davey chart for the hexagonal system at an axial ratio of about 1.63.

The indices, together with the values of $\sin^2\theta$, are given in Table III. The only missing reflections are those corresponding to (hhl) with $l = 2n$, and hence five space groups are possible. Further information

Table II. Diffraction Data for $TaCr_2$ Low Temperature Form

hkl	d kX	$\sin^2\theta$ Observed	$\sin^2\theta$ Calculated	Relative Intensity Observed	Relative Intensity Calculated
111	3.97	0.0373	0.0367	m	332
220	2.44	0.0982	0.0979	s	750
311	2.08	0.1353	0.1346	s	1000
222	2.00	0.1478	0.1469	w	92
400	1.74	0.1952	0.1958	vvw	29
331	1.59	0.2338	0.2326	w	76
422	1.414	0.2953	0.2938	m	283
511-333	1.335	0.3315	0.3305	m	284
440	1.225	0.3938	0.3917	m	293
531	1.174	0.4288	0.4284	w	59
620	1.096	0.4920	0.4896	w	126
533	1.059	0.5269	0.5263	w	111
622	1.043	0.5411	0.5396	vw	52
444	1.000	0.5909	0.5875	vvw	8
551-711	0.9723	0.6250	0.6242	vw	42
642	0.9281	0.6863	0.6854	w	221
553-731	0.9045	0.7223	0.7222	m	324
800	0.8680	0.7843	0.7834	vw	72
733	0.8482	0.8205	0.8201	vvw	29
822-660	0.8189	0.8812	0.8813	m	258
555-751	0.8023	0.9180	0.9180	m	316

Table III. Diffraction Data for $TaCr_2$ High Temperature Form

hkl	d kX	$\sin^2\theta$ Observed	$\sin^2\theta$ Calculated	Relative Intensity Observed	Relative Intensity Calculated
100	4.23	0.0331	0.0327	w	220
002	4.03	0.0365	0.0366	vw	83
101	3.72	0.0428	0.0419	w	400
102	2.92	0.0695	0.0693	w	296
110	2.45	0.0969	0.0962	s	725
103	2.26	0.1161	0.1151	s	1000
200	2.12	0.1319	0.1309	w	160
112	2.09	0.1357	0.1349	ms	375
201	2.06	0.1397	0.1400	ms	435
004			0.1463		45
202			0.1675		1
104			0.1792		25
203	1.67	0.2126	0.2133	w	87
210	1.60	0.2316	0.2290	vw	34
211	1.57	0.2405	0.2382	vw	34
105	1.51	0.2600	0.2616	m	148
122	1.491	0.2667	0.2656	vw	51
204			0.2774		1
300	1.418	0.2944	0.2945	m	130
123	1.380	0.3113	0.3114	ms	460
006			0.3296		340
302	1.339	0.3307	0.3311	ms	295
205	1.285	0.3591	0.3598	ms	244
106			0.3623		43
124	1.255	0.3764	0.3753	vvw	14
220	1.227	0.3938	0.3926	m	191
310			0.4254		1
116			0.4278		28
222	1.178	0.4287	0.4293	vw	28
311			0.4345		31
213			0.4579		120
206	1.138	0.4578	0.4605	m	60
312			0.4620		22
313	1.080	0.5083	0.5078	m	190
400			0.5235		18
401	1.052	0.5357	0.5327	w	91
224			0.5391	w	31
216	1.031	0.5578	0.5587	vw	39
402			0.5601		1
314			0.5719		8
403			0.6059		20
320			0.6217		10
306	0.9750	0.6237	0.6241	vvw	19
321			0.6308		10
315	0.9528	0.6534	0.6543	w	95
322			0.6583	w	17
404			0.6760		1
410	0.9316	0.6832	0.6871	m	190
323			0.7041		170
226	0.9049	0.7241	0.7223	m	97
412			0.7247	m	195
405	0.8876	0.7526	0.7524	m	140
316			0.7550	m	18
324			0.7682		8
500	0.8547	0.8116	0.8150	vvw	6
501			0.8271		6
325	0.8343	0.8518	0.8506	m	126
406			0.8531	m	60
502			0.8546		11
330	0.8214	0.8703	0.8834	vw	73
503			0.9064		8
420			0.9162		55
332	0.8018	0.9220	0.9201	w	168
421			0.9253		163

about the structure was then obtained by analogy with other intermetallic compounds of the AB_2 type. As pointed out by Laves,[7] the three typical structures MgCu$_2$ (face-centered cubic), MgZn$_2$ (hexagonal with $c/a = 1.64$), and MgNi$_2$ (hexagonal with $c/a = 3.26$) have very closely related atomic arrangements. Since the low temperature form of TaCr$_2$ has the MgCu$_2$ cubic structure, it was anticipated that the hexagonal high temperature form might be isostructural with either MgZn$_2$ or MgNi$_2$. Since the structure could be indexed on the basis of a hexagonal cell with an axial ratio of about 1.63, the possibility of a MgZn$_2$ type structure was first investigated. The structure is described as follows: space group D^4_{6h} — $C\,6/mmc$, 2 chromium in a, 6 chromium in h with $x = 1/6$, and 4 tantalum in f with $z = 1/16$.

On the basis of this structure, the intensities computed by means of eq 1 are given in Table III. The agreement between observed and calculated intensities is quite satisfactory, except for the first four reflections. These four reflections, corresponding to small Bragg angles, are probably weakened because of the high absorption factor of tantalum. The structure of the high temperature form of TaCr$_2$ is therefore hexagonal and isomorphous with MgZn$_2$. The lattice parameters are $a = 4.915$ kX, $c = 8.046$ kX, and $c/a = 1.637$.

Summary

In the Ta–Cr and Cb–Cr systems, the only intermediate phase is located around the stoichiometric compositions TaCr$_2$ or CbCr$_2$. The crystal structure of CbCr$_2$ is face-centered cubic, MgCu$_2$ type, with 24 atoms per unit cell. The TaCr$_2$ phase has a polymorphic transformation at a temperature between 1375° and 1590° C. The low temperature form is isomorphous with CbCr$_2$ (MgCu$_2$ type). The high temperature form is hexagonal, MgZn$_2$ type, with 12 atoms per unit cell.

Acknowledgment

This work was done at the Jet Propulsion Laboratory, California Institute of Technology, under contract number DA-04-495-ORD-18 with the Army Ordnance Department, Washington, D. C. The authors wish to thank this agency for permission to publish the results of this investigation.

References

[1] O. Kubaschewski and A. Schneider: Measurements on the Oxidation-Resistance of High-Melting Point Alloys. *Journal* Inst. Metals (1949) **75**, pp. 403-416.

[2] O. Kubaschewski and H. Speidel: Oxidation-Resistance and Some Phase Relationships in the System Chromium-Tantalum-Nickel. *Journal* Inst. Metals (1949) **75**, pp. 417-430.

[3] C. H. Schramm, P. Gordon, and A. R. Kaufmann: The Alloy Systems Uranium-Tungsten, Uranium-Tantalum, and Tungsten-Tantalum. *Trans.* AIME (1950) **188**, pp. 195-204; JOURNAL OF METALS (January 1950).

[4] P. Duwez and J. L. Taylor: A Partial Titanium-Chromium Phase Diagram and the Crystal Structure of TiCr$_2$. Paper submitted for publication to the American Society for Metals.

[7] F. Laves and H. Witte: The Crystal Structure of MgNi$_2$ and Its Relation to the MgCu$_2$ and MgZn$_2$ Types. *Metallwirtschaft* (1935) **14**, pp. 645-649.

Technical Note

A Sensitive Method for Thermal Analysis of Very Low Melting Alloys

by R. M. Evans, E. O. Fromm, and R. I. Jaffee

IN connection with a research on gallium alloys, a method for the thermal analysis of very low melting alloys was developed, which appeared to be worthy of more than passing interest. As used, the method was suitable for work in the temperature range, −72° to 250° C. However, with suitable adjustment, the method could be adapted for use over broader temperature ranges.

The Rosenhain temperature gradient furnace,[1] adapted for low-temperature use, was the basis for the method. The gradient was set up in a stainless steel tube. The specimens were lowered through it at a constant rate while time-temperature or inverse rate data were taken. It was essential to maintain careful control of the top and bottom temperatures of the gradient. Also essential was good heat transfer from the walls to the specimen. This was accomplished by a liquid heat-transfer medium.

R. M. EVANS, Member AIME, E. O. FROMM, and R. I. JAFFEE, Member AIME, are associated with Battelle Memorial Institute, Columbus, Ohio.

TN 98E. Manuscript, Sept. 14, 1951.

[1] Rosenhain, Some Appliances for Metallographic Research, Journal Inst. Metals (1913) **10**, p. 150.

Fig. 1—Thermal analysis furnace and auxiliary equipment.

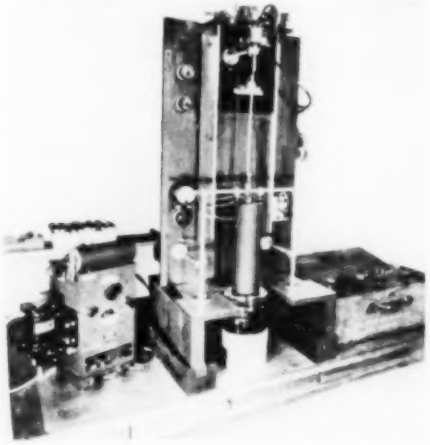

Fig. 1 is a photograph of the thermal-analysis equipment. Details of the furnace and the specimen holder are shown diagrammatically in Fig. 2. The furnace tube was made from a 2-in. round stainless-steel shaft, 16.5 in. long. A 0.75-in. hole was bored from the top to within 0.25 in. of the bottom. The top 3 in. were wound with 8 ft of 18-gage Chromel-A heating wire, and the bottom 3 in. were finned to promote good heat transfer to the cooling bath. The whole tube, except for the finned bottom, was insulated with 1 in. of natural asbestos. In use, the finned bottom section was held in an equilibrium mixture of dry ice and alcohol at −72°C. The top section was heated to varying temperatures, up to about 250°C, depending on the maximum temperature desired for thermal analysis of a particular alloy.

Melts of 2 g were prepared, and then transferred to either a rubber finger cot for the lower melting liquid, or a glass thimble for the higher melting liquids. The thimble or cot was then hung on the lowering device and a thermocouple and stirrer inserted in preparation for the actual thermal analysis. To provide good thermal contact and to prevent uneven cooling by air currents, the furnace cavity and the thimble were filled with a low-pour-point synthetic oil.

To insure uniform temperature distribution throughout the melt, a small stirrer having a combined rotary and vertical motion was used. Sufficient agitation was obtained with the stirrer rotated at 6 rpm and a two-cycle vertical amplitude of $\frac{1}{8}$ in.

Bare copper-constantan thermocouples were used, with the melt serving as the hot junction. New ends of the wire were presented to each melt to eliminate possible thermocouple contamination. A Leeds and Northrup semiprecision potentiometer was used to measure the thermal emf's set up by the couple. Temperatures measured were considered accurate to 0.5°C.

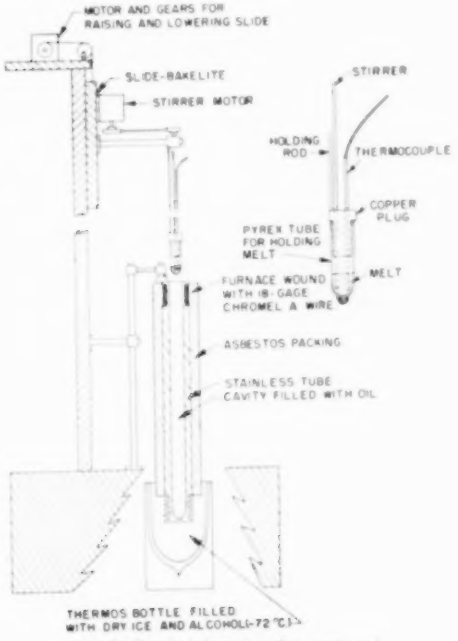

Fig. 2—Detail of thermal-analysis equipment.

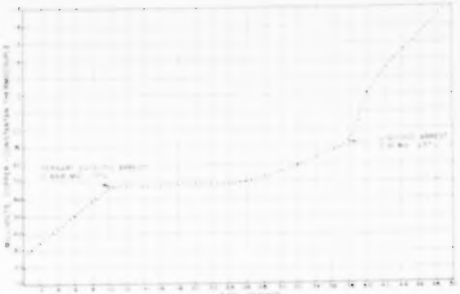

Fig. 3—Typical time-temperature curve obtained on heating Ga-Sn-Zn alloy.

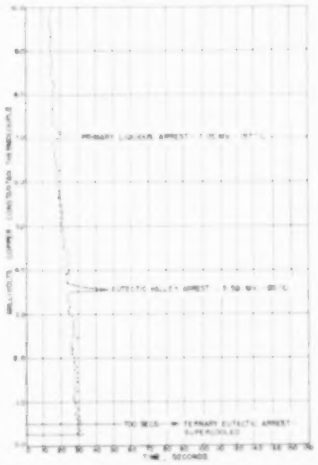

Fig. 4—Typical inverse rate curve obtained on cooling Ga-Sn-Zn alloy.

The rate of lowering, or raising, through the temperature gradient varied from 1° to 2.5°C per min, depending on the top temperature used.

Using the furnace described above, very satisfactory thermal-analysis curves were obtained. Typical curves for gallium-rich alloys are shown in Figs. 3 and 4.

Good liquidus arrests could be obtained during cooling, and, if a wide enough range existed between the liquidus and solidus, intermediate eutectic line arrests could be obtained. The eutectic component of the alloy usually supercooled to a considerable degree, so that eutectic or solidus arrests on cooling were not reliable. Heating curves were found to be better for determining these solidus temperatures. Conversely, heating curves were unreliable for liquidus arrests. Gallium is well known for its supercooling tendencies. Thus, for gallium-rich alloys, time-temperature curves, rather than inverse-rate curves, gave more reliable data.

Acknowledgment

This work was done under the auspices of the Department of the Navy, Bureau of Ships.

Rolling Textures in Face-Centered Cubic Metals

by Hsun Hu, P. R. Sperry, and Paul A. Beck

As described by means of quantitative pole figures, the inside texture of highly rolled aluminum and copper strips may be approximately described by four equivalent ideal orientations near (123) [121]. If rolled in reversed passes, the surface texture of copper is also near (123) [121], that of aluminum is (100) [011]. The inside texture of highly rolled brass is (110) [112]. The surface texture is the same, if rolled in reversed passes. The surface texture of all three metals is related to the inside texture, but asymmetrical, if rolled without reversal between passes.

MANY previous investigations dealing with the subject of the present work were reviewed by Wassermann,[1] Barrett,[2] Brick,[3] and Richards.[4] The recent introduction of quantitative methods for pole figure determination by Decker, Asp, and Harker,[5] Schulz[6] and others made it possible to reinvestigate some of the finer points which the earlier more qualitative photographic methods left undecided.

The rolling textures of silver and of 70-30 cartridge brass have been quite consistently characterized by the ideal orientation of (110) parallel to the plane of rolling and [112] parallel to the rolling direction. On the other hand, it has been recognized by several investigators that certain other face-centered cubic metals, such as copper and aluminum, developed rolling textures rather different from that of brass. These textures have been variously described by the following ideal orientations, singly or in combinations with each other: (110) [112]; (112) [111]; (135) [335]; (135) [211], etc. The discrepancies usually have been attributed to the lack of sharpness in the textures and to the attendant difficulty of associating "ideal orientations" with pole figures showing great scatter of orientations. It seemed desirable to investigate by the new quantitative methods to what extent the apparent lack of sharpness may have been brought about by the qualitative methods used previously, rather than by the textures themselves, and to decide, if possible, between the various ideal orientations which have been proposed.

Another problem, not satisfactorily settled by earlier investigations, concerns surface textures in rolled metals. For instance, in rolled aluminum the surface texture in some cases appeared to be similar to the texture inside the sheet, whereas in other cases it was reported to be entirely different.[7] The conditions under which such differences may have arisen, and the possibility of the occurrence of different surface textures in other face-centered cubic metals do not appear to have been examined in detail.

The present work was undertaken to investigate the above questions. Some of the results obtained have been described briefly.

Experimental Procedure

Specimen Preparation: In the present investigation 2S aluminum, electrolytic tough-pitch copper, and commercial 70-30 brass were used. These materials were available in the form of cold-drawn rods, 1 in. diam for tough-pitch copper and commercial 70-30 brass and 1½ in. diam for 2S aluminum.

The cold-drawn bars were alternately annealed and rolled 30 pct lengthwise in several cycles until a penultimate thickness of 0.500 in. was reached. The intermediate and the penultimate anneals were carried out for 30 min at 380°C with 2S aluminum, and for 30 min at 550°C with 70-30 brass. For tough-pitch copper, the intermediate anneals were 30 min

H. HU, Student Associate AIME, with the Institute for the Study of Metals, University of Chicago, Chicago, and P. A. BECK, Member AIME, Research Professor of Physical Metallurgy, University of Illinois, Urbana, were both formerly associated with the University of Notre Dame. P. R. SPERRY is with the Dept. of Metallurgy, University of Notre Dame, Notre Dame, Ind.

Discussion on this paper, TP 3207E, may be sent, 2 copies, to AIME by April 1, 1952. Manuscript, July 2, 1951. New York Meeting, February 1952.

Part of this paper represents a portion of thesis by Hsun Hu submitted in partial fulfillment of requirements for the degree of Doctor of Philosophy to the Graduate School of the University of Notre Dame.

at 650 C, and the penultimate anneal 30 min at 400 C. All annealing operations were carried out in constant-temperature salt baths. Penultimate grain size in each material was determined before final rolling. The average grain size values found were: 0.18 mm for 2S aluminum, 0.03 mm for tough-pitch copper, and 0.023 mm for commercial 70-30 brass.

The final rolling operation was carried out in two different ways: Procedure *a*—the strip was passed through the rolls in the same direction in successive passes, and procedure *b*—the strip was reversed end to end between successive passes.

The final rolling reduction in thickness was 95 pct for 2S aluminum and commercial 70-30 brass, with a reduction of approximately 10 pct in each pass. The final thickness of the rolled 2S aluminum strip and of the rolled commercial 70-30 brass strip was 0.024 in. The final rolling reduction given the tough-pitch copper strip was 96 pct, giving a final thickness of 0.020 in. The rolls used for all rolling operations were $3\frac{1}{2}$ in. diam, and were frequently lubricated with light mineral oil in order to reduce surface friction.

X-ray specimens were prepared of both the inside material of the cold-rolled strips (at approximately the center of the strip thickness) and the surface. The specimens were about 1 in. long and $\frac{3}{4}$ in. wide. The inside specimens were obtained by etching the strip in dilute hydrochloric acid solution (for 2S aluminum) and in 50 pct nitric acid solution (for tough-pitch copper and commercial 70-30 brass) at both surfaces until the thickness was reduced to 0.004 in. (for 2S aluminum) and to 0.002 in. (for tough-pitch copper and commercial 70-30 brass). The surface specimens were prepared by etching the strip on one surface only, until the same thickness (0.004 in. for 2S aluminum specimens and 0.002 in. for tough-pitch copper and commercial 70-30 brass specimens) was reached, while the other surface of the strip was protected from the acid by a painted layer of Glyptal. The texture of the surface material (surface texture) and of the inside material ("inside texture") was determined for strips of aluminum, copper, and brass rolled according to procedures *a* and *b*. Corresponding to the multiplicity of conditions and materials just described 12 specimens were prepared.

Quantitative Texture Determination: Texture determinations were made by using a General Electric Geiger counter X-ray spectrometer, which allows the quantitative determination of diffracted beam intensities. $CuK\alpha$ radiation was used throughout. The center portion of the pole figures (up to 40° away from the center) was determined by the Schulz reflection method,[7] which made it necessary to make corrections for absorption and for irradiated volume. It was found, however, that beyond about 40° away from the normal of the reflecting specimen surface the measured X-ray intensity rapidly decreased.[8] A full discussion of the variables bearing on this effect will be given in a paper by Chernock and one of the present authors.[9] Because of this intensity decrease, the peripheral part of the pole figures (from 40° to 90° away from the center) was determined by the Decker, Asp, and Harker transmission method,[10] using calculated correction factors for absorption and irradiated volume. The procedure is not given here, since it is available in the literature.[11] The reflection specimen holder used in the present work was so constructed as to allow scanning of an area of at least $0.5 \times 1\frac{1}{4}$ in. of the specimen surface. During scanning the reflecting specimen surface remained parallel with itself, and the counting device integrated the diffracted X-ray intensities. This procedure gave satisfactory results even with annealed specimens up to a uniform grain size of approximately 0.017 mm. No scanning and integration was used in conjunction with the transmission method.

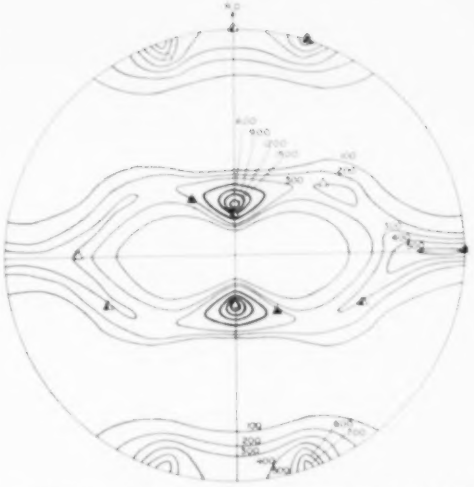

Fig. 1—(111) pole figure for the inside texture of 95 pct rolled 2S aluminum strip.

Rolled strip thickness 0.024 in., specimen 0.004 in. thick from center portion of strip. Open triangle indicates the position of (111) poles for ideal orientation (7, 12, 22) (345) (near (123) (121)). The (110) (112) and (112) (111) orientations, previously proposed in the literature, are indicated by the solid and the half-filled triangles, respectively. Intensities in arbitrary units.

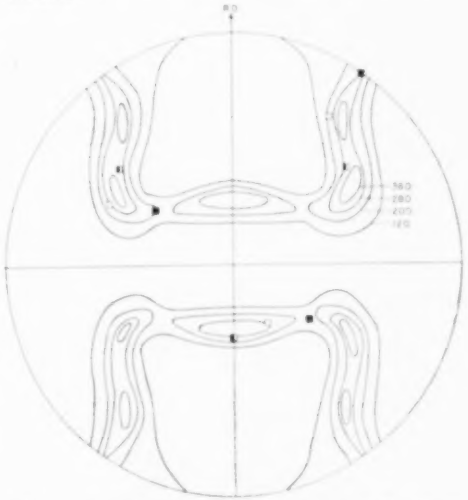

Fig. 2—(200) pole figure for the rolling texture of 2S aluminum strip obtained from the same specimen used for Fig. 1.

Open square indicates (7, 12, 22) (345) (near (123) (121)); solid square, (110) (112); half-filled square, (112) (111). Intensities in arbitrary units.

Fig. 3—(111) pole figure for the inside texture of 96 pct rolled strip of tough pitch copper.

Specimen 0.007 in. thick, from center portion of 0.070 in. thick rolled strip. Open triangle indicates (358) [352] (near (123) [121]); solid triangle (1, 9, 11) [945] (near (146) [211]). Intensities in arbitrary units.

In determining the center portion of the pole figure by the reflection method two quadrants (quadrants I and III) were experimentally determined, the other two quadrants were drawn as mirror images of quadrants I and III with respect to the rolling direction. The intensity measurements were in most cases taken at 10° intervals of rotation of the specimen in its own plane (corresponding to the azimuthal angle in the pole figure) and at 5° intervals of rotation of the specimen about axes in the plane of rolling (corresponding to the radial angle from the center of the pole figure). In high intensity regions intensity measurements were taken at 1° or 2° intervals in order to accurately locate the intensity maxima in the pole figure. In determining the peripherial portion of the pole figure by the transmission method, measurements were made in all four quadrants at angle intervals similar to those just described.

At 40° away from the center of the pole figure, the diffracted beam intensities were measured by both the reflection and the transmission methods. This overlapping was used to establish the intensity ratio between the transmitted and the reflected intensities under a certain set of conditions. In order to construct a complete pole figure, the reflected intensities were converted into corresponding transmitted intensities, and intensity contour lines were drawn at suitably selected intensity levels.

Results and Discussion

Inside Textures: The pole figures obtained for the inside texture of aluminum, copper, and brass rolled according to procedure *a* were practically the same as those for the same metals rolled according to procedure *b*. Fig. 1 shows the (111) pole figure quantitatively determined for the inside texture of the 95 pct rolled 2S aluminum strip, procedure *b*. The outstanding new feature of this pole figure is the occurrence of rather sharp high intensity maxima, such as the two located 25° from the center of the pole figure toward the rolling direction and the reverse rolling direction, respectively. The particular maxima mentioned, representing by far the

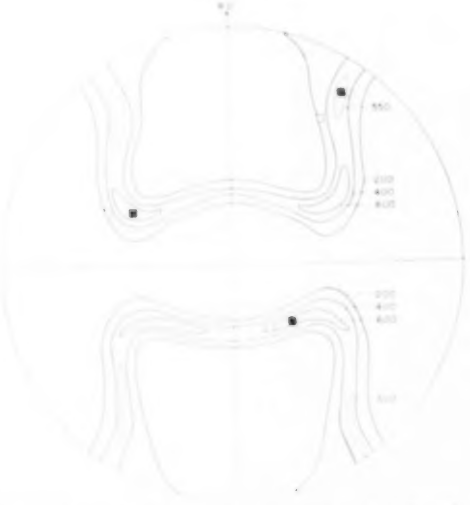

Fig. 4—(200) pole figure for the rolling texture of tough pitch copper strip.

Same specimen as in Fig. 3. Open square indicates (358) [352] (near (123) [121]); solid square (1, 9, 11) [945] (near (146) [211]). Intensities in arbitrary units.

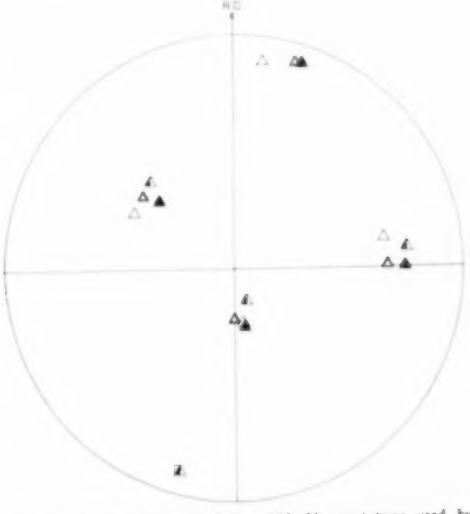

Fig. 5—(111) pole figure showing "ideal" orientations used by various investigators for the rolling textures of aluminum, copper, and a 48 pct Ni-Fe alloy.

Triangle in triangle indicates (2, 12, 22) [845] "ideal" orientation (near (123) [121]), for the rolling texture of aluminum (this paper); open triangle, "ideal" orientation for the rolling texture of aluminum, designated as (135) [335] by Goetzel and Sachs; solid triangle, (135) [211] "ideal" orientation for the rolling texture of copper, reported by Barrett and Steadman; half-filled triangle, "β-texture," used by Masters to describe the rolling texture of a 48 pct Ni-Fe alloy.

Fig. 6—(111) pole figure for the inside texture of 95 pct rolled strip of commercial 70-30 brass.

Specimen 0.002 in. thick, from center portion of 0.024 in. thick rolled strip. Triangle indicates (110) [112] orientation. Intensities in arbitrary units.

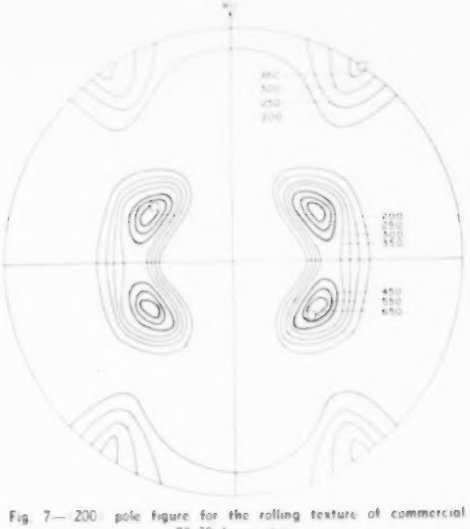

Fig. 7—(200) pole figure for the rolling texture of commercial 70-30 brass strip.

Same specimen as used for Fig. 6. Square indicates (110) [112] orientation. Intensities in arbitrary units.

highest intensities in the whole pole figure, are not satisfactorily accounted for by the (110) [112] ideal orientation, which has often been considered as the principal orientation in cold-rolled face-centered cubic metals.[5] It may be stated that the (111) poles for neither the (110) [112] orientation nor for the (112) [111] orientation, indicated by solid and half-filled triangles, respectively, fit the maxima found in the pole figure. On the other hand, it was found that the rolling texture may be reasonably well described as scatter around four ideal orientations corresponding to (7, 12, 22) parallel to the rolling plane and [845] parallel to the rolling direction. This orientation is not far from (123) [121]. The four symmetrical, crystallographically equivalent orientations of this type are shown in the pole figure by the open triangles. It is seen that these orientations account very well for the strongest intensity maxima near the center, fairly well for the four second highest intensity maxima at the periphery, but only approximately for the other high intensity areas. Fig. 2 shows the corresponding (200) pole figure, obtained with the same specimen.

Fig. 3 shows the (111) pole figure for the inside texture of the 96 pct rolled strip of tough-pitch copper, rolling procedure *b*. This pole figure is very similar to that of aluminum (compare Fig. 3 with Fig. 1), although there are some minor differences. For copper the two highest intensity maxima near the center are slightly closer to the center (22°) than they are for aluminum (25°). Nevertheless, the rolling texture of tough-pitch copper is also clearly of the (123) [121] type. Pole positions of approximately (358) [352] orientation and of approximately (2, 9, 11) [945] orientation are indicated in the pole figure by the open triangles and solid triangles, respectively. The (3, 5, 8) [352] orientation accounts fairly well for all the high intensity areas except those on the equator. The corresponding (200) pole figure for the same specimen is shown in Fig. 4.

The present results are in fairly good agreement with the earlier paper by Goeler and Sachs,[4] where the (135) [335] orientation was proposed, and particularly with Barrett and Steadman,[5] who found that (135) [211] is a principal orientation in the rolling texture of copper, and with Guinier and

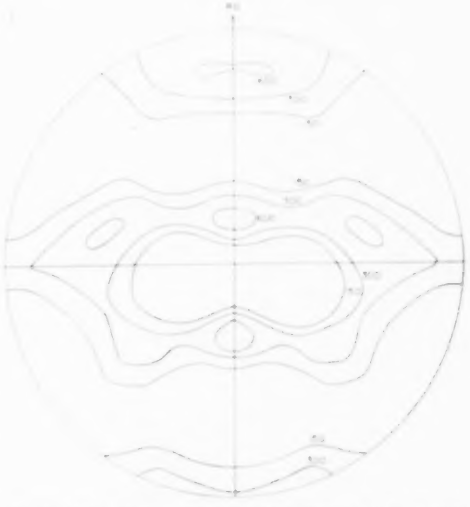

Fig. 8—(111) pole figure for the surface texture of 95 pct rolled 2S aluminum strip (rolled in one direction without reversing strip end for end between successive passes).

Strip 0.025 in. thick, specimen 0.001 in. thick from surface of strip. Intensities in arbitrary units.

Fig. 9—111 pole figure for the surface texture of 96 pct rolled tough pitch copper strip rolled in one direction without reversing strip end for end between successive passes

strip 0.078 in. thick, specimen 0.007 in. thick from surface of strip. Intensities in arbitrary units

Tennevin,[7] Custers[8] showed that the major part of the rolling texture of a face-centered cubic 48 pct Ni-Fe alloy corresponds to the so-called "Z-orientation," which also is fairly close to the (123) [121] type orientations, as obtained for aluminum and copper in the present investigation. The ideal orientations according to Goeler and Sachs for aluminum, Barrett and Steadman for copper, and Custers for a 48 pct Ni-Fe alloy, together with the ideal orientation obtained for aluminum in the present investigation, are shown in Fig. 5.

Fig. 10—111 pole figure for the surface texture of 95 pct rolled commercial 70-30 brass strip rolled in one direction without reversing strip end for end between successive passes

strip 0.013 in. thick, specimen 0.007 in. thick from surface of strip. Intensities in arbitrary units

The quantitatively determined pole figures for the inside texture of the 95 pct rolled 70-30 brass strip, procedure *b*, are shown in Figs. 6 and 7 for (111) poles and (200) poles, respectively. These pole figures are in excellent agreement with the results previously reported by various investigators and with the conventional (110) [112] ideal orientation (as indicated by the triangles in Fig. 6 and the squares in Fig. 7). This texture consists of two fairly sharply developed twin-related components. The difference between the rolling texture of brass, on the one hand, and that of aluminum and copper, on the other, is very obvious when their quantitative pole figures are compared. The fundamental reasons for this difference are not clear; they may possibly lie in differences with respect to the formation of deformation bands.

Surface Textures. Fig. 8 shows the (111) pole figure obtained for the rolling texture of the surface material of the 2S aluminum strip which was final-rolled according to procedure *a*, i.e., rolled in the same direction in successive passes. The general shape of the pole figure for this surface texture is similar to that for the inside texture of the strip, but there is a general shifting of all poles away from the direction of rolling, resulting in an asymmetrical pattern.*

The surface texture of the 2S aluminum strip final-rolled according to procedure *b*, i.e., by reversing it end to end between successive passes, is, however, entirely different. It corresponds to a (100) [011] orientation, as found previously by Vargha and Wassermann.[3] The (100) [011] type surface texture was obtained by those investigators with an aluminum strip of 5 mm thickness; in thinner strips (1 mm or less) they found a surface texture similar to the inside texture. For this reason, they associated the occurrence of the (100) [011] surface texture with a large strip thickness. The present results indicate that both types of surface texture may be obtained at the same strip thickness, depending on the rolling procedure employed.

In analogy to aluminum, the surface textures in tough-pitch copper and in commercial 70-30 brass final-rolled according to procedure *a* show asymmetrical pole figures (Figs. 9 and 10). In the case of brass (Fig. 10), the shifting of the poles from their symmetrical position in the inside texture to their asymmetrical position in the surface texture may be approximately described as a 5° rotation around the cross-rolling direction, but no similarly simple description applies for the surface texture of either copper or aluminum.

The surface texture of tough-pitch copper and of commercial 70-30 brass final-rolled according to procedure *b*, that is, reversed between passes, is the same as their respective inside textures. These materials do not develop the (100) [011] surface texture found in aluminum after rolling in reversed passes. The different behavior of copper and aluminum in this respect is rather striking, since their rolling textures are otherwise very similar.

Summary

1—Quantitative pole figures were determined for both the inside texture and the surface texture of

* This shift was earlier erroneously described as one toward the direction of rolling.

highly rolled 2S aluminum, tough-pitch copper, and commercial 70-30 brass strips with two different rolling procedures: *a*—rolled in the same direction in successive passes, and *b*—rolled by reversing the strip end to end between successive passes.

2—For each material the inside texture is the same regardless of whether the strip was rolled according to procedure *a* or *b*.

3—The inside texture in rolled 2S aluminum and in tough-pitch copper strips is nearly the same. This texture may be approximately described as scatter around four symmetrical, crystallographically equivalent orientations, not far from (123) [121]. On the other hand, the inside texture of rolled commercial 70-30 brass corresponds well to the ideal orientation (110) [$\bar{1}$12].

4—The surface textures of all three materials, when rolled according to procedure *a*, is somewhat similar to their respective inside textures, except for a general shifting of all poles away from the direction of rolling. This shift results in asymmetrical pole figures.

5—The surface textures of tough-pitch copper and of commercial 70-30 brass rolled according to procedure *b* show no difference from their respective inside textures; that of rolled 2S aluminum exhibits an entirely different texture corresponding to the (100) [011] orientation, previously described by Vargha and Wassermann.[17] The present results indicate that this type of surface texture in aluminum is a result of the reversal of the rolling direction between passes.

Acknowledgment

This work was supported by the Office of Naval Research, U. S. Navy, Contract No. N6ori-165, T. O. 1.

References

[1] G. Wassermann: *Texturen Metallischer Werkstoffe* (1939) Berlin.

[2] C. S. Barrett: *Structure of Metals*. 1st ed. p. 395 (1943) New York. McGraw-Hill Book Co.

[3] R. M. Brick: Deformation Textures. *Cold Working of Metals*. p. 99 (1949) Cleveland. A.S.M.

[4] T. Ll. Richards: Preferred Orientation in Non-ferrous Metals. *Progress in Metal Physics*. Edited by B. Chalmers. Vol. I, p. 281 (1949). London and New York.

[5] B. F. Decker, E. T. Asp, and D. Harker: Preferred Orientation Determination Using a Geiger Counter X-ray Diffraction Goniometer. *Journal of Applied Physics* (1948) **19**, p. 388.

[6] L. G. Schulz: A Direct Method of Determining Preferred Orientation of a Flat Reflection Sample using a Geiger Counter X-ray Spectrometer. *Journal of Applied Physics* (1949) **20**, p. 1030.

[7] G. Vargha and G. Wassermann: Uber die Abhangigkeit d. Kristallitanordnung in gewalzten Aluminium blechen von der Blechdicke. *Metallicirtschaft* (1933) **12**, p. 511.

[8] Hsun Hu and P. A. Beck: Rolling Texture in Aluminum. JOURNAL OF METALS (October 1950) p. 1214.

[9] Hsun Hu: Annealing Textures in Face-centered Cubic Metals. Thesis, University of Notre Dame (1951).

[10] W. P. Chernock and P. A. Beck: Analysis of Certain Errors in the X-ray Reflection Method for the Quantitative Determination of Preferred Orientations. To be published in *Journal of Applied Physics*.

[11] V. Goeler and G. Sachs: Walz- und Rekristallisation stextur regulaer-flaechen-zentrierter Metalle I. *Ztsch. f. Physik* (1927) **41**, p. 873.

[12] C. S. Barrett and F. W. Steadman: Structure of Copper After Rolling. *Trans.* AIME (1942) **147**, p. 57.

[13] J. F. H. Custers: Uber die (111)-Reflexe im Gewalzten und Rekristallisierten Nickeleisen. *Physica* (1941) **8**, p. 771.

[14] Tentative Method for Preparing Quantitative Pole Figures of Metals. A.S.T.M. Designation: E81-49T (1949).

[15] A. Guinier and J. Tennevin: Nouvelle Methode d'Etude aux Rayons X des Textures Cristallines. *Revue Metallurgie* (1948) **45**, p. 277.

Technical Note

Method for Locating Two-Liquid Immiscibility Limits

by R. E. Bish

IN an effort to distinguish experimentally between the radically different limits of two-liquid immiscibility reported for the Cu-Pb system by Bornemann and Wagenmann and by Briesemeister (see Fig. 1), it was found that the high temperature homogeneous liquid containing between 41 and 93 pct Pb could not be frozen without separation into two liquids with the fastest cooling technique that could be devised. Thus, the two-phase state could not be distinguished with certainty from the one-phase state by the examination of quenched samples. To overcome this obstacle the following method for detecting the presence of an interface between two immiscible conducting liquids at temperature was developed. Measurements made by the new method substantiate the Briesemeister diagram in its general form.

The method consists essentially in the measure-

R. E. BISH is with Materials Engineering Dept., Westinghouse Electric Corp., East Pittsburgh, Pa.

TN 97E. Manuscript, Sept. 25, 1951.

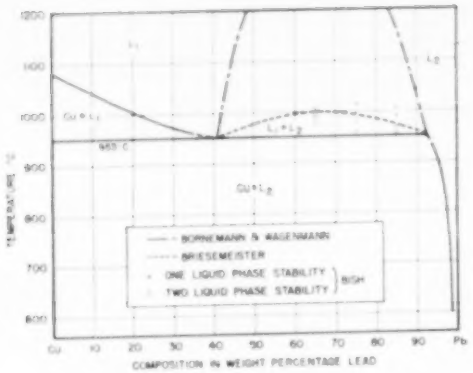

Fig. 1—left—Cu Pb phase diagram.

Fig. 4—below—Comparison of curves for an alloy of 65 pct Pb-35 pct Cu illustrating sudden resistance change with depth when two liquid phases are present.

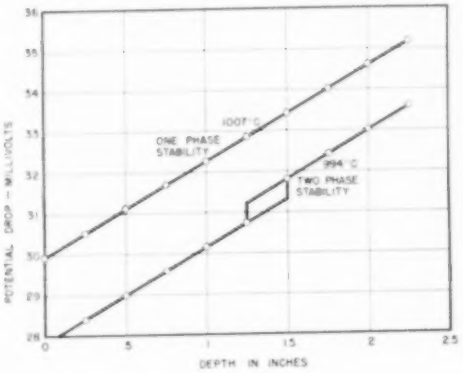

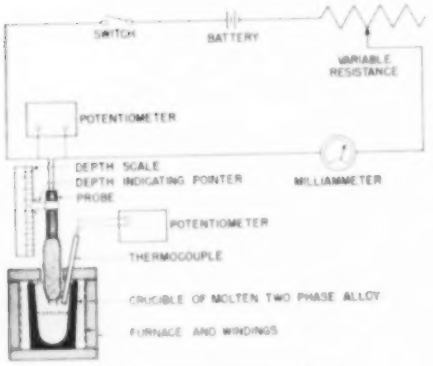

Fig. 2—Diagram of equipment layout.

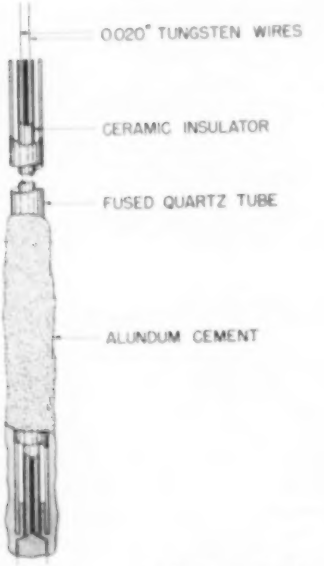

Fig. 3—Diagram of probe.

ment of the local electrical resistivity at a sequence of levels in the molten bath. Where a change of phase is encountered, the resistivity changes sharply. This measurement is made by the use of a (tungsten wire) probe consisting of a pair of wires, insulated except at their ends and kept at a fixed distance apart by a two-hole refractory tube. This probe is mounted upon a vertical slide directly above the crucible of metal, permitting it to be lowered by predetermined increments into the melt, Fig. 2. The vertical position of the probe is read from a scale upon the vertical slide and the resistance is read by means of a conventional potentiometric circuit.

An enlarged view of the probe is shown in Fig. 3. A pair of 18 gage tungsten wires are passed through a two-hole ceramic insulator. Enclosing this (except at the ends) is a fused quartz protection tube and a wash of white alundum cement is applied to the tip of the probe (except the wires) to seal and protect it from the molten metal.

As the probe is lowered into the molten bath the voltage read on the potentiometer increases directly (due to the heating of the probe wires). If only one phase is present at the temperature level under investigation, then a straight-line plot of voltage vs. depth will be obtained. If, on the other hand, two phases are stable at this temperature, there will be a sudden change in the voltage occurring at the interface between the two immiscible liquids. The magnitude of the change depends only upon the temperature under investigation, while the depth at which the interface occurs should vary both with composition and temperature. When the depth of the interface has been determined, tie-line phase relationships may be used to calculate the compositions of each liquid present at the temperature under investigation. Typical curves are shown in Fig. 4. These curves were obtained for an alloy containing 65 pct Pb-35 pct Cu. For this alloy, only one phase is stable at 1007°C, while two phases are stable at 994°C.

Annealing Textures in Rolled Face-Centered Cubic Metals

by Paul A. Beck and Hsun Hu

As described by means of quantitative pole figures, the annealing texture of highly rolled aluminum consists of the four retained components of the rolling texture near (123) [121], rather more sharply developed, and of a cube texture component. Local reorientation corresponds fairly well to 40° rotation around a [111] axis. In copper strip rolled 96 pct, the annealing texture is mainly the cube texture, with the four twin orientations as minor components. The annealing texture of highly rolled brass strip consists of four components of the (225) [734] type.

REVIEWS by Wassermann,[1] Barrett,[2] Dunn,[3] and Richards[4] give detailed accounts of the numerous publications dealing with annealing textures in rolled polycrystalline metals. Although a considerable amount of information of an empirical nature has been available for many years, even relatively recently the state of recrystallization-texture theory was considered uncertain. The reviews referred to above deal mainly with the description of experimental results, without developing generally applicable principles, suitable for explaining the observed annealing textures.

The investigations of Burgers and Louwerse[5] and Barrett[2] showed that in deformed single crystals of aluminum the orientation of the recrystallized grains deviates drastically from that of the deformed matrix. According to Barrett and to Beck and Hu,[6] the relationship between the two orientations can be best described as a rotation of about 40° around a [111] axis. Recent investigations led to similar orientation relationships for various face-centered cubic metals with a simple texture, regardless of whether the annealing process was recrystallization (strain-free grains growing in a highly deformed large crystal of aluminum[7] or copper,[8] or in deformed cube texture copper[9]) or coarsening (strain-free grains growing at the expense of an essentially strain-free, fine grained, polycrystalline matrix of single orientation texture copper,[10] aluminum,[11] or nickel-iron[12]). Barrett[2] pointed out the possibility that this orientation relationship may be a result of the orientation dependence of the rate of grain boundary migration. More recently, considerable evidence became available in favor of this view.[13,14]

In apparent contradiction to the above results, it has been known for a long time that the recrystallization texture of polycrystalline metals is often similar to the deformation texture. This was found, in particular, for the fiber textures obtained by wire drawing, compression, or compression rolling.[15] Following a suggestion by Barrett,[2] Kronberg and Wilson[16] and Beck and Hu[6] described a mechanism by which a [111] fiber texture, resulting from plastic deformation, may be retained upon recrystallization, even though the orientation of individual recrystallized grains differs from that of the local area of the matrix in which they grow. This mechanism assumes that the reorientation corresponds to a rotation around the [111] axis, which is also the fiber axis.

The present investigation was undertaken to examine in detail the orientation relationship between deformation texture and recrystallization texture in rolled face-centered cubic metals, using the quantitative methods of texture determination that have recently become available.[17,18] Quantitative pole figures for the rolling textures of such metals were reported recently.[19] Quantitative pole figures for annealing textures are given in the present paper. It was planned to investigate whether or not the orientation relationship previously found for the recrystallization of deformed single crystals, and for coarsening of single-orientation texture material, is capable of accounting for the observed, often complex, annealing textures in rolled polycrystalline metals. The question whether local reorientation is predominant, even in the early phases of the annealing process, was to be studied with high purity aluminum, by making use of an oxide film and sensitive tint illum-

P. A. BECK, Member AIME, Research Professor of Physical Metallurgy, University of Illinois, Urbana, and H. HU, Student Associate AIME, with the Institute for the Study of Metals, University of Chicago, were both associated with the University of Notre Dame, Notre Dame, Ind.

Discussion on this paper, TP 3206E, may be sent, 2 copies, to AIME by April 1, 1952. Manuscript, July 16, 1951. New York Meeting, February 1952.

This paper represents a portion of a thesis by Hsun Hu submitted in partial fulfillment of requirements for the degree of Doctor of Philosophy to the Graduate School of the University of Notre Dame. The other parts of this thesis have been published previously. See refs. 7, 12, and 16. Portions of the present work were published briefly in the form of a Research in Progress abstract, ref. 40.

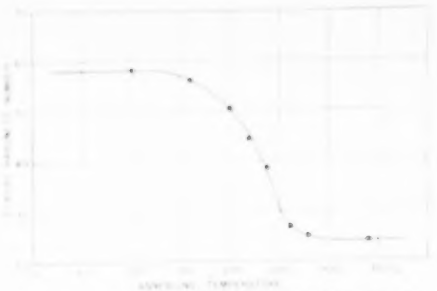

Fig. 1—Change of hardness in 95 pct rolled 2S aluminum strip as a function of annealing temperature.

Annealing time 5 min. Specimens corresponding to open circles were used for quantitative texture determination.

ination technique, which allows the estimation of orientations at high magnification in microscopically small areas of the specimen. The advantages of studies of this sort were pointed out by Lacombe and Beaujard.[3]

Experimental Procedure

In determining the annealing textures of rolled 2S aluminum, electrolytic tough-pitch copper, and commercial 70-30 brass, a number of specimens were cut from each of the strips previously used for the determination of the rolling textures.[1] The rolling reductions were 95 pct for aluminum, 96 pct for copper, and 95 pct for brass. The specimens were annealed in salt bath for 5 min at 20°C intervals in the temperature range of recrystallization. Vickers hardness measurements were made on each annealed specimen, and the average of four readings was plotted as a function of temperature. The results are shown in Figs. 1, 2, and 3 for 2S aluminum, tough-pitch copper, and commercial 70-30 brass, respectively. The annealing texture was quantitatively determined for each material annealed at the lowest temperature giving complete recovery of the hardness increase due to cold rolling. Only the "inside textures" of the annealed strips were determined.

Fig. 2—Change of hardness in 96 pct rolled electrolytic tough pitch copper strip as a function of annealing temperature.

Annealing time 5 min. Specimens corresponding to open circles were used for quantitative texture determination.

The preparation of the specimens for X-ray diffraction and the quantitative determination of the pole figures were carried out as described previously.[1]

A microscopic method was developed, making it possible to study the approximate orientation of deformation bands and of individual crystallites in high purity aluminum at magnifications up to X1000. The method is a variant of that described by Lacombe and Beaujard[3] and by Hone and Pearson.[4] The specimens were first electrolytically polished in a Buehler-Waisman Electro-Polisher with an electrolyte consisting of 2 parts of methyl alcohol and 1 part of concentrated nitric acid. The voltage employed was 12 v, the current density 10 milliamperes per sq mm, and the time of polishing 3 to 4 min. A thin oxide film was then formed on the polished surface by electrolytic etching in a mixture of phosphoric acid and carbitol solution. The composition of this solution is given in Table I.

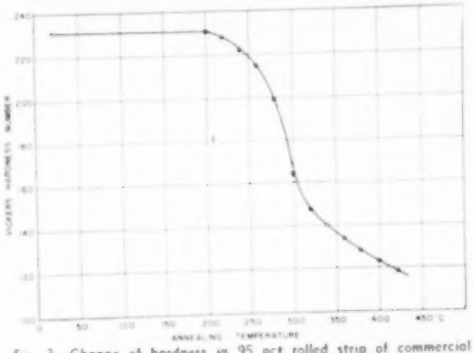

Fig. 3—Change of hardness in 95 pct rolled strip of commercial 70-30 brass strip as a function of annealing temperature.

Annealing time 5 min. Specimens corresponding to open circles were used for quantitative texture determination.

If a voltage of approximately 40 v and etching time of about 1 to 2 min is used,[5] the oxide film produced is suitable for magnifications up to about X200. Using sensitive tint illumination, bright color effects are observed, the color varying with the orientation of the underlying aluminum crystals. Thus, the orientation of small areas in the specimen could be estimated by observing the color. However, the oxide layer produced by the above method was too coarse grained for observation at high magnifications. A modified technique, developed in the present work, consisted of using a lower voltage (10 to 14 v) and longer time of etching (14 to 7 min). Under such conditions, the oxide film produced was very fine grained. Specimens prepared in this manner had a smooth appearance and satisfactory color contrast in sensitive tint illumination, even at magnifications as high as X1000, and visual observation at X1500 was possible.

Results

Fig. 4 shows the quantitative pole figure determined for the inside texture of the rolled and annealed 2S aluminum strip. The specimen was annealed for 5 min at 300°C, which was just sufficient to completely recover the hardness increment due to rolling, Fig. 1. The average recrystallized grain size after this annealing was about 0.017 mm. The pole figure shows that the four crystallographically equivalent "ideal orientations" of the (123) [121] type, which are present in the rolling texture,[1] are

Table I. Composition of Electrolyte Used for Producing a Thin Oxide Film on High Purity Aluminum

Materials	cc
Phosphoric acid	400
Carbitol	150
Water	140
Hydrofluoric acid	6

essentially retained in the annealing texture. In fact, they are here more sharply developed, as seen by comparing Fig. 4 with Fig. 1 of ref. 16. In addition, a new component appears in the annealing texture, which has the (100) (001), or "cube orientation." The existence of the "cube texture" component was confirmed by a rough determination of the (200) pole figure.

By means of the oxide film and sensitive tint illumination method, 95 pct rolled high purity aluminum* crystals in a coarse grained specimen were studied. In the as-rolled condition the deformed grains consisted of more or less clearly defined deformation bands, which appeared alternately yellow and blue, without sharp boundaries between them. The absence of sharp boundaries and the gradual merging of the color, i.e. orientation, of one band into that of its neighbors, Fig. 5, was confirmed at the highest available magnification.

It is interesting to note that the microscopic method shows only two major components in the rolling texture (corresponding to blue and yellow colors) while X-ray diffraction indicates four such components, Fig. 6. It was observed that, in rotating the stage of the microscope, all grains revert to their original color after a rotation of 180°. The method is, therefore, not capable of differentiating between two orientations related to each other by a 180° rotation around the optical axis. Since in the present work the optical axis always coincided with the rolling plane normal, it is understandable that component I of the rolling texture (see Fig. 6) should have the same color as component III, and II the same as IV. Neighboring deformation bands within the same grain, which appear alternately blue and yellow, may have an orientation relationship corresponding to that between components I and II (a rotation of 38° around the common [111] axis, marked Y in Fig. 6), or to that between components

Fig. 4—{111} pole figure for the annealing texture of 25 aluminum strip, rolled 95 pct and annealed 5 min at 300°C.

Specimen 0.004 in. thick, from center portion of 0.024 in. thick strip. Open triangle indicates (7, 12, 22) [8, 4, 5] orientation; circle in triangle, (100) [001] orientation. Intensities in arbitrary units.

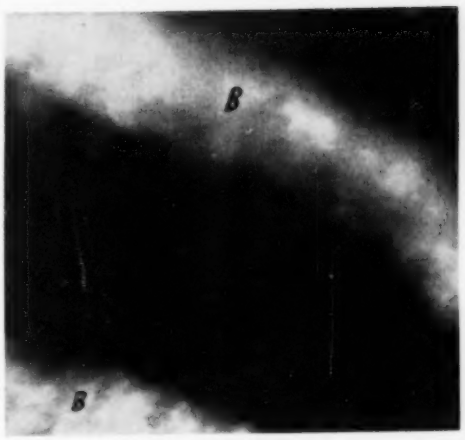

Fig. 5—High purity aluminum crystal, 95 pct rolled, showing deformation bands parallel to the rolling direction, with no sharp boundaries visible between regions of different orientations.

Specimen electrolytically polished, and anodically etched to produce thin oxide film. Alternate deformation bands appear yellow (Y) and blue (B) with the sensitive tint illumination used. X250.

Fig. 6—{111} pole figure showing the four symmetrical, crystallographically equivalent components of the rolling texture of 25 aluminum.

Their orientation is approximately (7, 12, 22) [8, 4, 5] which is near (123) [421]. Components I and II are related by a rotation of 38° around the common (111) pole Y. Components I and IV are related by a rotation of 55° around the common (111) pole Z. Components I and III are, in rough approximation, related by a rotation of about 45° around their (111) poles near the periphery, which are 10° apart. The relationship of components I and III can be accurately described as a 180° rotation around the rolling plane normal (the center of the pole figure).

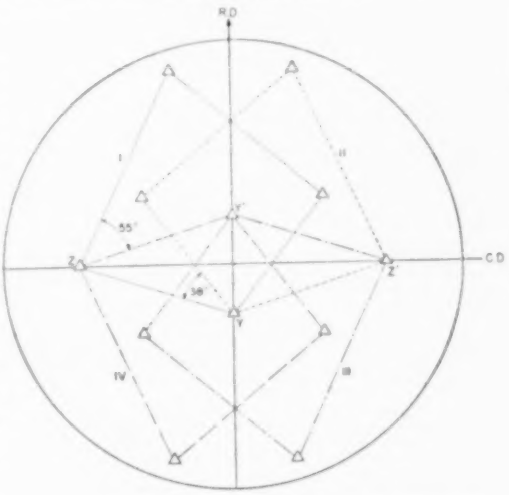

* Reported analysis: Cu, 0.002 pct; Si, 0.002 pct; Mg, 0.003 pct; Fe, 0.002 pct; Al, balance.

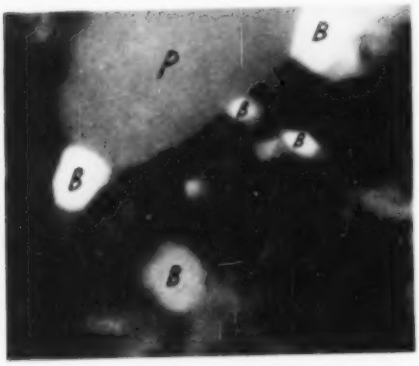

Fig. 7—High purity aluminum crystal, 95 pct rolled and annealed for 5 min at 340° C.

shown in the sensitive tint illumination used are several blue recrystallized grains (B), and a large pink recrystallized grain (P) in a matrix of yellow deformation band (Y), which has undergone recrystallization in situ and which consists of domains appearing in slightly varying shades of yellow. Specimen preparation the same as for Fig. 5. X150

I and IV (a rotation of 55° around the common [111] axes marked Z in Fig. 6). An orientation relation of the latter type, with a rotation axis (Z) near the cross-rolling direction, has been established earlier in a rolled aluminum single crystal by direct optical goniometer measurements.

After annealing the rolled high purity aluminum specimens over a rather wide range of temperatures, the colors (i.e. the orientations) observed with the oxide film and sensitive tint illumination method were largely the same as in the cold-rolled condition, namely yellow and blue. The only new color observed after annealing was pink, always associated with recrystallized grains. Fig. 7 shows such a pink grain in a yellow matrix. Other recrystallized grains in Fig. 7 have blue color. It was found that the blue recrystallized grains occur in yellow bands and vice versa, but that the pink recrystallized grains occur in both yellow and blue deformation bands. In all these cases of recrystallization the local orientation changes. However, the recrystallized grains of yellow and blue color have orientations which, although different from that of their immediate surroundings, are already present in other parts of the structure. Microscopic observation thus supports the idea that recrystallization with local reorientation is a mechanism leading to the retainment of the rolling texture in aluminum upon annealing. The orientation of the recrystallized grains of pink color was determined by means of etch pits and of X-ray diffraction, with specimens where these grains were sufficiently large. It was found that the pink grains have (100) approximately parallel to the rolling plane (which is parallel to the surface of the microscopic specimen), and [100] approximately parallel to the rolling direction. The pink grains, therefore, correspond to the "cube texture" component of the annealing texture, as shown in Fig. 4.

Careful microscopic examination, at high magnification and with critical adjustment of the color resolution, revealed that, in those areas of the deformation bands that have not been absorbed by the growing recrystallized grains, sharply defined boundaries emerge in the course of annealing. In place of the gradual variation of colors in the deformation band as-rolled, stepwise, or discontinuous color, i.e. orientation, changes along these new boundaries became increasingly evident during annealing. This structural change, which was observed to take place in severely rolled, high purity aluminum even at room temperature over long periods of time, proceeded within a few minutes at around 200° C. It left the local orientation of the deformation bands unchanged, while they became subdivided into large numbers of slightly disoriented domains, Fig. 7. The process is apparently identical with that designated by Crussard[7] as "recrystallization in situ," which is generally supposed to take place by the mechanism of "polygonization," as defined by Cahn.[8] In the rolled and annealed specimens the domain boundaries do not appear to have any crystallographic definition; the irregular network of the domain boundaries was found rather similar to that of ordinary grain boundaries. It may be concluded from the microscopic observations that "recrystallization in situ" is an important mechanism leading to the retainment of the deformation texture upon annealing in high purity aluminum.

Fig. 8—High purity aluminum crystal, 95 pct rolled and annealed for 5 min at 270° C and for 5 min at 310° C.

The domains formed by recrystallization in situ, and the grains formed by recrystallization with reorientation, show considerable growth. Specimen preparation the same as for Figs. 5 and 7. X150

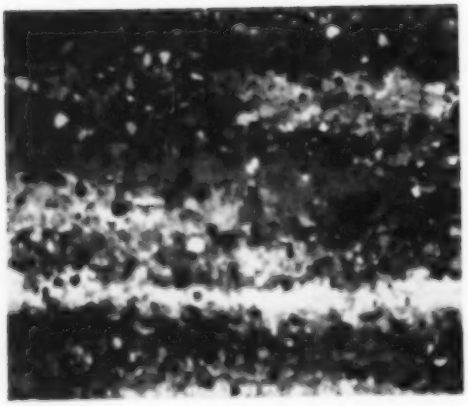

In severely rolled, high purity aluminum the average size of the domains formed by recrystallization in situ was found to be in the order of 2 microns. Similar size domains in highly deformed aluminum were previously reported by Keller, Hirsh, and Thorp[9] as a result of X-ray diffraction work by means of a microbeam method, and by Heidenreich[10] using electron transmission microscopy. Similar but apparently larger domains were observed by McLean, Tate, and Farmer[11] in hot-rolled aluminum, with the help of a microscopic method analogous to that used in the present work. It was observed that the domains, which become microscopically visible during annealing after severe cold rolling, usually do not perceptibly grow with further annealing, until the structure is finally swept by the boundary of a growing recrystallized grain of a different orientation. However, the interplay between recrystallization in situ and recrystallization with reorientation varies greatly between individual deformed grains of aluminum and, even in the same deformed grain, between the two sets of deformation bands. In some areas the domain boundaries hardly become discernible when recrystallized grains of a widely dif-

ferent orientation absorb the whole region. In other areas recrystallization with reorientation is greatly delayed, and recrystallization *in situ* leads to an apparently complete return to the fully annealed condition. In some cases such structures could be heated up to about 330 C for 5 min without much recrystallization involving reorientation, Fig. 8. At these relatively high annealing temperatures gradual growth was observed, in some cases increasing the average domain size to the order of 20 microns. At the same time, the orientation differences between neighboring domains become distinctly larger, so that in this condition the domains could be described without hesitation as grains. It was often observed that at still higher annealing temperatures (400 or 450 C), such fine grained areas, which have become fully annealed by recrystallization in situ and by domain growth, are eventually absorbed by large grains of a different orientation (usually near the cube orientation).

The inside texture determined for annealed electrolytic tough-pitch copper strip (annealed for 5 min at 200 C with a resulting average recrystallized grain size of 0.013 mm) is composed mainly of the (100) [001] orientation, or cube texture, with a minor component consisting of four (122) [21$\bar{2}$] type orientations, which are in the twin position with respect to the cube texture. The (111) pole figure and the (200) pole figure are shown in Figs. 9 and 10.

After completely recrystallizing the 95 pct rolled commercial 70-30 brass by annealing for 5 min at 340 C, an extremely fine grain size of approximately 0.002 mm was obtained. The inside texture determined for the recrystallized material is shown in Figs. 11 and 12, which represent the (111) pole figure and the (200) pole figure, respectively. Ideal pole positions for the (113) [21$\bar{1}$] orientation, frequently used to describe the recrystallization texture of brass, are indicated by solid symbols and those for the (225) [73$\bar{4}$] orientation are indicated by open triangles and squares in the pole figures. It appears that under the conditions of the present work the (225) [73$\bar{4}$] ideal orientation describes better the recrystallization texture of brass than the conventional (113) [21$\bar{1}$] orientation.

Discussion of Results

The present quantitative texture determinations confirm earlier statements found in the literature[7] that rolled commercial aluminum to a large extent retains its texture during annealing. However, it was found that, in addition to the four retained texture components, the texture also contains a fairly strong cube texture component. The occurrence of what was apparently a predominantly cube texture in rolled and annealed aluminum in a specific instance has been reported by Schmid and Wassermann.[8]

The microscopic observations clearly indicate that the retainment of the rolling texture in aluminum upon annealing is a result of both recrystallization in situ (relief of strain with practically no local orientation change), as described by Crussard,[9] and recrystallization with local reorientation. The latter contributes to texture retainment by producing orientations, which, although locally new, are prevalent in the texture as a whole.

It is interesting that the four retained components of the annealing texture of 2S aluminum correspond

Fig. 9—(111) pole figure for the annealing texture of electrolytic tough pitch copper strip, rolled 96 pct, annealed 5 min at 200 C. Specimen 0.002 in. thick, from center portion of 0.020 in. thick strip. Open triangle indicates (100) [001] orientation; solid triangle, (122) [21$\bar{2}$] orientation. The (111) pole, which these two orientations have in common is marked by half-filled triangle. Intensities in arbitrary units.

even more closely to the (123) [12$\bar{1}$] type "ideal orientation" than the four components of the rolling texture, for which this orientation was originally proposed. A decrease of the scatter around the "ideal orientation," that is, a sharpening of the texture, has been repeatedly found as a result of annealing. This sharpening may be due to either one of two mechanisms, both based on the orientation dependence of grain boundary mobility: 1—Preferential growth of large grains favorably oriented (for high

Fig. 10—(200) pole figure for the annealing texture of electrolytic tough pitch copper strip.

Same specimen as in Fig. 9. Open square designates (100) [001] orientation; solid square, (122) [21$\bar{2}$] orientation. Intensities in arbitrary units.

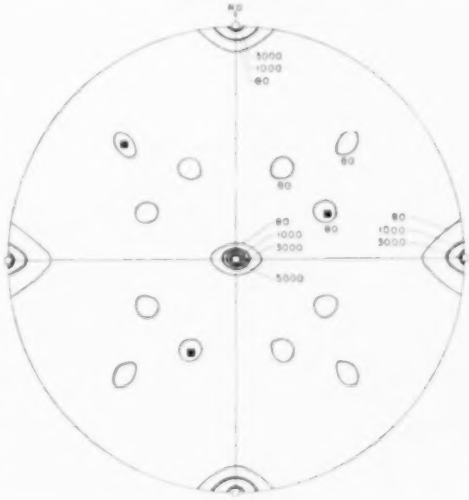

Fig. 11— [111] pole figure for the annealing texture of commercial 70-30 brass strip, rolled 95 pct and annealed 5 min at 340° C. Specimen 0.005 in. thick, from center portion of 0.025 in. thick strip. Open triangle denotes (225) [158] orientation, solid triangle (113) [211] orientation. Intensities in arbitrary units.

boundary mobility) with respect to the average orientation of the surrounding fine grained matrix. This may result in a sharp texture of the coarse grains in spite of large scatter of orientations in the fine grained matrix.” 2—Preferential absorption of small grains with orientations deviating considerably from that of the dominating texture, as a result of the greater mobility of their higher energy boundaries.[9] In view of the microscopic observations reported in the present paper, it is probable that both mechanisms play a role in the case of rolled aluminum.

The local reorientation upon recrystallization in highly rolled aluminum crystals, which results in orientations already present in other parts of the structure, should produce a local orientation change either of a type corresponding to the orientation relationship between components I and II, or of a type corresponding to that between components I and IV of the rolling texture, Fig. 6. The fact that the observations can be satisfactorily accounted for on the basis of a [111] rotation of 38° (corresponding to the orientation relationship between components I and II) is significant. It was found previously that a [111] rotation of approximately 40° may be used to describe the reorientation occurring in the spontaneous recrystallization in highly deformed aluminum single crystals and also in the texture-dependent coarsening of aluminum.[7] This orientation relationship corresponds to the highest grain boundary mobility for aluminum.[7,10]

The local reorientation connected with the growth of recrystallized grains of the cube orientation is shown in Fig. 13. The four [111] axes of the cube orientation approximately coincide with a [111] axis of each one of the four orientations of the rolling texture components in aluminum. The cube orientation is approximately related to each one of these four (123) [121] type orientations by a [111] rotation of 40°. The reorientation upon annealing of cold-rolled aluminum, leading to the formation of the cube texture is, therefore, again of a type to be expected on the basis of the orientation dependence of boundary mobility. An important difference between the grains of cube orientation on the one hand, and the recrystallized grains of the orientation of one of the retained texture components on the other, is that the former are favorably oriented for growth at the expense of either one of the four retained components, but the latter are favorably oriented with respect to two components only. Moreover, one of these two components is, in general, not in direct contact with the growing grain. A result of this difference is that upon further annealing, particularly at higher temperatures, the grains of cube orientation can grow readily, even after they become larger than the thickness of the deformation band in which they originated, but the recrystallized grains of the other type can grow at a high rate only within the deformation band in which they formed; after reaching the boundaries of this deformation band, their growth becomes much slower, because of unfavorable orientation. The conditions just described offer a satisfactory explanation for the effects of penultimate grain size, final rolling reduction, and final annealing temperature upon the formation of the cube texture,[7] in accordance with the observations recorded in the literature.

Previous investigations by Dahl and Pawlek,[7] Cook and Richards,[8] and Baldwin[9] showed that in rolled copper the relative amount of the cube texture after annealing increases with increasing rolling reduction and with decreasing penultimate grain size. The rather complicated pole figures obtained by Yen[7] for the annealing texture of 88 pct rolled copper strip may be interpreted to indicate partial retainment of the rolling texture, together with a cube texture component, and four components corresponding to annealing twins in the cube texture. The fact that in the present work the annealing texture of copper, Figs. 9 and 10, did not contain any retained texture component, but consisted only of the cube texture and its annealing twins, is satisfactorily accounted for by the high degree of def-

Fig. 12— [200] pole figure for the annealing texture of commercial 70-30 brass.

Same specimen as in Fig. 11. Open square indicates (225) [158] orientation, solid square, (113) [211] orientation. Intensities in arbitrary units.

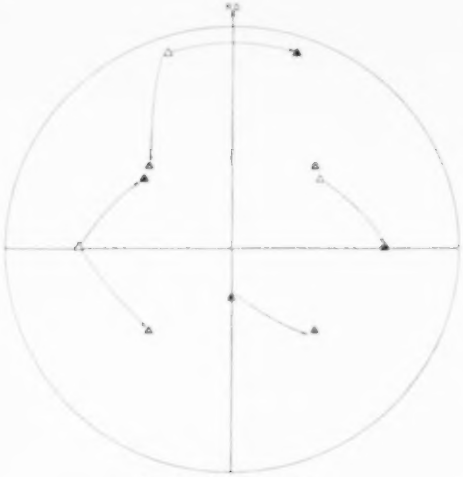

Fig. 13—(111) pole figure.

Orientation relationship is shown between two (7, 12, 22) [8, 4, 5] type orientations (open and solid triangles) and the (100) [001] orientation (circle in triangle). A (111) pole of each (7, 12, 22) [8, 4, 5] type orientation (rolling texture component) and a (111) pole of the (100) [001] orientation (cube texture) nearly coincide. The cube texture can be approximately derived from either one of the four components of the rolling texture by a 111 rotation of 10°.

ormation (96 pct reduction) and by the small penultimate grain size (0.03 mm). The similarity of the rolling textures[7] and of the annealing textures of copper and aluminum is striking. The principal differences in the annealing textures are the relative preponderance of the cube texture (perhaps as a result of the usually much smaller penultimate grain size and of the smaller width of deformation bands) and the presence of a much larger twin component in copper. It is significant that for the group of face-centered cubic metals which exhibit the phenomenon of the cube texture after rolling and annealing, such as copper, aluminum, and the 50-50 Ni-Fe alloy, the rolling texture is of the (123) [121] type. The addition to copper of certain alloying elements in solid solution, such as 5 pct Zn or 0.05 pct P, has the as yet unexplained effect of changing the rolling texture into the (110) [112] type, from which no cube texture develops upon annealing.

During the annealing process in highly rolled aluminum a large portion of the material undergoes microscopically visible recrystallization in situ, before being absorbed by growing grains of different orientations. The latter process could then be more properly designated as a type of discontinuous grain growth or coarsening, rather than as recrystallization, since the material absorbed is evidently no longer in the cold-worked condition at the time of its absorption, rather it is essentially strain free. As suggested by Smith,[9] the driving energy of the process must be the surface energy of the domain boundaries, rather than strain energy remaining from plastic deformation.

In 70-30 brass, where the reality of ordinary recrystallization and the absence of recrystallization in situ, at least during the greater part of annealing, is attested by the presence of slip bands in the material just being absorbed by grains of different orientation,[8] the rolling texture is, significantly, not retained upon annealing. If at all present in brass, recrystallization in situ must be relatively very slow and, therefore, unimportant in comparison with recrystallization involving reorientation. The rolling texture in brass is such that reorientation, of the type typical for face-centered cubic metals, does not result in orientations already present in the deformation texture and, therefore, recrystallization with reorientation also does not produce texture retainment. Cook and Richards[10] proposed a [111] rotation to describe the orientation relationship between rolling texture and recrystallization texture in brass. The present quantitative pole figures allow, at least in first approximation, an orientation relationship corresponding to [111] rotations of 30° (Fig. 14). The deviations may well be due to the fact that the recrystallized grains here are growing in a matrix consisting of not one but two major texture components. The additional reorientation resulting from grain growth at higher annealing temperatures, discovered by Wilson and Brick,[11] may be described by similar rotations in the reverse direction,[7] resulting in the approximate re-establishment of the deformation texture. Similar conditions were recently identified by Rost and Alexander,[12] for grain growth in silver, so that the analogy of textures in brass and in silver is now established for all three conditions: as-rolled, as-recrystallized, and after grain growth. It appears that for these metals the annealing textures are determined by the rolling texture, and by reorientations corresponding to maximum boundary mobility, but recrystallization in situ plays no significant role.

Summary

1—Quantitative pole figure determinations indicate that the annealing texture of 2S aluminum (penultimate grain size: 0.18 mm, rolled 95 pct and annealed for 5 min at 300°C) consists of four components of the (123) [121] type, retained from the rolling texture, and of a (100) [001], or cube texture component.

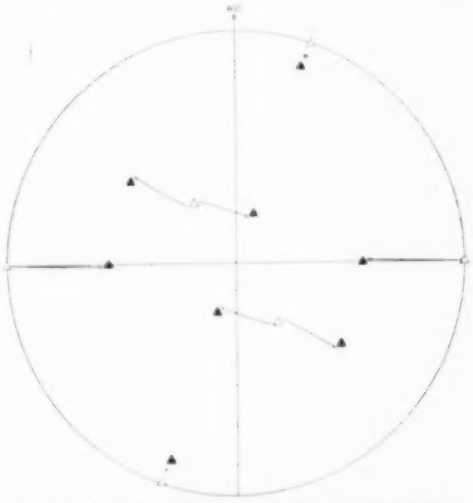

Fig. 14—(111) pole figure showing the orientation relationship between the rolling texture and the annealing texture of 70-30 brass. Open triangle indicates a (110) [112] orientation (component of the rolling texture); solid triangle, two (225) [334] orientations (components of the annealing texture). Arrows indicate rotations of 30° around *N*, which is at intermediate position between two approximately coinciding (111) poles of the above orientations.

2—Macroscopic study of the annealing process in 95 pct rolled, large grained, high purity aluminum by means of the oxide-film and sensitive tint illumination technique, shows that the retainment of the rolling texture is a result of both recrystallization in situ and recrystallization with local reorientation, where the orientation of the recrystallized grains is different from that of their local surroundings, but it is similar to an orientation prevalent in the rolling texture as a whole.

3—The local reorientations of the type leading from one major component of the rolling texture to another as a result of annealing, and those of the type leading from all four major components of the rolling texture to the cube texture, may be described approximately as 40° rotations around [111] axes. This orientation relationship between growing grain and matrix was previously found to correspond to maximum grain boundary mobility in aluminum.[35]

4—The quantitative pole figure for 96 pct rolled electrolytic tough-pitch copper (penultimate grain size: 0.03 mm), annealed for 5 min at 200°C, shows no retained rolling texture component. The annealing texture consists mainly of the cube texture, with four minor components corresponding to the annealing twins of the cube texture.

5—The annealing texture of 70-30 brass (penultimate grain size: 0.023 mm, rolled 95 pct and annealed for 5 min at 340°C) consists of four major components of the (225) [734] type, which may be approximately derived from the rolling texture by 30° rotations around [111] axes.

Acknowledgment

This work was supported by the Office of Naval Research, U. S. Navy, Contract No. N6ori-165, T. O. 1.

References

[1] G. Wassermann: *Texturen Metallischer Werkstoffe* (1939) Berlin.

[2] C. S. Barrett: *Structure of Metals*, 1st ed. p. 420 (1943) New York, McGraw-Hill Book Co.

[3] G. G. Dunn: Recrystallization Textures. Symposium on Cold Working of Metals. A.S.M. (1949) p. 113.

[4] T. Ll. Richards: Preferred Orientation in Non-ferrous Metals. *Progress in Metal Physics*. Edited by B. Chalmers. Vol. I, p. 281 (1949) London and New York.

[5] W. G. Burgers and P. C. Louwerse: Über den Zusammenhang Zwischen Deformationsvorgang und Rekristallisationstextur bei Aluminium. *Ztsch. f. Physik* (1931) **67**, p. 605.

[6] C. S. Barrett: Recrystallization Texture in Aluminum after Compression. *Trans.* AIME (1940) **137**, p. 128.

[7] P. A. Beck and H. Hu: Recrystallization Texture and Contrasting Texture in High Purity Aluminum. *Trans.* AIME (1949) **185**, p. 627; JOURNAL OF METALS (September 1949).

[8] P. A. Beck: Orientation in Recrystallization and Grain Growth. *The Physics of Powder Metallurgy*, p. 40 (1951) New York, McGraw-Hill Book Co.

[9] M. L. Kronberg and F. H. Wilson: Secondary Recrystallization in Copper. *Trans.* AIME (1949) **185**, p. 501; JOURNAL OF METALS (August 1949).

[10] J. S. Bowles and W. Boas: The Effect of Crystal Arrangement on "Secondary Recrystallization" in Metals. *Journal* Inst. Metals (1948) **74**, p. 501.

[11] G. W. Rathenau and J. F. H. Custers: Secondary Recrystallization of Face-Centered Nickel-iron Alloys. *Philips Research Reports* (1949) **4**, p. 241.

[12] P. A. Beck, P. R. Sperry, and H. Hu: The Orientation Dependence of the Rate of Grain Boundary Migration. *Journal of Applied Physics* (1950) **21**, p. 420.

[13] P. A. Beck: Theory of Annealing Textures. *Trans.* AIME (1951) **191**, p. 475; JOURNAL OF METALS (June 1951).

[14] B. F. Decker, E. T. Asp, and D. Harker: Preferred Orientation Determination using a Geiger Counter X-ray Diffraction Goniometer. *Journal of Applied Physics* (1948) **19**, p. 388.

[15] L. G. Schulz: A Direct Method of Determining Preferred Orientation of a Flat Reflection Sample Using a Geiger Counter X-ray Spectrometer. *Journal of Applied Physics* (1949) **20**, p. 1030.

[16] H. Hu, P. R. Sperry, and P. A. Beck: Rolling Textures in Face-centered Cubic Metals. This issue, p. 76.

[17] P. Lacombe and L. Beaujard: Etude Microscopique de l'écrouissage et de la recristallization de l'aluminium extra-pur. *Revue Metallurgie* (1947) **44**, p. 71.

[18] P. Lacombe and L. Beaujard: Etude metallographique et cristallographique de la croissance et de la structure des pellicules d'oxydation anodique de l'aluminium. In the book published by the Comite General D'Organisation des Industries Mécaniques. *Etudes sur les Aspects des Pellicules D'Oxydation Anodique Formées sur L'Aluminium et ses Alliages* (1944).

[19] A. Hone and E. C. Pearson: Grain Orientation in Aluminum revealed by Anodic Film. *Metal Progress* (1948) **53**, p. 363.

[20] P. R. Sperry: Method for Studying Grain Boundary Migration in Aluminum. *Trans.* AIME (1950) **188**, p. 103; JOURNAL OF METALS (January 1950).

[21] C. Crussard: Etude du Recuit de l'aluminium. *Revue Metallurgie* (1944) **41**, p. 140.

[22] R. W. Cahn: Recrystallization of Single Crystals after Plastic Bending. *Journal* Inst. Metals (1949) **76**, p. 121.

[23] J. N. Keller, P. H. Hirsch, and J. S. Thorp: An X-ray Micro-beam Examination of a Plastically Deformed Metal. *Nature* (1950) **165**, p. 554.

[24] R. D. Heidenreich: Electron Transmission Through Thin Metal Sections. Bell Telephone Lab., Inc. (1951).

[25] D. McLean, A. E. L. Tate, and M. H. Farmer: Subcrystals in Aluminum Observed with Polarized Light. *Nature* (1950) **165**, p. 70.

[26] V. Goeler and G. Sachs: Walz- und Rekristallisationstextur regulaer—flaechen zentrierter Metalle I. *Ztsch. f. Physik* (1927) **41**, p. 873.

[27] E. Schmid and G. Wassermann: Zur Rekristallisation von Aluminiumblech. *Metallwirtschaft* (1931) **10**, p. 409.

[28] Answer to the discussion of ref. 7. *Trans.* AIME (1950) **188**, p. 1057; JOURNAL OF METALS (August 1950).

[29] G. W. Rathenau and G. Baas: Grain Growth in a Texture, Studied by Means of Electron-Emission Microscopy. *Physica* (1951) **17**, p. 117.

[30] P. A. Beck: Origin of the Cube Texture in Face-Centered Cubic Metals. *Trans.* AIME (1951) **191**, p. 474; JOURNAL OF METALS (June 1951).

[31] O. Dahl and P. F. Pawlek: Kornordnung und Kornwachstum bei Walzblechen. *Ztsch. f. Metallkunde* (1936) **28**, p. 266.

[32] M. Cook and T. Ll. Richards: The Self-Annealing of Copper. *Journal* Inst. Metals (1944) **70**, p. 159.

[33] W. H. Baldwin: Effect of Rolling and Annealing upon the Crystallography, Metallography and Physical Properties of Copper Strip. *Trans.* AIME (1946) **166**, p. 591.

[34] M. K. Yen: A Study of Textures and Earing Behavior of Cold-rolled (87-89 pct) and Annealed Copper Strips. *Trans.* AIME (1949) **185**, p. 59; JOURNAL OF METALS (January 1949).

[35] C. S. Smith: Discussion of ref. 8, p. 50.

[36] J. E. Burke: Personal communication.

[37] M. Cook and T. Ll. Richards: The Structural Changes Effected in 70-30 Brass Strip by Cold Rolling and Annealing. *Journal* Inst. Metals (1943) **69**, p. 351.

[38] F. H. Wilson and R. M. Brick: Textures, Anisotropy and Earing Behavior of Brass. *Trans.* AIME (1945) **161**, p. 173.

[39] F. D. Rosi and B. H. Alexander: Measurements on the Rate of Secondary Recrystallization in High Purity Silver. JOURNAL OF METALS (October 1950) p. 1217.

[40] P. A. Beck and H. Hu: Annealing Texture in Rolled Aluminum Strip. JOURNAL OF METALS (October 1950) p. 1215.

On the Solution of Diffusion Problems Involving Concentration-Dependent Diffusion Coefficients

by Carl Wagner

This paper contains solutions of the differential equation of diffusion in binary alloys if the diffusion coefficient is an exponential function of the concentration of one of the components.

THE general differential equation for one-dimensional diffusion in a binary system can be written as:

$$\frac{\partial c}{\partial t} = \frac{\partial}{\partial x}\left(D\frac{\partial c}{\partial x}\right) \qquad [1]$$

where c is the concentration of one of the two components in any suitable units; x, the distance from a reference plane; t, time; and D, the diffusion coefficient.

Hartley and Crank[1] have pointed out that eq 1 with conventional length units for measuring the distance x holds only if the alloy can be regarded as a rigid framework. In general, this is not the case, especially if the lattice parameter varies appreciably with composition. If a modified coordinate system is used instead of an orthodox system based on the centimeter as length unit, eq 52 is obtained, which has the same general form as eq 1 and is generally valid. The necessary transformations are presented in the appendix.

If D is independent of concentration, analytical solutions of eq 1 are known for numerous boundary conditions. If D depends on concentration, solutions based on known analytical functions are not available. Among others, Boltzmann[2] and Matano[3] have shown that the concentration c depends only on $(x/t^{1/2})$ in the case of diffusion between two semi-infinite spaces with uniform initial concentrations:

$$\begin{aligned} c &= c_1 \text{ for } x < 0,\ t = 0, \text{ i.e., } x/t^{1/2} = -\infty \\ c &= c_2 \text{ for } x > 0,\ t = 0, \text{ i.e., } x/t^{1/2} = +\infty \end{aligned} \qquad [2]$$

Moreover, Boltzmann and Matano have shown how D may be calculated as a function of concentration over the whole range of composition from $c = c_1$ to $c = c_2$ if c as a function of $(x/t^{1/2})$ for the initial conditions stated in eq 2 has been determined experimentally. Thus, for instance, in principle, the diffusion coefficient in silver-gold alloys may be calculated as a function of concentration for the whole range of composition from only one diffusion experiment with a couple of pure silver and pure gold welded together.

If the diffusion coefficient D as a function of concentration c is known, a solution of eq 1 for boundary conditions as stated in eq 2 with arbitrarily chosen values of c_1 and c_2 may be wanted. For instance, if the diffusion coefficient in an alloy A-B as a function of concentration has been derived from an experiment with a diffusion couple involving 0 and 30 pct B as initial concentrations, the calculation of the concentration distribution in a diffusion couple involving other initial concentrations, e.g., 5 and 20 pct B, may be desired. This problem may be solved by numerical or graphical integration of eq 1. The solution of an ordinary differential equation of second order, which results from using $(x/t^{1/2})$ as an independent variable, can be computed quite rapidly if two conditions for the same value of the independent variable are given. In eq 2, however, two conditions are given for two

C. WAGNER, Member AIME, is Visiting Professor of Metallurgy, Dept. of Metallurgy, Massachusetts Institute of Technology, Cambridge, Mass.

Discussion on this paper, TP 3209E, may be sent, 2 copies, to AIME by April 1, 1952. Manuscript, Aug. 10, 1951. New York Meeting, February 1952.

Fig. 1—Auxiliary parameter γ as a function of z

different values of the independent variable, viz., for $(x/t^{1/2}) = -\infty$ and $(x/t^{1/2}) = +\infty$. In this case a solution of eq 1 with D as an empirical function of c is not easy to compute.

If, however, D as a function of c is represented either by a linear or an exponential function, it is possible to calculate the value of c for given values of x and t with the aid of appropriately defined auxiliary functions, which can be computed quite easily and can be tabulated in the same manner as other transcendent functions, e.g., the error function.

In view of available results for the systems Fe-C,[1] Cu-Zn,[2,3] Cu-Al,[2,3] Cu-Be, Cu-Si, Cu-Sn,[2,3] Fe-Mn, Fe-Ni,[4] the assumption of an exponential function for $D(c)$ seems to have a wider applicability than the assumption of a linear relation between D and c. Thus, the following analysis is based on the relation:

$$D = D_1 \exp\{\beta[c - \tfrac{1}{2}(c_1 + c_2)]\} \qquad [3]$$

where D_1 is the diffusion coefficient for the average concentration $c_1 = \frac{1}{2}(c_1 + c_2)$ and β is a constant to be calculated from the slope of a plot of the logarithm of D vs. c:

$$\beta = d \ln D/dc \qquad [4]$$

Such an analysis presupposes, of course, that the diffusion coefficient is a single-valued function of composition, temperature, and pressure, which may be considered as the independent thermodynamic variables. In other words, each volume element is assumed to represent a state of local thermodynamic equilibrium. In the case of Cu-Zn alloys, this assumption does not hold according to da Silva and Mehl[5] because of local degeneracies of the lattice. Such cases are excluded from the present treatment.

Calculation of the Concentration Distribution in Diffusion Couples

The dimensionless group

$$z = x/[2(D_1 t)^{1/2}] \qquad [5]$$

is introduced as an independent variable with D_1 as the diffusion coefficient for $c = c_1$, i.e., the concentration at the Matano interface, $x = 0$, which is determined by the condition that:

$$\int_{c_2}^{c_1} (c - c_2)\, dx = \int_{c_1}^{c_2} (c_1 - c)\, dx \qquad [6]$$

The calculation of c from given values of c_1 and c_2 is shown below in eq 21.

To express the concentration, the dimensionless group

$$\epsilon = \frac{c - \tfrac{1}{2}(c_1 + c_2)}{\tfrac{1}{2}(c_1 - c_2)} \qquad [7]$$

is introduced whereupon the inverse relation is obtained:

$$c = \tfrac{1}{2}(c_1 + c_2) + \tfrac{1}{2}(c_1 - c_2)\,\epsilon \qquad [8]$$

Substituting eqs 8, 3, and 5 in eqs 1 and 2, the following is obtained:

$$\frac{d}{dz}\left[e^{\frac{1}{2}q\epsilon}\left(1 - \epsilon^2\right)\frac{d\epsilon}{dz}\right] + 2z\frac{d\epsilon}{dz} = 0 \qquad [9]$$

$$\epsilon(z = -\infty) = -1;\ \epsilon(z = +\infty) = +1 \qquad [10]$$

where $\epsilon = \epsilon(z = 0)$ and q is a parameter defined as the dimensionless group:

$$q = \beta(c_1 - c_2) \qquad [11]$$

which according to eq 4 equals the natural logarithm of the ratio of the diffusion coefficients for the concentrations c_1 and c_2.

The function ϵ defined by eqs 9 and 10 may be regarded as a modified error function; it becomes identical with the error function for $q = 0$.

To compute numerical values of the function $\epsilon(z, q)$, another dimensionless group is introduced as:

$$\gamma = \beta(c - c_1) \qquad [12]$$

whereupon eq 3 becomes:

$$D = D_1 e^{\gamma} \qquad [13]$$

with D_1 as diffusion coefficient for $c = c_1$. Substitution of eqs 5, 12, and 13 in eq 1 gives:

$$\frac{d}{dz}\left(e^{\gamma}\frac{d\gamma}{dz}\right) + 2z\frac{d\gamma}{dz} = 0 \qquad [14]$$

Introducing the auxiliary variable:

$$u = e^{\gamma} \qquad [15]$$

into eq 14, gives:

$$u(d^2u/dz^2) + 2z(du/dz) = 0 \qquad [16]$$

Solutions of eq 16 from $z = -\infty$ to $z = +\infty$ for the initial conditions:

$$\gamma = 0 \text{ or } u = 1 \text{ at } x = 0,\ g = (d\gamma/dz)_{z=0} = (du/dz)_{z=0} = 0.2, 0.4, \ldots, 2.4 \qquad [17]$$

have been obtained with the aid of the M.I.T. differential analyzer.

For each auxiliary parameter g there are two limiting values, $\gamma_1 = \gamma(z = -\infty)$ and $\gamma_2 = \gamma(z = +\infty)$, with opposite signs. In view of eq 12, these values are related to the initial concentrations c_1 and c_2 by:

$$\gamma_1 = \beta(c_1 - c_1) \qquad [18]$$

$$\gamma_2 = \beta(c_2 - c_1) \qquad [19]$$

Upon substracting corresponding sides of eqs 18 and 19, the following is obtained with the aid of eq 11:

$$\gamma_2 - \gamma_1 = \beta(c_2 - c_1) = q \qquad [20]$$

Fig. 1 shows the relation between $\gamma_2 - \gamma_1$ and the parameter g.

Moreover, it follows from eqs 18 and 19 that:

$$c_1 = \tfrac{1}{2}(c_1 + c_2) - \tfrac{1}{2}(\gamma_1 + \gamma_2)/\beta \qquad [21]$$

Substitution of eq 21 in eq 3 gives:

$$D_c = D(c = c_c) = D_c \exp [-\tfrac{1}{2}(\gamma_c + \gamma_c)] \quad [22]$$

To facilitate the computation of D_c, a graph for $\tfrac{1}{2}(\gamma_c + \gamma_c)$ as a function of g is shown in Fig. 2.

According to eqs 12 and 7, the values of z are obtained from the relation:

$$z = \frac{\gamma - \tfrac{1}{2}(\gamma_c + \gamma_c)}{\tfrac{1}{2}(\gamma_c - \gamma_c)} \quad [23]$$

Numerical values of the function $z(z, g)$ are compiled in Table I. For negative values of the parameter g the following relation may be used:

$$z(z, -g) = -z(-z, g) \quad [24]$$

In view of the regularity of differences between z values for different g values but equal z values, it is believed that the error in z is, in general, not greater than one figure in the last decimal, except for $g = -1.6$ to $g = -2.4$ for which the accuracy is less because of rather sudden changes in the values of the first derivative of z as a function of z.

In order to obtain the concentration distribution for a diffusion couple with given initial concentrations c_c and c_c and known values of D_c and β, the procedure is as follows:

1—Read the value of the auxiliary parameter g for the known value of $(\gamma_c - \gamma_c) = \beta(c_c - c_c)$ from Fig. 1.

2—Read the value of $\tfrac{1}{2}(\gamma_c + \gamma_c)$ for the auxiliary parameter g from Fig. 2.

3—Calculate the value of D_c from eq 22.

4—Plot z for the auxiliary parameter g as a function of z with the aid of Table I.

In view of eqs 5 and 8 the plot z vs. z gives the concentration c at any distance x from the Matano interface and any time t.

Instead of using Figs. 1 and 2, the values of g and $\tfrac{1}{2}(\gamma_c + \gamma_c)$ may be calculated from the empirical interpolation formulas:

$$g = 0.564(\gamma_c - \gamma_c) - 5 \cdot 10^{-3}(\gamma_c - \gamma_c)^2 + 6.4 \cdot 10^{-5}(\gamma_c - \gamma_c)^3 \quad [25]$$

$$\tfrac{1}{2}(\gamma_c + \gamma_c) = -0.144g^2 - 0.0038g^4 \quad [26]$$

The flux S_c across the Matano interface at $x = 0$ equals according to Fick's first law and eqs 8 and 5:

$$S_c = -D_c(\partial c/\partial x)_{x=0} = -\tfrac{1}{4}(D_c^{1/2}/t^{1/2})(c_c - c_c)(dz/dz)_{z=0} \quad [27]$$

where S_c is the transport rate in the direction of the x-axis in g-atoms per sq cm per unit time if the concentration c is expressed in g-atom per cu cm. Using eqs 7, 3, and 5, an empirical relation between g and $(\gamma_c - \gamma_c)$ is obtained:

$$(dz/dz)_{z=0} = g/[\tfrac{1}{2}(\gamma_c - \gamma_c)] = 1.128 - 0.030g^2 \quad [28]$$

For the extreme case $g = 2.4$ (corresponding to a ratio $D(c_c)/D(c_c) = 150$) the value of $(dz/dz)_{z=0}$ equals 0.96 and thus does not differ widely from the value of 1.128 for $g = 0$, valid if the diffusion coefficient is independent of concentration. Conse-

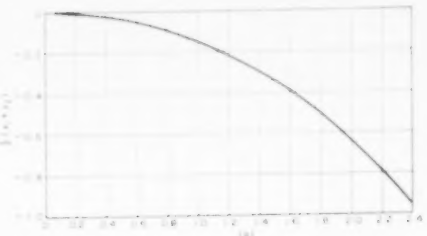

Fig. 2—$\tfrac{1}{2}(\gamma_c + \gamma_c)$ as a function of g.

Table I. Numerical Values of the Function $1000\,z(z, g)$

z	$g = 0.0$	0.2	0.4	0.6	0.8	1.0	1.2	1.4	1.6	1.8	2.0	2.2	2.4
2.0	995	998	1000										
1.9	983	986	989	1000									
1.8	969	974	978	990									
1.7	954	960	966	978	1000								
1.6	936	944	952	966	989	1000							
1.5	916	926	935	952	977	999	1000						
1.4	892	904	916	935	963	997	999						
1.3	864	878	892	915	946	994	998	1000					
1.2	830	845	862	888	926	985	996	999					
1.1	789	806	826	856	902	972	987	996	1000				
1.0	743	760	784	820	875	945	969	987	997	1000	1000		
0.9	690	708	736	778	842	901	943	968	986	998	999		
0.8	630	648	680	730	801	834	870	912	952	984	997	1000	
0.7	563	581	617	674	741	774	817	869	928	975	996	1000	
0.6	490	508	548	612	680	717	778	837	901	965	988	998	1000
0.5	412	430	474	545	618	658	721	785	865	946	978	993	998
0.4	329	347	396	474	553	598	672	738	829	923	965	984	994
0.3	243	261	314	400	486	536	621	691	793	899	951	975	988
0.2	154	172	230	324	417	472	568	643	756	874	936	965	981
0.1	62	80	144	246	347	407	514	595	719	849	921	955	974
0.0	0	32	64	167	276	341	459	546	681	824	906	945	967
+0.1	112	143	174	285	405	474	603	696	842	998	890	934	959
+0.2	225	256	278	305	332	359	385	411	436	462	487	511	535
+0.3	329	352	374	397	420	442	465	487	508	530	552	572	593
+0.4	429	445	462	481	499	517	535	553	570	589	607	624	642
+0.5	520	531	543	555	568	582	596	611	624	640	654	668	684
+0.6	604	608	614	622	631	640	650	661	672	684	696	709	720
+0.7	678	677	678	681	686	691	698	706	713	723	732	740	751
+0.8	742	737	733	733	734	736	740	745	750	757	764	771	779
+0.9	797	788	781	778	776	775	777	779	782	787	792	798	804
+1.0	843	831	823	816	812	810	809	809	810	813	817	820	825
+1.1	880	868	858	849	844	839	837	836	835	837	839	841	845
+1.2	910	899	886	878	871	865	861	859	857	858	858	859	862
+1.3	934	922	911	901	894	888	883	879	878	876	876	876	877
+1.4	952	941	931	921	913	906	901	897	894	892	891	890	891
+1.5	966	956	947	938	930	924	917	913	909	906	905	903	903
+1.6	976	968	959	951	943	937	931	926	922	919	917	915	915
+1.7	984	977	969	962	955	948	943	938	933	930	928	924	924
+1.8	989	984	977	971	964	958	953	948	943	940	937	934	933
+1.9	993	989	983	978	972	966	961	956	952	949	946	943	941
+2.0	995	992	988	983	978	973	968	964	959	956	952	950	948

Fig. 3—Concentration distribution in a Cu–Cu, Al diffusion couple after 305 hr at 889°C.

quently, the flux S across the Matano interface is nearly the same even when the diffusion coefficient varies considerably with concentration, provided that in eq 27 the diffusion coefficient D is employed. In the case of a concentration-dependent diffusion coefficient, however, the concentration distribution on the two sides of the Matano interface is remarkably asymmetric as shown in Fig. 3 for $g = 1.7$, corresponding to a value of $D(c_1)/D(c_2) = 26$.

Thus far it has been assumed that the diffusion coefficient is an exponential function of the concentration in accordance with eq 3. If this assumption does not hold strictly, the foregoing analysis may be used as an approximation. It is recommended that the analysis be based on the diffusion coefficients for the concentrations $c' = \frac{1}{2}(c_1 + c_2) - \frac{1}{4}(c_1 - c_2)$ and $c'' = \frac{1}{2}(c_1 + c_2) + \frac{1}{4}(c_1 - c_2)$ as the most representative values, corresponding to the average concentration $\frac{1}{2}(c_1 + c_2) \pm 25$ pct of the total concentration difference $(c_1 - c_2)$. Thus:

$$\beta = \frac{1}{\frac{1}{2}(c_1 - c_2)} \ln \frac{D[c = \frac{1}{2}(c_1 + c_2) + \frac{1}{4}(c_1 - c_2)]}{D[c = \frac{1}{2}(c_1 + c_2) - \frac{1}{4}(c_1 - c_2)]} \quad [29]$$

$$D_0 = [D[c = \tfrac{1}{2}(c_1 + c_2) + \tfrac{1}{4}(c_1 - c_2)]]^{0.5} \cdot [D[c = \tfrac{1}{2}(c_1 + c_2) - \tfrac{1}{4}(c_1 - c_2)]]^{0.5} \quad [30]$$

For the sake of illustration, these equations are applied to experimental data reported by da Silva and Mehl.[6] Fig. 3 shows the concentration distribution for a diffusion couple consisting of pure copper and a Cu-Al alloy with 16 atomic pct Al (sample B 39-1) after heating the sample 305 hr at 889°C. The concentrations c_1 and c_2 in mol fractions are 0.00 and 0.16, respectively. According to Fig. 32 of da Silva and Mehl's paper, $D(c = 0.04) = 1.4 \cdot 10^{-9}$ sq cm per sec and $D(c = 0.12) = 7.2 \cdot 10^{-9}$ sq cm per sec whence according to eqs 29 and 30, $\beta = 29.5$ and $D_0 = 3.2 \cdot 10^{-9}$ sq cm per sec. Following the procedure outlined above, the following is obtained consecutively: $\beta(c_1 - c_2) = 3.28$; $g = 1.7$; $\frac{1}{2}(c_1 + c_2) = 0.45$; $c_s = 0.102$; $D_s = 5.0 \cdot 10^{-9}$ sq cm per sec. With the aid of these data and Table I the solid curve in Fig. 3 has been drawn. Minor deviations between observed values (indicated by open circles) and the calculated curve are due to uncertainties of the experimental values and to the fact that the concentration dependence of the diffusion coefficient is not strictly exponential.

Calculation of the Concentration Distribution for Diffusion from or to the Surface of a Sample

If a substance diffuses from the interior of a sample with uniform initial bulk concentration c_i to the surface, or vice versa, eq 1 must be solved with the boundary conditions:

$$\left.\begin{aligned} c &= c_i \text{ at } x > 0,\ t = 0 \\ c &= c_s \text{ at } x = 0,\ t > 0 \end{aligned}\right\} \quad [31]$$

where x is the distance from the surface and c_s denotes the surface concentration for $t > 0$.

For an exponential dependence of the diffusion coefficient D on concentration it follows that:

$$D = D_s \exp[\beta(c - c_s)] \quad [32]$$

where D_s is the diffusion coefficient for the surface concentration c_s.

Solutions for special values of β have already been reported by Crank and Henry[7] in a paper dealing with diffusion of plasticizers into air from high polymer foils.

Upon introduction of eq 32 and the auxiliary variables:

$$z = x/[2(Dt)^{0.5}] \quad [33]$$

$$\chi = (c - c_s)/(c_i - c_s) \quad [34]$$

Eqs 1 and 31 become:

$$\frac{d}{dz}\left(e^{\chi}\frac{d\chi}{dz}\right) + 2z\frac{d\chi}{dz} = 0 \quad [35]$$

$$\chi(z = 0) = 0;\ \chi(z = \infty) = 1 \quad [36]$$

Table II. Numerical Values of the Function $1000\ \chi(z, \beta)$

z	β = +.4	+.2	+.0	−.2	−.4	−.6	−.8	−1.0	−1.2	−1.4	−1.6	−1.8	−2.0	−2.2	−2.4
0.0	0	0	0	0	0	0	0	0	0	0	0	0	0	0	0
0.1	86	87	84	83	86	90	96	99	102	105	107	110	112	115	117
0.2	162	165	159	161	166	206	204	207	210	214	217	220	223	226	228
0.3	229	233	225	222	221	222	222	223	224	225	225	228	229	230	231
0.4	290	295	287	278	269	257	249	243	239	235	233	230	229	227	226
0.5	377	375	359	350	324	309	300	294	291	288	286	284	282	280	279
0.6	395	395	390	353	375	357	344	338	334	331	329	327	325	324	322
0.7	1000	997	961	944	898	881	871	862	857	853	850	848	846	844	843
0.8		1000	999	997	992	978	966	957	951	946	943	940	938	936	935
0.9			1000	999	999	976	944	915	896	880	870	862	856	852	849
1.0				1000	999	999	974	953	929	905	883	862	843	826	811
1.1					1000	999	999	976	958	939	919	899	880	863	848
1.2						999	999	988	977	961	945	928	910	896	879
1.3						1000	999	995	987	977	964	949	934	919	905
1.4							999	998	994	986	977	963	952	939	926
1.5							1000	999	997	992	986	977	966	955	943
1.6								1000	999	996	992	985	976	967	956
1.7									1000	998	995	990	984	976	967
1.8										999	998	994	989	983	976
1.9										1000	999	997	993	988	982
2.0											1000	999	995	992	987

z	β = −2.6	−2.8	−3.0	−3.2	−3.4	−3.6	−3.8	−4.0	−4.2	−4.4	−4.6	−4.8	−5.0	−5.2	−5.4
0.0	0	0	0	0	0	0	0	0	0	0	0	0	0	0	0
0.1	119	121	124	126	128	130	132	134	136	138	140	142	144	146	148
0.2	231	233	236	238	240	242	244	246	248	250	252	254	256	258	260
0.3	333	334	335	336	338	339	340	341	342	344	345	346	347	348	349
0.4	423	424	424	423	423	422	422	422	422	422	422	422	422	422	422
0.5	505	502	499	497	495	494	492	491	491	489	488	487	486	485	484
0.6	567	563	559	556	553	550	548	546	544	542	540	538	536	534	532
0.7	626	620	615	610	606	602	599	596	593	590	587	584	581	578	575
0.8	677	670	664	658	653	648	644	640	636	632	628	624	620	616	612
0.9	715	707	700	694	688	683	678	673	668	663	658	653	648	643	638
1.0	742	732	723	715	707	700	694	688	683	677	672	666	660	654	648
1.1	759	749	739	730	721	713	706	699	693	687	681	675	669	663	657
1.2	770	760	750	740	731	723	715	708	701	695	689	683	677	671	665
1.3	778	768	758	748	739	730	722	715	708	702	696	690	684	678	672
1.4	784	774	764	754	745	736	728	721	714	708	702	696	690	684	678
1.5	790	780	770	760	751	742	734	727	720	714	708	702	696	690	684
1.6	796	786	776	766	757	748	740	733	726	720	714	708	702	696	690
1.7	802	792	782	772	763	754	746	739	732	726	720	714	708	702	696
1.8	808	798	788	778	769	760	752	745	738	732	726	720	714	708	702
1.9	814	804	794	784	775	766	758	751	744	738	732	726	720	714	708
2.0	820	810	800	790	781	772	764	757	750	744	738	732	726	720	714

where τ is a parameter defined as the dimensionless group:

$$\tau = \beta(c_s - c_i) \qquad [37]$$

which according to eq 32 equals the natural logarithm of the ratio of the diffusion coefficients for the concentrations c_s and c_i.

The function χ defined by eqs 35 and 36 may be considered as another type of modified error function.

Substituting eqs 32 and 33 and

$$\gamma = \beta(c - c_i) \qquad [38]$$

in eq 1, eq 14 with z_1 instead of z is obtained. In view of eqs 31 and 38 the integration is to be performed with $\gamma = 0$ for $z_1 = 0$ as lower limit. Thus the values of γ calculated above can be used. In view of eqs 31 and 34:

$$\gamma(z = \infty) = \tau = \beta(c_s - c_i) \qquad [39]$$

$$\chi = \gamma/\gamma(z_1 = \infty) \qquad [40]$$

Fig. 4 shows the limiting values of $\gamma(z_1 = \infty)$ as a function of the auxiliary parameter g used for the integration of eq 16. Numerical values of $\chi(z_1, g)$ are compiled in Table II.

In order to obtain the concentration distribution for diffusion from the surface to the interior of a sample, or vice versa, the procedure must be as follows:

1—Read the value of the parameter g for the value of $\gamma(x = \infty) = \beta(c_s - c_i)$ from Fig. 4.

2—Plot χ for the parameter g as a function of z_1 with the aid of Table II.

From eqs 33 and 34 it follows that the concentration c at any distance x and any time t equals:

$$c = c_i + (c_s - c_i)\,\chi(z_1, g) \qquad [41]$$

Instead of using Fig. 4, the values of g may be calculated with the aid of the empirical interpolation formula:

$$g = \frac{1.128\,\gamma(z_1 = \infty)}{1 - 0.177\,\gamma(z_1 = \infty)} = \frac{1.128[\beta(c_s - c_i)]}{1 - 0.177[\beta(c_s - c_i)]} \qquad [42]$$

According to Fick's first law and eqs 4 and 33, the flux $S(x = 0)$ across the surface becomes:

$$S(x = 0) = -D_i(\partial c/\partial x)_{x=0} = -[1/2D_i/t^{1/2}](c_s - c_i)(d\chi/dz_1)_{z_1=0} \qquad [43]$$

From eqs 17, 40, and 42 it follows that:

$$(d\chi/dz_1)_{z_1=0} = g/\gamma(z_1 = 0) = \frac{1.128}{1 - 0.177[\beta(c_s - c_i)]} \qquad [44]$$

If β is positive (i.e., the diffusion coefficient increases with concentration) and if the substance diffuses from the surface into the interior of a sample with zero initial concentration (i.e., $c_s - c_i > 0$), the value of g is negative. For relatively high negative values of g (≤ -1.6), there is a remarkably sharp decrease of the concentration at a certain distance from the surface. Thus there is virtually a "front" of the diffusing substance as has been pointed out by Crank and Parker[7] in regard to diffusion of plasticizers into high polymers. A similar situation is found if the diffusion coefficient is proportional to concentration. In this case, the concentration does not decrease asymptotically to zero, but there is a definite distance beyond which the concentration is zero.[10]

Summary

1—A solution for the concentration distribution in diffusion couples is presented for the case where the diffusion coefficient is an exponential function of the concentration of one of the components of a binary alloy. Numerical values for the new function χ are compiled in Table I.

2—A solution has been worked out for diffusion of an alloying element to or from the surface of a sample, if the diffusion coefficient is an exponential function of the concentration. Numerical values for the new function χ are compiled in Table II.

3—On the basis of a paper by Hartley and Crank, definitions of modified coordinate systems are given in order to obtain the conventional generalized form of Fick's second law if an alloy cannot be regarded as a rigid framework.

Acknowledgment

This work was done as a part of an investigation sponsored by Atomic Energy Commission under Contract No. AT(30-1)-1002. The author wishes to express his gratitude to Z. Kopal and F. M. Verzuh for advice and performing the numerical integrations with the aid of the M.I.T. differential analyzer.

Appendix

The conditions for the validity of the conventional generalized form of Fick's second law in eq 1 have been stated by Hartley and Crank.[7] By and large, a modified coordinate ξ has to be used instead of x in cm, if the alloy cannot be regarded as a rigid framework. The appropriate definition of ξ depends on the choice of units for concentrations. In the case of alloys, there are mainly two possibilities if the cross-sectional area in sq cm is constant. This condition is probably satisfied whenever the breadth of the sample is much greater than the effective depth of the diffusion zone.

In the first place, the concentrations of a binary alloy A-B may be indicated in mol fractions N_A and N_B, especially in the case of substitutional alloys.

According to Hartley and Crank the coordinate ξ may then be defined so that equal increments of ξ correspond to equal increments of the total number of gram-atoms of the alloying elements. To this end, the following definition may be used:

$$d\xi = (V_i/V)\,dx \qquad [45]$$

where V is the local atomic volume (i.e., the volume per 1 g-atom of the alloying elements), and V_i is the atomic volume of a suitable reference alloy. Thus, the total number of gram-atoms of the alloying elements

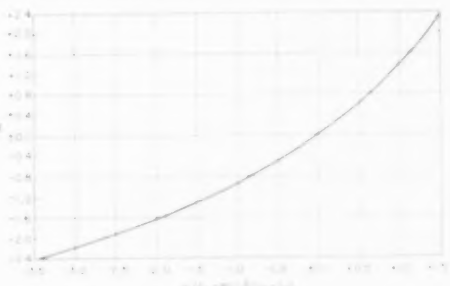

Fig. 4—Auxiliary parameter g as a function of $\gamma(z_1 = \infty) = \beta(c_s - c_i)$.

between the coordinates ξ and $\xi + d\xi$ equals $(A/V_v)d\xi$, where A is the cross-sectional area in sq cm, supposedly independent of x.

Upon integration of eq 45, the following is obtained:

$$\xi = \int_0^x (V_v/V)\,dx \qquad [46]$$

which equation is to be used for practical computations of ξ if the local composition and thus V for given values of x is known.

Conversely, if the solution of the generalized form of Fick's second law in eq 54 has been obtained and thus the mol fraction and V as functions of ξ are known, the inverse relation must be used:

$$x = \int_0^\xi (V/V_v)\,d\xi \qquad [47]$$

For substitutional alloys with a cubic structure, eq 45 may be written as:

$$d\xi = (a_v/a)^3 dx \qquad [48]$$

where a is the local lattice parameter and a_v is the lattice parameter of a reference alloy.

For the number n_A of gram-atoms of component A of a binary alloy A-B passing a cross-section at a fixed value of ξ per unit time:

$$n_A = -{}^1\mathcal{D}_A A \frac{\partial}{\partial \xi}\left(\frac{N_A}{V_v}\right) + \frac{N_A A v}{V} \qquad [49]$$

as the generalized equation of Fick's first law where ${}^1\mathcal{D}_A$ denotes the "intrinsic diffusion coefficient" of component A (defined for N_A/V_v as a measure of the concentration of component A according to Hartley and Crank) and v is the displacement of a physical cross-section (eventually indicated by markers) per unit time in cm per sec with respect to the ξ coordinate system at the point under consideration.

Likewise, then for component B:

$$n_B = -{}^1\mathcal{D}_B A \frac{\partial}{\partial \xi}\left(\frac{N_B}{V_v}\right) + \frac{N_B A v}{V} \qquad [50]$$

In view of the definition for ξ in eq 45, the change in the total number of gram-atoms in a volume element between ξ and $\xi + d\xi$ vanishes. Thus

$$\partial(n_A + n_B)/\partial\xi = 0 \qquad [51]$$

Upon combining eqs 49 to 51, v may be eliminated and the net gain of component B in the volume element may be calculated between ξ and $\xi + d\xi$. Dividing this value by $(A/V)dx = (A/V_v)d\xi$, i.e., the total number of gram-atoms of the alloying elements in this volume element, the following is obtained:

$$\frac{\partial N_B}{\partial t} = \frac{\partial}{\partial \xi}\left(D\frac{\partial N_B}{\partial \xi}\right) \qquad [52]$$

where

$$D = N_A {}^1\mathcal{D}_B + N_B {}^1\mathcal{D}_A \qquad [53]$$

is the "interdiffusion coefficient" in accordance with Darken.[11]

Eq 52 has the generalized form of Fick's second law, which has been stated in eq 1 with c instead of N_B and x instead of ξ.

Under most conditions, use of ξ instead of x in cm is an academic problem, for, in general, solid solutions extend over a wide range of composition only if the atomic radii do not differ considerably. As an exceptional case there is the system Au-Ni where the volume of the unit cell, a^3, varies from 43.3 to 67.4 A^3. This variation seems particularly important if the position of the Matano interface is calculated from experimental data.

Da Silva and Mehl[5] have suggested measuring the distance in the direction of the diffusion current by the number of lattice spacings. This procedure is equivalent to the introduction of a dimensionless variable ξ' defined by the relation:

$$d\xi' = dx/a \qquad [54]$$

Upon multiplying ξ' by a_v as a constant factor, a form similar to eq 48 is obtained:

$$d\xi'' = a_v d\xi' = (a_v/a)\,dx \qquad [55]$$

Use of the coordinates defined by eqs 54 and 55 would lead to a relation of the general form in eq 52 only if the cross-sectional area in terms of the number of unit-cell areas were independent of x. However, this is not the case in the experiments reported by da Silva and Mehl, for the cross-section of the initial and the heated sample was constant regardless of variations of the lattice parameter. If the cross-section in sq cm is constant, use of eqs 54 and 55 leads to an equation which is more involved than eq 1 or eq 52. From a practical point of view it is desirable to obtain the form of eq 1. Consequently, for concentrations in mol fractions and a constant cross-sectional area in sq cm, eq 45 must be used, or eventually eq 48, rather than eqs 54 and 55. Fortunately, use of eq 48 instead of eq 54 does not materially affect the evaluation of the experiments of da Silva and Mehl (except for the calculation of the Kirkendall effect in Cu-Al alloys).

In the case of interstitial cubic alloys with atoms of component B on interstitial sites, the foregoing equations also hold except that eq 48 must be replaced by:

$$d\xi = [N_{Av} a_v^3/N_A a^3]dx \qquad [56]$$

where N_{Av} is the mol fraction of component A in the reference alloy. The expression in brackets in eq 56 is equal to the volume ratio V_v/V as follows readily from an elementary calculation.

Eventually, the concentration in interstitial alloys may be expressed by the atomic ratio of the two components, $y = N_B/N_A$. Then, according to Hartley and Crank, eq 45 must be used with V' instead of V where V' is the volume of an amount of alloy containing 1 g-atom of component A, since for use of the concentration y equal increments of ξ must correspond to equal increments of the number of gram-atoms of component A. Instead, eq 48 for cubic structures may be used without change. Following these recommendations, the general form of eq 1 is obtained with y instead of c and ξ instead of x.

If concentrations are expressed by weight fractions, specific volumes (i.e., volumes per 1 g of alloy) must be substituted for atomic volumes in eq 45. This procedure has been suggested by Hartley and Crank[1] for systems involving high polymers but does not seem profitable in the case of alloys, since use of mol fractions or atomic ratios gives a better basis for subsequent theoretical evaluations.

References

[1] G. S. Hartley and J. Crank: *Trans.* Faraday Soc. (1949) **45**, p. 801.

[2] L. Boltzmann: *Wiedem. Ann. Physik* (1894) **53**, p. 960.

[3] C. Matano: Japanese *Journal of Physics* (1933) **8**, p. 109.

[4] C. Wells and R. F. Mehl: *Trans.* AIME (1940) **140**, p. 279.

[5] F. N. Rhines and R. F. Mehl: *Trans.* AIME (1938) **128**, p. 185.

[6] L. C. Correa da Silva and R. F. Mehl: *Trans.* AIME (1951) **191**, p. 155; JOURNAL OF METALS (February 1951).

[7] C. Wells and R. F. Mehl: *Trans.* AIME (1941) **145**, p. 315.

[8] C. Wells and R. F. Mehl: *Trans.* AIME (1941) **145**, p. 325.

[9] J. Crank and M. E. Henry: *Trans.* Faraday Soc. (1950) **45**, p. 1119.

[10] C. Wagner: *Journal of Chemical Physics* (1950) **18**, p. 1227.

[11] L. S. Darken: *Trans.* AIME (1948) **175**, p. 184.

AIME OFFICERS
President—
Vice Presidents—
Vice President and Treasurer—
AIME STAFF
Secretary—
Ass't Secretaries—
Ass't. to Secretary—
Ass't. Treasurer—

aime NEWS

Program of the Metals Branch

American Institute of Mining and Metallurgical Engineers Annual Meeting
Hotel Statler, New York, Feb. 18 to 21, 1952

The Program Committees of each of the three Metals Divisions have developed a substantially complete program for the Metals Branch Annual Meeting. A few papers subsequently may be added to the program. Highlights of the Iron and Steel Div. program are the Howe Memorial Lecture and two symposia, one on *Oxygen in Steelmaking* and one on *Manganese Conservation*, jointly with the Extractive Metallurgy Div. The Extractive Metallurgy Div. again has provided an extensive and timely program. Two sessions on *Manganese Conservation*, one jointly with the Minerals Beneficiation Div. and the other with the Iron and Steel Div., are included. Four sessions on *Addition Agents in Electro Metallurgy* promise to be a highlight on the program, as do also three sessions on the *Physical Chemistry of Nonferrous Extractive Metallurgy*. An innovation this year is a session on *Training of Extractive Metallurgists*. The three *Uncommon Metals* sessions include unique and interesting papers.

The Institute of Metals Div., Program Committee again has included three features in addition to the Institute of Metals Division Annual Lecture: *A Research in Progress* session, a two session *Seminar on the Theory of Metals* and a panel discussion on *High Temperature Alloys*.

These additional features have made it necessary to schedule more of the classical technical papers per session in order to include all of them on the program. The Program Committee, however, feels that since most of these papers are prepublished, it will not be necessary to allow more than 10 min for presentation. Authors are being requested to indicate the significance of their paper in the short time allotted, since the audience will have had an opportunity to read the details of the paper prior to the meeting. This should allow ample time for discussion of each paper.

SUNDAY, FEBRUARY 17

1:00 p.m., AIME
Student Relations Committee Meeting

2:00 p.m., AIME
Board of Directors Meeting

8:00 p.m., IMD
Program Committee Meeting
P. A. Beck, Chairman

MONDAY, FEBRUARY 18

10:30 a.m., EMD

Copper and Lead

J. G. Leckie and P. R. Drummond, Associate Chairmen

Operations at the Monterrey Refinery of the Compania Metallurgica Penoles SA: G. Ross, S. A. Peabody, Cia Metallurgica Penoles, S. A., Monterrey, N. L., Mexico.
Investigation of Certain Copper Converter Reactions: S. T. Ross, Harrison Radiator Div., General Motors Corp.; J. L. Bray, Purdue University, W. Lafayette, Ind.

9:30 a.m., IMD

Properties

T. E. Leontis, Chairman; R. L. Fullman, Secretary

Effect of Varying the Rate of Reduction on the Magnetic Properties, Ultimate Tensile Strength, and Resistivity of 18/8 Stainless Steel Wire: S. Storchheim, Sylvania Electric Products, Inc., Bayside, L. I. JOURNAL OF METALS, December 1951.
Properties of Mg-Th and Mg-Th-Ce Alloys: T. E. Leontis, Dow Chemical Co., Midland, Mich.
Tensile Properties of Wrought Austenitic Manganese Steel in the Temperature Range from 100°C to 196°C: H. C. Doepken, Manganese Steel Forge Co.
Low-Melting Gallium Alloys: R. M. Evans, R. I. Jaffee, Battelle Memorial Institute, Columbus, Ohio.

9:30 a.m., IMD

Solidification and Physical Metallurgy

John P. Nielson, Chairman; Ben H. Alexander, Secretary

Solidification Mechanism of Steel Ingots: H. F. Bishop, F. A. Brandt, W. S. Pellini, Naval Research Laboratory, Washington, D. C. JOURNAL OF METALS, January 1952.
Model for Dendrite Growth Form in Metals and Alloys: R. B. Pond, S. W. Kessler, Johns Hopkins University, Baltimore, Md. JOURNAL OF METALS, December 1951.
Origin of Porosity in Castings of Magnesium-Aluminum and other Alloys: E. J. Whittenberger, Aluminum Co. of America, Cleveland; F. N. Rhines, Carnegie Institute of Technology, Pittsburgh.
Cast Molybdenum of High Purity: G. W. P. Rengstorff, R. B. Fischer, Battelle Memorial Institute, Columbus, Ohio.
Mechanism of Grain Refinement in Aluminum Alloys: F. A. Crossley, L. F. Mondolfo, Illinois Institute of Technology, Chicago. JOURNAL OF METALS, December 1951.
On the Mechanism of Precipitation in Copper-Beryllium Alloys: A. H. Geisler, J. H. Mallery, General Electric Co., Schenectady, N. Y.; F. E. Steigert, University of Indiana, Bloomington.
Metallurgical Mechanism for Mercury Stress Cracking of Copper Alloys: W. D. Robertson, Yale University,

New Haven, Conn. JOURNAL OF METALS, December 1951.

10:00 a.m.

Metals Branch Council Meeting

C. C. Long, Chairman

2:00 p.m., EMD

Zinc

R. A. Young and L. P. Davidson, Associate Chairmen

Cyclone Vs. U Tubes for Cooling Purposes: H. E. Hoon, Northern Blower Co., Cleveland.

Description of the Electrolytic Zinc Plant at the American Zinc Co., Monsanto, Ill.: L. P. Davidson, American Zinc Co. of Ill., Monsanto, Ill.

Relationship Between Germanium and Cadmium in the Electrolysis of Zinc Sulphate Solution: S. T. Ross, Harrison Radiator Div., General Motors Corp.; J. L. Bray, Purdue University, W. Lafayette, Ind. JOURNAL OF METALS, June 1951.

Interactions Between Certain Impurities Present in the Electrolysis of Zinc Sulphate Solutions: T. J. Hughel, J. L. Bray, Purdue University, W. Lafayette, Ind.

Progress Report on Slag Fuming.

2:00 p.m., EMD

Training of Extractive Metallurgists

Round Table Discussion

A. W. Schlechten and R. Schuhmann, Jr., Associate Chairmen

2:00 p.m., IMD

Orientation and Plasticity

J. E. Burke, Chairman; D. C. Jillson, Secretary

Rolling Textures in Face-centered Cubic Metals: H. Hu, University of Chicago, Chicago; Paul A. Beck, University of Illinois; P. R. Sperry, University of Notre Dame, Notre Dame, Ind. JOURNAL OF METALS, January 1952.

Annealing Textures in Rolled Face-centered Cubic Metals: P. A. Beck, University of Illinois; H. Hu, University of Chicago, Chicago. JOURNAL OF METALS, January 1952.

Preferred Orientation in Zirconium: R. K. McGeary; B. Lustman, Westinghouse Electric Corp., Pittsburgh. JOURNAL OF METALS, November 1951.

Preferred Orientation of Arc-Cast Molybdenum Sheet: M. Semchyshen, G. A. Timmons, Climax Molybdenum Co., Detroit.

Plasticity of Molybdenum Single Crystals: N. K. Chen, R. Maddin, Johns Hopkins University, Baltimore, Md. JOURNAL OF METALS, October 1951.

Plastic Deformation of Magnesium Single Crystals: E. C. Burke, Dow Chemical Co., Midland, Mich.; W. R. Hibbard, Jr., General Electric Co., Schenectady, N. Y.

Delay Time for the Initiation of Slip in Metal Single Crystals: I. R. Kramer, Horizons, Inc., Princeton, N. J.; R. Maddin, Jr., Johns Hopkins University, Baltimore, Md.

Recrystallization of Al Single Crystals after Plastic Extension: N. K. Chen, Johns Hopkins University, Baltimore, Md.; C. H. Mathewson, Yale University, New Haven, Conn.

2:00 p.m., IMD

Research in Progress

Abstracts of papers to be presented on this session will appear in the February issue of the JOURNAL OF METALS, see page 1213 December issue. Opportunity will be afforded to present current research for discussion.

2:00 p.m., IMD

Executive Committee Meeting

R. M. Brick, Chairman

4:30 p.m., IMD

Membership Committee Meeting

W. J. Harris, Jr., Chairman

TUESDAY, FEBRUARY 19

7:30 a.m., IMD

Publications Committee Breakfast Meeting

M. Gensamer, Chairman

9:00 a.m., EMD

Physical Chemistry of Extractive Metallurgy

H. H. Kellogg and A. J. Phillips, Associate Chairmen

Volatility and Stability of Metallic Sulphides: C. M. Hsiao, A. W. Schlechten, Missouri School of Mines, Rolla. JOURNAL OF METALS, January 1952.

Thermodynamics of Iron-Silicate Slags—Slags Saturated with Solid Silica: R. Schuhmann, Jr., E. J. Michal, Massachusetts Institute of Technology, Cambridge.

Constitution of the FeO-Fe$_2$O$_3$-SiO$_2$ System at Smelting Temperatures: R. Schuhmann, Jr., R. Guy Powell, E. J. Michal, Massachusetts Institute of Technology, Cambridge.

Mechanism of the Reduction of Oxides and Sulphides to Metals: Carl Wagner, Massachusetts Institute of Technology, Cambridge.

9:00 a.m., EMD

Manganese Conservation

Jointly with MBD

J. H. Jacobs and John Sullivan, Associate Chairmen

Shifts in U. S. Manganese Sources and their Significance: N. B. Melcher, U. S. Bureau of Mines, Washington, D. C.

Manganese Extraction by Carbamate Solutions and the Chemistry of New Manganese-Ammonia Complexes: R. S. Dean, Consulting Engineer, Washington, D. C.

Upgrading of Low Grade Manganese Ores by Caustic Leaching: R. V. Lundquist, U. S. Bureau of Mines, San Francisco.

Hydrometallurgical Methods for the Use of Domestic Manganese Ores: K. M. Leute, Lithium Corp. of America, Inc., Minneapolis, Minn.; R. S. Dean, Consulting Engineer, Washington, D. C.

9:00 a.m., IMD

Seminar: Theory of Metals

The field will be reviewed and brought up to date in a comprehensive manner.

R. F. Mehl and B. L. Averbach, Associate Chairmen

Electrons, Bands, and the Behavior of Metals: Frederick Seitz, University of Illinois, Urbana.

Conductivity and Magnetism: Clarence Zener, Westinghouse Electric Corp., E. Pittsburgh.

9:00 a.m., ISD

General Session

H. B. Emerick and B. M. Larsen, Associate Chairmen

A Corrected CO/CO$_2$ Ratio for Blast Furnaces: S. T. Killian, Johnstown, Pa.

The Effect of Alloying Elements on the Mechanism of Sulphur Transfer across a Slag-Metal Interface—Si, Mn, C, Al: K. Goldman, W. O. Philbrook, G. Derge, Carnegie Institute of Technology, Pittsburgh.

11:00 a.m., ISD

Howe Memorial Lecture

M. L. Haider and T. L. Joseph, Associate Chairmen

Chromium Carbide in Stainless Steel: Augustus B. Kinzel, Union Carbide & Carbon Research Laboratories, Inc., New York.

12:15 p.m., EMD

Physical Chemistry of Extractive Metallurgy Committee Luncheon Meeting

H. H. Kellogg, Chairman

12:30 p.m., ISD

Executive Committee Luncheon Meeting

T. L. Joseph, Chairman

2:00 p.m., EMD

Physical Chemistry of Extractive Metallurgy

L. M. Pidgeon and R. Schuhmann, Jr., Associate Chairmen

Distillation of Binary Alloys at Low Pressure. I—Lead-base Alloys, II—Tin-base Alloys: H. W. St. Clair, U. S. Bureau of Mines, Washington, D. C.; M. J. Spendlove, U. S. Bureau of Mines, College Park, Md.; H. S. Caldwell, Jr., U. S. Bureau of Mines.

Separation of Constituents of Binary Lead Alloys: H. W. St. Clair, U. S. Bureau of Mines, Washington, D. C.; D. D. Blue, U. S. Bureau of Mines, Silver Spring, Md.

Surface Tension in the System Liquid Copper-Sulphur: C. F. Baes, H. H. Kellogg, Columbia University, New York.

Optical Temperature Scale and Emissivities of Liquid Iron-Copper Nickel Alloys: D. B. Smith, J. Chipman, Massachusetts Institute of Technology, Cambridge.

2:00 p.m., ISD, EMD—Joint Session

Symposium on Manganese Conservation

O. C. Ralston and Shadburn Marshall, Associate Chairmen

Production of Spiegeleisen from Open Hearth Slag in an Experimental Blast Furnace: R. C. Buehl, M. B. Royer, U. S. Bureau of Mines, Pittsburgh.

Production of High Mn Slags by the Selective Oxidation of Spiegeleisen: R. C. Buehl, M. B. Royer, U. S. Bureau of Mines, Pittsburgh.

Effect of Various Elements on the Hot Working Characteristics and Physical Properties of Iron-Carbon Alloys—Sulphur: C. Travis Anderson, U. S. Bureau of Mines, Redding, Calif.

Manganese Distribution under Blast Furnace Conditions: J. E. Stukel, Youngstown Sheet & Tube Co., Youngstown, Ohio.

2:00 p.m., IMD

Seminar: Theory of Metals

R. F. Mehl and B. L. Averbach, Associate Chairmen

Theory of Alloys: G. V. Raynor, University of Birmingham, England; presently at Institute for the Study of Metals, University of Chicago.

Critical Evaluation of Electron Theory of Metals: J. C. Slater, Massachusetts Institute of Technology, Brookhaven National Laboratory.

Discussion

6:00 p.m.

Metals Branch Cocktail Party

7:00 p.m.

Metals Branch Annual Dinner

Toastmaster: C. C. Long, Director, Research Dept., St. Joseph Lead Co. of Pa.

WEDNESDAY, FEBRUARY 20

9:00 a.m., EMD

Physical Chemistry and Uncommon Metals

N. Arbiter and O. C. Ralston, Associate Chairmen

Exploration with the High-Temperature Microscope: Moving picture, Carborundum Co.

Preparation of Iodide Titanium: O. J. C. Runnalls, L. M. Pidgeon, University of Toronto, Toronto, Ontario.

Panel Discussion, Potential Importance of Liquid-Liquid Extraction in Extractive Metallurgy:

a. *Relative Stability of Chelate Compounds with Reference to Liquid-Liquid Extraction:* W. C. Fernelius, Pennsylvania State College, State College, Pa.

b. *Some Examples of Liquid-Liquid Extraction in Metal Purification:* Clarence E. Larson, Oak Ridge National Laboratories.

c. *General Panel Discussion.*

9:00 a.m., EMD

Addition Agents in Electro Metallurgy

Round Table Discussion

Lawrence Addicks, Honorary Chairman

S. Skowronski and P. R. Drummond, Associate Chairmen

Introduction and Historical: S. Skowronski, Raritan Copper Works, Perth Amboy, N. J.

Theoretical: W. B. Kleiner, Rutgers University, New Brunswick, N. J.

9:00 a.m., IMD

Crystal Structure

R. Maddin, Chairman; R. G. Treuting, Secretary

Crystal Structure of $TaCr_2$ and $CbCr_2$: P. Duwez, H. Martens, California Institute of Technology, Pasadena. JOURNAL OF METALS, January 1952.

Diffraction Patterns and Crystal Structure of Si_3N_4 and Ge_3N_4: W. C. Leslie, K. G. Carroll, R. M. Fisher, United States Steel Co., Kearny, N. J.

Crystal Structure of $TiAl$: P. Duwez, J. L. Taylor, California Institute of Technology, Pasadena. JOURNAL OF METALS, January 1952.

Influence of Carbon on Lattice Parameter of Molybdenum: R. Speiser, J. W. Spretnak, Ohio State University; W. E. Few, R. M. Parke, Battelle Memorial Institute, Columbus.

Crystal Structure of Ti_2Sn: P. Pietrokowsky, California Institute of Technology, Pasadena.

10:45 a.m., IMD

Annual Business Meeting
Institute of Metals Division

R. M. Brick, Chairman

11:00 a.m., IMD

Annual Lecture, Institute of Metals Division

W. M. Peirce and R. M. Brick, Associate Chairmen

Solid State Physics in Electronics and Metallurgy: William Shockley, Bell Telephone Laboratories, Murray Hill, N. J.

12:30 p.m., EMD

Executive Committee Luncheon Meeting

O. C. Ralston, Chairman

12:30 p.m., ISD

Luncheon Meeting

Physical Chemistry of Steelmaking Committee

M. Tenenbaum, Chairman

2:00 p.m., EMD

Addition Agents in Electro Metallurgy

Round Table Discussion

S. Skowronski and P. R. Drummond, Associate Chairmen

(Contd.)

Addition Agents in the Refining of Copper:

A. Glue; B. Glue and Goulac; C. Glue, Goulac and Oils; D. Casein and Glue; E. Casein, Glue and Goulac; F. Thiourea; G. The Functions of Chlorine as an Addition Agent; H. Possibility of Other Types of Addition Agents; I. Estimation of Addition Agents.

2:00 p.m., IMD

Panel Discussion High Temperature Alloys

Norman Mochel, Chairman

Composition and Properties of Alloys for High Temperature Service: Paul de Huff, Westinghouse Electric Corp., Philadelphia.

Problems in Testing High Temperature Materials: James W. Freeman, University of Michigan, Ann Arbor.

Requirement and Outlook for High Temperature Materials: Howard Croff, Battelle Memorial Institute, Columbus, Ohio.

Following the initial presentations, discussion from the floor will be invited.

2:00 p.m., ISD

Symposium on Oxygen in Steelmaking

N. J. Grant and D. E. Babcock, Associate Chairmen

Iron Oxide Activity and Oxygen Distribution between Slag and Liquid Iron: E. T. Turkdogan, British Iron & Steel Research Assn., London, England.

Deoxidation Studies under FeO-MnO-SiO$_2$ Slags: P. T. Carter, Royal Technical College, Glasgow, Scotland.

Silicon-Oxygen Equilibrium in Liquid Iron: Nevzat A. Gokcen, Lafayette College, Easton, Pa.; John Chipman, Massachusetts Institute of Technology, Cambridge.

Oxygen Equilibria and the Carbon-Oxygen Reaction in Steelmaking: P. Herasymenko, New York.

4:45 p.m., EMD

Annual Business Meeting, Extractive Metallurgy Division

O. C. Ralston, Chairman

THURSDAY, FEBRUARY 21

9:00 a.m., EMD

Uncommon Metals

S. F. Urban and A. U. Seybolt, Associate Chairmen

Direct Chlorination of Zirconium Oxide: W. W. Stephens, H. L. Gilbert, U. S. Bureau of Mines, Albany, N. Y.

Vacuum Reduction of Some Metallic Oxides Using Zirconium: T. T. Magel, Massachusetts Institute of Technology, Cambridge.

Induction Melting of Reactive Metals Without Refractory Containers: T. T. Magel, P. Kulin, A. R. Kaufman, Massachusetts Institute of Technology, Cambridge.

Malleable Arc Melted Chromium Metal: H. L. Gilbert, H. I. Johansen, U. S. Bureau of Mines, Albany, N. Y.

9:00 a.m., EMD

Addition Agents in Electro Metallurgy

Round Table Discussion
(Contd.)

H. R. Hanley and S. Skowronski, Associate Chairmen

Addition Agents in the Refining of Other Metals:
A. Silver
B. Lead
C. Tin
D. Lead-Tin

Addition Agents in the Winning of Metals (Insoluble Anodes):
A. Copper
B. Zinc—In charge of Prof. Hanley

9:00 a.m., IMD

Transformation and Hardening

V. N. Krivobok, Chairman; George A. Roberts, Secretary

Habit Phenomenon in the Martensitic Transformation: E. S. Machlin, Morris Cohen, Massachusetts Institute of Technology, Cambridge. JOURNAL OF METALS, November 1951.

Isothermal Mode of the Martensitic Transformation: E. S. Machlin, Columbia University, New York; Morris Cohen, Massachusetts Institute of Technology, Cambridge.

Isothermal Martensite Formation in an Iron-Chromium-Nickel Alloy: S. A. Kulin, G. R. Speich, Westinghouse Research Laboratory, East Pittsburgh, Pa.

Isothermal Transformation Characteristics of an Iron-Chromium Alloy of Titanium: C. W. Phillips, University of Michigan, Ann Arbor; D. N. Frey, Ford Motor Co., Dearborn, Mich.

Work Hardening Reannealing Cycle of Pure Silver: M. Balicki, G. Leeds, Polytechnic Institute of Brooklyn, Brooklyn, N. Y. JOURNAL OF METALS, January 1952.

Kinetics and Orientation Relationship of Secondary Recrystallization in Silver: F. D. Rosi, B. H. Alexander, C. A. Dube, Sylvania Electric Products, Inc., Bayside, L. I.

Dislocation Collision and the Yield Point of Iron: A. N. Holden, General Electric Co., Schenectady, N. Y.

Strain-hardening and Recovery—Effect of Prior Strain at Low Temperatures on the Properties of Some Close-packed Metals at Room Temperatures: E. S. Greiner, W. C. Ellis, Bell Telephone Laboratories, Murray Hill, N. J.

9:00 a.m., IMD

Constitutional Diagrams

F. N. Rhines, Chairman; L. A. Willey, Secretary

Analytical Representation of Certain Phase Boundaries: W. Rostoker, Armour Research Foundation, Chicago. JOURNAL OF METALS, December 1951.

Zirconium-Chromium Phase Diagram: E. T. Hayes, A. H. Robertson, M. H. Davies, U. S. Bureau of Mines, Albany, Ore.

Lead-Uranium System: R. J. Teitel, Brookhaven National Laboratory, Upton, L. I.

Constitution of Titanium-Aluminum Alloys: H. R. Ogden, D. J. Maykuth, R. I. Jaffee, Battelle Memorial Institute, Columbus, Ohio; W. L. Finlay, Rem-Cru Titanium, Inc., Midland, Pa. JOURNAL OF METALS, December 1951.

Contribution to the Metal-Carbon-Boron System: F. W. Glaser, American Electro Metal Corp., Yonkers, N. Y.

Solubility of Gaseous Nitrogen in Gamma Iron and the Effect of Alloying Constituents—Aluminum Nitride Precipitation: L. S. Darken, R. P. Smith, E. W. Filer, United States Steel Co., Kearny, N. J. JOURNAL OF METALS, December 1951.

Constitution and Properties of Some Iron-Bearing Cupro-nickel: E. W. Palmer, F. H. Wilson, American Brass Co., Waterbury, Conn.

9:00 a.m., ISD

Symposium: Oxygen in Steelmaking

G. Derge and D. J. Girardi, Associate Chairmen

Chromium Distribution between Liquid Iron and Slags: N. J. Grant, John Chipman, Massachusetts Institute of Technology, Cambridge.

Electrical Conductivity in Wustite Melts: Henry Inouye, John Chipman, Massachusetts Institute of Technology, Cambridge; John Tomlinson, British Iron & Steel Research Assn., London, England.

The Liquidus Surface of the Iron-Sulphur-Oxygen System: D. C. Hilty, Walter Crafts, Union Carbide & Carbon Research Laboratories, Inc., Niagara Falls.

Metallic Oxidation in Stainless Steel Melting: D. C. Hilty, G. W. Healey, Walter Crafts, Union Carbide & Carbon Research Laboratories, Niagara Falls, N. Y.

12:30 p.m., IMD

Luncheon Meeting

Powder Metallurgy Committee
J. J. Cordiano, Chairman

2:00 p.m., EMD

Uncommon Metals

B. W. Gonser and A. R. Kaufmann, Associate Chairmen

Metallurgical Products as a Source of Trace Elements in Agriculture: John H. Carter, Battelle Memorial Institute, Columbus, Ohio.

Discovery, Occurrence, Concentration, Extraction, and Chemical Properties of Rhenium: A. D. Melaven, University of Tennessee, Knoxville.

A Fume Collecting and Absorption System for Special Metallurgical Products: L. Troutman, G. White, G. G. Simons, Beryllium Corp. of America.

Some Applications of Amalgam Metallurgy: R. B. MacMullen, R. B. MacMullen Associates, Niagara Falls.

2:00 p.m., EMD

Addition Agents in Electro Metallurgy

Round Table Discussion
Continued

H. R. Hanley and S. Skowronski, Associate Chairmen

2:00 p.m., IMD

Physical Properties

M. A. Williamson, Chairman; R. I. Jaffee, Secretary

Surface Tension of Solid Silver: E. R. Funk, H. Udin, J. Wulff, Massachusetts Institute of Technology, Cambridge. JOURNAL OF METALS, December 1951.

Surface Tension of Solid Gold: F. H. Buttner, H. Udin, J. Wulff, Massachusetts Institute of Technology, Cambridge. JOURNAL OF METALS, December 1951.

Viscous Creep of Gold Wires near the Melting Point: F. H. Buttner, E. R. Funk, H. Udin, Massachusetts Institute of Technology, Cambridge.

Vapor Pressures of Zinc over Ag-Zn Alloys: E. E. Underwood, B. L. Averbach, Massachusetts Institute of Technology, Cambridge. JOURNAL OF METALS, December 1951.

On the Solution of Diffusion Problems Involving Concentration Dependent Diffusion Coefficients: Carl Wagner, Massachusetts Institute of Technology, Cambridge. JOURNAL OF METALS, January 1952.

Free Energy of Formation of Cementite and the Solubility of Cementite in Austenite: L. S. Darken, R. W. Gurry, United States Steel Co., Kearny, N. J. JOURNAL OF METALS, November 1951.

Effect of Temperature on the Lattice Parameters of Magnesium Alloys: R. S. Busk, Dow Chemical Co., Midland, Mich.

Correlation Between Electrical Conductivity and Temperature Coefficient of Resistance of Solid-Solution Alloys: M. Hansen, W. R. Johnson, J. M. Parks, Armour Research Foundation, Chicago. JOURNAL OF METALS, December 1951.

Internal Friction Measurements on Iron Wires of Commercial Purity: Ake Josefsson, Eric Kula, Kopparbergs Bergslags AB, Domnarvet, Sweden.

2:00 p.m., ISD

Symposium: Oxygen in Steelmaking

D. L. McBride and R. E. Birch, Associate Chairmen

Evaluation of the Bomb Sampling Technique: J. G. Huff, U. S. Steel Co. Laboratories, Pittsburgh.

Determination of Oxygen in Iron in the Presence of Sulphur by the Vacuum Fusion Method: H. L. Hamner, R. M. Fowler, Union Carbide & Carbon Research Laboratories, Inc., Niagara Falls, N. Y.

Chemical Effect of the Oxygen Lance in Steelmaking and the Carbon-Oxygen Equilibrium: D. J. O. Brandt, British Iron & Steel Research Assn., London, England.

Use of the Oxygen Lance in Steelmaking: P. M. Hulme, Air Reduction Co., New York.

2:30 p.m., IMD

Powder Metallurgy Seminar
Metal Ceramic Materials

John C. Redmond, Presiding

Introduction: L. D. Richardson, Wright Air Development Center, Wright Patterson Air Force Base, Dayton, Ohio.

Theory of Metal Carbide and Similar Combinations: John T. Norton, Massachusetts Institute of Technology, Cambridge.

Theory of Metal-Oxide Combinations: W. B. Crandall, New York State College of Ceramics, Alfred, N. Y.

Cemented Carbide Combinations: John W. Graham, Kennametal, Inc., Latrobe, Pa.

Metal Oxide Combinations: T. S. Shevlin, Ohio State University, Columbus.

IMD Fall Meeting Paper Deadline

Apr. 15, 1952 is the deadline for all Institute of Metals Div. papers to be presented at the fall meeting, Oct. 20 to 22, at the Hotel Adelphia, Philadelphia.

Post Convention Cruise Planned

PLANS are underway for the annual meeting of AIME, to be held in New York, February 17 to 21. The technical program includes meetings of all divisions of all three branches, Mining, Metals, and Petroleum. The bulk of the technical sessions will be held at the Statler hotel, and the annual banquet will be held at the Waldorf-Astoria, Wednesday evening, February 20.

Then, after a full scale and possibly somewhat strenuous technical meeting, a post-meeting feature will appeal to many of the members. A restful cruise to Bermuda and Nassau is offered at special rates to AIME members and friends. The schedule is a 3:00 pm departure from New York on the "*Queen of Bermuda*" on Saturday, February 23; arrival at Bermuda at 7:00 am Monday, February 25; arrival at Nassau at noon, Wednesday, February 27; and the trip ending again in New York at 9:00 am, Saturday, March 1. Rates begin at $202.10 per person, with higher rates depending upon accommodations desired. The base rate includes outside room with private bath and all meals, as well as federal, Bermuda and Nassau taxes.

Reservations for the trip should be made immediately through Leon V. Arnold, 36 Washington Square West, New York 11. Mr. Arnold is in charge of the cruise arrangements.

Queen of Bermuda

M. L. Haider Named AIME President for 1952

No other nominations having been received, the ticket named by the Committee on Nominations for AIME officers in 1952 was declared elected at the November meeting of the Executive and Finance Committees. Names and biographical data were published in the July issues of the Institute's journals: President, M. L. Haider; President-elect, Andrew Fletcher; Vice-Presidents, O. B. J. Fraser and J. B. Morrow; Directors, C. H. Benedict, R. B. Caples, T. B. Counselman, T. L. Joseph, and C. F. Rettie, Jr.

Business Meeting Planned

The annual business meeting of the AIME will be held at the Hotel Statler, New York, at 4 pm, Tuesday, Feb. 19, 1952. Newly elected Directors and officers will assume their duties at this meeting. A report of the financial condition of the Institute will be made, as well as reports of the principal officers and standing committees. All AIME members are invited to attend. Immediately afterward, at 5 pm, the new Board will meet in executive session.

Membership Reinstatement Rules Revised

Former resolutions of the Board on delinquent dues and reinstatements of former AIME members were reaffirmed for 1952 at the meeting of the Board on Dec. 5. These provide for one month of grace, or until Jan. 31, 1952, for those who would otherwise be dropped from the Institute rolls at the end of December 1951 as owing two years' dues. Also, those who have made even a partial payment of their 1950 dues will be continued on the rolls for the entire year 1952. As to reinstatements of those who have formerly been dropped for nonpayment of dues, the reinstatement charge shall not exceed $20 in lieu of arrears in dues. In addition, dues for the year of reinstatement would be payable, and an initiation fee if none had ever been paid and if the reinstatement was for Member or Associate Member. This latter is payable in $5 annual instalments.

Tri-State Elects Directors

Newly elected Directors of the Tri-State Section for 1952 are Ernest Blessing and C. E. Stover, Miami, Okla.; J. C. Stipe and S. S. Clarke, Baxter Springs, Kan.; R. O. Cash, R. E. Illidge, Dan R. Stewart, and W. F. Netzeband, Joplin, Mo. W. F. Netzeband will serve as Chairman of the Section, R. O. Cash, as Vice-Chairman, Dan R. Stewart as Secretary-Treasurer, S. S. Clarke as Program Committee Chairman, and Ernest Blessing as Membership Committee Chairman.

Proposes Local Sections Be Set Up Branchwise

At recent meetings of the AIME Directors, there has been some discussion of a proposal made by Claude R. Hocott. He suggests that Local Sections be set up on a Branch rather than on a purely geographical basis. There might thus be two or three Local Sections in the same small area, if the membership of two or three Branches—Mining, Metals, or Petroleum—were large and concentrated. Present appropriations from the national treasury would be discontinued, Local Sections supporting themselves by dues or other means. The present Council of Section Delegates would be disbanded, for the three groups of Local Sections would have to do with the Branch councils instead of the Board of Directors. The proposed plan would go still farther than has so far been done in setting up the Institute organization on a purely professional basis.

The proposal has been considered by the executive committee of the Petroleum Branch, and has been referred to the AIME Board for study. Further discussion is expected at the meeting of the Board just previous to the Annual Meeting, on Sunday afternoon, Feb. 17.

Annual Meeting Committees Named

Arrangements Committee
Francis Cameron, Chairman

Chairmen of other committees and Executive Committee of New York Section.

Reception Committee
Philip D. Wilson, Chairman

Howland Bancroft Lester E. Grant
John G. Baragwanath

Banquet Committee
M. B. Gentry, Chairman
Louis C. Raymond, Vice-Chairman

Mrs. Domingo Moreno Frank G. Breyer
Mrs. Thorne E. Lloyd Fred W. Hanson
Parke A. Hodges J. R. Atkinson
Ernest V. Gent W. A. Clark, Jr.

Dinner-Smoker Committee
Louis C. Raymond, Chairman
Maxwell L. McCormack, Vice-Chairman

R. L. McCann David Swan
Frank R. Milliken

Welcoming Luncheon Committee
W. J. Turner, Chairman

Mrs. John P. Dyer R. D. Mollison
H. W. Bitzrot H. G. Moulton

Informal Dance Committee
Ira K. Hearn, Chairman

David T. Steele George P. Lutjen

Hotel Committee
Robert H. Ramsey, Chairman

John H. Ffolliott Howard L. Waldron
Robert B. Fulton

Information Committee
Alvin Knoerr, Chairman

George P. Lutjen Theodore Marvin

Cocktail Party Committee
Russell H. W. Chadwick, Chairman

C. Phillip Jenney Joseph A. Wiendl

Technical Publications Committee Appointed

Personnel of the AIME Technical Publications Committee, which took office for the ensuing year on Oct. 15, follows: J. I. Laudermilk, chairman; Charles H. Lambur and Vinton H. Clarke, vice-chairmen; E. J. Kennedy, Jr., secretary; Robert H. Aborn, J. R. Atkinson, W. H. Callahan, Charles W. Eichrodt, Francis B. Foley, E. V. Gent, M. B. Gentry, M. D. Hassialis, W. H. Loerpabel, Robert D. Nininger, Earl W. Palmer, and J. S. Smart, Jr.; with Joe B. Alford, John Beall, E. O. Kirkendall, R. E. O'Brien, and E. H. Robie members ex officio.

This committee relies to a large extent on Divisional Auxiliary Publications Committees for its action on the acceptance or rejection of papers, but considers matters of policy, and budgetary limitations.

Nominations Committee Personnel Expanded

Certain additions to the personnel of the Nominating Committee for AIME Officers in 1953 were approved at the Dec. 5 meeting of the Executive and Finance Committees. Proposed by the executive committee of the Council of Section Delegates—M. Gensamer, School of Mines, Columbia University, New York 27, N. Y. (with Max Ball, 1025 Vermont Ave., Washington 5, D. C., as alternate). Alternate from the Southern California Section: Basil Kantzer, Union Oil Co. of California, 617 W. 7th St., Los Angeles 14. These names should be added to the list published in the December issue.

Michigan Alumni to Meet

The New York section of the Michigan College of Mining & Technology Alumni Assn. will be hosts at a dinner for all Alumni, friends of the college, their wives and guests, on Tuesday, Feb. 9, 1952, in the Sky Top Room of the Statler Hotel. This will be in conjunction with the AIME annual meeting. Cocktails will be served at 6:30 pm, and dinner at 7:30 pm.

Dr. Grover C. Dillman, president of the college, will speak on "*Higher Education and its Meaning in the World Today.*" Reservations may be made at the reservation desk at the meeting, or through F. G. Woodruff, P.O. Box 392, Dover, N. J.

Chicago Section Hears A. J. Boynton on Seaway

Chicago Section, AIME, held a dinner meeting on Dec. 5, 1951, with F. M. Rich, Inland Steel Co., as technical chairman. Speaker for the evening was A. J. Boynton, A. J. Boynton & Co., and the topic was *The St. Lawrence Seaway.* Starting with a description of existing physical conditions, he outlined the historical background of the project and the proposals for its completion. The effect of the seaway on the transportation of wheat, coal, petroleum, and iron ore, both to and from this country was discussed.

On December 8, a tour aboard the *Wilfred Sykes*, largest ore carrier operating on the Great Lakes was arranged with Inland Steel Co. The group then visited Inland's new continuous tin plate mill.

"Ore Deposits of Western States" to be Republished

One of the outstanding special volumes published by the AIME was the Lindgren volume, "Ore Deposits of the Western States," which appeared in 1933. It has been out of print for several years. It has been decided to publish a totally new volume, again under the sponsorship of the Rocky Mountain Fund, the scope and content of which is to be directed by the following committee: John W. Vanderwilt, chairman; Carlton D. Hulin, T. S. Lovering, Charles F. Park, Harrison Schmitt, and Philip J. Shenon.

Credit Allowed Junior Members for Military Duty

Ordinarily, applicants for Junior Membership must not have passed their 30 birthday anniversary at the time their application is received by the Institute. By recent action of the Board, however, a credit of one year on this entrance age limit is given for each year of military service. A similar credit is given veterans in changing their status from Junior Member to Associate Member or Member, which must normally be done before their 33 birthday anniversary. Heretofore, these credits were extended only to veterans of World War II; now, all veterans are given this privilege.

Awards To Be Presented at the Annual Meeting

Robert W. Hunt Medal to G. Derge, W. O. Philbrook, and Kenneth M. Goldman.

J. E. Johnson, Jr. Award to William R. Bond.

C. H. Mathewson Gold Medal to C. G. Dunn, F. Lionetti, F. W. Daniels, and M. J. Bolton.

Robert H. Richards Award to John F. Myers.

Rossiter W. Raymond Memorial Award to Donald A. Dahlstrom.

Certificate of Honorary Membership to Everette De Golyer.

Student Chapter Okayed

A new Student Chapter of the AIME was authorized by the Board at its Dec. 5 meeting at the Texas College of Arts and Industries, Kingsville, Texas. The group is interested in petroleum and natural gas engineering, and the curriculum has been accredited by Engineers Council for Professional Development.

Student Papers Selected

At the Welcoming Luncheon to be held at the Statler Hotel, New York, on Feb. 18, 1952, checks for $100 each will be awarded to the winners of the tenth annual Student Prize Paper Contest. Winners in the undergraduate div. are: 1—Charles R. Rainesalo, Carnegie Institute of Technology; 2—Alfred F. Weinberg, Illinois Institute of Technology; and 3—William E. Bond, Carnegie Institute of Technology. The only award made in the graduate div. will go to John F. Radavich, Purdue University.

Annual Meeting Social Events

This is a tentative list of the social events of the Annual Meeting.

Monday, February 18

Welcoming Luncheon will have Harold R. Medina, famous jurist as guest speaker.

Cocktail Party, Statler Hotel. The mining companies in the New York area extend a cordial invitation to the registrants and their wives to attend this informal get-together session. The **Dinner-Smoker** will follow the Cocktail Party at the Statler. Entertainment will be by Nelba of the Cotillion Room in the Hotel Pierre. Following the dinner, there will be an hour show by entertainers that will lend a night club atmosphere to the event.

Tuesday, February 19

Informal Dance, Hotel Statler. Music by 12-piece orchestra. Refreshments and entertainment during the intermission.

Wednesday, February 20

The Annual Banquet will be held at the Waldorf-Astoria Hotel. The banquet will be preceded by the President's reception and followed by dancing.

T. J. McLOUGHLIN, U. S. Steel Co., Chairman of the Executive Committee, delivered the welcoming address at the Annual Dinner.

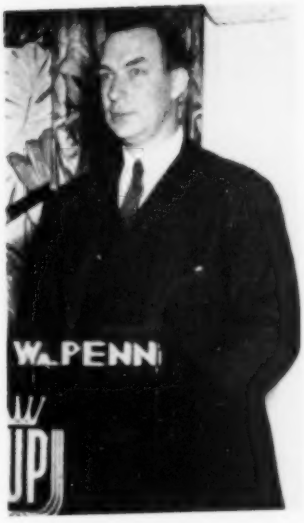

C. L. AUSTIN, Jones & Laughlin Steel Corp., was speaker for the Annual Dinner. His topic was "This Is Our Job."

Electric Furnace Steelmakers Hold Record Meeting In Pittsburgh

T. J. McLOUGHLIN, U. S. Steel Co., presents the Past Chairman Certificate and Perpetual Registration to J. A. Bowers, American Cast Iron Pipe Co.

TECHNICAL sessions on Availability and Conservation of Raw Materials, Special Features in Electric Furnace Practice, Stainless Steel, Bottom Maintenance and Furnace Design, Acid Vs. Basic Practice for Castings, and Refractories and Residual Elements, drew nearly 750 registrants to the Hotel William Penn, Pittsburgh, Dec. 6 to 8, 1951. An educational session on Procedure in Making a Heat of Steel was also held.

C. L. Austin, executive vice-president, Jones and Laughlin Steel Co., was introduced as speaker at the Annual Dinner by toastmaster C. B. Pollack, vice-president of production, Allegheny Ludlum Steel Corp. Mr. Austin's speech was entitled "*This Is Our Job.*"

R. H. Frank was elected chairman of the Executive Committee of the Electric Furnace Steel Committee for 1952, with W. M. Farnsworth chairman of the Conference Committee, and F. O. Lemmon vice-chairman of the Conference Committee.

The committees in charge of the ninth annual meeting included T. J. McLoughlin, chairman of the Executive Committee; R. H. Frank and W. M. Farnsworth, chairman and vice-chairman of the Conference Committee; R. K. Kulp, chairman of the Finance Committee; and A. E. Bickell, chairman of the Local Committee on Arrangements.

Scenes taken at random of some of the 500 members and guests that attended the Annual Dinner.

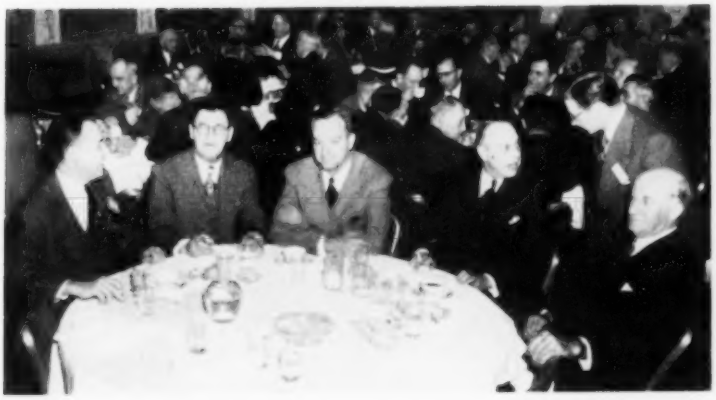

Obituaries

Charles N. Becker (Member 1936) died in May 1951. Mr. Becker was born in 1895 at Metuchen, N. J. From 1914 to 1916 he was employed by the Simplex Automobile Co., as assistant to the superintendent. He later joined the S. S. White Dental Mfg. Co., Staten Island, as cost accountant. After two years with this firm Mr. Becker became auditor for the Wright-Martin Aircraft Corp. at New Brunswick, N. J. In 1920 he went to Waukegan, Ill. as accountant with Southern Phosphate Corp. and Export Phosphate Co. He was made superintendent in 1923 and then assistant manager. At the time of his death he was employed by the R. H. Clark Equipment Co., Inc., Mulberry, Fla.

Adolph Bregman (Member 1921), consulting engineer of New York, died suddenly on October 4. Mr. Bregman was born in Minsk, Russia on Mar. 21, 1890. He attended the Ethical Culture School, New York and in 1914 received the degree of E.M. from the Colorado School of Mines, Golden. After graduation he was connected with the Wanakah Smelter as draftsman and designer. In 1916 he became experimental engineer for Nichols Copper Co., Laurel Hill, Long Island, N. Y. During the first world war he was in the Army and following his discharge he was a consulting metallurgical engineer. In 1919 he joined *The Metal Industry* as managing editor. In 1938 he opened his office as a consulting engineer.

Edward L. Clair (Member 1937) has died. Born at Washington, Pa., in 1894 he attended Carnegie Institute of Technology, and graduated in 1914. In 1920 he joined the Toledo Furnace Co. and was foreman and blast furnace superintendent, respectively. Three years later Mr. Clair was made blast furnace superintendent for the St. Louis Coke & Iron Co. In 1926 he joined the Interlake Iron Co., Toledo as blast furnace superintendent and was later made plant manager. At the time of his death he was located in Cleveland.

Will Lee Clark (Member 1903) died on Sept. 4, 1951 after a year's illness. Born at Denver in 1865 he went to New York in 1882 and attended the Lowville Academy. He returned to Butte to become clerk of the Superior Court and assistant business manager of a mining firm. In 1908 he was made assistant general manager of the United Verde Copper Co., Jerome, Ariz. Mr. Clark was later promoted to the position of general manager and in 1917 was appointed as United States Fuel Administrator for the state of Arizona. He lived in the west and at the time of his death was residing at Los Angeles.

Robert Saltzman Cockle (Member 1937) died on September 22 after a very short illness. Mr. Cockle was born in Denver on Sept. 22, 1911 and graduated from the Colorado School of Mines in 1933. He took a position with the Montezuma Apex mine at Plymouth, Calif. In 1937 he went to work on the Elton tunnel as surveyor on construction for the National Tunnel & Mines Co., Tooele, Utah. He later became an engineer for the Standard Silver-Lead Mining Co., Wilburn, Mont. He entered the Army Engineers as engineer instructor in January 1942 and in July of that year went overseas. He was discharged in 1945 with the rank of Lt. Colonel. Upon his discharge he took a position with Idarado Mining Co., Ouray, Colo. as engineer in October 1945. He soon was promoted to shift boss, mine superintendent and finally to assistant manager.

Harry A. Knowlton (Member 1947) died on August 31 after a brief illness. He was a metallurgical engineer in the employ of the International Harvester Co., Wisconsin Steel Div., Chicago. Born in Milwaukee on June 4, 1925, he received a B.S. degree in mechanical engineering from Illinois Institute of Technology and a B.S. degree in metallurgical engineering from Carnegie Institute of Technology. During World War II he was in the Naval Reserve in charge of training recruits at the Armory in Chicago. In 1946 he was with the Landberg Steel Treating Co., Chicago. He later joined the Air Reduction Sales Co. as a junior engineer, at Murray Hill, N. J.

H. D. Williamson (Member 1903) died on October 14. He served his apprenticeship as an engineer for the Northern Railway Locomotive Works at York, England. He was in Yokohama, Japan as assistant superintendent for the Rising Sun Petroleum Co. In 1915 he was located at Kent, England. Later Mr. Williamson was consulting engineer in London.

Eijiro Sagawa (Member 1920) and a Life Member of AIME, died in 1940, his death being recently reported to AIME headquarters. He was educated at Tokyo Imperial University, Berlin University, Freiberg Mining Academy and Wien University. He worked as geologist for Imperial Geological Survey of Japan; chief geologist for International Oil Co., Yokahama; assistant professor of the Imperial University, Tokyo; professor at Imperial University, Sendai; and chief geologist of Mitsui Mining Co., Tokyo.

Elwyn W. Stebbins (Member 1903), 80 years old, died May 21, 1950, at his home in San Francisco. A C.E. graduate of Massachusetts Institute of Technology and a M.E. graduate of University of California, he worked for Southern Pacific Railway Co., a surveyor and engineer for Liberty Bell Gold Mining Co., Telluride, Colo., and until the time of his death was engaged principally in examining and reporting on mining properties.

NECROLOGY

Date Elected	Name	Date of Death
1948	E. W. K. Andrau	Oct. 20, 1951
1905	Frank S. Ballie	Mar. 27, 1951
1922	Thomas Barrera	Unknown
1939	William R. Burgoyne	Oct. 19, 1951
1951	Donald A. Callahan	Oct. 24, 1951
1927	Richard J. Ennis	Oct. 5, 1951
1915	John Herman	Oct. 8, 1951
1905	Thomas F. Holdreth	Unknown
1912	Karl F. Hoffmann	June 1951
1944	Charles E. Pittson	Unknown
1914	William N. Roseberg	Sept. 16, 1951
1916	J. Moore Samuel	Nov. 5, 1951
1948	Paul Semko	Unknown

PROFESSIONAL SERVICES

Limited to AIME members, or to companies that have at least one AIME member on their staffs. Rates $40 per year per inch.

MAX STERN
Consulting Engineer
Expert for Strata Control and Shaft Sinking in Mechanization of Room and Pillar Mines for Bituminous Coking Coals
150 Broadway New York 7, N. Y.

ST & CO. INC.
ENGINEERS
CONSULTANTS
METALLURGISTS
Small Jobs Welcomed
SAM TOUR & CO., INC.
Laboratories and offices
44 Trinity Place, New York 6, N. Y.
Testing—Certifying
American Standards Testing Bureau, Inc.

R. S. DEAN LABORATORIES, INC.
Consulting, Research Development Chemistry, Electrochemistry, & Metallurgy Laboratory Research on a Contract Basis
5810—47TH AVENUE AP. 2821
RIVERDALE, MD.

LEWIS B. LINDEMUTH
Consulting Engineer
140 CEDAR STREET NEW YORK 6, N. Y.
STEEL PRODUCTION
DESIGN - OPERATION - CONSTRUCTION - METALLURGY

Personals

George Thomas Motock is now with the Union Carbide & Carbon Research Laboratories, Niagara Falls, N. Y.

Louis Lionel Colin has resigned as government metallurgist to the Portuguese Government, Portuguese East Africa, and is setting up a private consulting practice in Umtali, Southern Rhodesia.

Robert J. Turney has joined the United Development Corp. Pty. Ltd., Sydney, Australia, as sales engineer.

R. F. Hollis is with the atomic energy div. of the American Cyanamid Co., Watertown, Mass.

T. V. Canning has joined the Oglebay Norton Co., Duluth, Minn. He had been with Allis-Chalmers Mfg. Co., Milwaukee.

Warren P. Chernock is now a junior metallurgical engineer, physical metallurgy section, Sylvania Electric Products, Inc., Bayside, N. Y.

Murray James Miller is now with the Republic Steel Corp., Gadsden, Ala.

John A. Brown, General Electric Co., Schenectady, is now at the aircraft nuclear propulsion project, metallurgical section, Oak Ridge, Tenn.

George C. Floyd has been elected president of the Vanadium Corp. of America. He was previously vice-president of Thomas Steel Co.

Sherman R. Lyle was recently appointed district manager of the steel and tube div., northern Pennsylvania and New York, Timken Roller Bearing Co. He will be located in Buffalo.

H. M. Griffith has been appointed assistant to the president of the Steel Co. of Canada, Ltd., Hamilton, Ont. He was works manager before his appointment. Mr. Griffith succeeds **R. M. Kelday,** who was recently appointed manager of the wire, wire products and screw div. **M. A. Leisbman** has been named works manager, Hamilton and Ontario Works; **G. W. Bruce,** assistant works manager; and **A. D. Fisher,** general superintendent.

H M GRIFFITH

J. Alfred Berger was recently appointed acting head of the metallurgical engineering dept. of the University of Pittsburgh. Dr. Berger joined the faculty of the University in 1940 and in 1949 was appointed associate professor of metallurgical engineering.

Gano Dunn, president of the J. G. White Engineering Corp., **William E. Moore,** president of W. E. Moore & Co. and chairman of Pittsburgh Lectromelt Furnace Corp., and **James M. Caird,** civil engineer, were awarded gold keys as tokens of 50-year membership in the Franklin Institute, Philadelphia.

Paul E. Rapp has joined Foote Mineral Co., Philadelphia, as assistant treasurer.

Charles H. Moore has been appointed head of the metal and ceramic div., P. R. Mallory & Co., Inc., Indianapolis. Dr. Moore, inventor and developer of Titania, formerly was with National Lead Co. of Ohio, as technical director.

CHARLES H MOORE

John G. Nelson, assistant secretary and assistant treasurer, American Steel & Wire Co., has retired after more than 42 years of service.

Kenneth W. Donle was recently appointed chief metallurgist of Tube Reducing Corp., Wallington, N. J. He had been associated with the National Tube Co., Gary, Ind., as assistant chief metallurgist.

Charles W. MacGregor, professor of applied mechanics and head of the materials div., Massachusetts Institute of Technology, has been named vice-president of the University of Pennsylvania in charge of engineering and scientific studies.

Vernor L. Barbor, Jr. and **Carl L. McVicker** have joined the staff of Exothermic Alloys Sales & Service, Inc. Mr. Barbor will be on the west coast and Mr. McVicker will be at the Chicago office.

KARL V. LINDELL

Karl V. Lindell has been appointed vice-president of Canadian Johns-Manville Co., Ltd. and general manager of the company's Asbestos Fiber Div. He was mine manager of the company's Jeffrey mine.

Herbert M. Meyer has joined the metals research staff of Armour Research Foundation, Chicago.

Paul L. Jackson is now a member of the engineering staff at the Ford Motor Co. scientific laboratory, Dearborn, Mich.

Elliott Willner has become a metallurgical trainee for the purchasing dept., Federated Metals Div., American Smelting & Refining Co., Whiting, Ind.

E. Arthur Laird has joined the Bethlehem Pacific Coast Steel Corp., Los Angeles, as chief observer.

Reginald Rowand is now production manager of the Baroid Sales Div., National Lead Co., Houston.

Lee S. Richardson has joined the Oak Ridge National Laboratory as junior metallurgist.

Richard N. Lutz is presently with the Crucible Steel Co. of America, Midland, Pa.

Karl W. Reber, Russell C. Nelson, and **Fred H. Eckert, Jr.** have joined the Oak Ridge National Laboratory, Carbide & Carbon Chemicals Co. **Robert M. Fuller, Jr.** is on the staff of the gaseous diffusion plant.

Bernard C. Case has been appointed manager of electrochemical development for Hanson-Van Winkle-Munning Co., Matawan, N. J.

Ralph Vernon Hilkert has been appointed chief, physical metallurgy, Titanium Alloys Mfg. Div., National Lead Co., Niagara Falls, N. Y. He had previously been associated with the Pullman Standard Car Mfg. Co., Hammond, Ind.

Alberto Enrique Brazzini has returned to Peru from Washington, D. C. where he was Peruvian delegate to the Materials Conference—Copper, Zinc, Lead Committee.

Ronald Sadler has accepted a position with the Pennsylvania Smelting & Refining Co., Philadelphia.

Bruce M. Shields has been made general supervisor, development and research, U. S. Steel Co., Duquesne, Pa.

W. A. Smith, Stewarts & Lloyds, Ltd., has been promoted to manager of the research and technical development dept. at Lanarkshire, England.

Robert Ford is with the Aluminum Co. of Canada, Ltd., Isle Maligne, P. Q.

Walther Mathesius, president of Geneva Steel Co., who has announced his retirement, will become a consultant for the Freyn Engineering Dept. of Koppers Co., Inc. He will move to Chicago, the headquarters of the Freyn Dept.

Clay Crawford, a member of the metallurgical staff at the Pueblo steel mills of Colorado Fuel & Iron, has been named process control metallurgist for the new seamless tubing mill.

E. C. Bunce, New Jersey Zinc Co. (of Pa.), is now at the New York office. He had been located at the central laboratory, Palmerton, Pa.

L. W. Spang has been appointed secretary of the M. A. Hanna Co.

Alver E. Peterson was appointed controller of the Brainard Steel Co., Warren, Ohio.

William W. Wanamaker, Brigadier General, U. S. Army, retired, has been appointed chief engineer of the Orinoco Mining Co.

William R. Miller has been named to the post of manager of the metallurgical dept., American Steel & Wire Co.

Morton H. Dorenfeld has joined the Southwestern Engineering Co., Los Angeles, as metallurgist. He had been employed by the Tennessee Copper Co.

Lawrence A. Roe is now with the mining and metallurgical section, Bjorksten Research Laboratories, Inc., Madison, Wis.

John Bidner has been appointed assistant to the general superintendent, Sharon Steel Corp., Sharon, Pa. He was formerly openhearth superintendent of the company's Roemer Works.

Winthrop Sargent, Jr. was elected a member of the board of directors of National Lead Co., New York. Mr. Sargent has been general manager of the Titanium Alloy Mfg. Div. since 1948.

Robert A. O'Brien, research manager for the ASME, has been appointed assistant to the chairman of the mechanism and propulsion research dept., Armour Research Foundation of Illinois Institute of Technology.

Durrel L. Brown has joined the Vanadium Corp. of America, Durango, Colo., as metallurgist.

Julian Street, Jr. was recently appointed a special assistant on the U. S. Steel Corp. New York public relations staff.

Ralph R. Kelley is now associated with Brooks & Perkins as general superintendent of the new magnesium rolling mill to be called the Livonia Mill Div. He will have complete charge of casting magnesium slabs and rolling sheet and plate. Mr. Kelley had been roll products engineer for the Aluminum Co. of America.

W. Cordes Snyder, Jr. has been elected president and chief executive officer of Blaw-Knox Co. He previously was a vice-president of the company in charge of its Lewis foundry and machine div. More recently he was vice-president of the Koppers Co. and manager of the metallurgical dept.

Proposed for Membership

Metals Branch AIME

TAKE *Lectromelt* FURNACES TO YOUR ORE AND SAVE ON TRANSPORTATION

Deloro Smelting & Refining Company, Ltd., employ three Lectromelt Furnaces here at Deloro, Ontario.

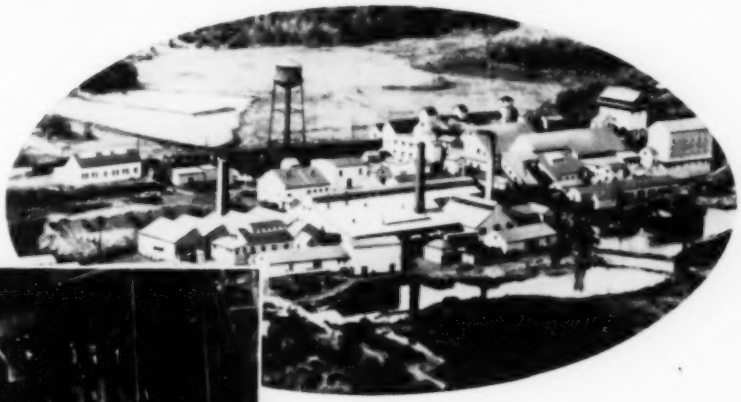

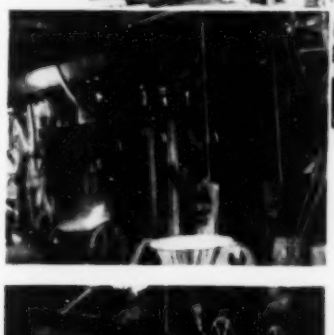

• This 150 kva. Lectromelt Furnace is smelting cobalt concentrates. Total charge 6-7 tons per day.

Silver concentrates are treated by this 100 kva. furnace at the rate of 3½ to 4 tons of charge per day.

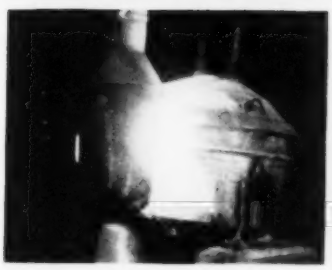

Cobalt alloys are melted and refined in this 250-pound lectromelt furnace. Another similar furnace is being added.

You have electric power at the mine site. Why not locate Lectromelt smelting furnaces there and avoid long, expensive hauls of bulky ores? You'll doubtless be money ahead.

Lectromelt Furnace equipment is dependable and long lived, so it can safely be installed away from service centers.

Our engineers are familiar with the use of electric arc furnaces for smelting, refining and melting operations. They can help you select the Lectromelt equipment you need and will advise on the designing of your furnaces. For Bulletin 104 telling you more about these furnaces and services, write Pittsburgh Lectromelt Furnace Corporation, 326 32nd Street, Pittsburgh 30, Pennsylvania.

Manufactured in . . . CANADA: Lectromelt Furnaces of Canada, Ltd., Toronto 2 . . . ENGLAND: Birlec, Ltd., Birmingham . . . AUSTRALIA: Birlec, Ltd., Sydney . . . FRANCE: Stein et Roubaix, Paris . . . BELGIUM: S. A. Belge Stein et Roubaix, Bressoux-Liege . . . SPAIN: General Electrica Espanola, Bilbao . . . ITALY: Forni Stein, Genoa

WHEN YOU MELT... MOORE RAPID *Lectromelt*

50 K.V.A. TO 50,000 K.V.A.

WHEREVER THE HOT STUFF HITS

USE NATIONAL CARBON

TRADE-MARK

For the cinder notch liner!

For the cinder notch plug!

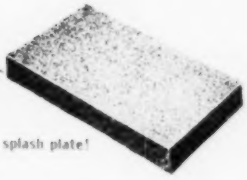

For the splash plate!

For the runout troughs!

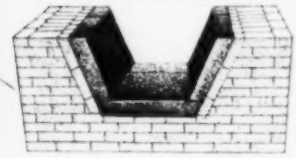

For the skimmer plate!

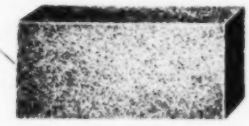

● "National" carbon is now firmly established for blast furnace linings. It is being used outside the furnace as well—wherever there is contact with molten material—for the splash plate, runout troughs—clear down to the ladle—skimmer plate, cinder notch liner and cinder notch plug.

The reasons?

"National" carbon has no melting point. It is highly resistant to slag attack and thermal shock . . . not wet by molten metal . . . has a low thermal expansion . . . and maintains its mechanical strength at elevated temperatures.

Use "National" carbon inside and outside your blast furnaces and you cut down maintenance, speed up production and save money. For more information, write to National Carbon Company, Dept. S.

The term "National" is a registered trade-mark of Union Carbide and Carbon Corporation

NATIONAL CARBON COMPANY

A Division of Union Carbide and Carbon Corporation

30 East 42nd Street, New York 17, N. Y.

District Sales Offices: Atlanta, Chicago, Dallas, Kansas City, New York, Pittsburgh, San Francisco

IN CANADA: National Carbon Limited
● Montreal, Toronto, Winnipeg